TECHNICAL
MEMORANDUM
NCSC TM 471-87

DECEMBER 1987

MEASUREMENTS OF THE HYDRODYNAMIC FORCE AND STRUM CHARACTERISTICS OF STRANDED CABLES

K. J. HORTON
C. M. FERRER
K. P. WATSON
D. CHARVOZ, DTNSRDC

Approved for public release; distribution is unlimited.

DESTRUCTION NOTICE

For classified documents, follow the procedures in DOD 5220.22M, Industrial Security Manual. Section II-19 or DOD 5200.1-R, Information Security Program Regulation, Chapter IX (chapter 17 of OPNAVINST 5210.1). For unclassified, limited documents, destroy by any method that will prevent disclosure of contents or reconstruction of the document.

NAVAL COASTAL SYSTEMS CENTER
NCSC
PANAMA CITY, FLORIDA 32407

NAVAL COASTAL SYSTEMS CENTER

PANAMA CITY, FLORIDA 32407-5000

CAPT M. W. GAVLAK, USN
Commanding Officer

DR. EDWARD B. TUNSTALL
Technical Director

ADMINISTRATIVE INFORMATION

This effort was completed during FY 86 by Code 4210, Hydromechanics Branch, of the Naval Coastal Systems Center (NAVCOASTSYSCEN), Panama City, Florida and Code 1541, Towed Systems Branch of the David Taylor Naval Ship Research and Development Center (DTNSRDC), Carderock, Maryland. The work was sponsored by the Seaborne Mine Countermeasures Block, NAVCOASTSYSCEN Block NC3A, of the Mine and Special Warfare Technology Project, PE 62315, from the Office of Naval Technology, Code 235.

E. H. Freeman, Head
Advanced Technology
Division

P. H. Kurtz, Head
Research Technology
Department

UNCLASSIFIED
SECURITY CLASSIFICATION OF THIS PAGE

REPORT DOCUMENTATION PAGE

1a. REPORT SECURITY CLASSIFICATION UNCLASSIFIED	1b. RESTRICTIVE MARKINGS
2a. SECURITY CLASSIFICATION AUTHORITY	3. DISTRIBUTION / AVAILABILITY OF REPORT Approved for public release; distribution is unlimited.
2b. DECLASSIFICATION / DOWNGRADING SCHEDULE	
4. PERFORMING ORGANIZATION REPORT NUMBER(S) NCSC TM 471-87	5. MONITORING ORGANIZATION REPORT NUMBER(S)
6a. NAME OF PERFORMING ORGANIZATION Naval Coastal Systems Center 6b. OFFICE SYMBOL (If applicable) Code 4210	7a. NAME OF MONITORING ORGANIZATION
6c. ADDRESS (City, State, and ZIP Code) Panama City, Florida 32407-5000	7b. ADDRESS (City, State, and ZIP Code)
8a. NAME OF FUNDING / SPONSORING ORGANIZATION Chief of Naval Research 8b. OFFICE SYMBOL (If applicable) Code 235	9. PROCUREMENT INSTRUMENT IDENTIFICATION NUMBER
8c. ADDRESS (City, State, and ZIP Code) Office of Naval Technology 800 North Quincy Street Arlington, VA 22217-5000	10. SOURCE OF FUNDING NUMBERS PROGRAM ELEMENT NO.: PE 62315 PROJECT NO.: TASK NO.: WORK UNIT ACCESSION NO.:

11. TITLE (Include Security Classification)
Measurements of the Hydrodynamic Force and Strum Characteristics of Stranded Cables

12. PERSONAL AUTHOR(S)
K. J. Horton, C. M. Ferrer, K. P. Watson, and D. Charvoz, DTNSRDC

13a. TYPE OF REPORT	13b. TIME COVERED FROM ____ TO ____	14. DATE OF REPORT (Year, Month, Day)	15. PAGE COUNT
		December 1987	179

16. SUPPLEMENTARY NOTATION

17. COSATI CODES		
FIELD	GROUP	SUB-GROUP

18. SUBJECT TERMS (Continue on reverse if necessary and identify by block number)
Hydrodynamic Forces; Measurement; Stranded Cables; Cables; Drag Measurement; Wire Rope; Lift; Towed Cables.

19. ABSTRACT (Continue on reverse if necessary and identify by block number)
The Naval Coastal Systems Center performed a series of cable tests in the high-speed tow basin at the David Taylor Naval Ship Research and Development Center. Steady and unsteady lift and drag characteristics and strum responses were measured for five twisted wire ropes. Fourteen-foot cable models were tensioned between two struts and towed over a velocity range of 2 to 10 knots with yaw angles varying from 20 to 90 degrees. From the mean steady force data, lift and drag loading functions were developed for each cable. The force and strum characteristics of the cables were compared with results from previous tests of circular cylinders and cables at yaw angles. Keywords:—

20. DISTRIBUTION / AVAILABILITY OF ABSTRACT	21. ABSTRACT SECURITY CLASSIFICATION
☐ UNCLASSIFIED/UNLIMITED ☒ SAME AS RPT. ☐ DTIC USERS	UNCLASSIFIED

22a. NAME OF RESPONSIBLE INDIVIDUAL	22b. TELEPHONE (Include Area Code)	22c. OFFICE SYMBOL
C. M. Ferrer	(904) 234-4146	Code 4210

DD FORM 1473, 84 MAR — 83 APR edition may be used until exhausted. All other editions are obsolete.

SECURITY CLASSIFICATION OF THIS PAGE
UNCLASSIFIED

GLOSSARY

A	Frontal Area
C_d	Coefficient of Drag
C_ℓ	Coefficient of Lift
C_{dn}	Normal Coefficient of Drag
$C_{\ell n}$	Normal Coefficient of Lift
D	Diameter
F_N	Force in Normal Direction
F_T	Force in Tangential Direction
F_L	Force in Lift Direction
F'_L	Maximum Lift Force per Unit Length
f	Cable Frequency at Midspan
f_n	Cable Natural Frequency
f_V	Vortex Shedding Frequency
$f(\beta)$	Trigonometric Loading Function
$f_n(\beta)$	Cable Loading Function in Normal Direction
$f_L(\beta)$	Cable Loading Function in Lift Direction
f_N	Normalized Force per Unit Length in Normal Direction
f_T	Normalized Force per Unit Length in Tangential Direction
f_L	Normalized Force per Unit Length in Lift Direction
L	Length
m	Mass
n	Mode Number

R	Normal Force per Unit Length at B = 90 degrees
Re	Reynolds Number
S	Strouhal Number
V	Velocity
Y	Y-Amplitude
β	Cable Angle
ρ	Fluid Density
ν	Kinematic Fluid Viscosity

CONTENTS

CONTENTS
(Continued)

ILLUSTRATIONS

ILLUSTRATIONS
(Continued)

ILLUSTRATIONS
(Continued)

ILLUSTRATIONS
(Continued)

TABLES

INTRODUCTION

A wide variety of towed marine systems are employed for purposes of naval defense, underwater environmental tests, and seabed mapping. Such systems consist of cables and hydrodynamic bodies. For configurations employing bodies which produce much larger hydrodynamic forces than the towed cables, the bodies dominate the system dynamics. However, for configurations in which the forces produced by the cables exceed the forces produced by the bodies, the cables dominate the system dynamics. This can be true even though the cable is a passive, uncontrolled member of the configuration while the body can be dynamically controlled.

The forces developed on towed cables include drag normal to the cable, drag tangential to the cable, and a lift force tranverse to the drag plane. The forces are illustrated in Figure 1. These forces can vary on the same cable with tow speed and fluid velocity (Reynolds number), and angle of incidence of the cable to the direction of tow. Thus, the fluid forces acting on a segment of a cable can be compared to the fluid forces developed on a towed body. Although towed body geometries are typically designed to produce specific lift and drag forces, the stranding geometry of towed cables is rarely chosen for the production of desired forces. However, some recently developed towed systems have required low drag tow cables which do not vibrate. As a result of that requirement a variety of tests have been completed since 1970 to precisely characterize some towed cables.

Characterizing the hydrodynamic properties of towed cables is an important step in creating the data base required for accurate towed system design. As the placement precision and accuracy requirements for towed systems become more stringent for the success of the system mission, greater design accuracy is required. Analytic methods of predicting the characteristics of cables of a given geometry have not been developed. Thus, measuring cable dynamic properties and predicting cable behavior under tow by means of semi-empirical methods is employed when designing towed systems.

Accurately predicting the configuration of a diverted towed system is an area of research under study. The task requires knowledge of both the forces produced by the towed bodies in their equilibrium condition in the system and the hydrodynamic forces produced by the towed cables. This investigation focuses on the latter as applied to mechanical minesweeps. The dynamic behavior of various wire ropes was tested and the data used to develop empirical expressions suitable for use in towed system design predictions. The wire ropes of interest were those considered suitable for mechanical minesweeping systems.

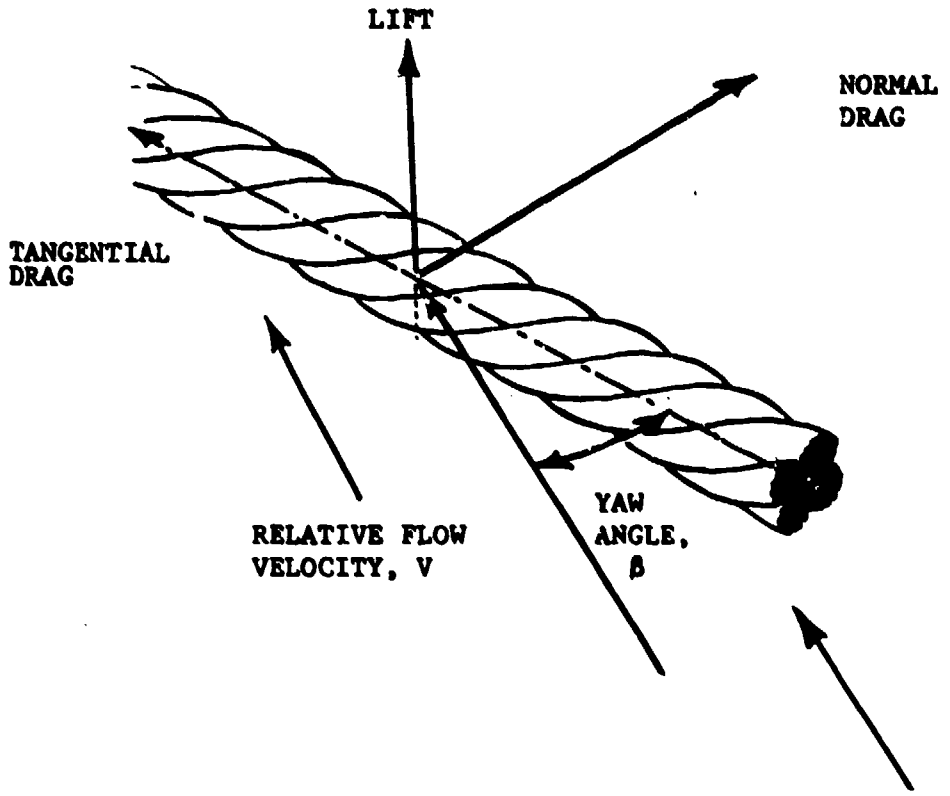

FIGURE 1. POSITIVE DIRECTION OF HYDRODYNAMIC FORCES, CABLE YAW ANGLE, AND RELATIVE FLOW VELOCITY

BACKGROUND

Mechanical minesweeps typically consist of a tow cable depressed to the desired sweep depth, followed by one or more sweep cables which are diverted by bodies maintained at the same depth. In mechanical sweep systems all the cables are twisted wire ropes and are referred to as either cables or wires. A hypothetical mechanical minesweep system is shown in Figure 2. The tow wire creates a catenary in a near vertical plane aft of the towpoint while the sweep wire creates a catenary in a near horizontal plane aft of the depressor. However, due to the hydrodynamic lift developed by wire ropes and the weight of the ropes, both the tow wire and the sweep wire maintain three-dimensional rather than perfectly planar configurations.

Wire ropes display a twisted geometry which is asymmetric. As a result of this asymmetry wire ropes under tow produce a steady-state lift force orthogonal to their steady normal and tangential drag forces (Figure 1). This lift is comparable to that produced by an airfoil and, similarly, the size of the lift changes with angle of incidence of the rope to its direction of tow. In the case of a depressed tow wire, the cable lift produces a side force causing the cable and depressor to kite to the lift side of the towpoint. In the case of a mechanical sweep

wire which is diverted, the cable lift produces a vertical force which causes the wire to hog (arc) if the lift is directed upward or sag if the lift is directed downward. Sweep wires constructed of wire rope are heavy in water, so if they did not produce lift they would always sag. However, tests have shown that because they do produce lift under some tow conditions, sections of a sweep wire can hog above its endpoints. The effect is that sweep wires can ride above mines intended to be swept.

Mechanical minesweeping wires were originally designed for their efficient cutting capability, not their hydrodynamic qualities. During their development prior to World War II, the main technology issue was to produce a sweep wire which would sever moorings by a sawing action.

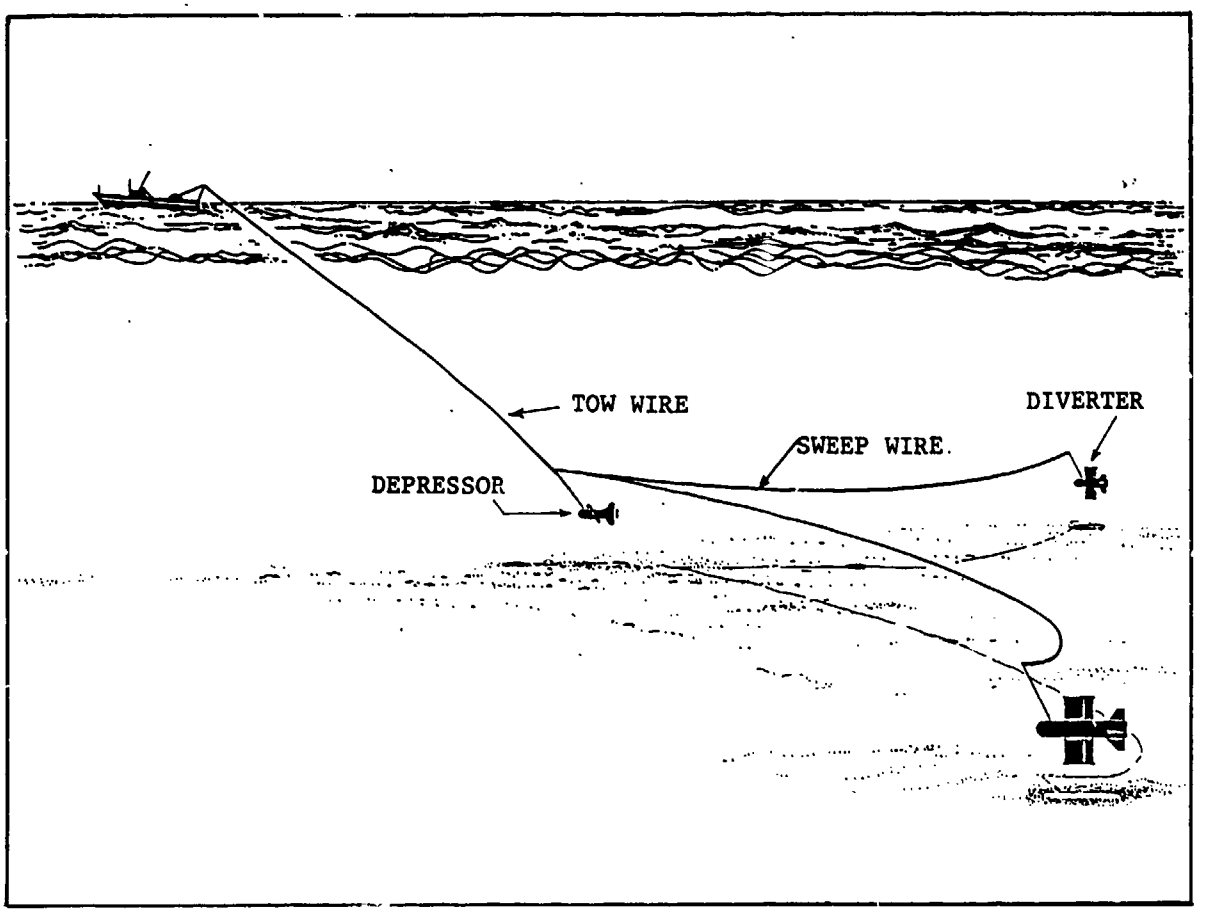

FIGURE 2. ELEMENTS OF A HYPOTHETICAL MECHANICAL MINESWEEPING SYSTEM

Today, however, one technology issue is precise placement of a mechanical minesweep. The solution to this problem requires sweep wires which will lie in a horizontal plane while under tow. In order to achieve this goal, information about wire hydrodynamics is required for accurate predictions of mechanical minesweep geometries during operations. The required information is typically in the form of trigonometric loading functions describing the cable normal drag, tangential drag, and lift forces developed for angle of incidence of the wire to the tow velocity. Two tests to characterize several wire ropes were performed in 1945 and 1962 at the David Taylor Model Basin wind tunnel.[1] [2] Although those tests were the best available at the time, they contain known interferences.

A second technology issue is the longevity of sweep wires. Sweep wires are currently retired due to fatigue, or the breakage of a specified number of wires per length of rope. Exposure, passes through sheaves, and imperfect winch operations are some causes of fatigue. In addition vibrations of the wire ropes under tow cause fatigue. These vibrations, commonly referred to as strumming, are caused by vortices periodically shed from the cable as a result of the fluid boundary layer separation. These shed vortices are also referred to as a "von Karman vortex street." Vortex shedding creates fluctuating pressure differentials around the wire which force it to vibrate. The vibrations resulting from vortex shedding are also known to increase the effective drag coefficients of wire ropes thus increasing the power required to tow them.

OBJECTIVES

In order to better characterize the hydrodynamics of wire ropes for application to mechanical minesweeping systems, a series of tests was completed. This test program was performed with two objectives:

1. Quantify the lift and drag forces produced by five potential sweep wires under normal tow speeds and angles of incidence to tow.

2. Qualitatively determine the relative strum amplitudes of each wire.

Prior to these tests no strum data existed for wire rope constructions, and the latest drag and lift data available as mentioned before were from wind tunnel tests performed in 1945 and 1962 at David Taylor Naval Ship Research and Development Center (DTNSRDC). The data

---

[1]David W. Taylor Model Basin Report R-312, "Wind-Tunnel Tests of Mine Sweeper Cables," Aero Report 705, December 1949.

[2]David W. Taylor Model Basin Report 1645, "Wind-Tunnel Determination of the Aerodynamic Characteristics of Several Twisted Wire Ropes," by M. P. Schultz, Aero Report 1028, June 1962.

collected in this test program are therefore expected to assist in the design of towed cable systems and the development of improved prediction methods. Data analysis of the results will determine drag and lift loading functions to use in predicting steady-state towed cable systems. The data can also be used for fatigue analysis of cables. It is expected that the strum characteristics will aid in cable selection for towed systems. This report documents the test procedures and preliminary data reduction and analysis.

THEORY

The two objectives of the test program described were accomplished by measuring the mean steady drag and lift characteristics of the cable models and the overlying unsteady drag and lift characteristics including the cable vibrational, or strum, response. The steady and unsteady characteristics of cables are closely related. Both the steady and unsteady data are required for a complete analysis of the cable dynamics. The following section provides the reader with a brief discussion of the production and analysis of steady drag and lift, and strum vibrations.

STEADY DRAG AND LIFT

Cables under tow produce mean steady drag and lift forces which are overlaid by fluctuating forces. A stranded cable produces a steady drag force in the cable flow plane, and a steady lift force transverse to the cable flow plane. Defining the mean steady forces arising on a cable under tow is required to predict its configuration. In the past, estimates of the cable forces have been adequate to predict the rough placement of a towed system before it was deployed. However, the system placement requirements today are more stringent than in the past. As a result more precise methods and data on which to base system predictions are required for design studies.

The drag vector acting on a cable under tow can be resolved into components normal and tangential to the cable. The normal drag component represents form or profile drag while the tangential component represents frictional drag. Each of these drag components can be represented by a function of the angle the cable makes to the flow (β).

Cable drag is typically expressed in terms of the flow dynamic pressure, the frontal area, a force coefficient, and a trigonometric function of yaw angle:

$$F = qAC_d * f(\beta) \qquad (1)$$

where

F = drag force

q = 1/2 * fluid density * velocity squared

A = cable diameter x cable length

C_d = drag force coefficient

β = cable angle

$f(\beta)$ = trigonometric loading function for cable angle.

One common form of the loading function is that given by Springston:[3]

$$f(\beta) = A_o + A_1 * \cos(\beta) + B_1 * \sin(\beta) + A_2 * \cos(2\beta) + B_2 * \sin(2\beta) \quad (2)$$

where the coefficients A and B are empirical constants for each cable. The normal and tangential drag components can each be represented by functions of this form with different coefficients. This loading function form was determined for drag forces based on analyses performed over a period of years by various scientists.

In addition to drag being a function of yaw angle, normal drag coefficients are also Reynolds number dependent. They are also increased significantly by strum vibrations of the cable. By repressing strumming cable drag coefficients can be reduced by up to 75 percent. Normal drag is generally assumed to be independent of tangential drag for a cable at an angle of yaw.

The steady lift force produced by a yawed cable is small compared to the drag force. However, for mechanical minesweep systems the lift forces are large enough to govern the success of such a system. Although it is well known that stranded cables produce a mean steady lift, steady lift development has been quantified for only a few cables.[1 2 4] The flow patterns leading to the production of steady lift

---

[1] op. cit.

[2] op. cit.

[3] David W. Taylor Naval Ship Research and Development Center Report 2424, "Generalized Hydrodynamic Loading Functions for Bare and Faired Cables in Two-Dimensional Steady-State Cable Configurations," by G. B. Springston, Jr., June 1967.

[4] Imperial College of Science and Technology Report 117, "Lift and Drag Measurements on Stranded Cables," by J. Counihan, United Kingdom, 1963.

on either strumming or nonstrumming cables have not been qualitatively or quantitatively measured. Two different theories regarding the production of mean steady lift by stranded cables have been postulated. The first theory reflects the concept of the cable acting as an airfoil. When a cable is yawed to the flow, the upper and lower surfaces of the cable profile as viewed in the flow plane are not symmetric. This causes a low pressure region to arise over the rougher surface. The lift mechanism is therefore due to the profile geometry of the cable. The geometric asymmetry varies widely for yaw angle. Figure 3 displays the profile geometry in the flow plane of a wire rope at two yaw angles. The second theory proposes that the varying geometry about the cable causes separation to occur earlier on one side of the cable than on the other for the turbulent boundary layer regime. The assertion is that measurable lift is produced by asymmetric separation of the turbulent boundary layer. The steady lift is produced by surface pressure differences caused by the difference in separation points from the top and bottom of the cable.[5]

Based on available lift data the functional form used to predict drag can be applied to the prediction of lift forces.[1,2,4] One study also shows the lift coefficient to be Reynolds number dependent.[4] The relationships between lift and drag, and between mean steady lift and fluctuating lift, have not been determined. Drag and lift loading functions will be expressed by Springston's recommended form (Equation (2)) in this report.

CABLE STRUMMING

Cable strum vibrations result from unsteady cyclic forces produced by the alternate shedding of vortices from the cable. Strumming affects cables in two ways. First, strumming increases the drag of a towed system, thus affecting the catenary the cable assumes and increasing the power required to tow it. Second, the fluctuating forces imposed during vibrations due to strumming cause fatigue, limiting the service life of a cable. Defining the strum response of a cable is important in order to predict the effectiveness of a planned cable-towed system which is to provide long term service.

---

[1]op. cit.

[2]op. cit.

[4]op. cit.

[5]Simpson, A., "Fluid Dynamic Stability Aspects of Cables," Proceedings of the Mechanics of Wave-Induced Forces on Cylinders, T. L. Shaw, ed., Pitman Advanced Publishing Program, London, 1979, pp. 90-132.

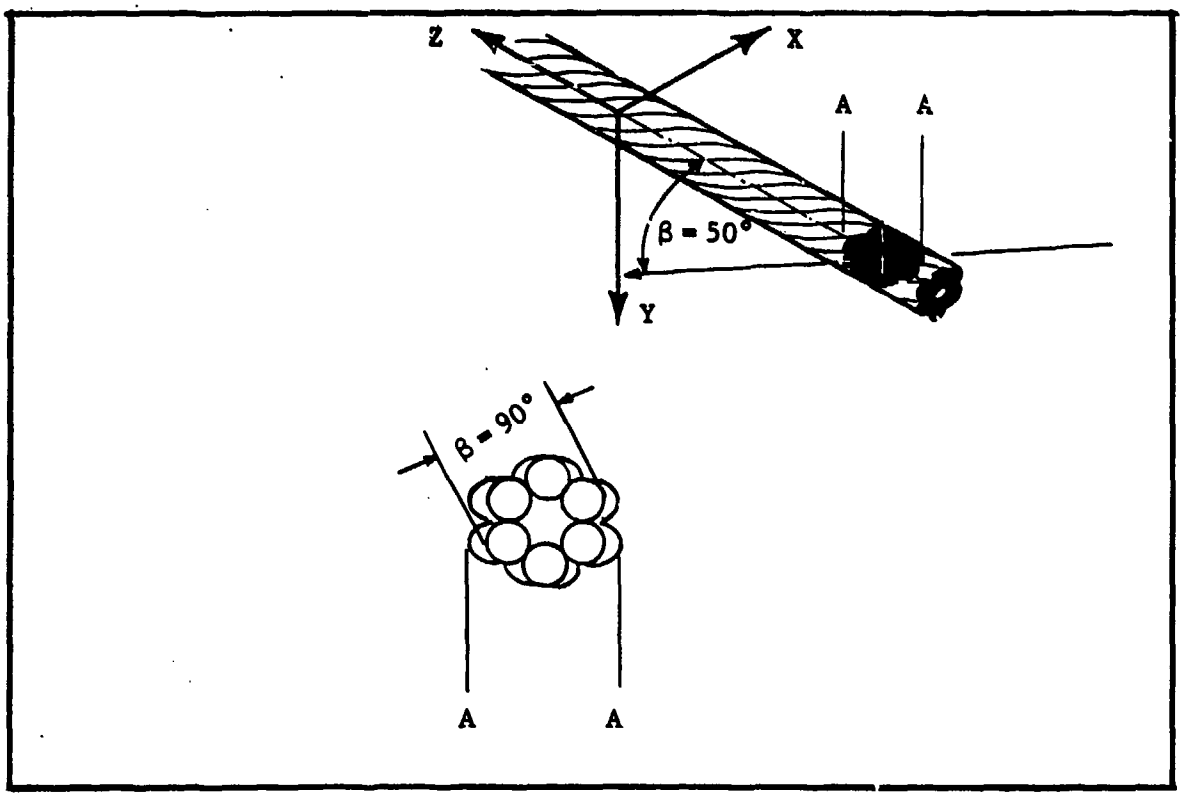

(a)

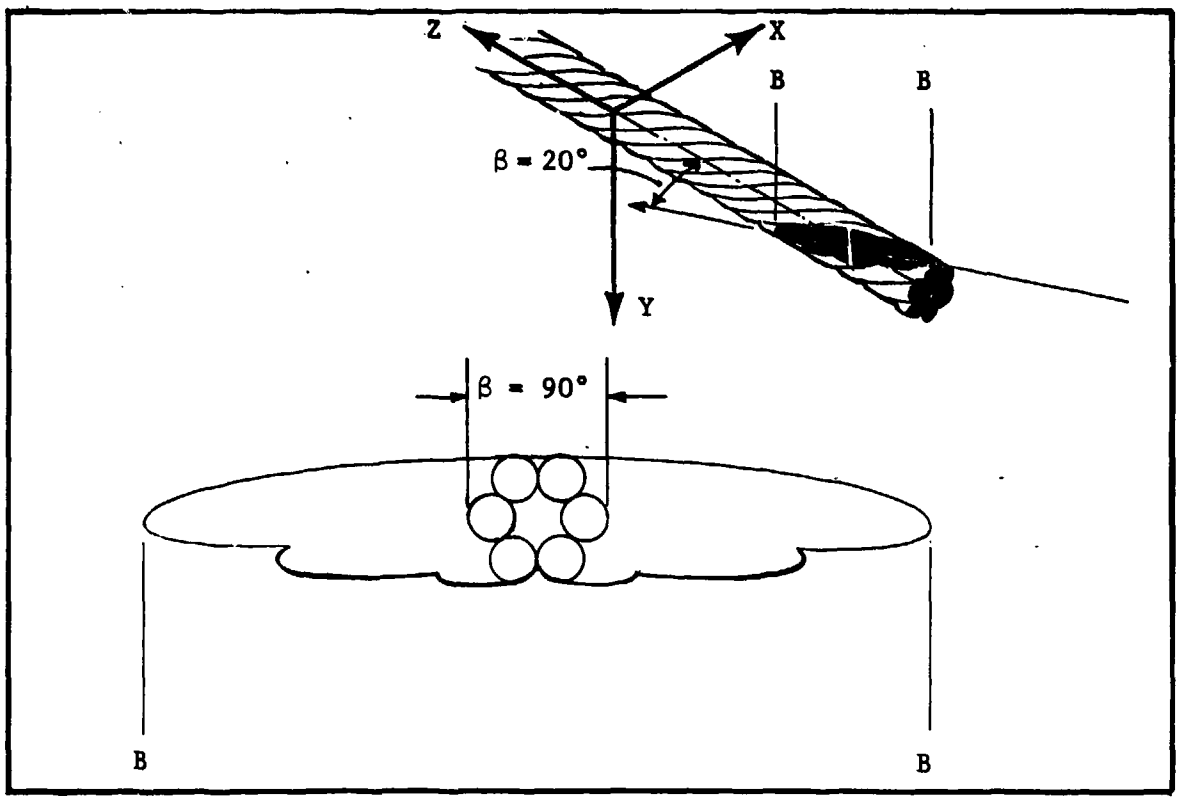

(b)

FIGURE 3. CROSS SECTIONS THROUGH A 6-STRAND CABLE YAWED AT 50 DEGREES (a) AND 20 DEGREES (b) TO THE FLOW

The dynamic characteristics of interest in a rudimentary strum analysis are the strum frequency and the resulting vibrational amplitude of the cable. Comprehensive discussions of the analysis of vortex-induced vibrations are given by Simpson,[5] Diggs,[6] and Griffin, et al.[7] The reader is referred to Appendix A for indepth descriptions of the strumming phenomenon and advanced analysis techniques.

Information about circular cylinders is used as a baseline in the analysis of wire ropes. A number of recent experiments have been performed to characterize the wake of circular cylinders. The wake patterns of cylinders immersed in a flow are governed by the Reynolds number based on cylinder diameter:

$$Re = \frac{VD}{\nu}$$

where V is the freestream velocity, D is the cylinder diameter, and ν is the fluid kinematic viscosity.

Figure 4 illustrates the wake patterns under various flow regimes. For mechanical minesweeping systems, the Reynolds number range of interest is $1 \times 10^4 < Re < 1 \times 10^5$. Figure 4 shows that in this flow regime the wake is composed of turbulent vortices shed alternatively from the top and bottom of the cylinder. A fluctuating pressure field around the cylinder occurs with the vortex shedding. Strumming is the structural response of the towed cable to the fluctuating pressure field.

The Strouhal number, S, is a nondimensional parameter used to relate the frequency of the shed vortices to the cylinder diameter and flow velocity. The Strouhal number for circular cylinders has been determined empirically for Reynolds number and the results are shown in Figure 5. In order to determine this relationship the vortex shedding frequencies for nonvibrating circular cylinders were measured in a variety of experiments and the resulting nondimensional parameter

$$S = \frac{f_v D}{V} \qquad (3)$$

---

[5]op. cit.

[6]MAR, Inc. Technical Report 122, "A Survey of Vortex Shedding from Circular Cylinders with Application Toward Towed Arrays," by J. S. Diggs, July 1974.

[7]Naval Civil Engineering Laboratory Technical Note 1608, "The Strumming Vibrations of Marine Cables: State of the Art," by O. M. Griffin, S. E. Ramberg, and R. A. Skop, May 1981.

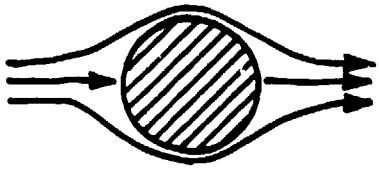

Re < 5 REGIME OF UNSEPARATED FLOW.

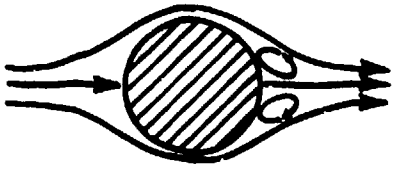

5 TO 15 < Re < 40 A FIXED PAIR OF FOPPL VORTICES IN THE WAKE.

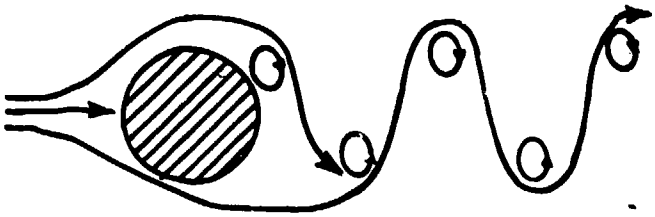

40 < Re < 90 AND 90 < Re < 150

TWO REGIMES IN WHICH VORTEX STREET IS LAMINAR
- PERIODICITY GOVERNED IN LOW Re RANGE BY WAKE INSTABILITY
- PERIODICITY GOVERNED IN HIGH Re RANGE BY VORTEX SHEDDING.

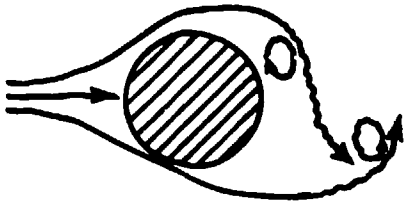

150 < Re < 300 TRANSITION RANGE TO TURBULENCE IN VORTEX.

300 < Re $\lesssim$ 3×10^5 VORTEX STREET IS FULLY TURBULENT.

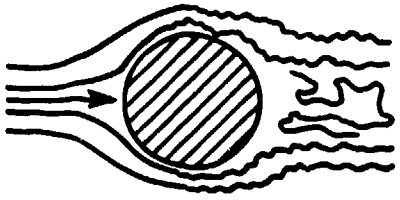

$3 \times 10^5 \lesssim$ Re < 3.5×10^6

LAMINAR BOUNDARY LAYER HAS UNDERGONE TURBULENT TRANSITION. THE WAKE IS NARROWER AND DISORGANIZED. NO VORTEX STREET IS APPARENT.

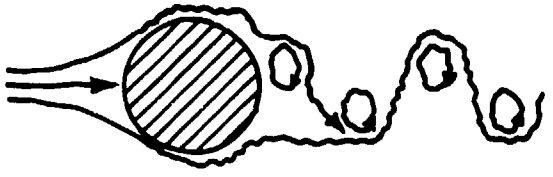

3.5×10^6 < Re < ∞ (?)

RE-ESTABLISHMENT OF THE TURBULENT VORTEX STREET THAT WAS EVIDENT IN 300 < Re $\lesssim$ 3×10^3. THIS TIME THE BOUNDARY LAYER IS TURBULENT AND THE WAKE IS THINNER.

FIGURE 4. VORTEX STREET FORMATION FLOW REGIMES

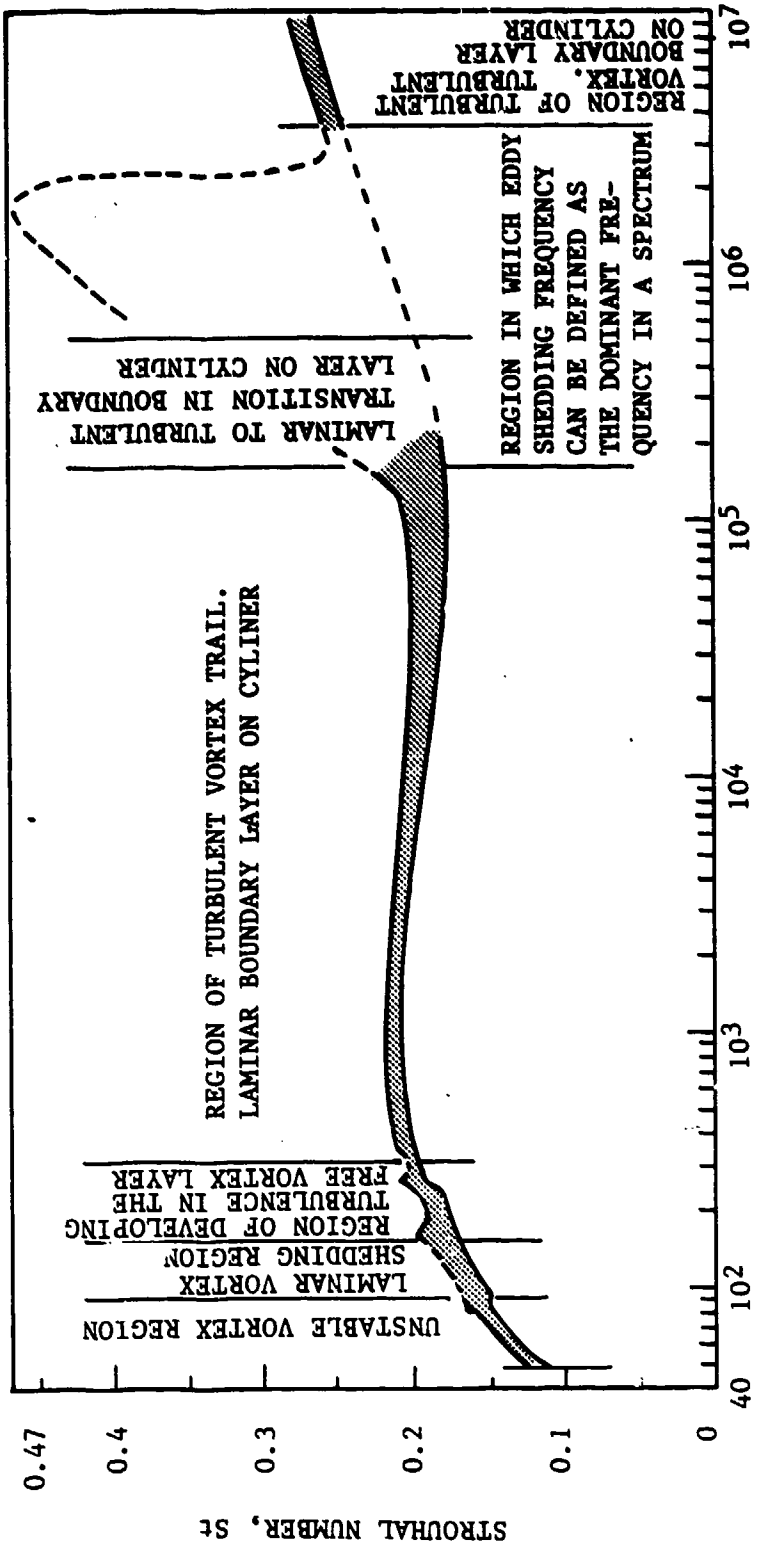

FIGURE 5. STROUHAL-REYNOLDS NUMBER RELATIONSHIP FOR CYLINDERS NORMAL TO THE FLOW

where f_v is the shedding frequency in cycles per second (hertz, Hz), was determined for each case. The Strouhal number for circular cylinders for the stated Reynolds number range of interest has been measured at 0.18 to 0.21.

Inversely, the shedding frequency can be inferred from Equation (3) as

$$f_v = \frac{SV}{D} \tag{4}$$

if the Strouhal number is known.

The above expression for f_v applies to a cylinder normal to the flow. When the cylinder is yawed the frequency of shedding is altered. Equation (4) may be used to predict f_v for a yawed cylinder if the equation is expressed in terms of the normal velocity component, V sin (β), which gives

$$f_v = (SV/D) \sin(\beta) \quad . \tag{5}$$

This is a result of the well-known Independence Principle which states that the fluid dynamic properties of a yawed cylinder are governed by the normal component of the flow. The tangential flow component is assumed to have no effect on the shedding frequency and strum amplitude. Equation (5) predicts the maximum f_v when the cylinder is normal to the flow ($\beta = 90$). As the yaw angle is reduced the frequency likewise decreases.

As stated previously, fluctuating asymmetric pressure distributions about the cable are created by the vortex shedding process. One complete vortex shedding cycle consists of two vortices of opposite sign shed from alternate sides of the cable. For flow in the horizontal plane, one cycle consists of a vortex shed from the bottom of the cable followed by a vortex shed from the top of the cable. During this cycle the cable is forced to vibrate, or strum, due to the alternating pressure distribution. One shedding cycle causes the cable to respond with one vibrational cycle transverse to the wake and two vibrational cycles in line with the wake. This is because one vibrational cycle in the horizontal plane is caused by each shed vortex, while one vibrational cycle in the vertical plane is caused by two shed vortices, or one vortex cycle. Again for horizontal flow, this is one vibrational cycle in the vertical direction and two cycles in the horizontal direction. The transverse vibrational frequency corresponds to the wake shedding frequency, and the in line vibrational frequency corresponds to twice the wake shedding frequency.

During cable strum vibrations, the wake shedding frequency is influenced by the structural natural frequency. The natural frequency, f_n, of a taut cable can be approximated by the stretched string wave equation solution:

$$f_n = \frac{n}{2L}\sqrt{\frac{T}{m}} \tag{6}$$

where n is the mode number, i.e., 1, 2, 3, ..., T is the cable tension, L is the cable length, and m is the cable mass per unit length.

In the case of nonvibrating circular cylinders, if the flow velocity is increased smoothly, the wake shedding frequency also increases smoothly. However, for cylinders or cables free to vibrate, as the flow velocity is increased smoothly, the wake frequency increases in steps corresponding to jumps from lower mode natural frequencies to higher mode natural frequencies. This is illustrated in Figure 6. Previous tests have confirmed that the wake shedding frequency will "lock-on" to within 25 percent of the nearest structural natural frequency, causing the cable to vibrate at or near one of its structural natural frequencies.[7]

Lock-on affects the cable wake by increasing the length of cable over which the wake is coherent, or in phase.[7] The coherence is determined by the length of cable over which the vortices are shed as a uniform vortex street and the extent to which the vortices along that length are in phase. As the coherence increases, the length of cable experiencing the same cross-sectional pressure distribution increases. In turn, the strum amplitude is influenced by the spanwise coherence of the vortex street. Maximum strum amplitudes occur when the wake is most coherent. Circular cylinder vibration amplitudes due to strumming have been shown to be self-limiting to approximately one diameter. At larger vibration amplitudes the vibration itself causes the wake to lose its coherence.[8]

Although a cable is often estimated by a circular cylinder there are important differences in the geometry of cables and cylinders. The geometry of a cable presented normal to the flow is noncircular, shaped somewhat like a cloverleaf. The "lumpy" cross section of a cable causes boundary layer transition from laminar to turbulent to occur earlier on cables than on circular cylinders.[4] The vortex shedding patterns for

---

[4]op. cit.

[7]op. cit.

[8]Blevins, R. D., Flow-Induced Vibration, Van Nostrand Reinhold Company, New York, 1977, Ch. 3, pp. 11-54.

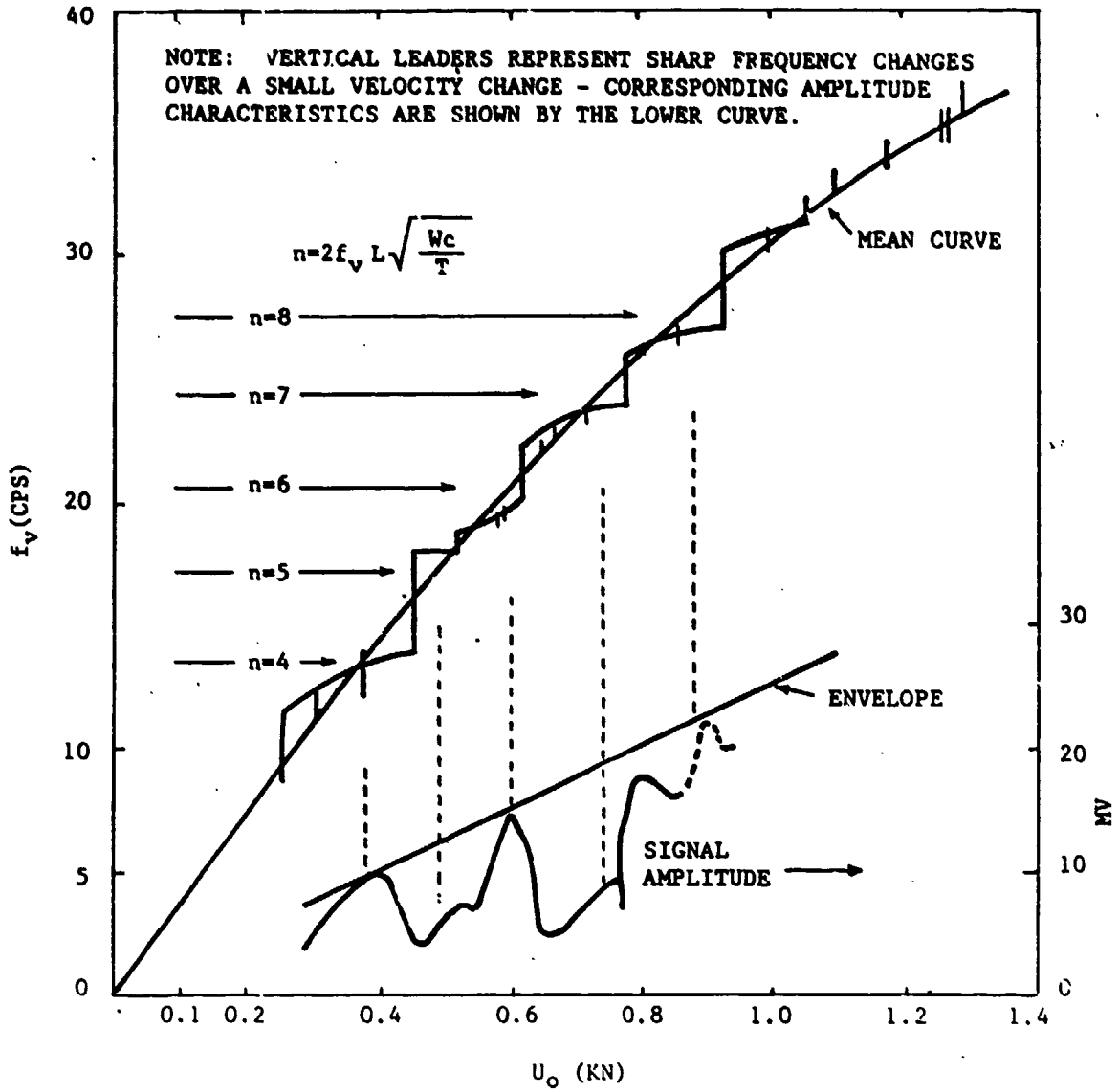

FIGURE 6. FREQUENCY CHARACTERISTICS FOR 6-FOOT-LONG 0.1-INCH-DIAMETER FLEXIBLE CABLE

the laminar, transitional, and turbulent boundary layer regimes are somewhat different. The main difference is that during the transition range regularly shed vortices are replaced by a general turbulence in the wake. Post transition and pretransition wake characteristics are similar except for the later separation observed in the post transition regime.

The effect of the cable stranding on vortex coherence is not clearly established. The cross section of a cable varies in shape at each station along the length of the cable as a result of its stranding. The local diameter in the flow plane varies with the twist of the rope. Because the local wake frequency is determined by the local transverse cable diameter, the frequencies of the shed vortices might vary along the cable, decreasing wake coherence.

TEST PLAN

The tests were performed at the David Taylor Naval Research and Development Center (DTNSRDC) in its high-speed tow basin. Fourteen-foot lengths of five wire ropes were each tensioned between two faired struts on the tow carriage. The cable models were immersed in the water and towed horizontally at various yaw angles over a speed range. The dynamic normal, tangential, and transverse forces were measured at one end of the cable. The horizontal and vertical accelerations of the center point of the cable were also measured. Data from this test were then reduced and analyzed in support of the test objectives. The following sections describe the specifics of the cable strumming tests.

TEST RIG

The DTNSRDC rig was developed in 1975.[9] It is used to measure the strumming phenomena of cables in both uniform and non-uniform flow conditions. The rig is a rotatable twin-strut assembly attached to the towing carriage with a bracket and turntable which allows tow angles between 0 and 90 degrees to the flow. Fairings that are self-aligning to the flow are attached at the bottom of each strut. They provide protection for any sensors which are placed at this location and minimize strut interference on the cable that might occur during testing. The strut assembly allows tow speeds up to 20 knots. The entire assembly can be raised out of the water to facilitate cable and cable angle changes. A photo of the rig is shown in Figure 7.

---

[9]David W. Taylor Naval Ship Research and Development Center Report SPD 766-01, "Measurement Technique to Obtain Strumming Characteristics of Model Mooring Cables in Uniform Currents," by J. H. Pattison, April 1977.

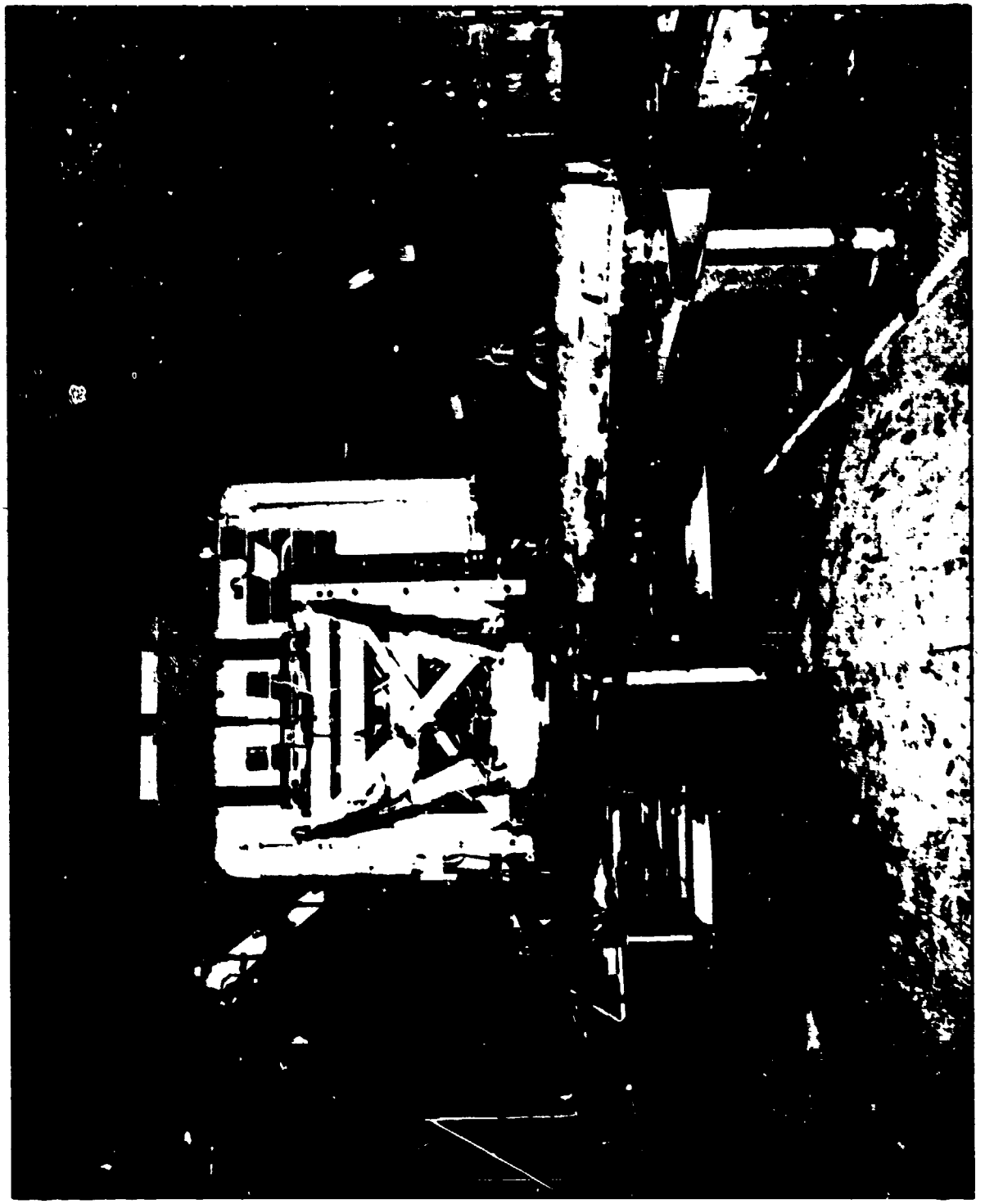

FIGURE 7. DTNSRDC CABLE FORCE AND STRUM MEASUREMENT TEST RIG AT YAW ANGLE

The struts were designed to maintain a cable tension up to 1000 pounds. The self-aligning fairing design was examined for damping and interference effects on the cable. A two-dimensional potential flow panel program[10] was used to determine the angle at which flow interference effects result from the strut fairing. To prevent flow interference from the struts, minimum tow angles were limited to 20 degrees. The distance between the struts limited cable model lengths to 14 feet.

TEST PARAMETERS

The cable constructions chosen include models of 1 x 19, 7 x 7, 3 x 19, 4 x 7 serrated, and 6 x 25 lang lay wire ropes. In designating wire ropes, the first number refers to the number of strands, the second to the number of wires per strand. The 4 x 7 rope is termed serrated because one of the wires in each strand is actually composed of two wires twisted together. An important characteristic of wire ropes is the "lay" of the strands. The 3 x 19, 4 x 7 serrated, and 6 x 25 lang lay models are right lay, meaning that the strands pass from right to left around the cable. The remaining models are left lay. Another characteristic of wire rope is the direction of the wires within each strand. The wires in the strands are laid opposite in direction to the lay of the strands (regular lay) for all the models except the 6 x 25. For this model the wires are laid in the same direction as the lay of the strands (lang lay). The geometric properties of the cable models are listed in Table 1. The 4 x 7 and 1 x 19 cables are presently used

TABLE 1

PHYSICAL CHARACTERISTICS OF CABLE MODELS

Cable Construction	Nominal Diameter (in.)	Actual Diameter (in.)	Length (ft)	Weight Air/Water (lb)	Cable Lay
1 x 19	0.625	0.632	14	12.2/10.6	Left
7 x 7	0.625	0.640	14	10.1/8.8	Left
3 x 19	0.625	0.615	14	9.3/7.8	Right
4 x 7 serrated	0.797	0.700	14	11.0/9.3	Right
6 x 25 lang lay	0.625	0.625	14	10.6/8.9	Right

[10]National Aeronautics and Space Administration Report CR 134695, "Improved Solution for Potential Flow About Arbitrary Axisymmetric Bodies by the Use of a Higher-Order Surface Source Method, Part I, Theory," by D. M. Friedman, July 1974.

in seaborne and airborne minesweeping systems, respectively. The 3 x 19 and 7 x 7 cables are possible future seaborne minesweeping system tow cables. The 6 x 25 cable, chosen to provide additional quantitative data, is not used and is not planned for use in any minesweeping systems. It was chosen in order to investigate the effect of the lang lay construction on hydrodynamic forces developed. Figures 8 through 12 show profiles of the cable models. Figure 13 shows a sketch of the cross sections of the cable models. The 1 x 19, 6 x 25, and 7 x 7 cables are more nearly circular than the 3 x 19 and 4 x 7 cables.

In order to obtain sufficient data to develop drag and lift loading functions, measurements were performed with the cable models at eight angles to the flow. Although the tow angles desired were from 20 to 90 degrees in 10-degree increments, the angles chosen were 20, 30, 43, 50, 60, 71, and 90 degrees to the flow. Inability to obtain 40 and 70 degrees was due to the previous setup of the turntable on the rig. Angles less than 20 degrees were not chosen due to strut interference as previously discussed.

Tow carriage speeds were chosen to provide the same Reynolds number range encountered in seaborne minesweeping operations. The speeds chosen were 2, 5, 7, and 10 knots.

Cable tension was bounded primarily by the maximum tension supported by the struts being 1000 pounds, but also by the desire to limit the number of modes excited. From Equation (6) of the theory section, the mode number is given by:

$$n = 2L\, f_n \sqrt{\frac{m}{T}} \quad . \tag{7}$$

The structural mode stimulated in response to vortex shedding can be determined by substituting the vortex frequency f_v for the natural frequency f_n. By increasing tension the mode number is decreased for all other conditions being equal. Two tensions were selected to provide cable data at different ranges of modes. A high tension of 850 pounds and a low tension of 550 pounds were chosen.

Each test run was performed at a single speed, angle, and tension. All combinations of tension, angle, and speed were run on the 1 x 19, 7 x 7, 3 x 19, and 4 x 7 serrated cable models for a total of 64 runs per cable. The 6 x 25 lang lay model was tested at each speed and tension at 30, 60, and 90 degrees to the flow. Test runs on the 6 x 25 were limited by available tow basin time.

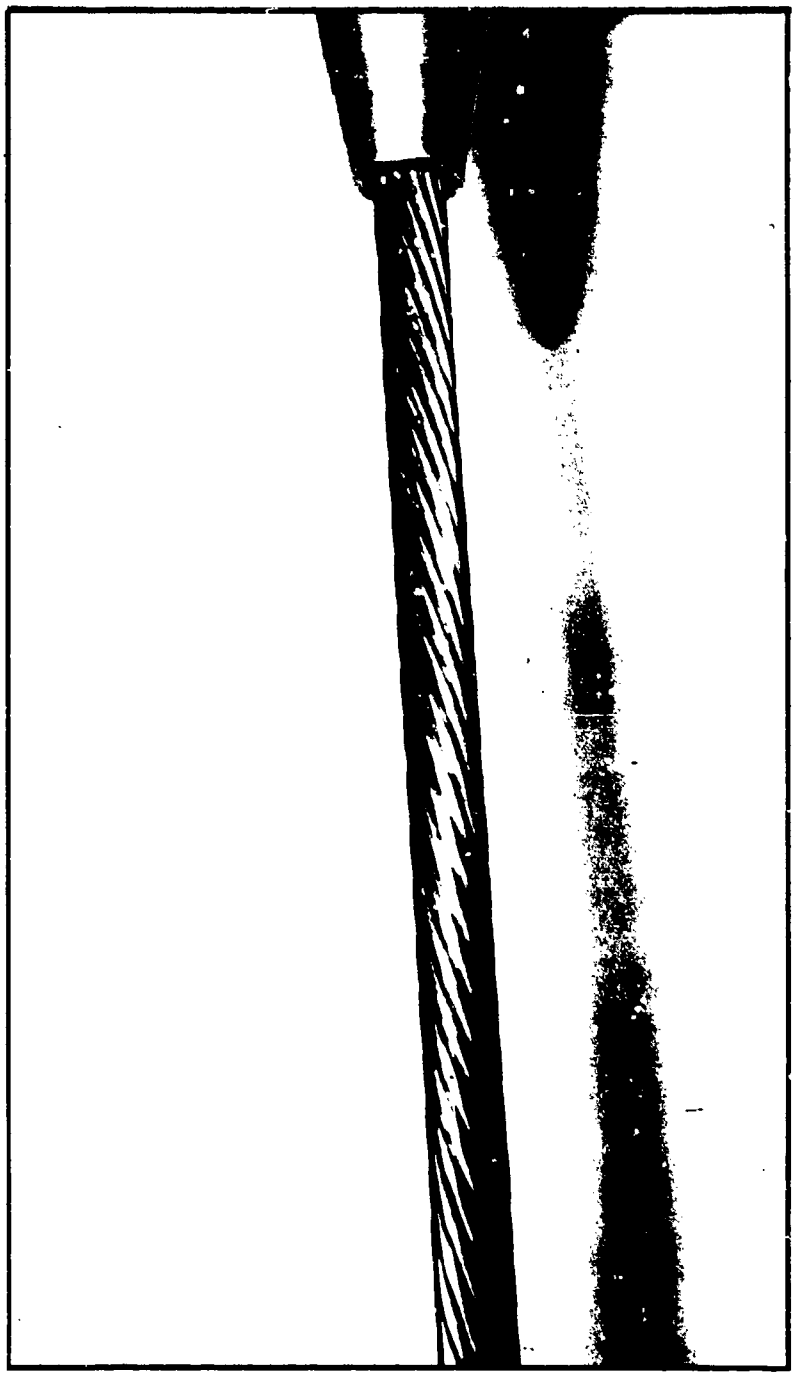

FIGURE 8. 1 x 19 CABLE MODEL

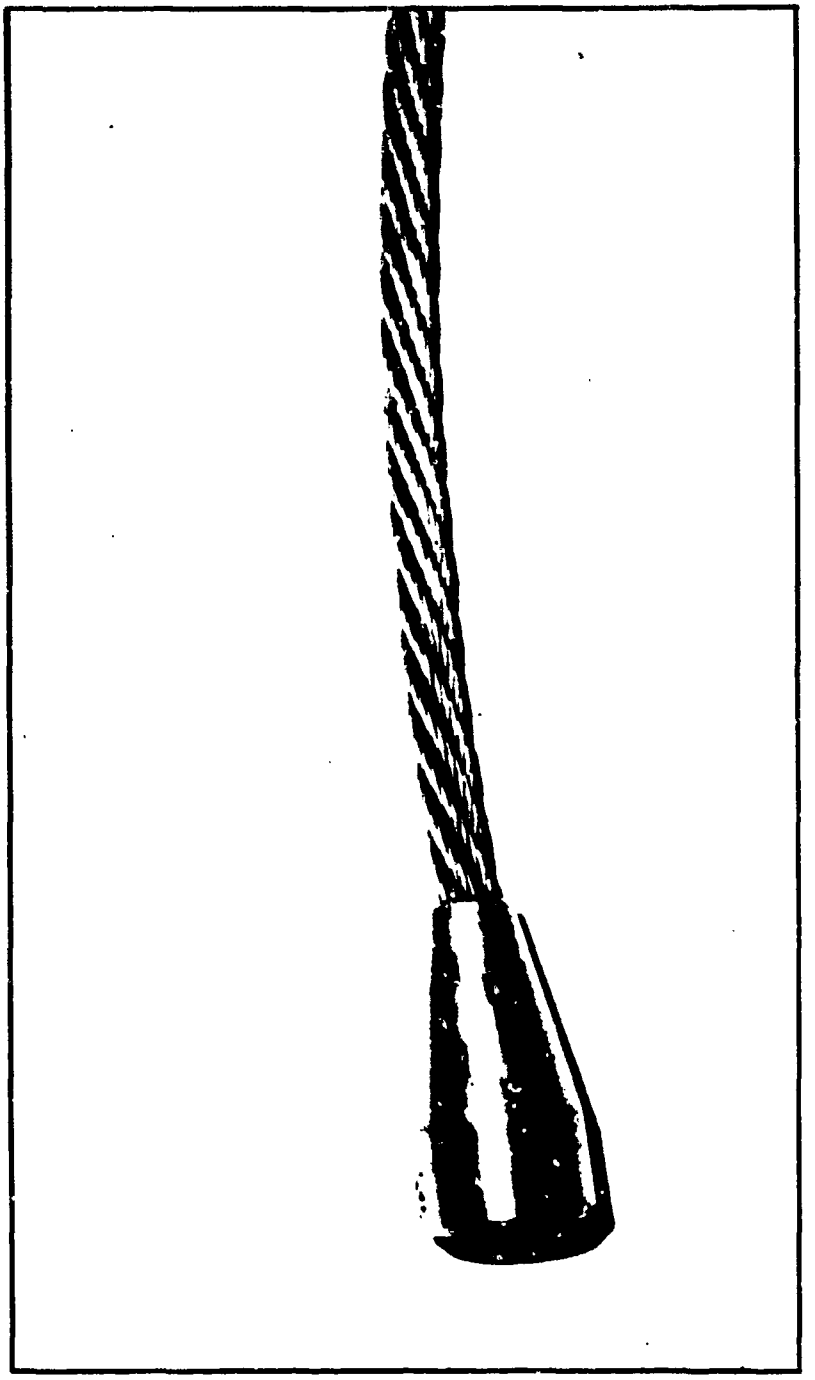

FIGURE 9. 7 x 7 CABLE MODEL

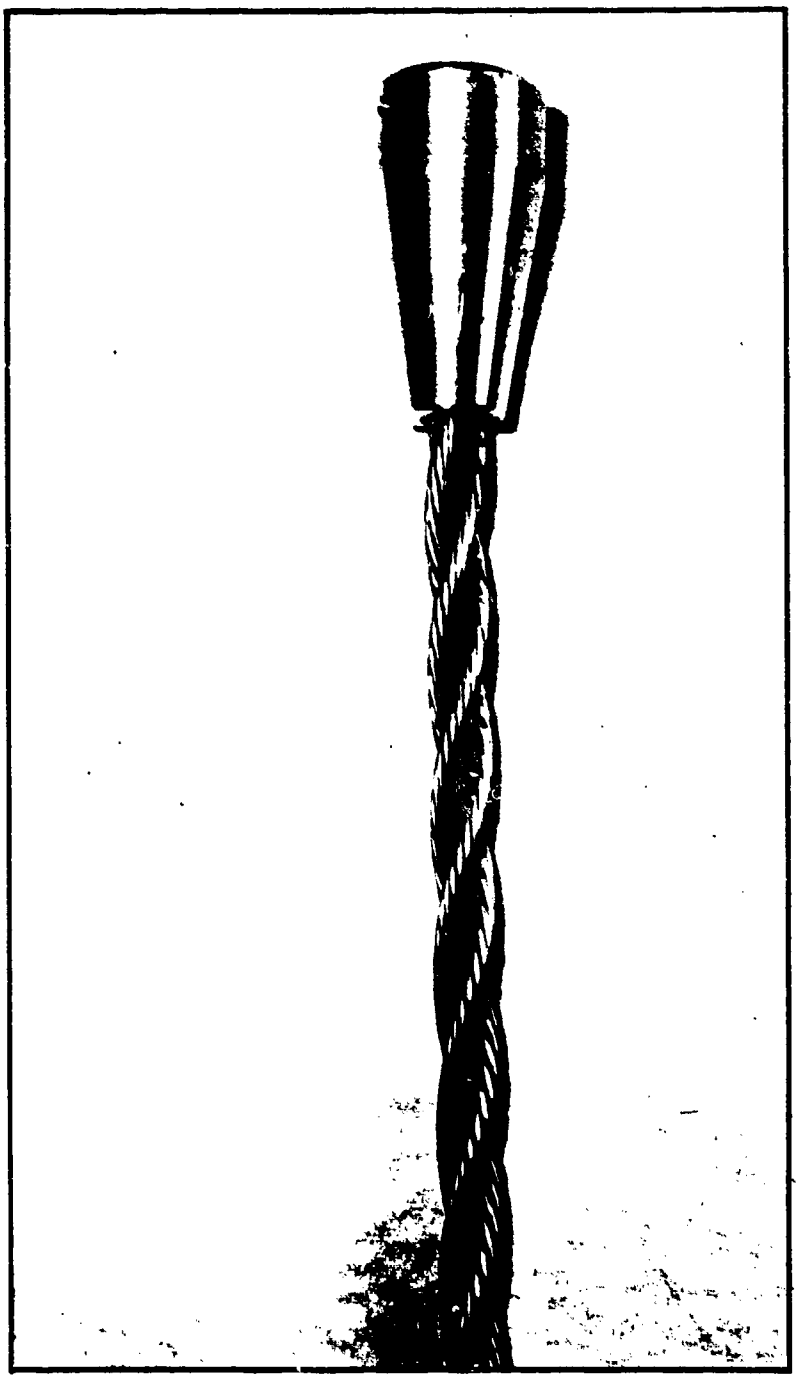

FIGURE 10. 3 x 19 CABLE MODEL

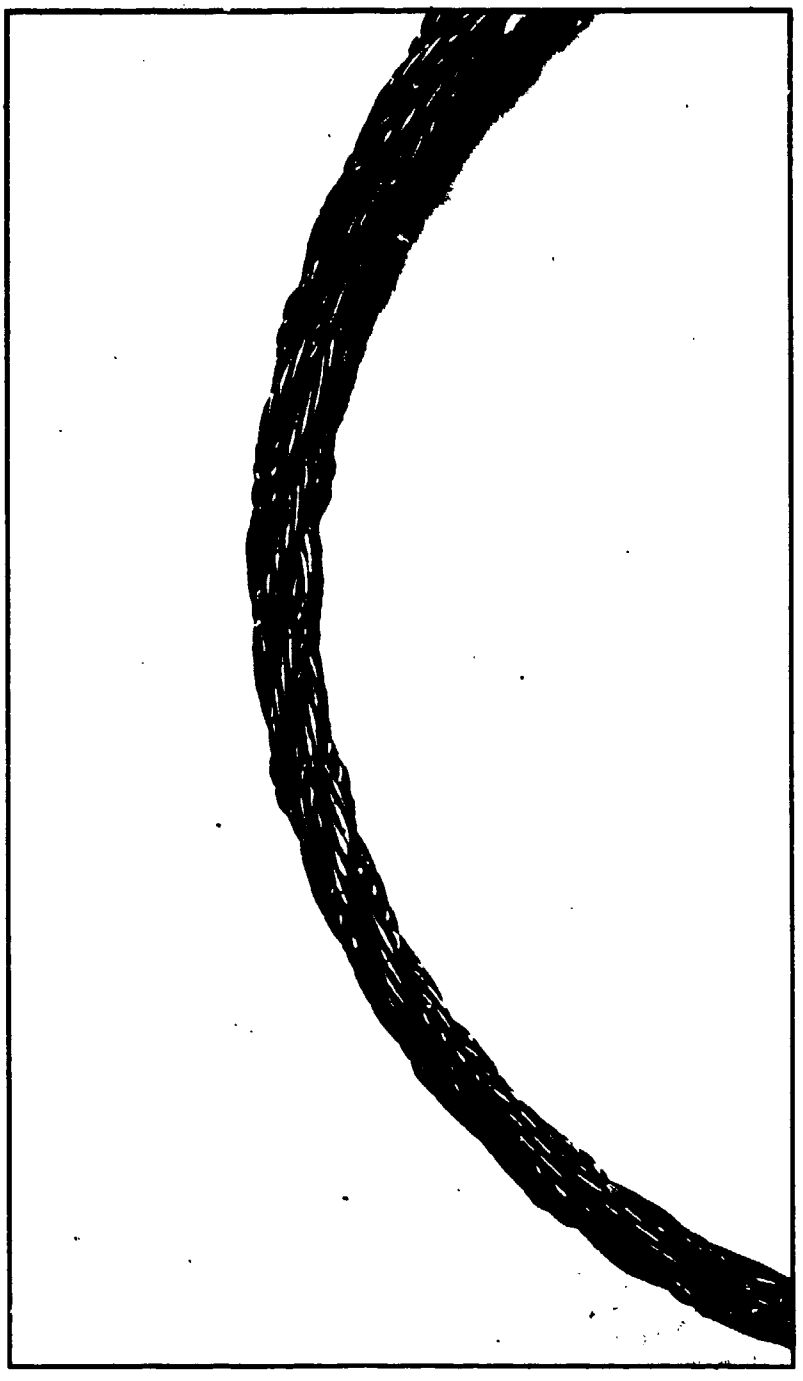

FIGURE 11. 4 x 7 SERRATED CABLE MODEL

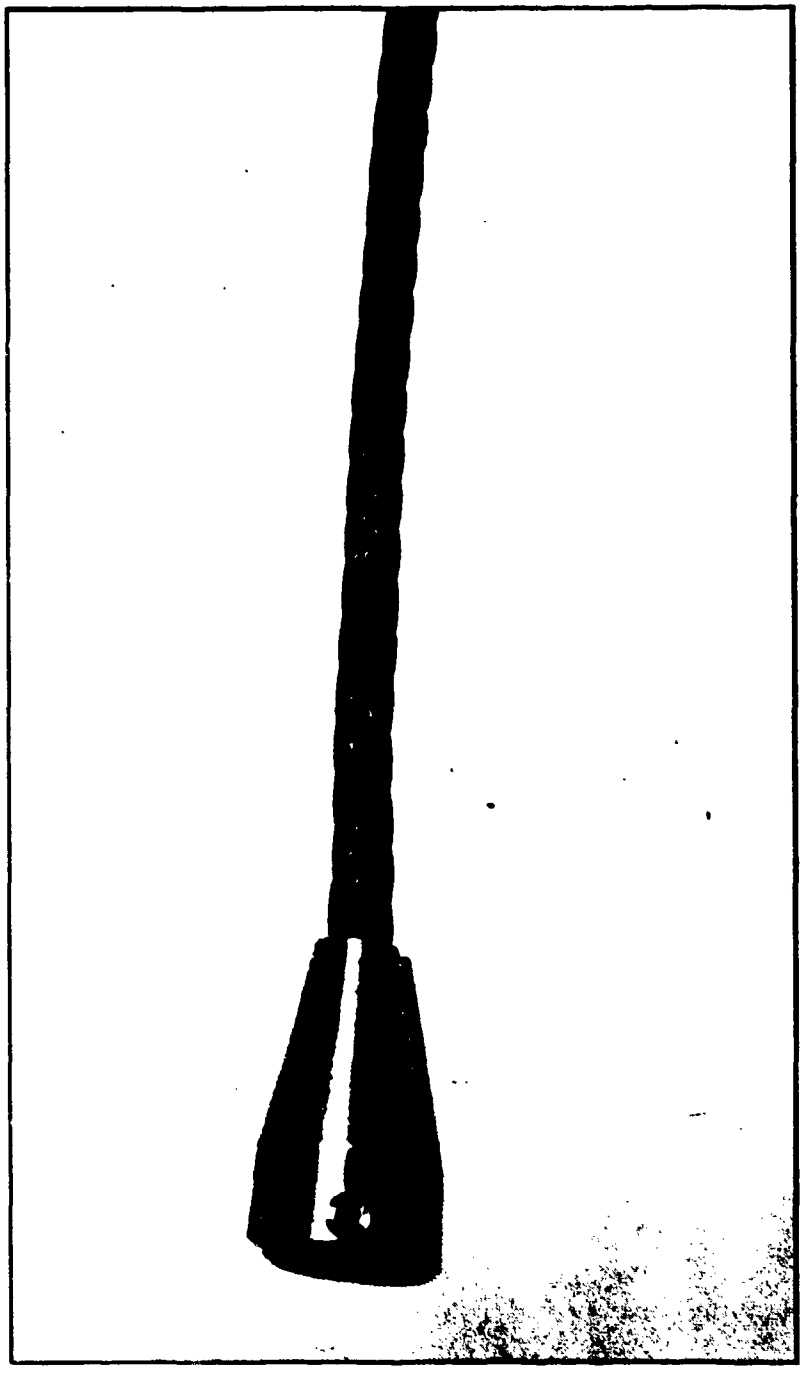

FIGURE 12. 6 x 25 LANG LAY CABLE MODEL

CABLE CONSTRUCTION	NOMINAL / ACTUAL DIAMETER (IN)	WEIGHT AIR/WATER (LB)	CABLE LAY
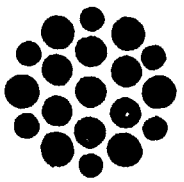 1 x 19	0.625/0.632	12.2/10.6	LEFT
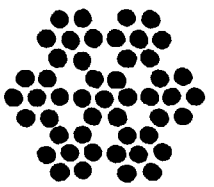 7 x 7	0.625/0.640	10.1/8.8	LEFT
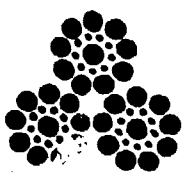 3 x 19	0.625/0.615	9.3/7.8	RIGHT
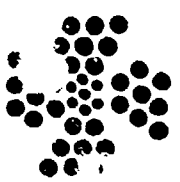 4 7 SERRATED	0.797/0.700	11.0/9.3	RIGHT
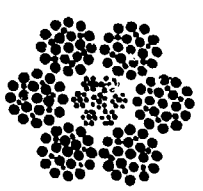 6 x 25 LANG LAY	0.625/0.625	10.6/8.9	RIGHT

FIGURE 13. SKETCH OF CABLE CROSS SECTIONS AND GEOMETRIC PROPERTIES

INSTRUMENTATION

The drag and lift forces, consisting of the steady and unsteady hydrodynamic forces exerted on the cable, were measured with a quartz force transducer, shown in Figure 14. Signal conditioning for the quartz force transducer or triaxial force gage was provided by three Kistler Model 504E Dual Mode Amplifiers. Long and short time constants were used for the steady and unsteady forces, respectively.

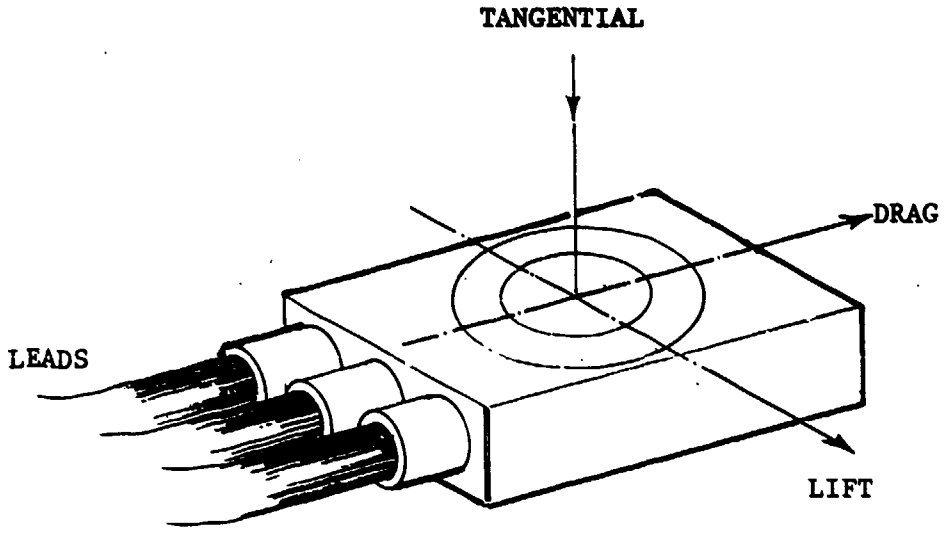

FIGURE 14. QUARTZ FORCE TRANSDUCER

The force transducer requires a high preload in the tangential direction to accurately measure forces in the lift and drag directions. The preload tension was measured with a strain gage ring dynamometer, and a control unit provided signal conditioning with a variable gain amplifier allowing readout in engineering units.

Acceleration of the cable model at midspan was measured in the drag and lift directions using Kistler accelerometers in conjunction with Kistler piexotron couplers which provided constant current excitation.

Table 2 provides a list of the various sensors used during the experiment. The range and accuracy of each device is also given.

TABLE 2

SENSOR DESCRIPTION AND ACCURACY

Sensor	Measurand	Model	Range	Accuracy
Magnetic Pickup	Carriage Velocity	N/A	N/A	±0.01 kt
Ring-Gage Dynamometer	Static Tension	TMB	0-500 lb	±0.5%
Accelerometer	Cable Accel. in Lift Direction	KISTLER 8616A500	500 g	±0.01 g
Accelerometer	Cable Accel. in Drag Direction	KISTLER 8616A500	500 g	±0.01 g
Steady: Unsteady Lift Force	Triaxial Force Gage	KISTLER 9251 SN Quartz Transducer	560 lb	±0.002 lb
Steady: Unsteady Drag Force	Triaxial Force Gage	KISTLER 9251 SN Quartz Transducer	560 lb	±0.002 lb
Steady: Unsteady Tangential Force	Triaxial Force Gage	KISTLER 9251 SN Quartz Transducer	1120 lb	±0.002 lb

All voltage signals from the sensors and signal condition units were recorded on an analog tape recorder, an Ampex Model FR1300, for post test data processing. Individual oscilloscopes, two strip chart recorders, and a spectral analyzer were used to monitor signals from the accelerometers and force gages to insure that they were functioning correctly. The two strip chart recorders, a six-channel Brush Model 260 and an eight-channel Brush Model 2800, were used to record time histories. The spectral analyzer, a Spectral Dynamics Model SD380 digital, two-channel signal analyzer, was used to obtain frequency spectra from the two accelerometers during the experiment and was used for analyzing the triaxial force gage data during the post test analysis. The accelerometer spectra were stored on the analyzer's micro floppy disk drive unit using 3.5-inch disks. A Hewlett Packard Model 7225B plotter was used for plotting the spectra.

TEST SETUP

Figure 15 shows a forward view of the cable model attached to the test rig. Both ends of the cable model were terminated to provide convenient attachment points for sensors and to prevent the cable from unraveling. The left end or downstream end of the cable model was attached to the strain gage ring dynamometer, contained in the strut housing. A 1/8-inch leader cable connected the cable model to the dynamometer through a pulley. Figure 16 shows a closeup view of the downstream end of the cable. The ring dynamometer was attached to a tensioning cylinder over a pulley by another 1/8-inch leader cable. A tensioning cylinder and nitrogen cartridge controlled the tension of the cable model. With a regulator, nitrogen was released from the cartridge to exert pressure on oil reservoirs in the tensioning cylinder. The tension on the cable model was increased or decreased by pressure relief valves.

The right end or upstream end of the cable model was attached to the triaxial force gage. The force gage lies within the strut housings. The signal transmission wires leading to the force gage were treated to be waterproof. Figure 17 shows a closeup view of the upstream end of the cable model.

Two accelerometer pairs were initially placed 6 feet and 7 feet from the upstream end. Accelerometer positions were chosen to provide sufficient information at even and odd modes not greater than 30 and to capture the peak displacement at these modes. Due to failure of one accelerometer pair during initial setup runs only one pair of accelerometers was used and was placed at the middle of the cable model. The wires leading to the accelerometers ran through struts covered with Fathom snap-on fairing. Figure 18 shows a closeup view of the accelerometers attached to the cable model and the snap-on fairing.

DATA ANALYSIS AND RESULTS

Data from the triaxial force gage and accelerometers were analyzed for each cable for hydrodynamic force and strum properties. Normal drag and lift loading functions were developed from the force data for each cable. The accelerometer data were used to determine strum amplitudes and frequencies.

A right-hand coordinate system, shown in Figure 19, is used throughout the analysis. The x- and z-axes define the cable-flow plane with the x-axis normal to the cable and the z-axis along the cable. The positive axes correspond to the normal and tangential drag directions. The y-axis lies transverse to the x- and z-axes according to the right-hand rule. Beta, β, is defined to be the angle between the z-axis and the relative flow velocity.

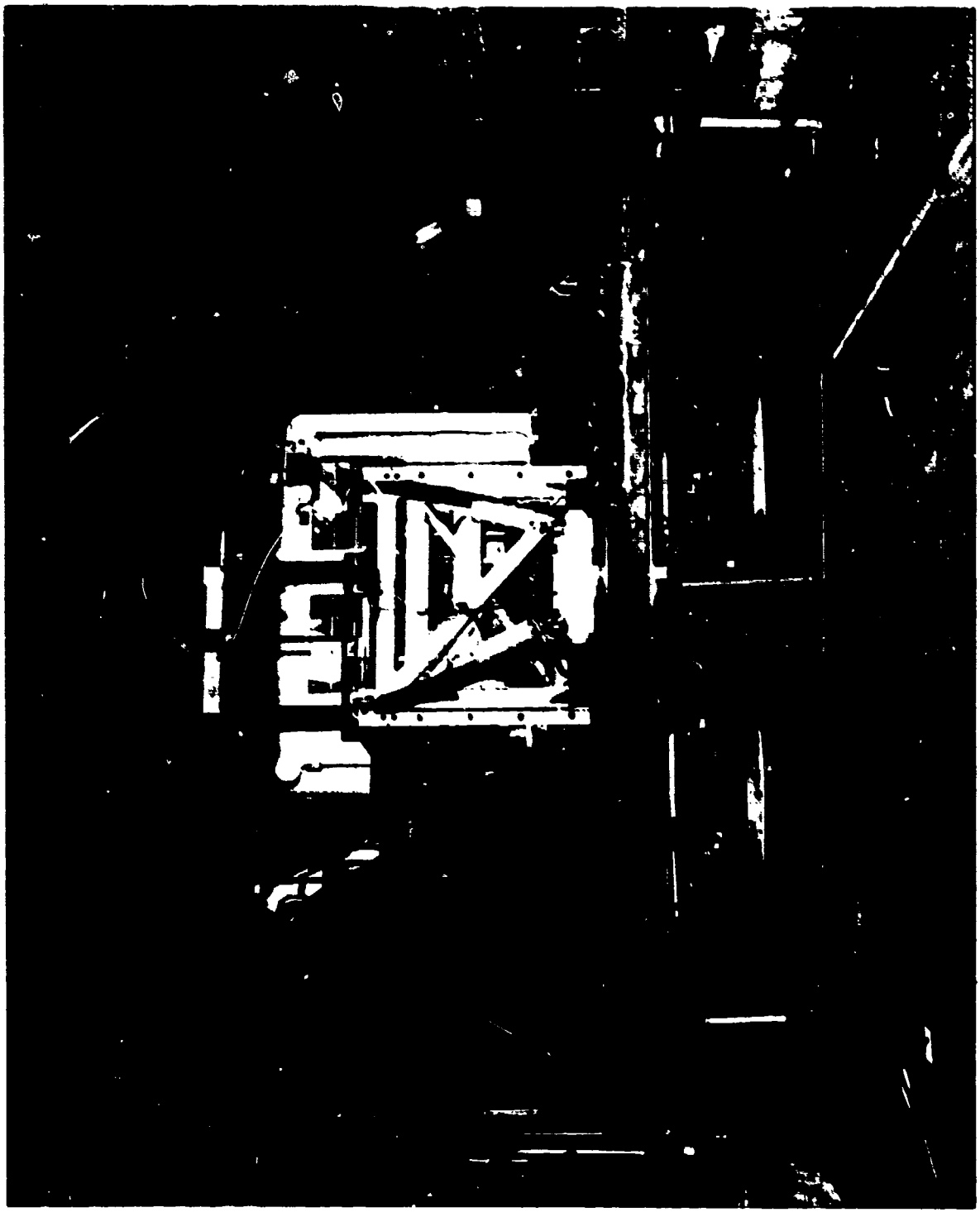

FIGURE 15. FORWARD VIEW OF DTNSRDC TEST RIG

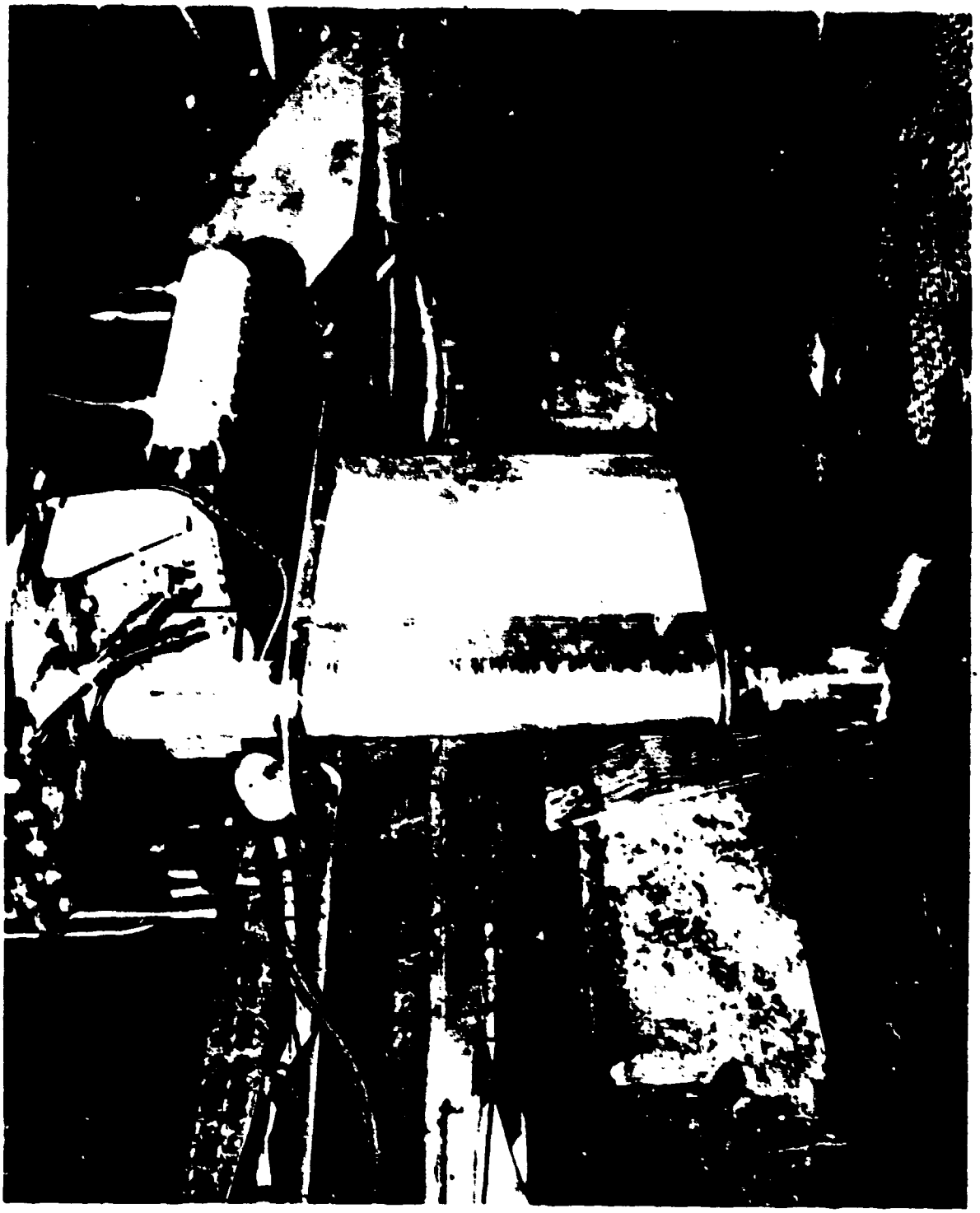

FIGURE 16. DOWNSTREAM END OF TEST RIG

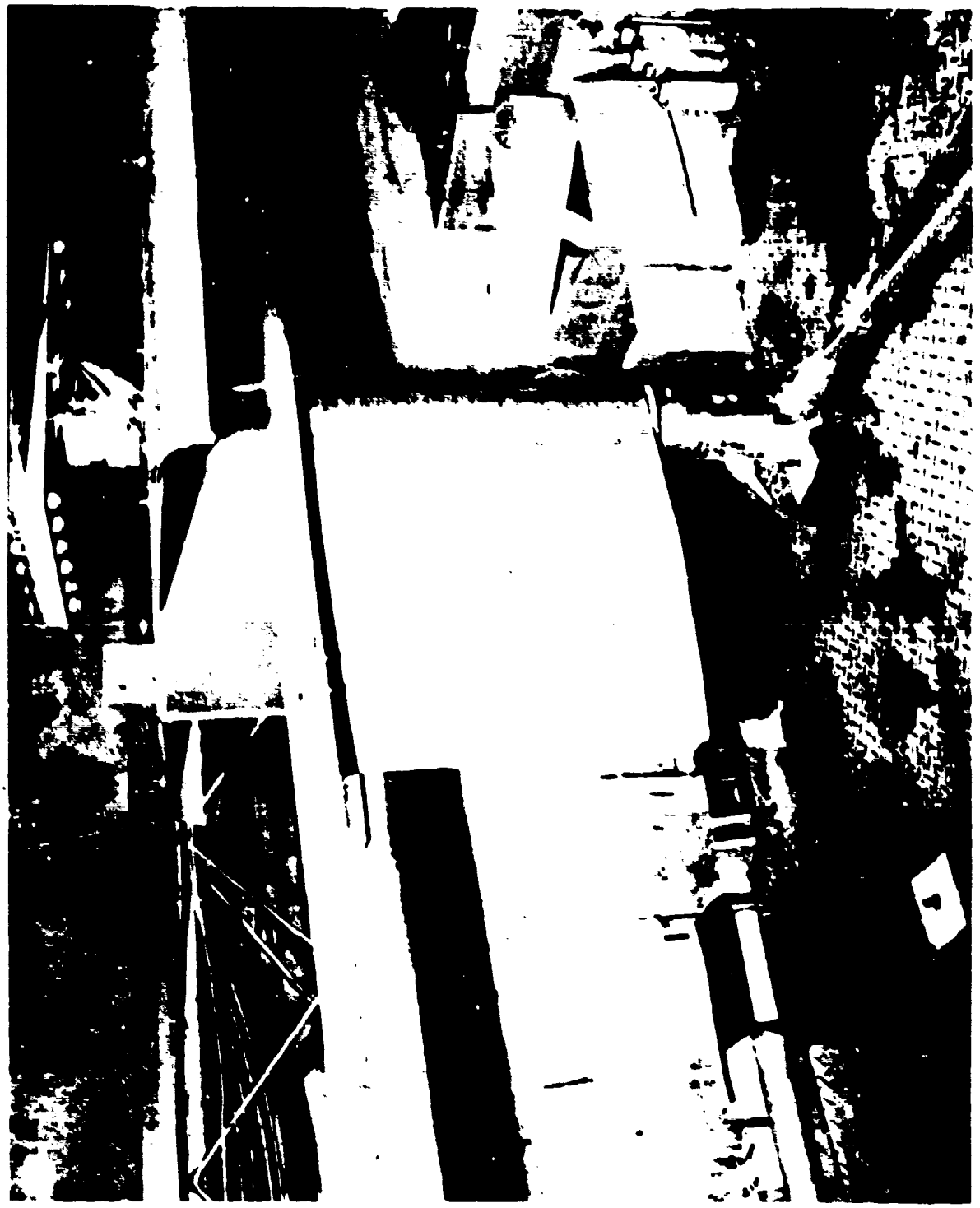

FIGURE 17. UPSTREAM END OF TEST RIG

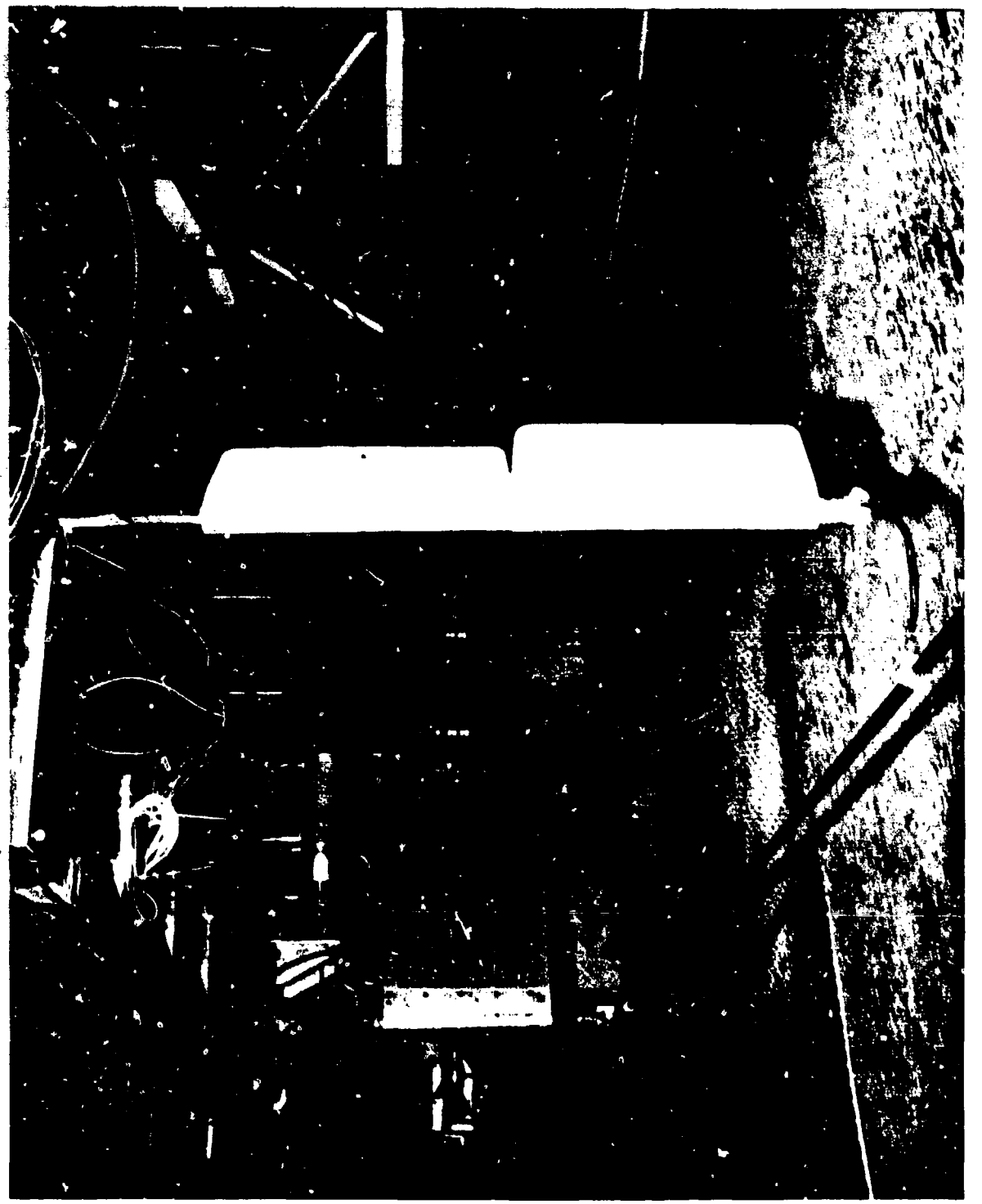

FIGURE 18. ACCELEROMETERS AND SNAP-ON FAIRING

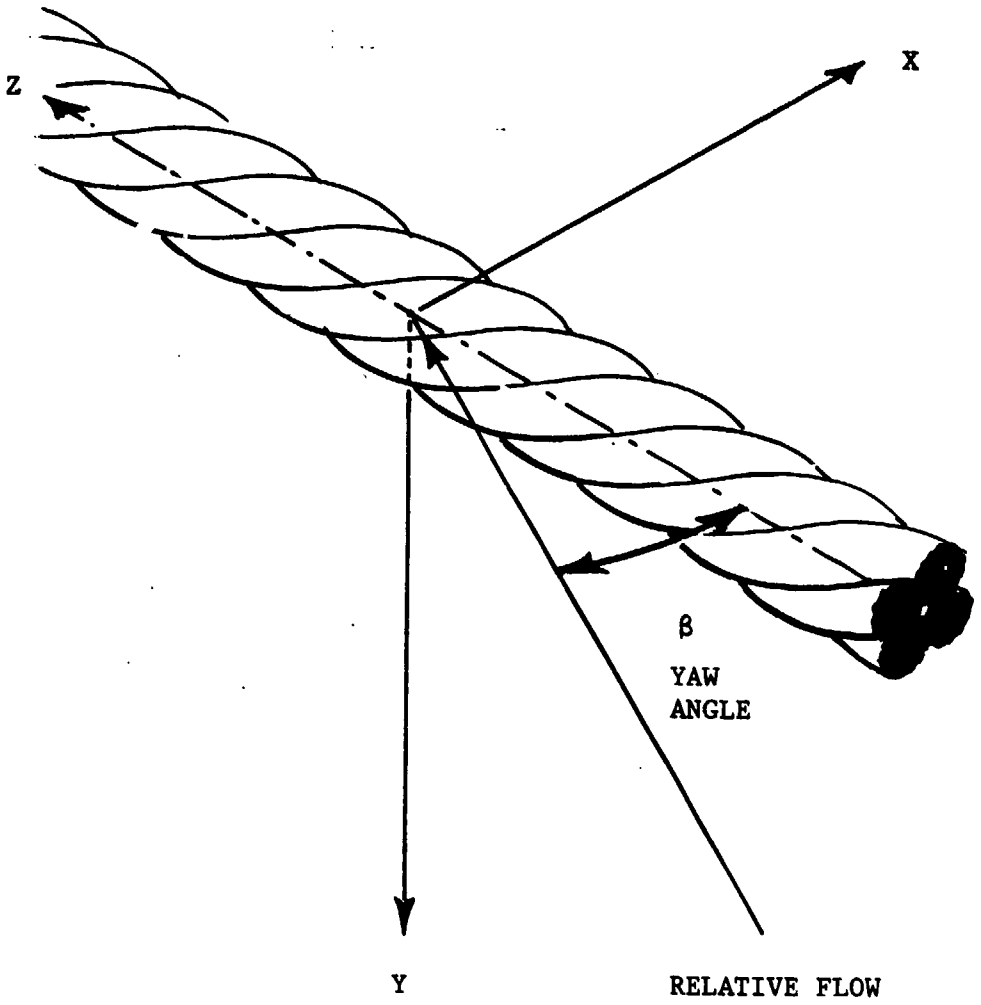

FIGURE 19. COORDINATE SYSTEM

For this test setup, all data reduction has been completed as if the coordinate system described in Figure 19 were applied to a left lay cable. From previous tests and tow experience it has been shown that the drag forces developed on right and left lay cables are equivalent at the same yaw angles.[1,2] The lift force developed on a right lay cable over the angle range $0° < \beta < 90°$ is equivalent to that developed by a left lay cable except the direction of the lift vector is reversed. All lift force data tabulated in Appendix B are listed as positive forces regardless of the lay of the corresponding cable tested. The reader who chooses to use the loading functions developed for system design must take care to insure the correct sign is attached to the lift loading function depending on whether the design cable is right or left lay.

LOADING FUNCTIONS

Hydrodynamic loading functions describe the variations in loading on a cable inclined to the flow and provide input parameters for computing tow cable catenaries. Present computer programs generally accept the loading function terms in nondimensional form; therefore, the terms are normalized by either the force per unit length for $\beta = 90$ degrees or the maximum force per unit length. The expressions for the normalized terms in the normal, tangential, and lift force directions are:

$$f_N = \frac{F_N(\beta, Re)}{R(Re)} \tag{8}$$

$$f_T = \frac{F_T(\beta, Re)}{R(Re)} \tag{9}$$

$$f_L = \frac{F_L(\beta, Re)}{F'_L(Re)} \tag{10}$$

where f_N is the normal force per unit length, f_T is the tangential force per unit length, f_L is the lift force per unit length, R is the normal force per unit length for $\beta = 90$ degrees, F'_L is the maximum lift force per unit length, Re is the Reynolds number based on diameter, and β is the cable yaw angle.

As seen from the above equations the actual forces acting on the cables are both Reynolds number and yaw angle dependent. However, the normalized terms for a particular cable at a single speed are dependent on yaw angle only and can be represented by a trigonometric series of the form (3):

---

[1] op. cit.

[2] op. cit.

$$f(\beta) = A_o + \sum_{n=1}^{\infty} \{A_n \cos(\beta) + B_n \sin(\beta)\} \quad . \qquad (11)$$

The first two terms of the series are typically used to describe the cable loading:

$$f(\beta) = A_o + A_1 \cos(\beta) + B_1 \sin(\beta) + A_2 \cos(2\beta) + B_2 \sin(2\beta) \quad . \qquad (12)$$

When normalized force data over several speeds are used to determine a loading function for a cable, any Reynolds number effects on the forces have been averaged and are therefore not explicitly accounted for. The data analysis provided the coefficients for this expression for the 1 x 19, 7 x 7, 3 x 19, and 4 x 7 models for normal drag and lift force. The data for the 6 x 25 lang lay model were limited to three yaw angles (β = 30, 60, 90°) and, therefore, the 6 x 25 model is not included in the analysis.

Normal Drag Loading Functions

The dynamic normal drag forces were measured with the triaxial force gage. The steady drag forces were determined from the long time constant data. The data were reproduced through an averaging voltmeter to obtain the average direct current (dc) voltage for each force direction. The average voltage was multiplied by the calibration constant for each direction, resulting in dimensional force values in pounds. The measured drag at one end of the cable was assumed to be one-half the total drag. For the 1 x 19 and 3 x 19 cable models the unsteady drag forces were determined in the same fashion as the steady forces except the short time constant data was used from the force gage. A comparison of the mean unsteady to steady drag forces for these cable models reveals the unsteady to steady force ratio of 1:20. Thus, the measured unsteady drag forces are a small percentage of the mean steady drag forces.

Dimensional normal drag data for each cable model are shown in Figure 20 for the full range of angles, speeds, and tensions. The normal force per unit length is plotted as a function of yaw angle for the four cable models. Data for the two tensions show that the normal drag forces are not affected by tension. Each cable model develops a maximum load of about 20 pounds per foot near β = 90 degrees for the highest speed, V = 10 knots. This corresponds to a total normal drag of 280 pounds acting on the 14-foot cable model. The average total normal forces at 90 degrees for each speed, which are used to normalize the forces to obtain loading functions, are listed in Table 3.

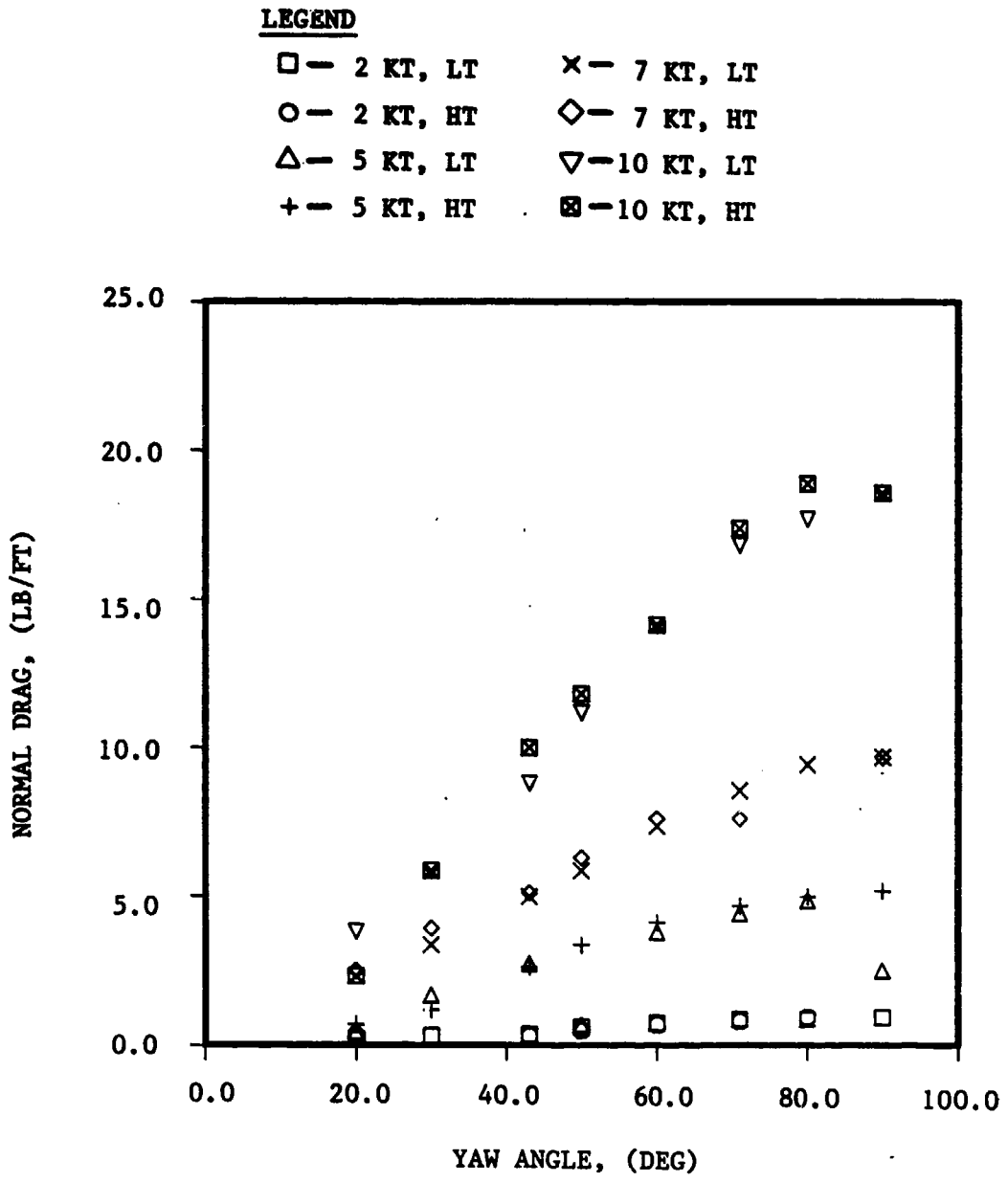

FIGURE 20(a). MEASURED NORMAL DRAG VERSUS CABLE YAW ANGLE
1 x 19 CABLE (Sheet 1 of 4)

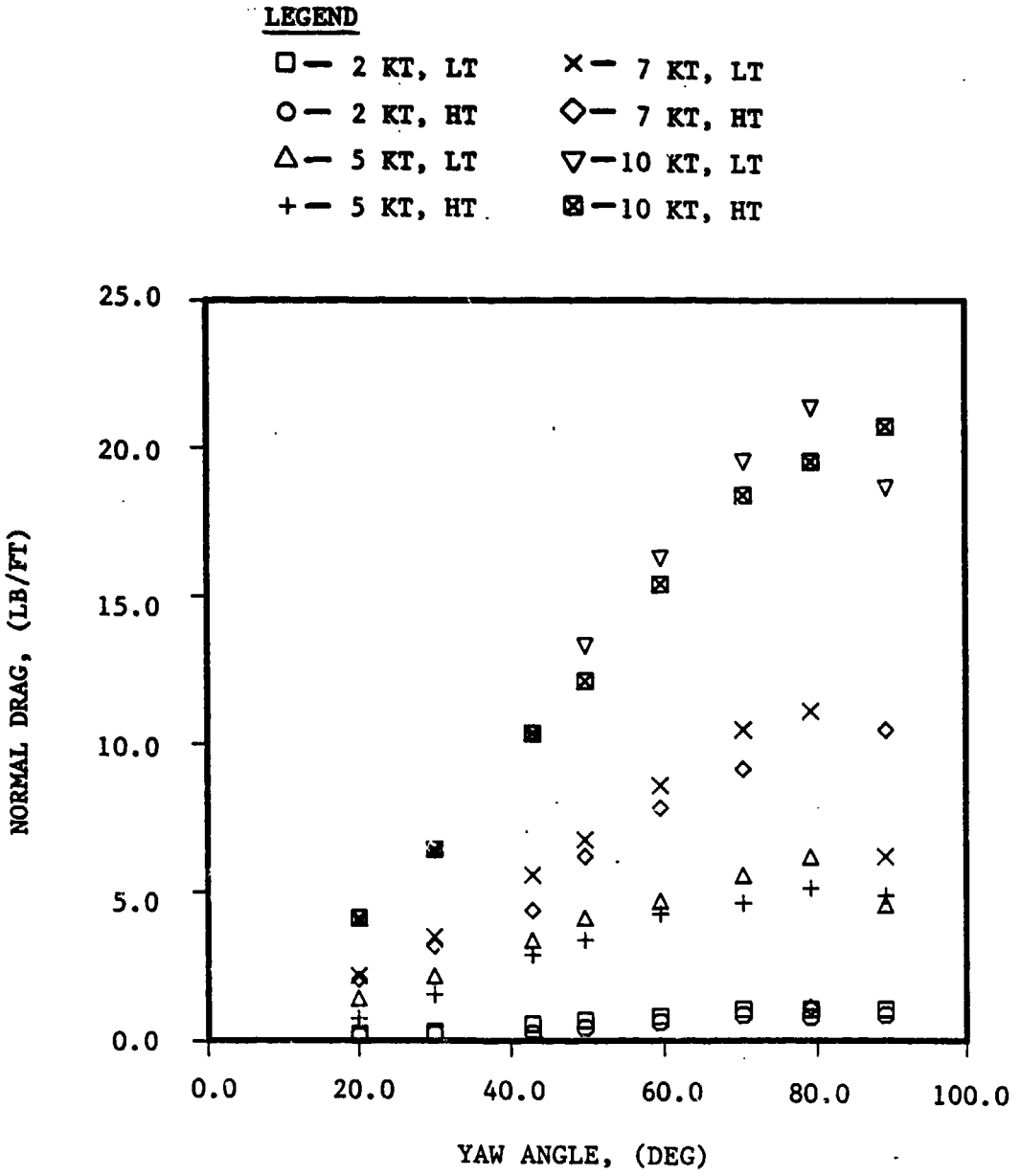

FIGURE 20(b). 7 x 7 CABLE (Sheet 2 of 4)

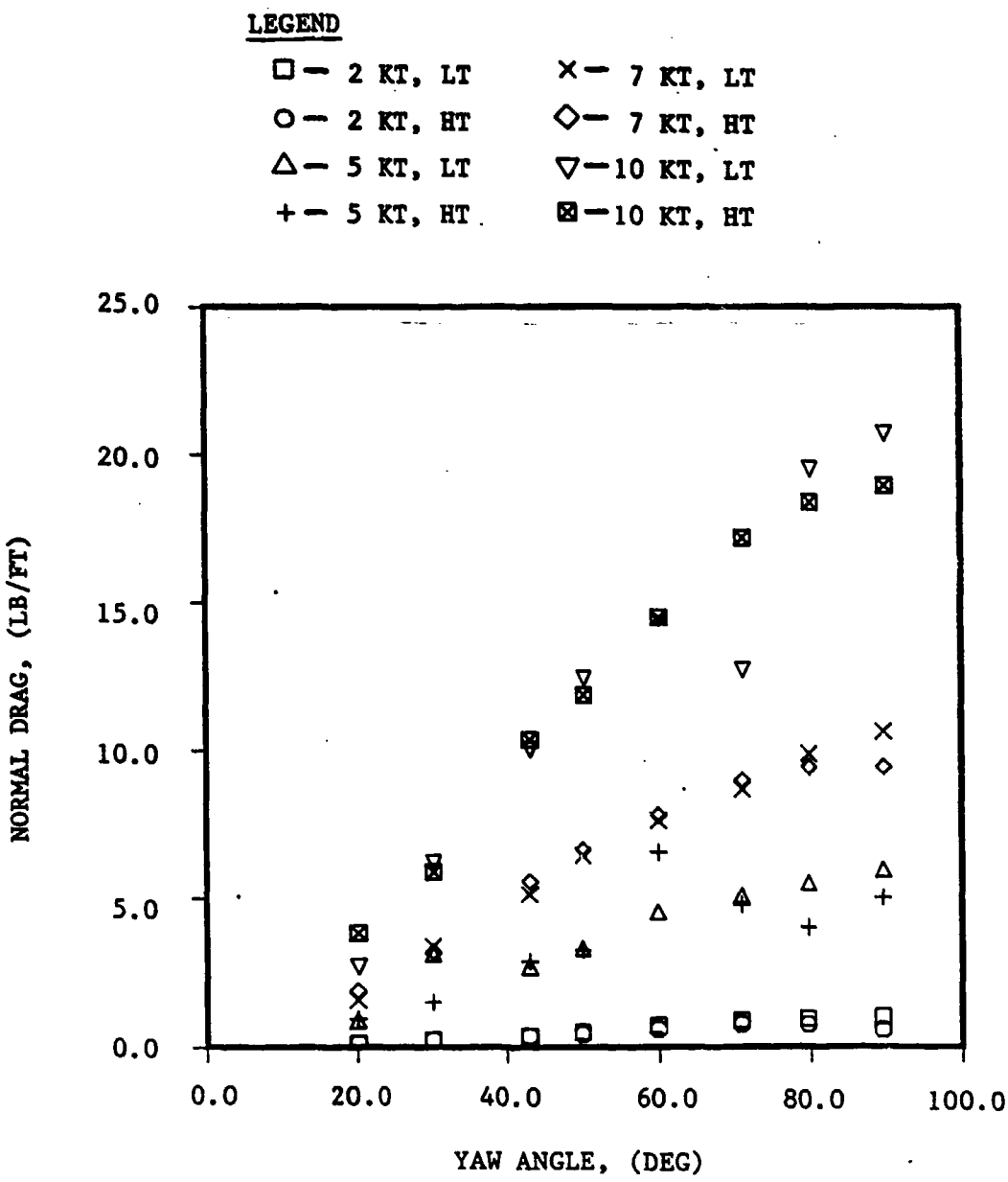

FIGURE 20(c). 3 x 19 CABLE (Sheet 3 of 4)

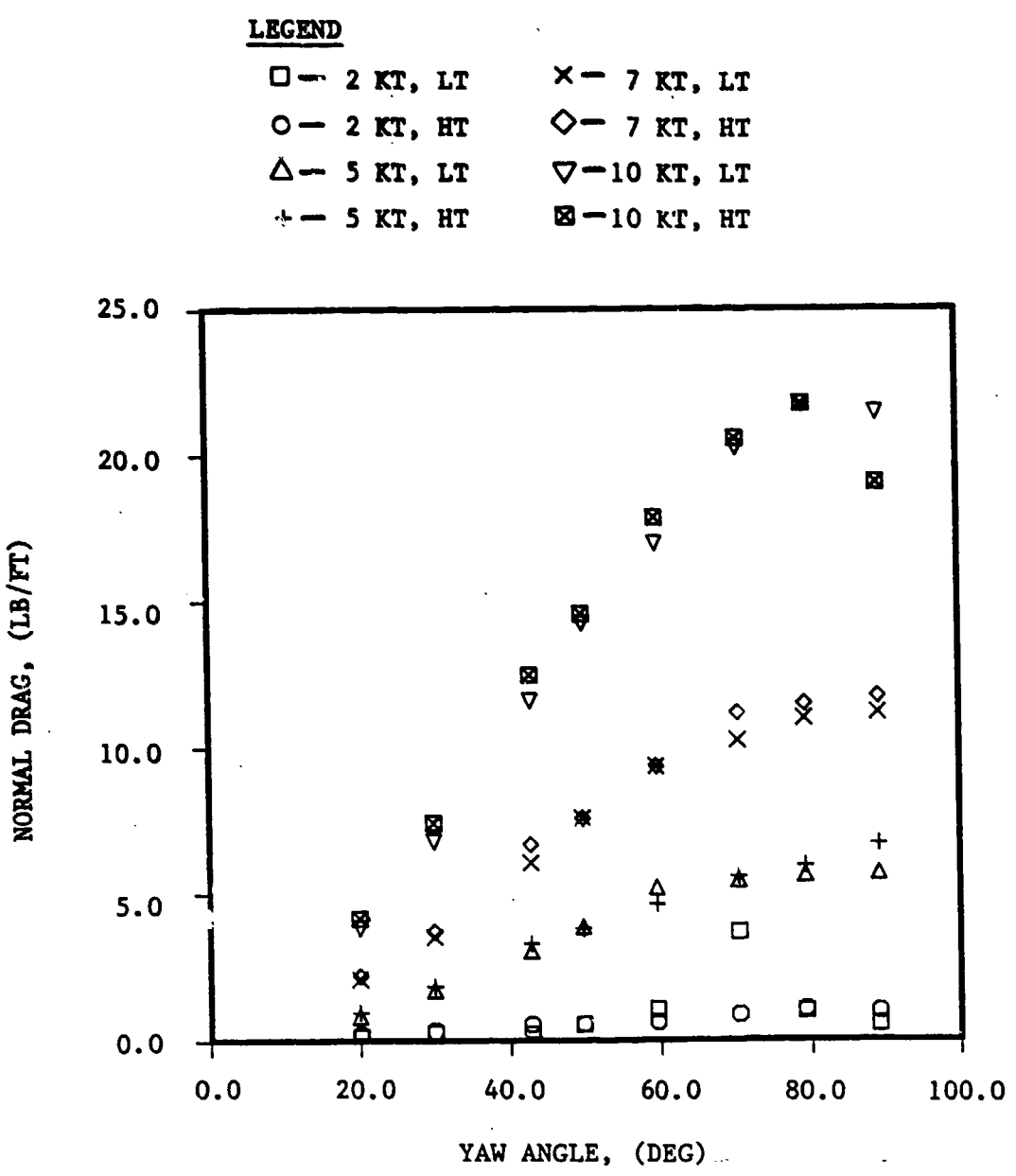

FIGURE 20 . 4 x 7 CABLE (Sheet 4 of 4)

TABLE 3

AVERAGE NORMAL FORCE PER UNIT LENGTH AT 90 DEGREES FOR THE FOUR CABLE MODELS

Cable Model	Speed (kt)			
	2	5	7	10
1 x 19	0.94	5.14	9.72	18.73
7 x 7	0.95	4.72	8.17	19.62
3 x 19	0.85	5.54	10.02	19.77
4 x 7	0.75	6.13	11.35	20.06

The drag is nondimensionalized into the form of a drag coefficient, C_d. The drag coefficient is a function of Reynolds number. The expressions for drag coefficient and Reynolds number are as follows:

$$C_d = \frac{R}{\frac{1}{2} \rho V^2 D}$$

$$Re = \frac{V D}{\nu}$$

where R is the normal drag per unit length, ρ is the fluid density, V is the freestream velocity, D is the cable diameter, and ν is the kinematic fluid viscosity.

Figure 21 shows C_d for the cable model perpendicular to the flow, β = 90 degrees, as a function of Re for all cable models (including the 6 x 25), for both the low and high tension cases. The combined averaged data results in a drag coefficient of 1.46 over the range of Re evaluated. The data scatter is greatest at the lowest Reynolds number, $Re = 1.8 \times 10^4$. For increasing Reynolds number the drag data are more closely grouped together. Previous measurements for cables and cylinders with surface roughness show a drop in the magnitude of the drag coefficient with increasing Re.[4] [11] This is caused by transition

[4] op. cit.

[11] Hoerner Fluid Dynamics, Fluid Dynamic Drag, Brick Town, NJ, 1965.

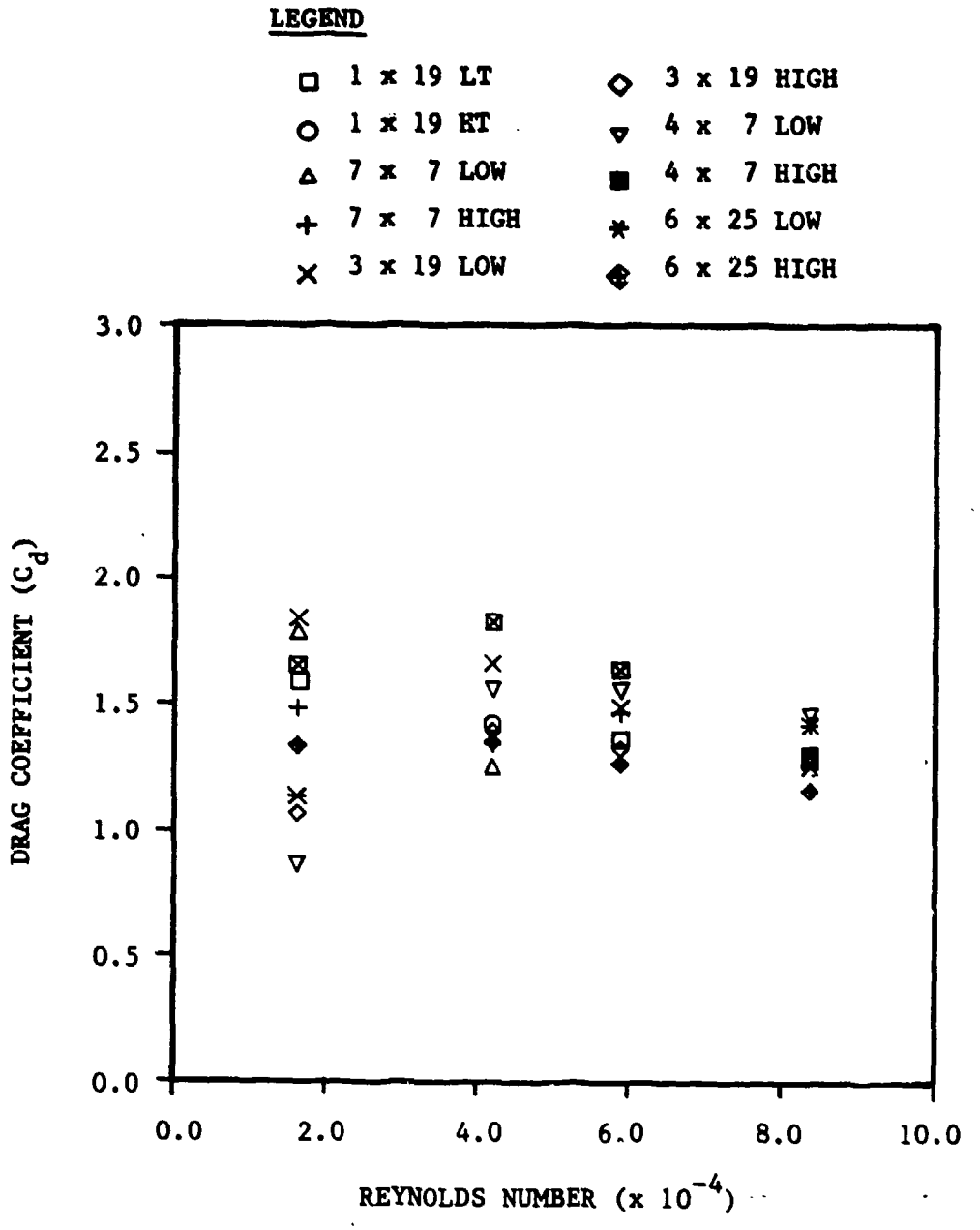

FIGURE 21. MEASURED DRAG COEFFICIENT VERSUS REYNOLDS NUMBER

of the boundary layer from laminar to turbulent. There is no evidence of transition in the drag data of Figure 21. The rough surface of the cable evidently maintains a turbulent boundary layer over the Reynolds number range considered.

Figure 22 shows the effects of yaw angle on the measured drag coefficients. Data for the four cable models and both tensions are plotted versus yaw angle for speeds of V = 2 and 10 knots. Comparing the results for the two speeds shows significantly more scatter in the 2-knot drag data throughout the range of yaw angles. At 10 knots the drag coefficients for the four cable models fall within a relatively narrow band width of $\Delta C_d = 0.25$, whereas for 2 knots the data are scattered over a range of $\Delta C_d = 0.5$. Cable geometry apparently has a more important effect on the magnitude of the drag coefficient at the lowest test speed. Unsteady cable strum effects, considered in a later section, may also contribute to the differences noted in the 2- and 10-knot data. Table 4 presents the average normal drag coefficients for each cable model evaluated.

TABLE 4

AVERAGE NORMAL DRAG COEFFICIENTS

Cable Model	Average Normal Drag Coefficient
1 x 19	1.43
7 x 7	1.44
3 x 19	1.44
4 x 7 Serrated	1.58
6 x 25 Lang Lay	1.30

The drag coefficients shown in Figure 22 are based on the total freestream velocity. Using the Independence Principle the normal drag coefficient, C_{dn}, is defined using the normal velocity component, V sin (β), to give:

$$C_{dn} = \frac{C_d}{\sin^2(\beta)} .$$

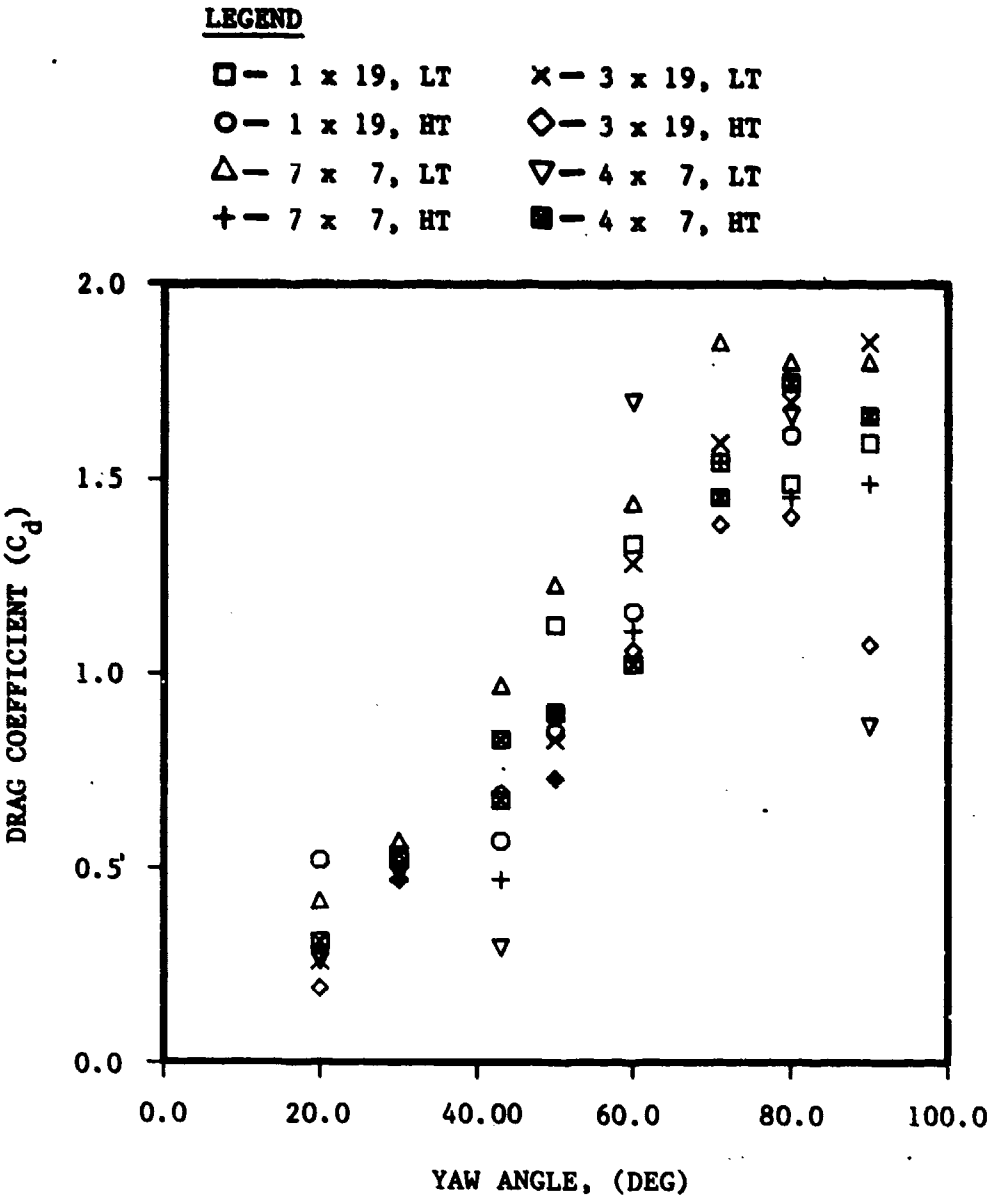

FIGURE 22(a). MEASURED DRAG COEFFICIENT VERSUS YAW ANGLE
V = 2 KNOTS (Sheet 1 of 2)

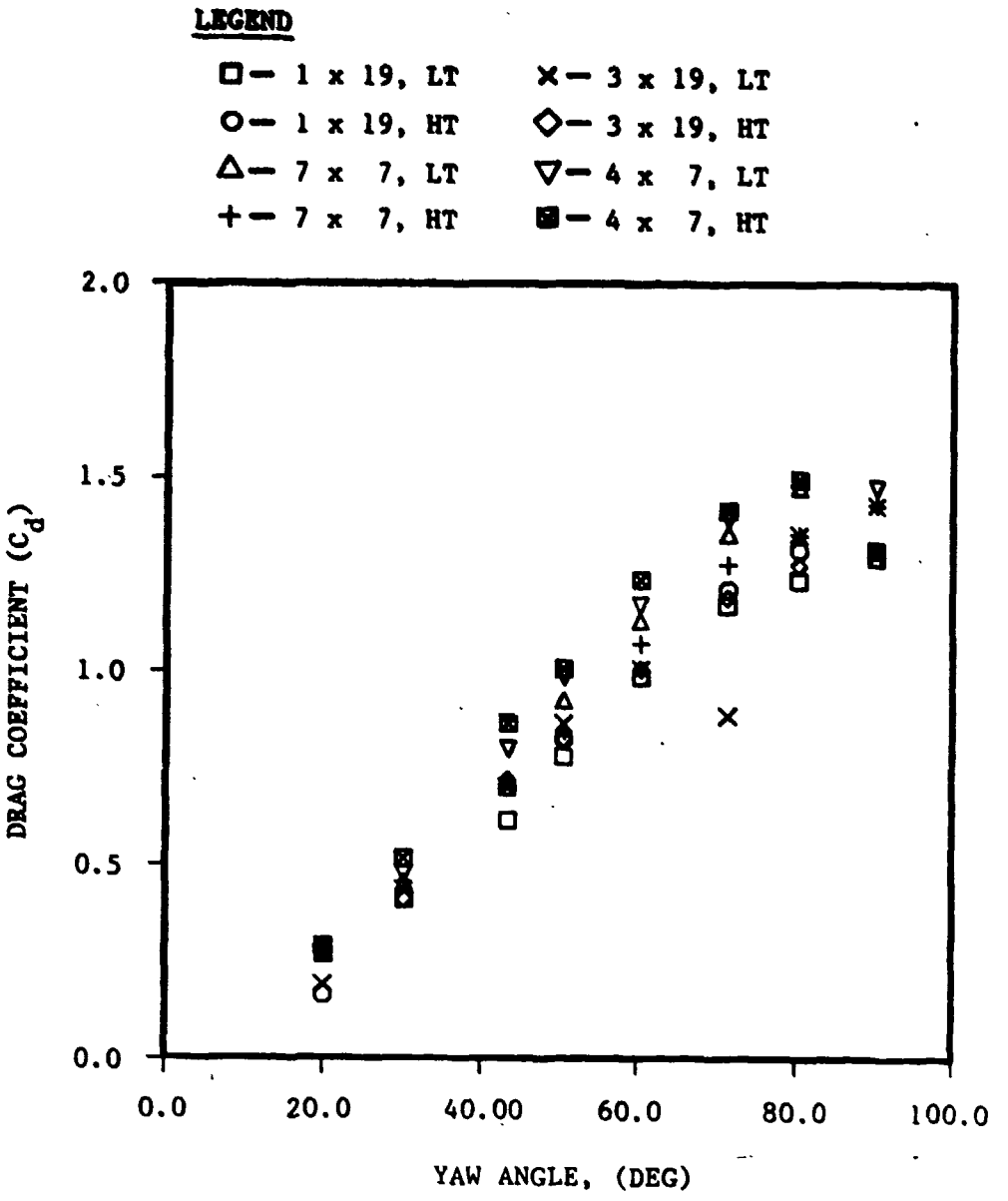

FIGURE 22(b). V = 10 KNOTS (Sheet 2 of 2)

Figure 23 shows the normal drag coefficient for each cable model as a function of the crossflow Reynolds number, $Re_n = V D \sin(\beta)/\nu$. The drag data are presented for the four test speeds at yaw angles of β = 50, 60, 71, 80, and 90 degrees. Data for angles lower than 50 degrees are excluded because the assumptions of the Independence Principle break down as the yaw angle becomes small. For each cable model shown in Figure 23 the normal drag coefficients are distributed in a manner similar to the drag data at β = 90 degrees in Figure 21. Values of C_{dn} for β = 50 to 90 degrees are roughly centered about the average drag coefficient of 1.46 derived for β = 90 degrees. The highest scatter in the data occurs at the lowest Reynolds number, and there is no drop in C_{dn} with increasing Re_n which would indicate boundary layer transition. Thus the results of Figure 23 shows that the drag coefficients based on the normal velocity component are constant for $50° < \beta < 90°$. The normal drag characteristics are independent of β over a wide range of yaw angles.

A least squares curve fit to the normalized forces was used to determine the coefficients of the loading functions of the form of Equation (12) using the boundary conditions $f_n(0) = 0$ and $f_n(90) = 1$.[12]

The low and high tension data were combined to obtain a single function for each cable model. The normal drag loading functions are shown in Figure 24. A "common" loading function is included which is the average of the four separate loading functions. Because the general shapes of the individual loading functions are similar, the common loading function is a good approximation for the normal drag of any of the four cable models. The loading functions shown in Figure 24 are similar to those developed from previous experiments.[3] The normal drag loading function coefficients are listed in Table 5.

The normal drag forces were normalized with the measured force at β = 90 degrees to obtain the coefficients. The maximum normal forces typically occur at 90 degrees; however, the 7 x 7 cable model shows coefficients in Figure 24(b) greater than 1.0 at angles between 80 and 90 degrees. This is caused by data scatter occurring in an area where the slope of the curve is approaching zero. Adding the boundary condition

$$\frac{df_n(\beta)}{d\beta} = 0 \text{ at } \beta = 90°$$

should correct the problem. This condition was not incorporated into the present effort.

---

[3]op. cit.

[12]Brogan, W. L., Modern Control Theory, Prentice-Hall, Inc./Quantum Publishers, Inc., NJ, 1982, pp. 90-92.

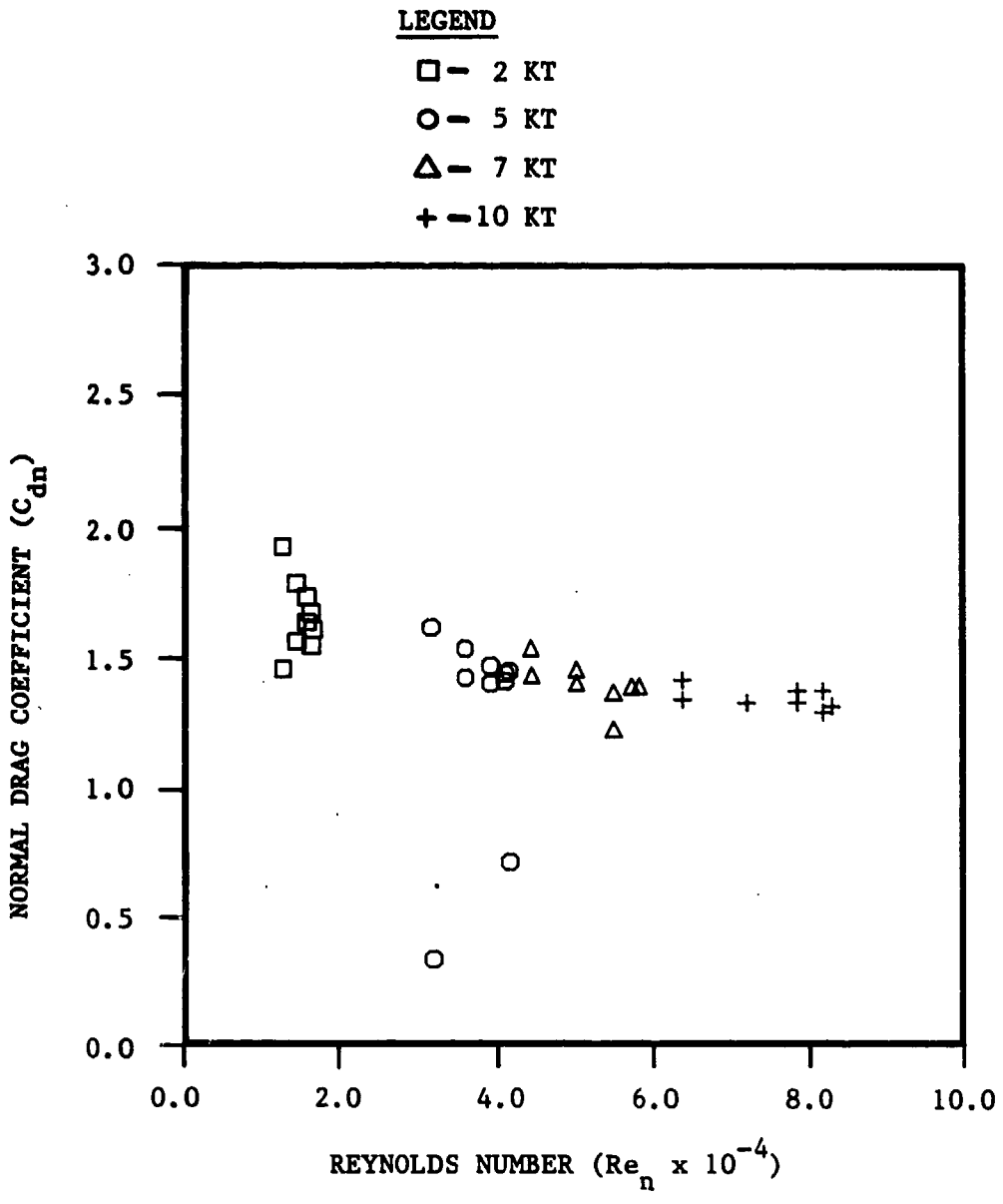

FIGURE 23(a). MEASURED NORMAL COEFFICIENT VERSUS CROSSFLOW REYNOLDS NUMBER - 1 x 19 CABLE (Sheet 1 of 4)

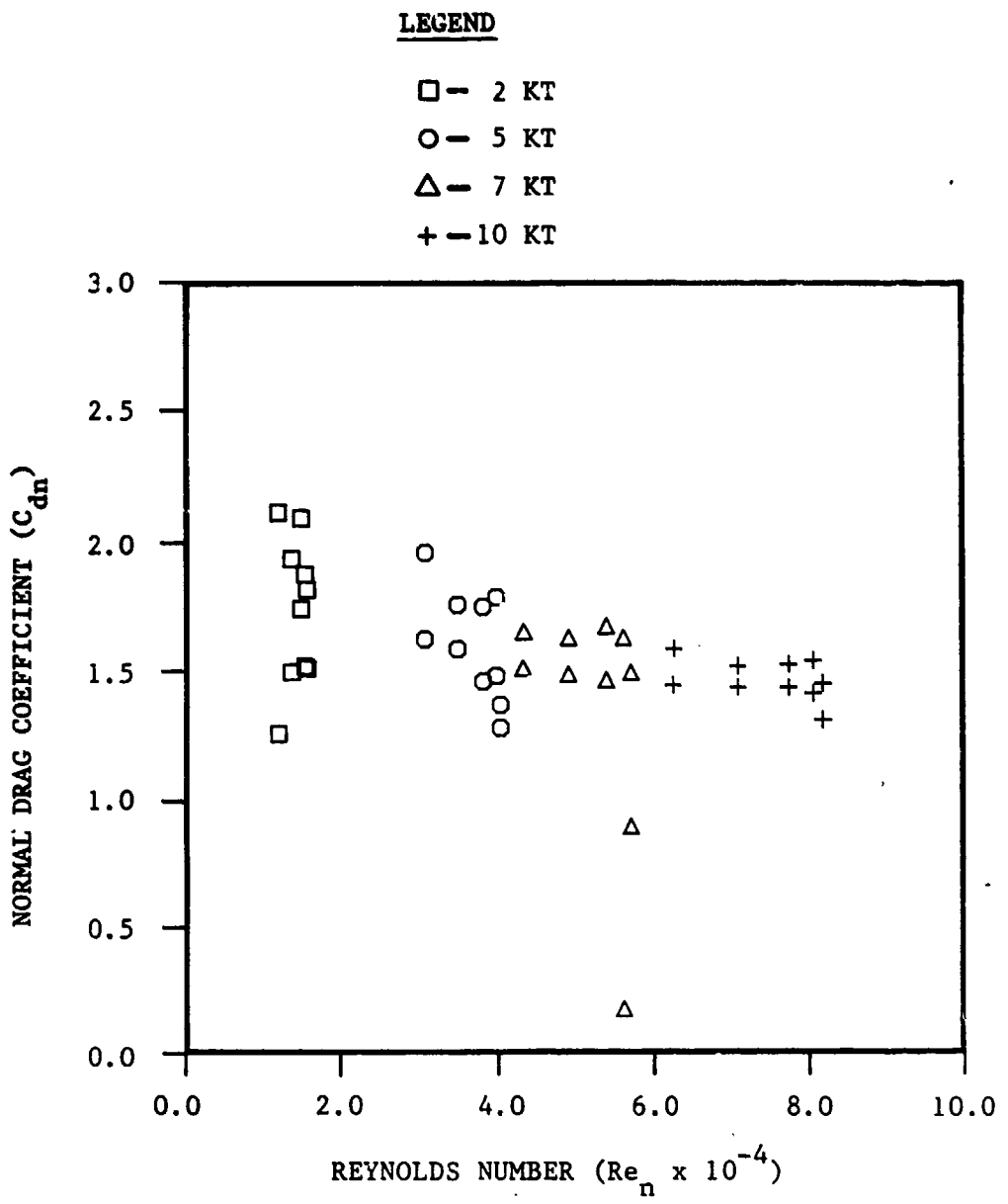

FIGURE 23(b). 7 x 7 CABLE (Sheet 2 of 4)

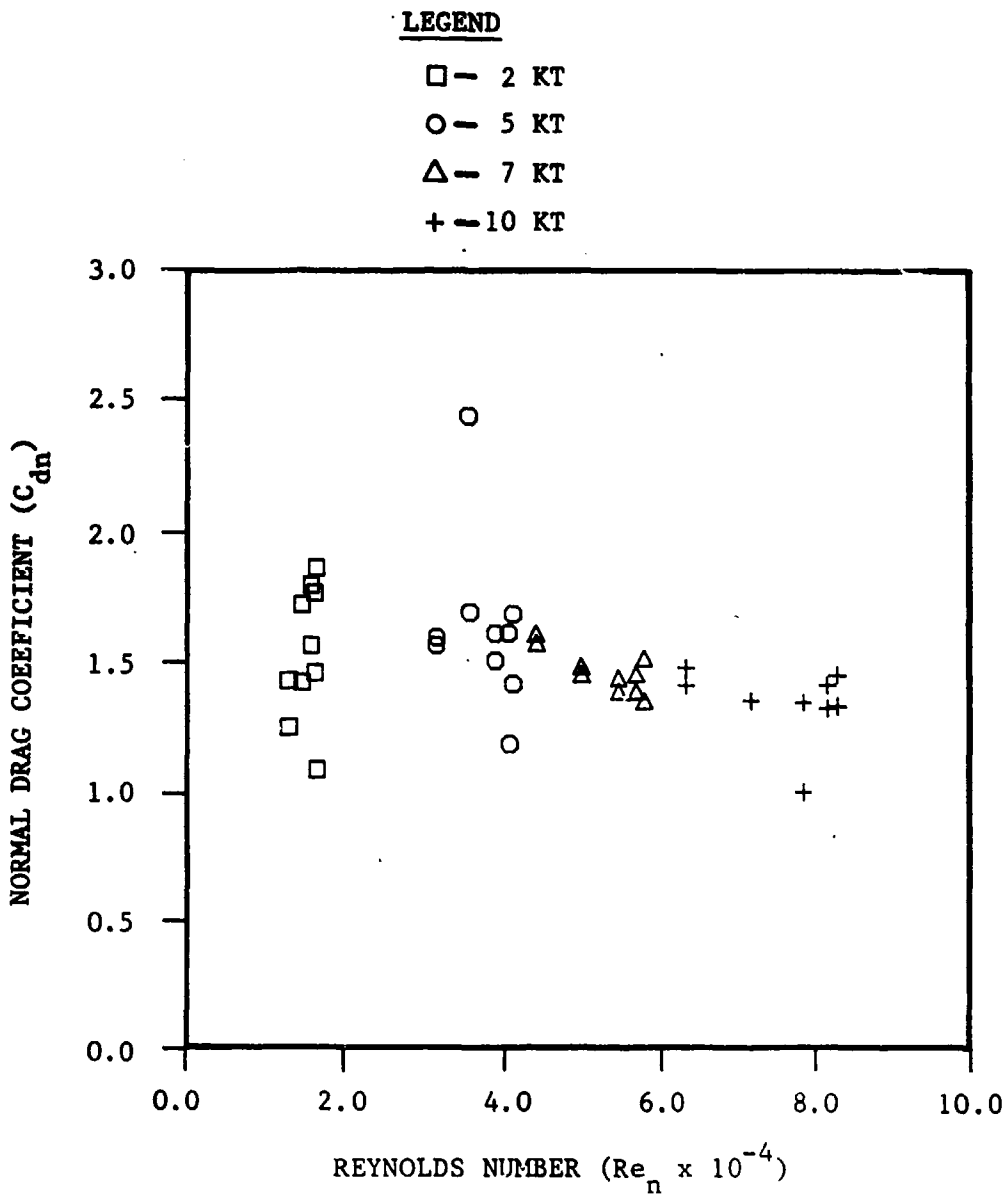

FIGURE 23(c). 3 x 19 CABLE (Sheet 3 of 4)

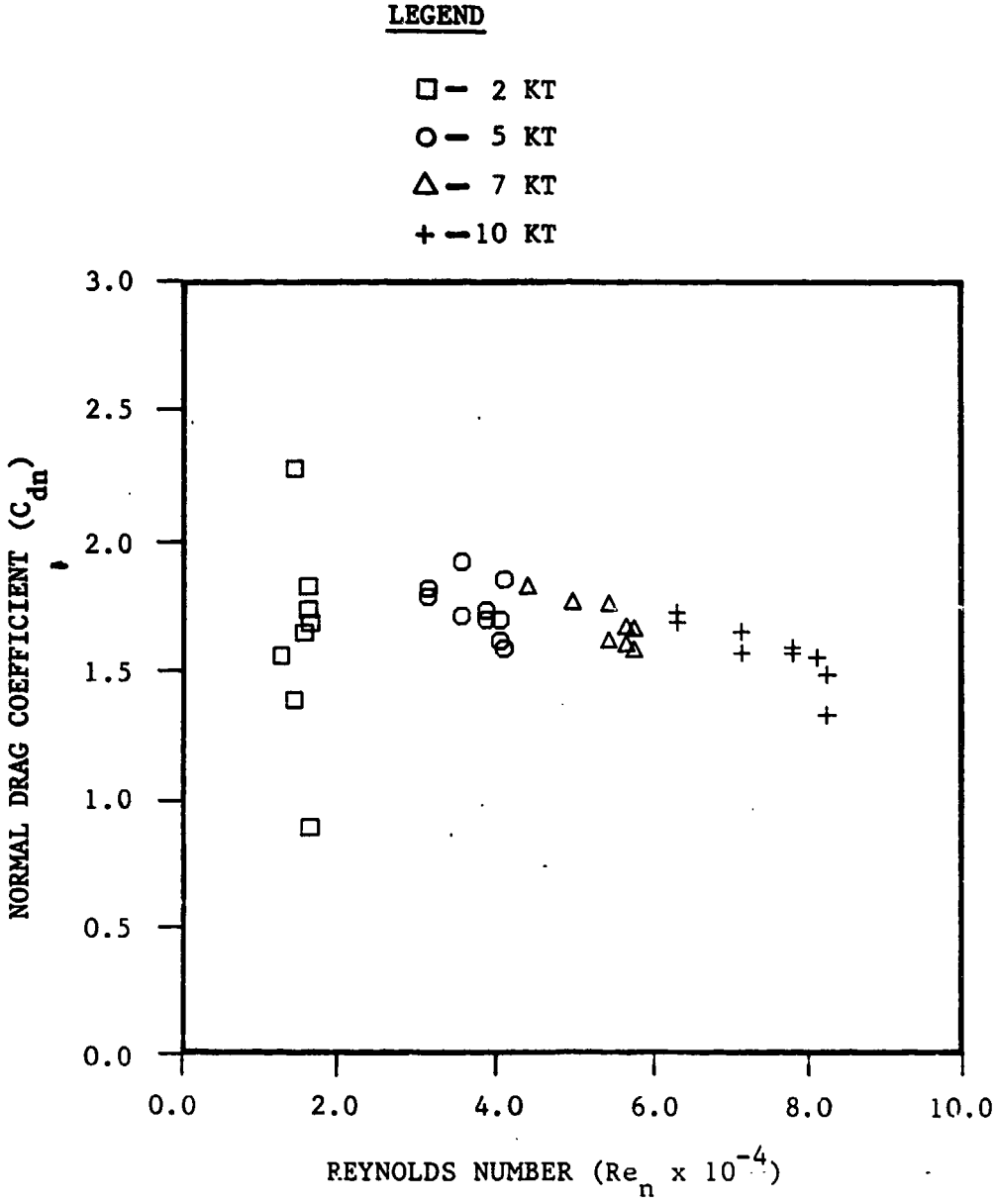

FIGURE 23(d). 4 x 7 CABLE (Sheet 4 of 4)

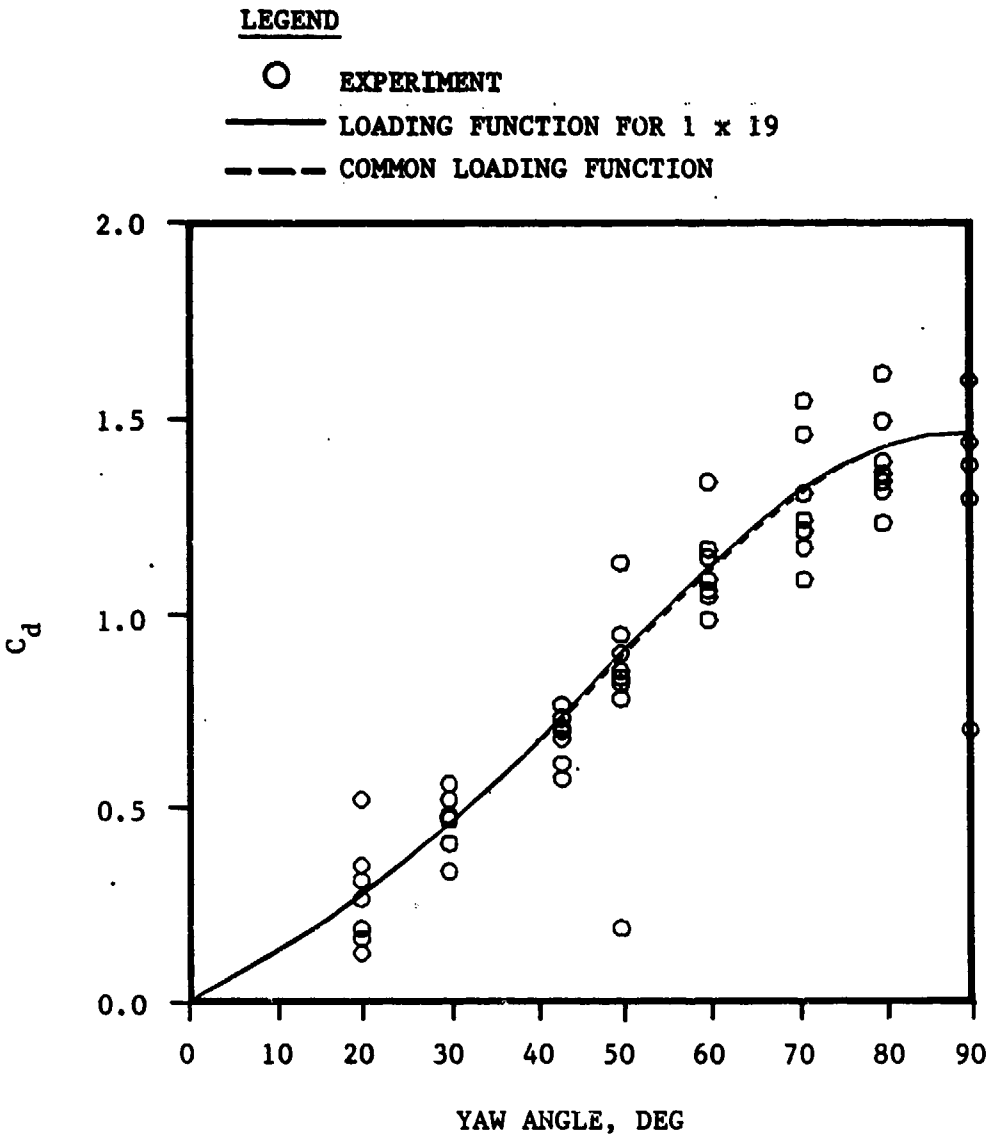

FIGURE 24(a). NORMAL DRAG LOADING FUNCTION VERSUS CABLE YAW ANGLE 1 x 19 CABLE (Sheet 1 of 4)

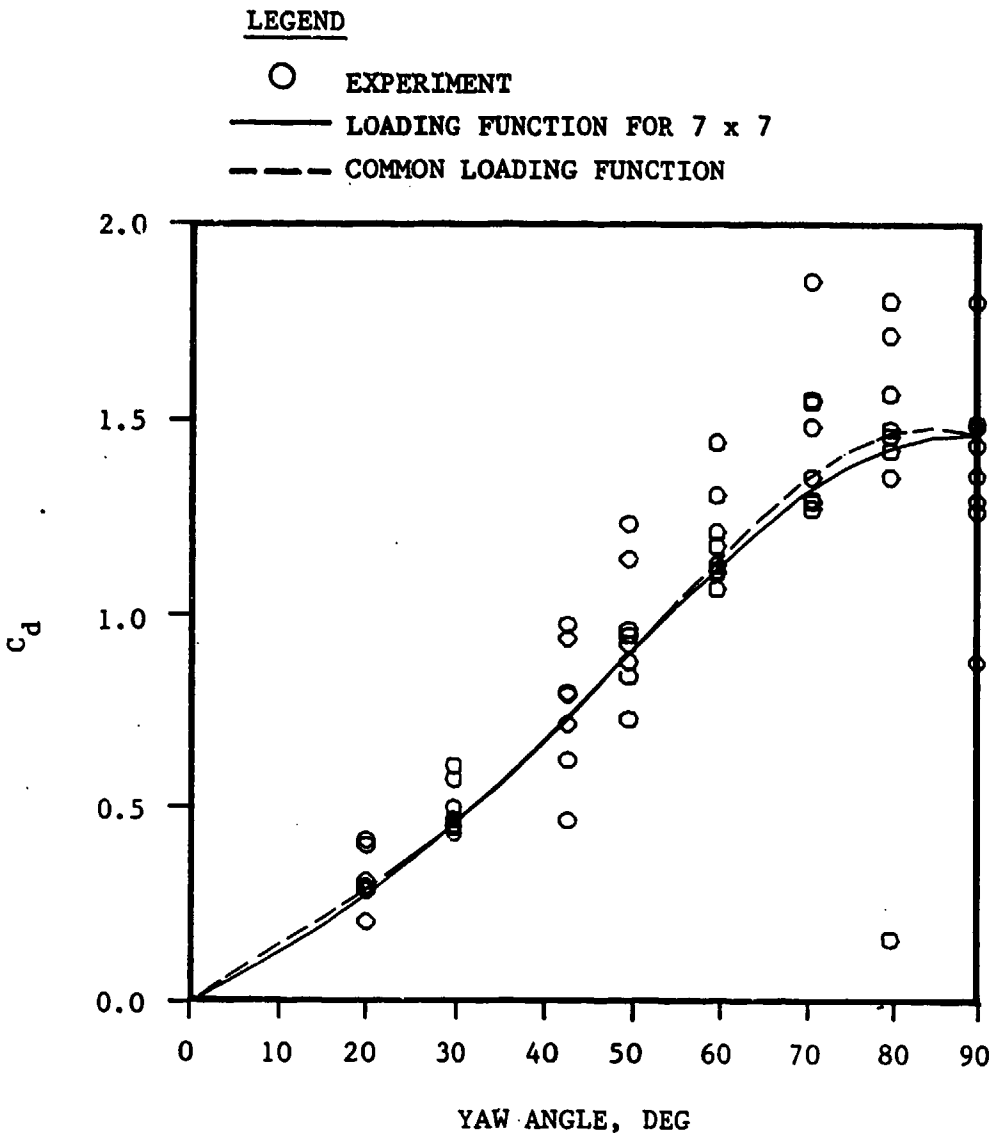

FIGURE 24(b). 7 x 7 CABLE (Sheet 2 of 4)

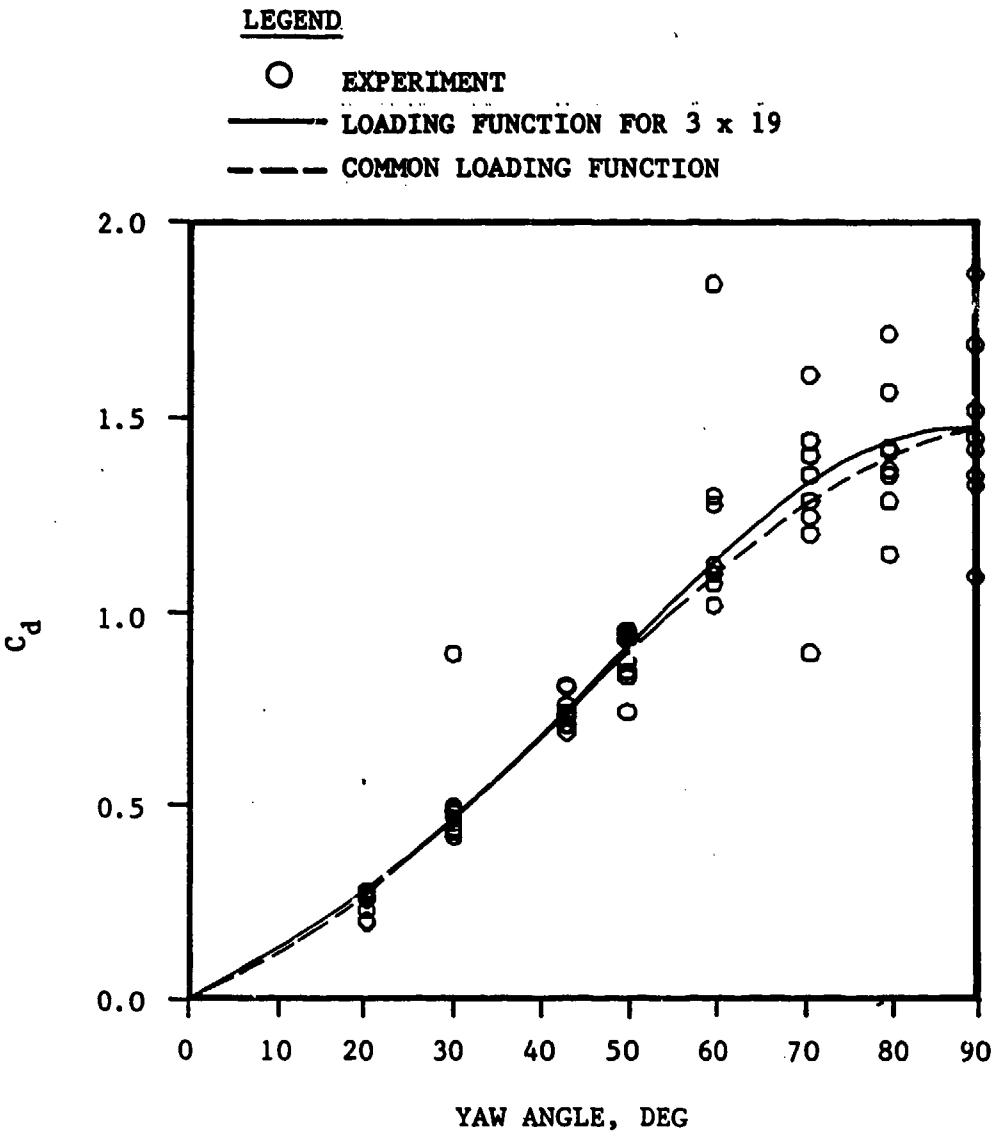

FIGURE 24(c). 3 x 19 CABLE (Sheet 3 of 4)

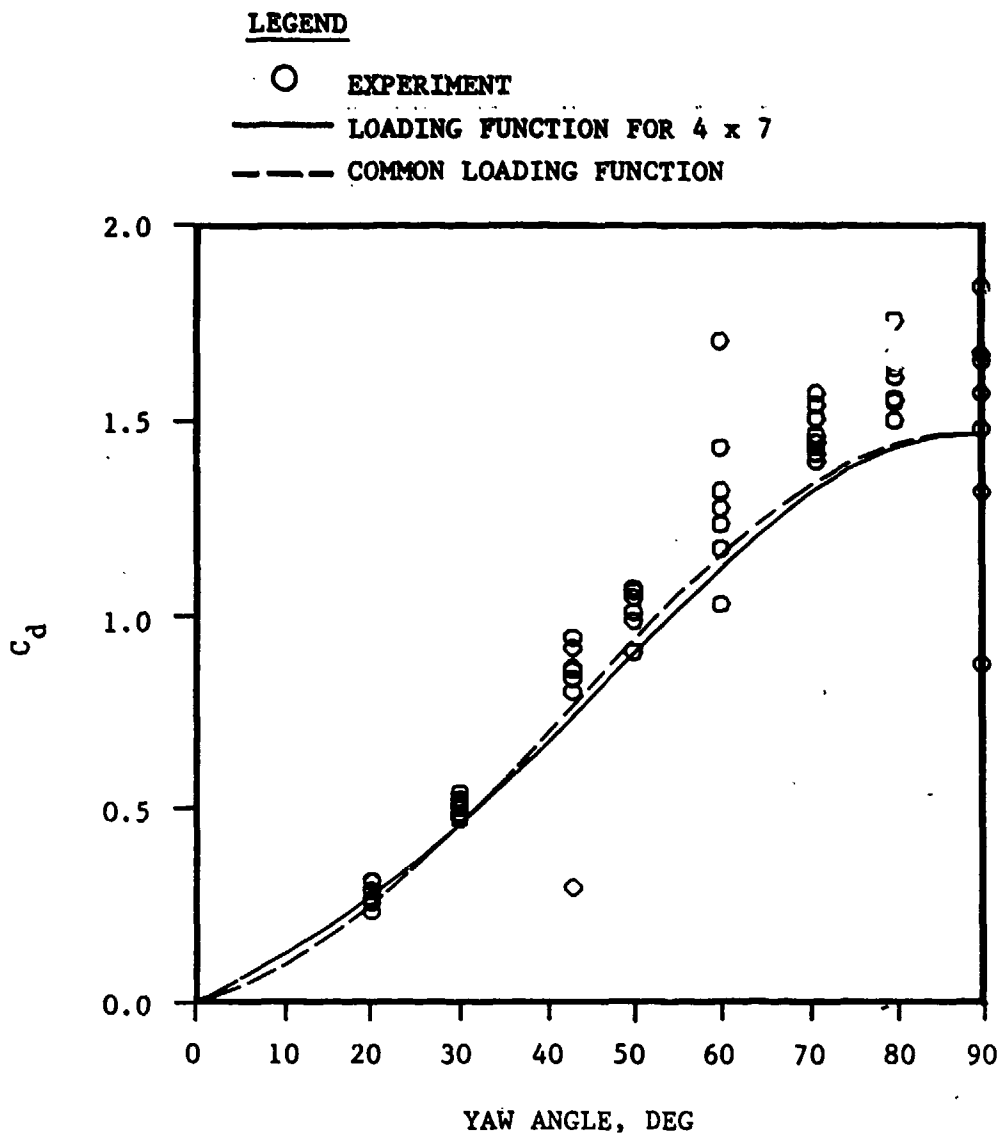

FIGURE 24(d). 4 x 7 CABLE (Sheet 4 of 4)

TABLE 5

HYDRODYNAMIC NORMAL DRAG LOADING FUNCTION COEFFICIENTS
FOR THE FOUR CABLE MODELS

Cable Model	Coefficients $f_n(\beta) = A_o + A_1 \cos\beta + B_1 \sin\beta + A_2 \cos 2\beta + B_2 \sin 2\beta$				
	A_o	A_1	B_1	A_2	B_2
1 x 19	-0.9300	1.2272	1.6328	-0.2972	-0.5643
7 x 7	-1.9580	2.3201	2.5960	-0.3621	-0.9870
3 x 19	0.4018	-0.1597	0.3561	-0.2421	-0.0126
4 x 7	0.1571	0.2518	0.4341	-0.4089	-0.0868

Lift Force Loading Functions

The steady and unsteady lift forces were determined similarly to the normal forces. Unsteady lift forces were determined for the 1 x 19 cable model. Figure 25 displays the unsteady and steady force ratio for this cable model for the complete set of angles, speeds, and tensions. The results of this figure show that the unsteady lift forces are significantly greater than the steady lift forces. The ratio of unsteady to steady forces are on the order of 5:1 for most runs. This ratio is one hundred times greater than that observed for the normal drag (1:20). The large unsteady to steady force ratio introduces scatter into the steady lift force data.

Dimensional lift force data for each cable model are shown in Figure 26 for the full range of angles, speeds, and tensions. The lift force per unit length is plotted versus yaw angle for the four cable models. The maximum lift force varies from about 2 pounds per foot for the 4 x 7 cable model to 4 pounds per foot for the 3 x 19 cable model. Table 6 gives the average maximum lift force for each cable model, which were used to normalize the data in obtaining the loading functions. The angle at which the maximum lift force is developed shows a wide variation for the four cable models with no apparent trend. Also, for a given speed, significant differences are noted between the force data for the two tensions.

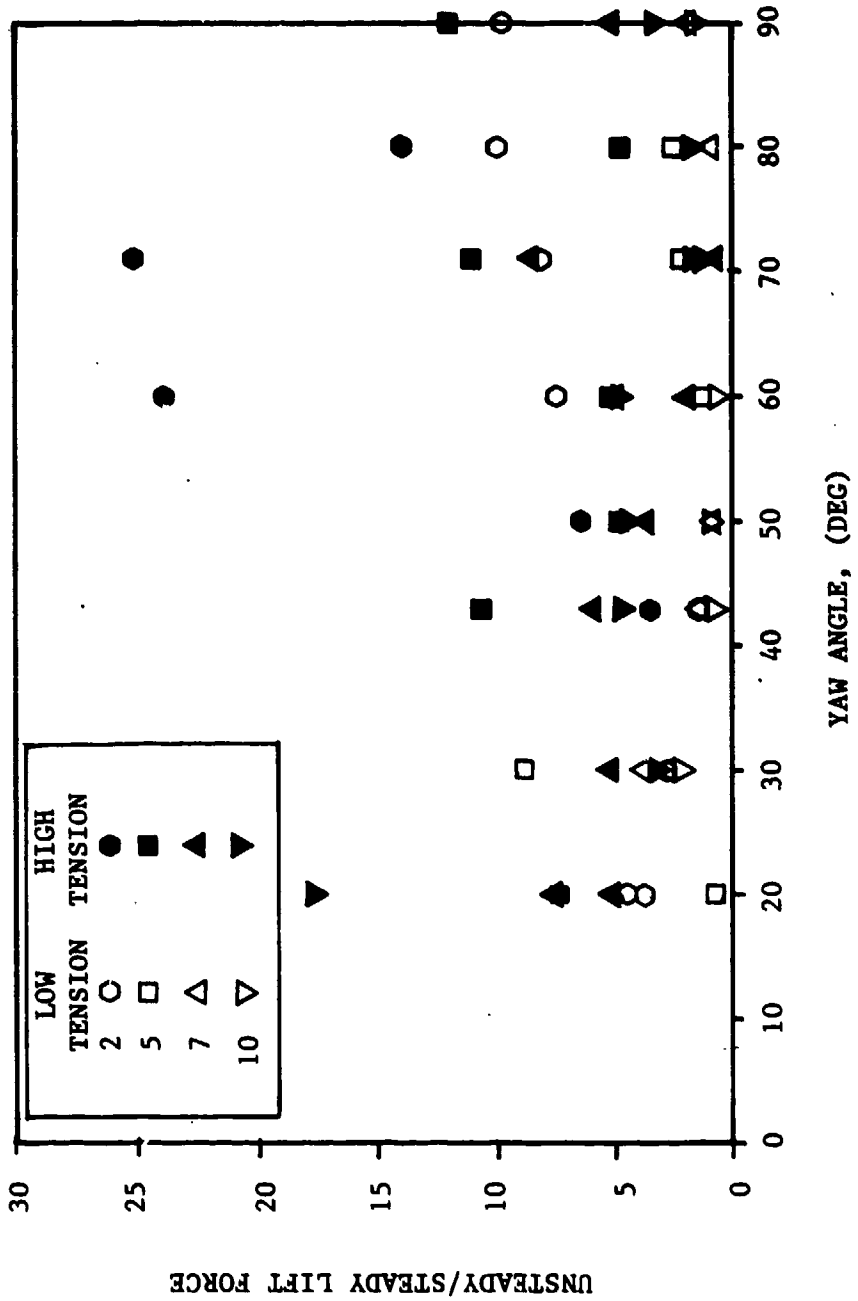

FIGURE 25. RATIO OF UNSTEADY LIFT FORCE TO STEADY LIFT FORCE FOR THE 1 x 19 CABLE MODEL AT TWO TENSIONS

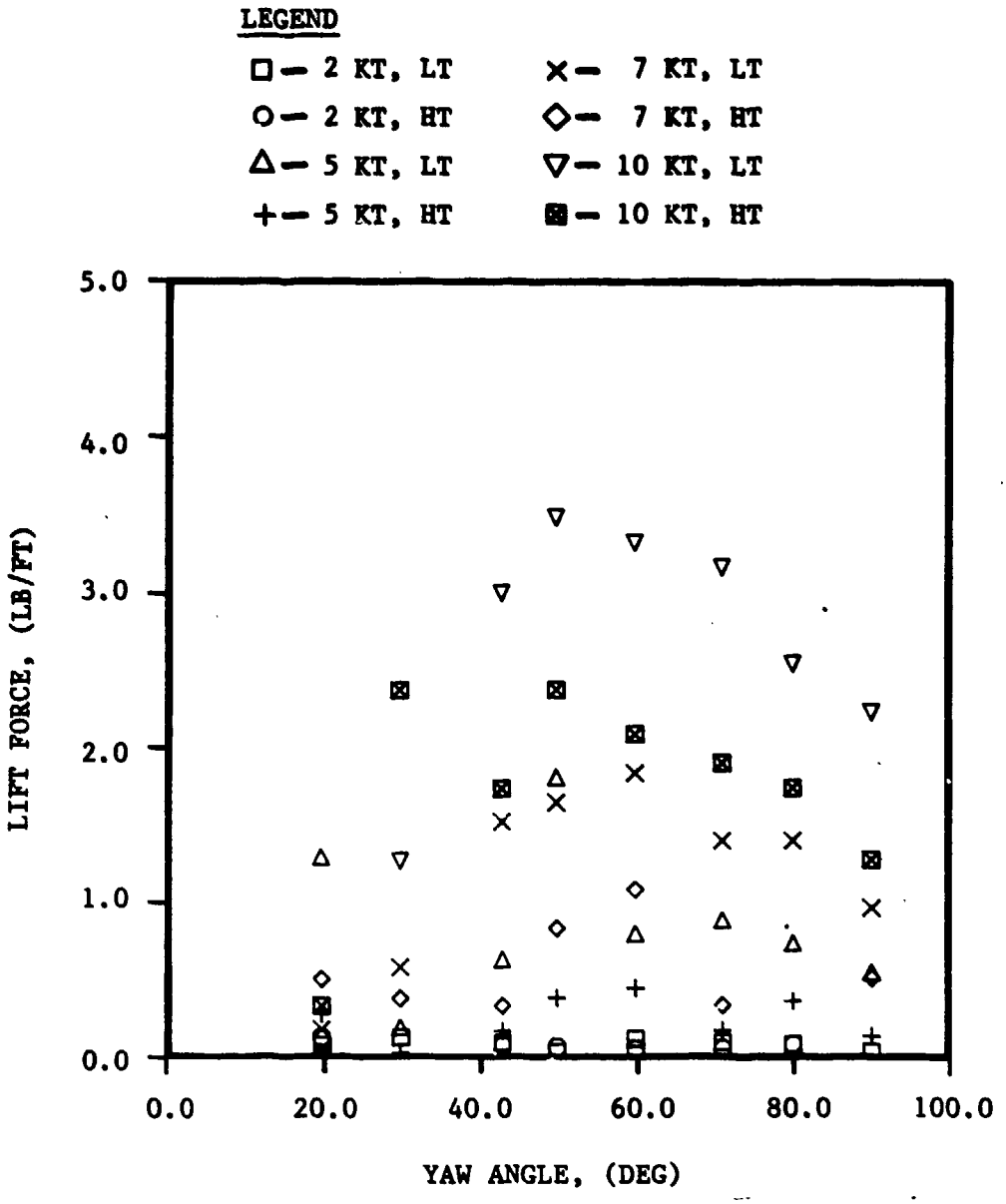

FIGURE 26(a). MEASURED LIFT FORCE VERSUS CABLE YAW ANGLE
1 x 19 CABLE (Sheet 1 of 4)

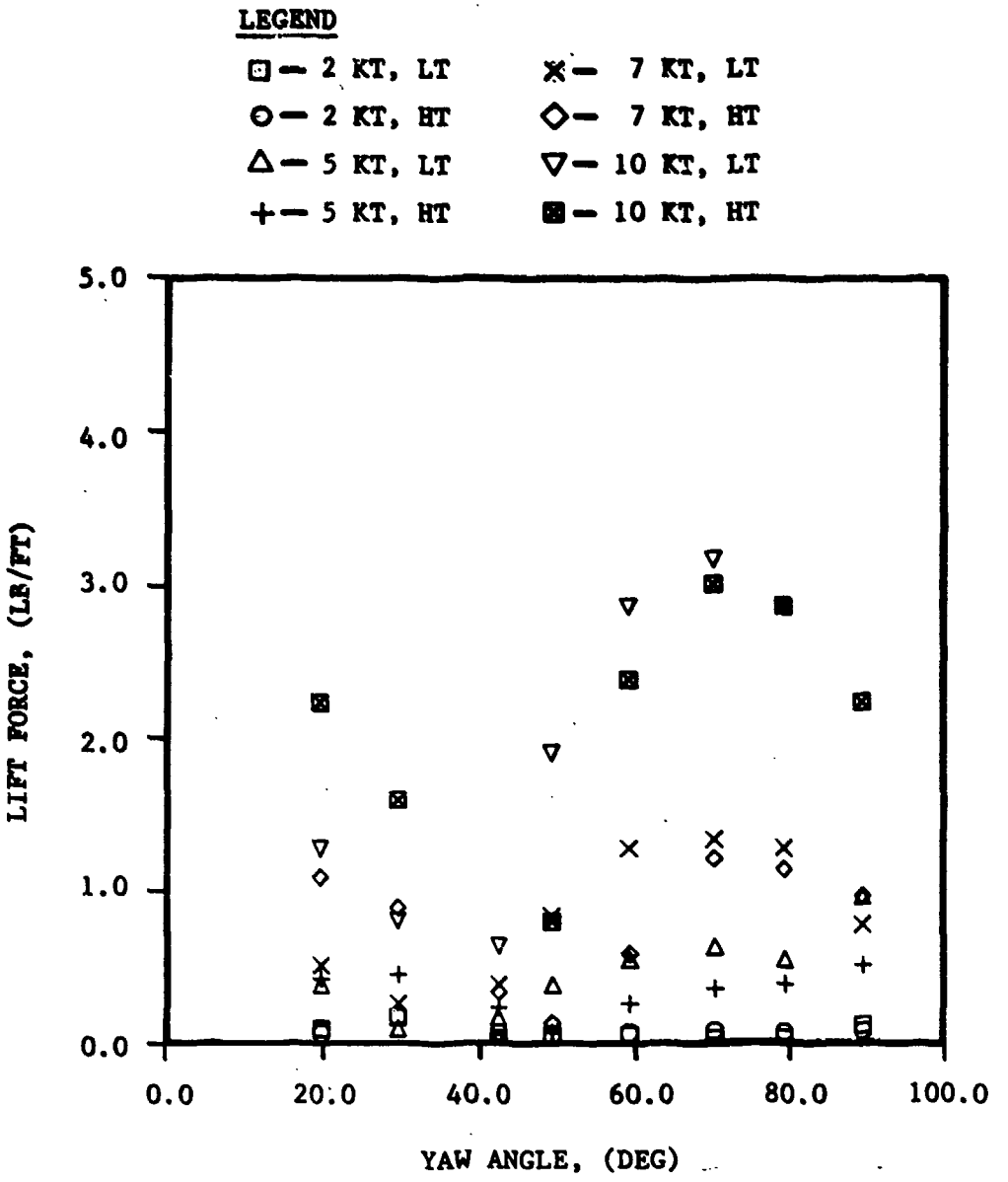

FIGURE 26(b). 7 x 7 CABLE (Sheet 2 of 4)

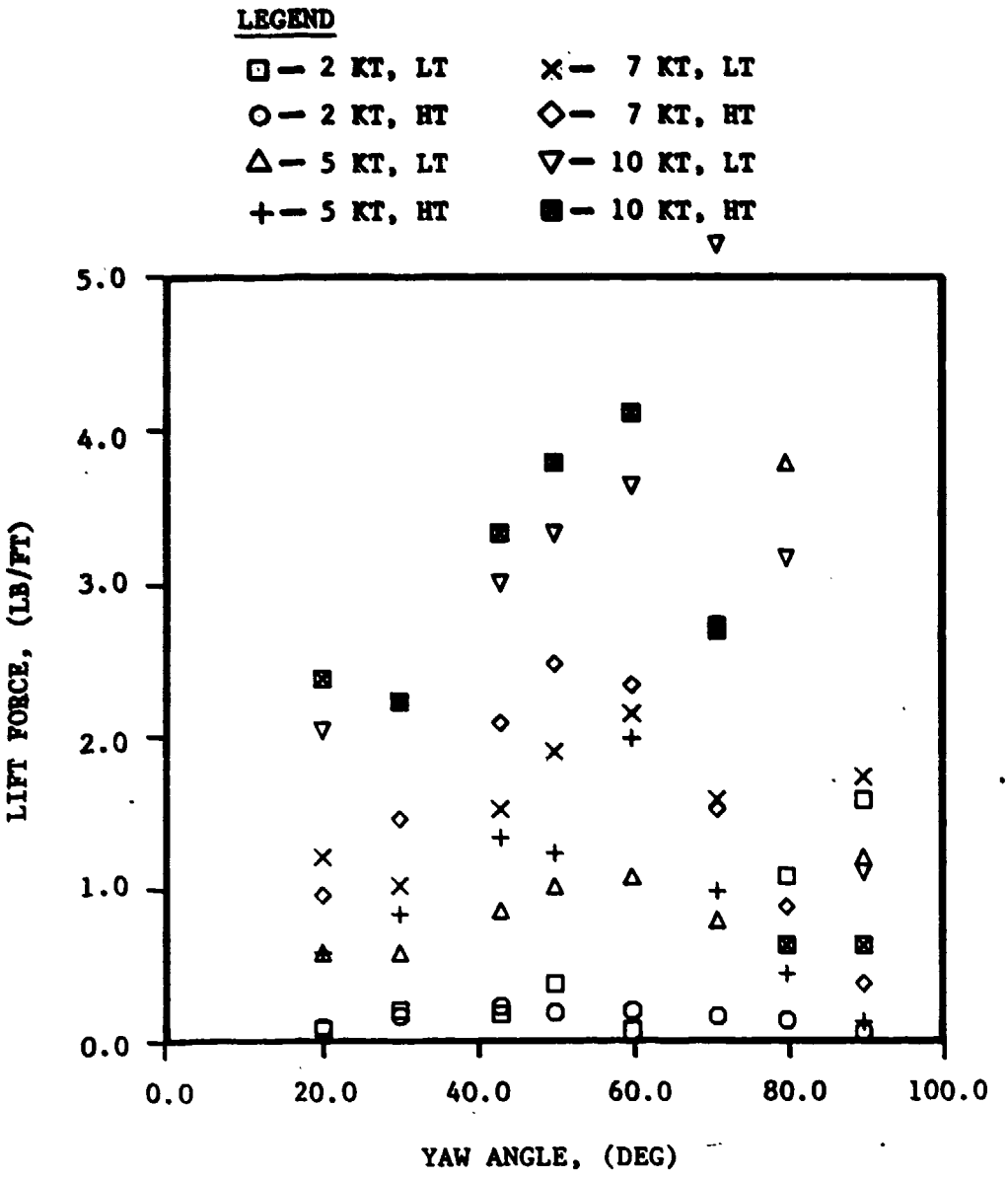

FIGURE 26(c). 3 x 19 CABLE (Sheet 3 of 4)

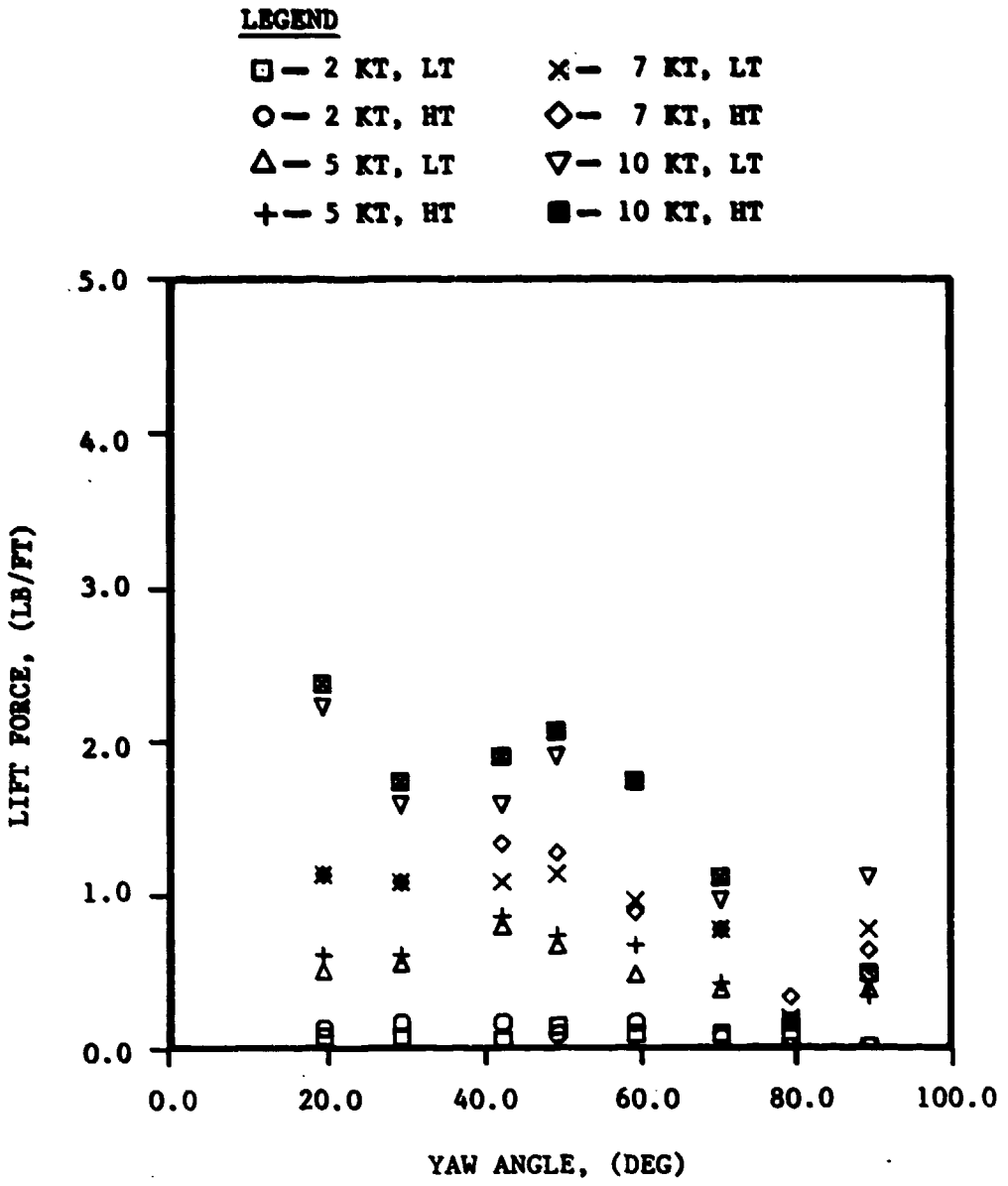

FIGURE 26(d). 4 x 7 CABLE (Sheet 4 of 4)

TABLE 6

AVERAGE MAXIMUM LIFT FORCE PER UNIT LENGTH
FOR THE FOUR CABLE MODELS

Cable Model	Lift Force/Length (lb/ft)			
	Speed (kt)			
	2	5	7	10
1 x 19	0.114	0.609	1.304	2.954
7 x 7	0.113	0.504	1.374	3.189
3 x 19	0.222	1.234	2.071	3.526
4 x 7	0.112	0.742	1.204	2.069

The lift coefficient, C_ℓ, is plotted as a function of yaw angle in Figures 27 through 30 for the four cable models. Unlike the normal drag coefficient data, the lift force data for all cable models show significant Reynolds number effects. The data for the four speeds are scattered along a wide bandwidth. No systematic effect due to Reynolds number is apparent. The distributions for the 1 x 19 and 3 x 19 cable models are somewhat similar, with maximum lift coefficients for the two cable models occurring at yaw angles between 50 and 70 degrees. The distribution for the 7 x 7 cable model shows a double peak at β = 20 and 70 degrees. Maximum values for the 4 x 7 cable model lie along a broad plateau of $10° < \beta < 50°$. The different distributions noted between the cable models suggest that the lift force is sensitive to cable geometry. Also, tension has an important effect on the magnitude of the lift force coefficients for the 1 x 19 cable model and a lesser effect on the other cable models. The average and standard deviation values of the lift coefficient data are listed in Table 7. Previous tests of cable models[1] [2] show lift force distributions comparable to those of Figures 27 through 30. Wind tunnel tests were conducted on 6 x 19 and 4 x 7 cable models[2] and a 1 x 19 cable model.[1] These tests show that the lift force coefficients are strongly affected by Reynolds number variations in the test range of $1.5 \times 10^4 < Re < 8.5 \times 10^4$.

The lift coefficient nondimensionalized by the normal velocity component is defined as

$$C_{\ell n} = \frac{f_\ell}{\frac{1}{2} \rho V^2 D \sin^2(\beta)} .$$

[1] op. cit.

[2] op. cit.

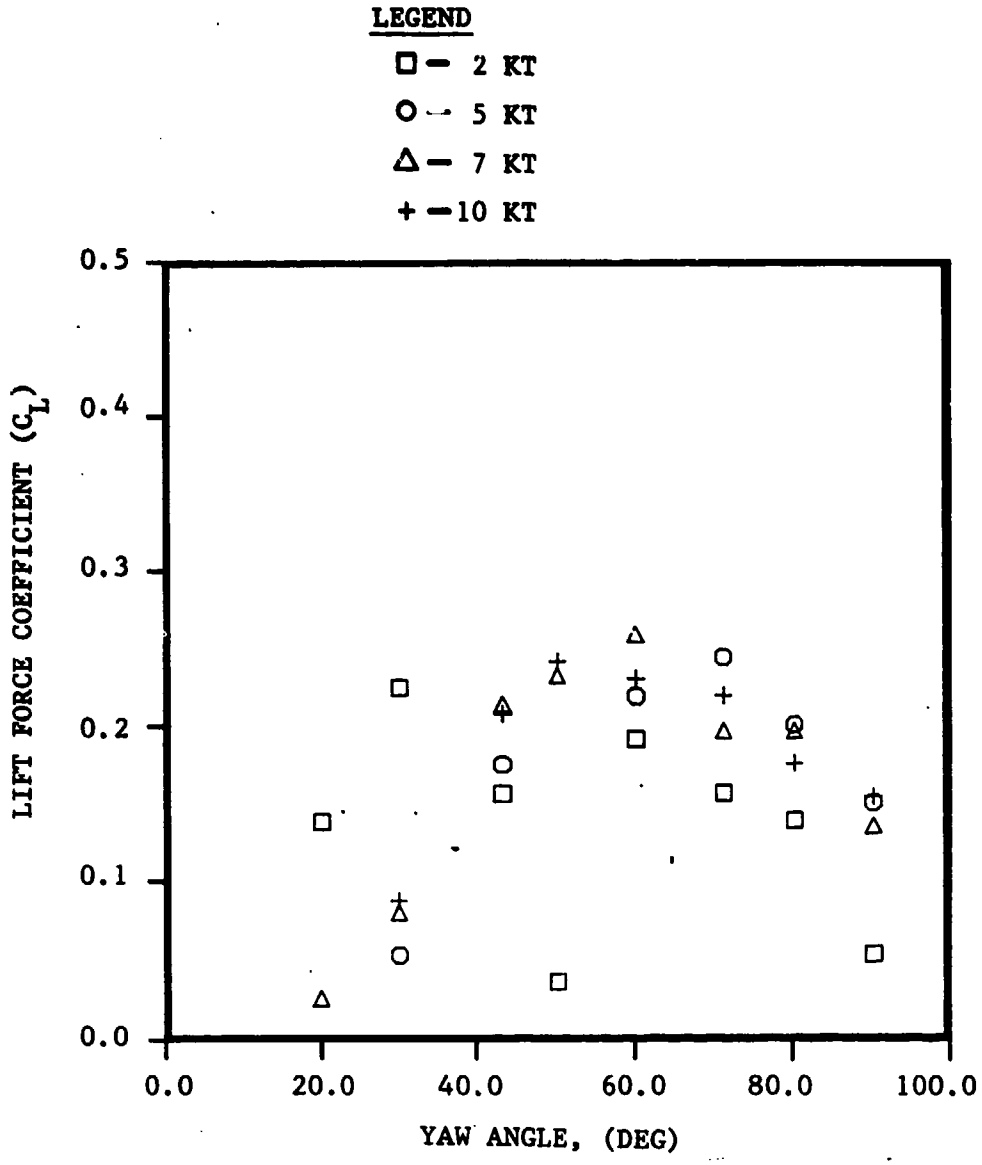

FIGURE 27(a). MEASURED LIFT FORCE COEFFICIENT VERSUS CABLE YAW ANGLE FOR THE 1 x 19 CABLE MODEL - LOW TENSION (Sheet 1 of 2)

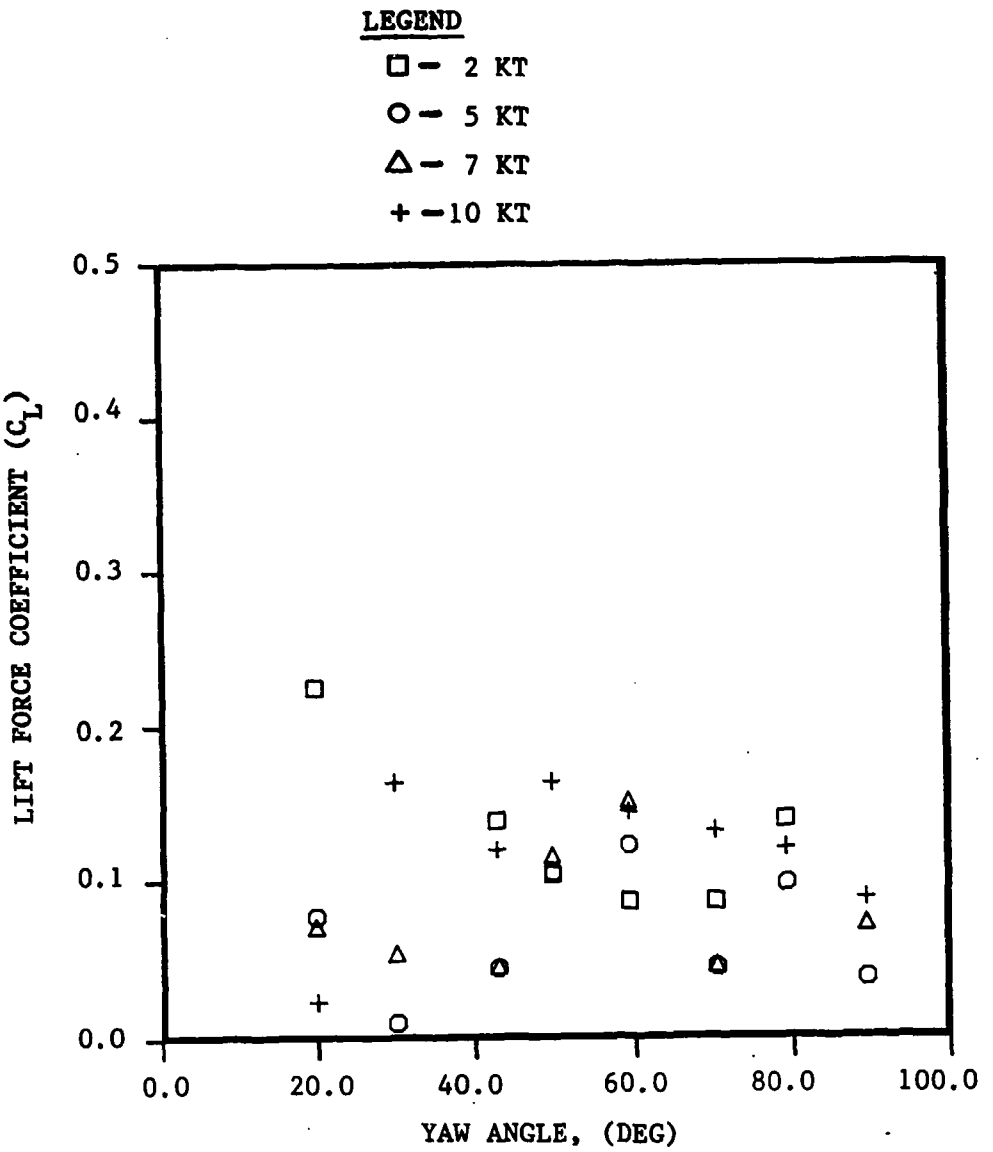

FIGURE 27(b). HIGH TENSION (Sheet 2 of 2)

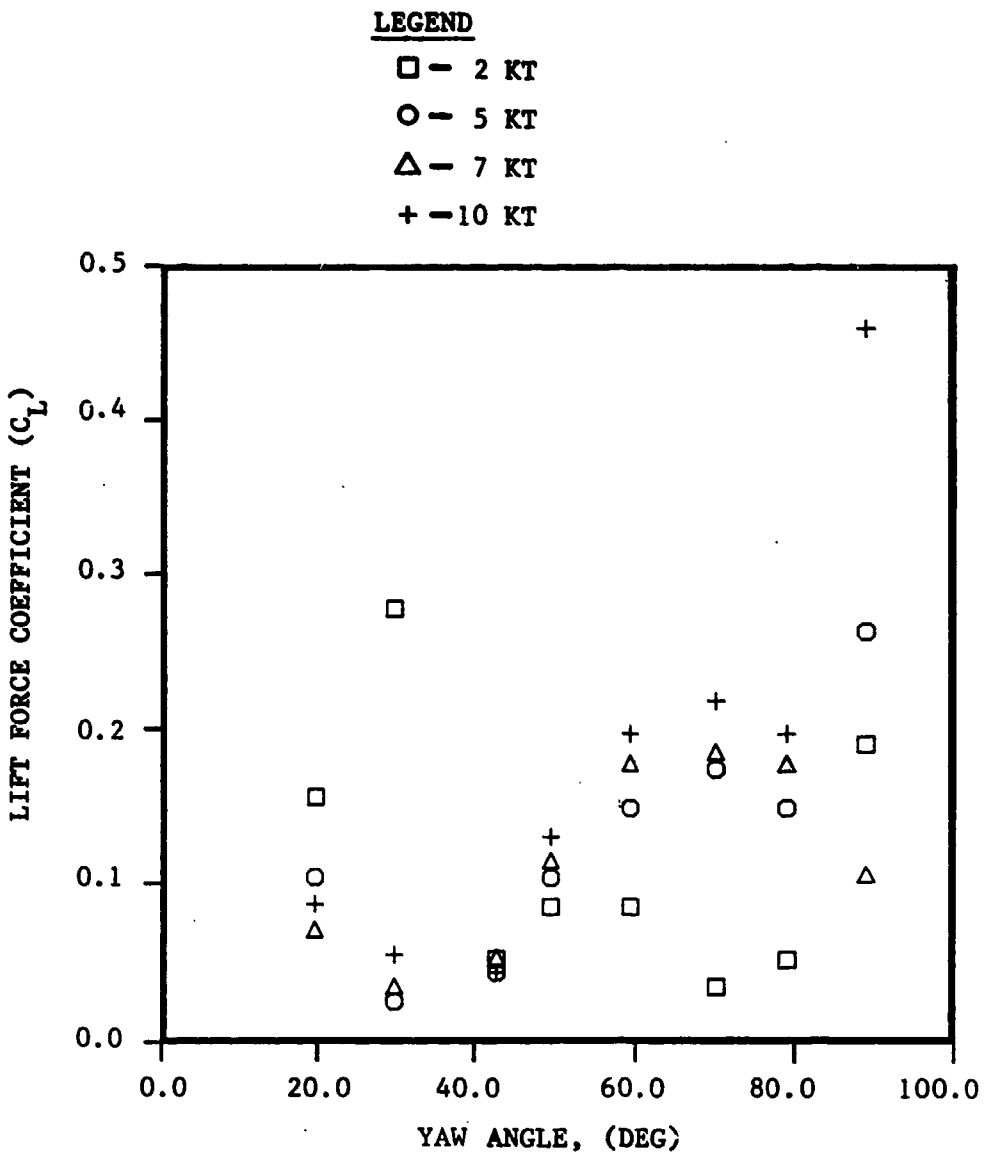

FIGURE 28(a). MEASURED LIFT FORCE COEFFICIENT VERSUS CABLE YAW ANGLE FOR THE 7 x 7 CABLE MODEL - LOW TENSION (Sheet 1 of 2)

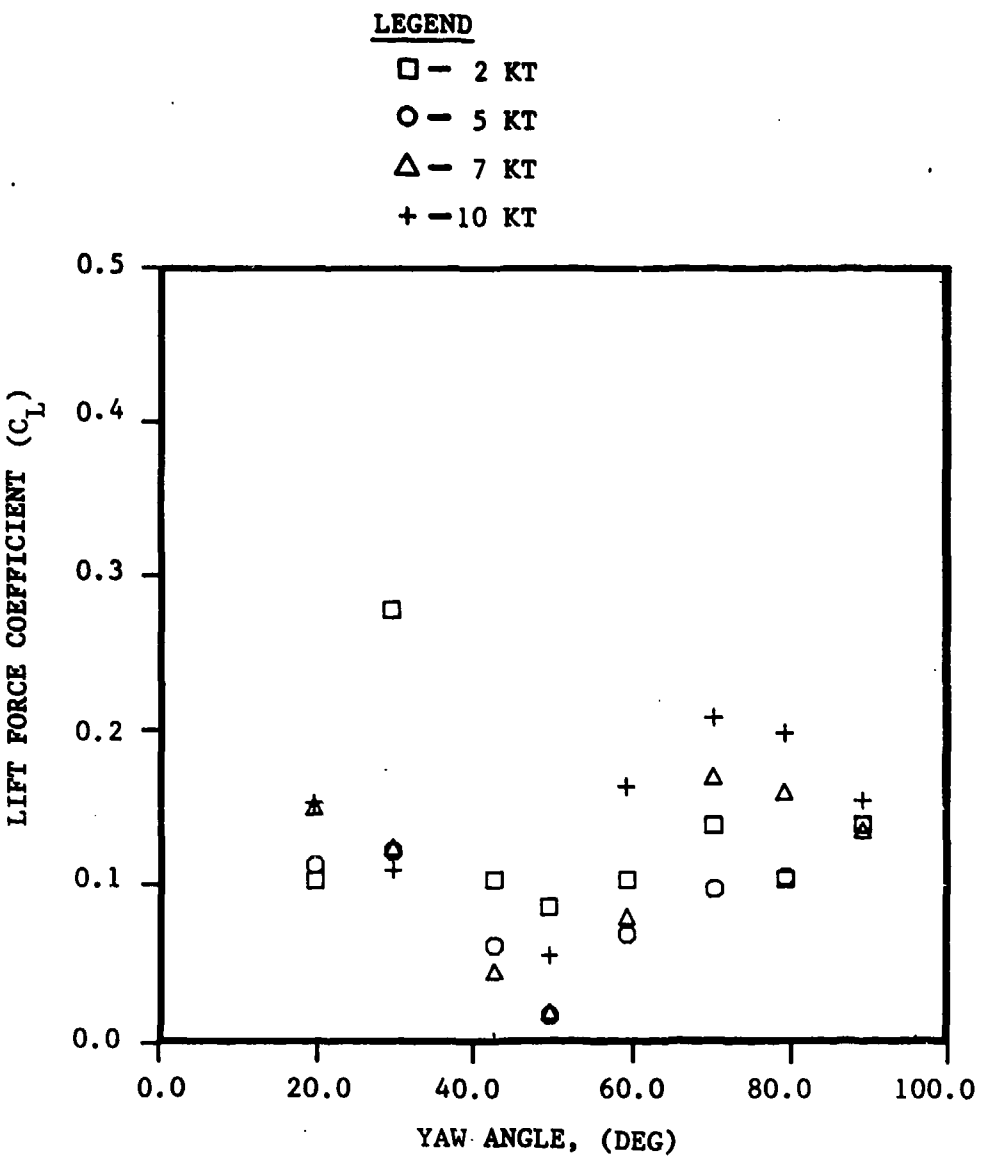

FIGURE 28(b). HIGH TENSION (Sheet 2 of 2)

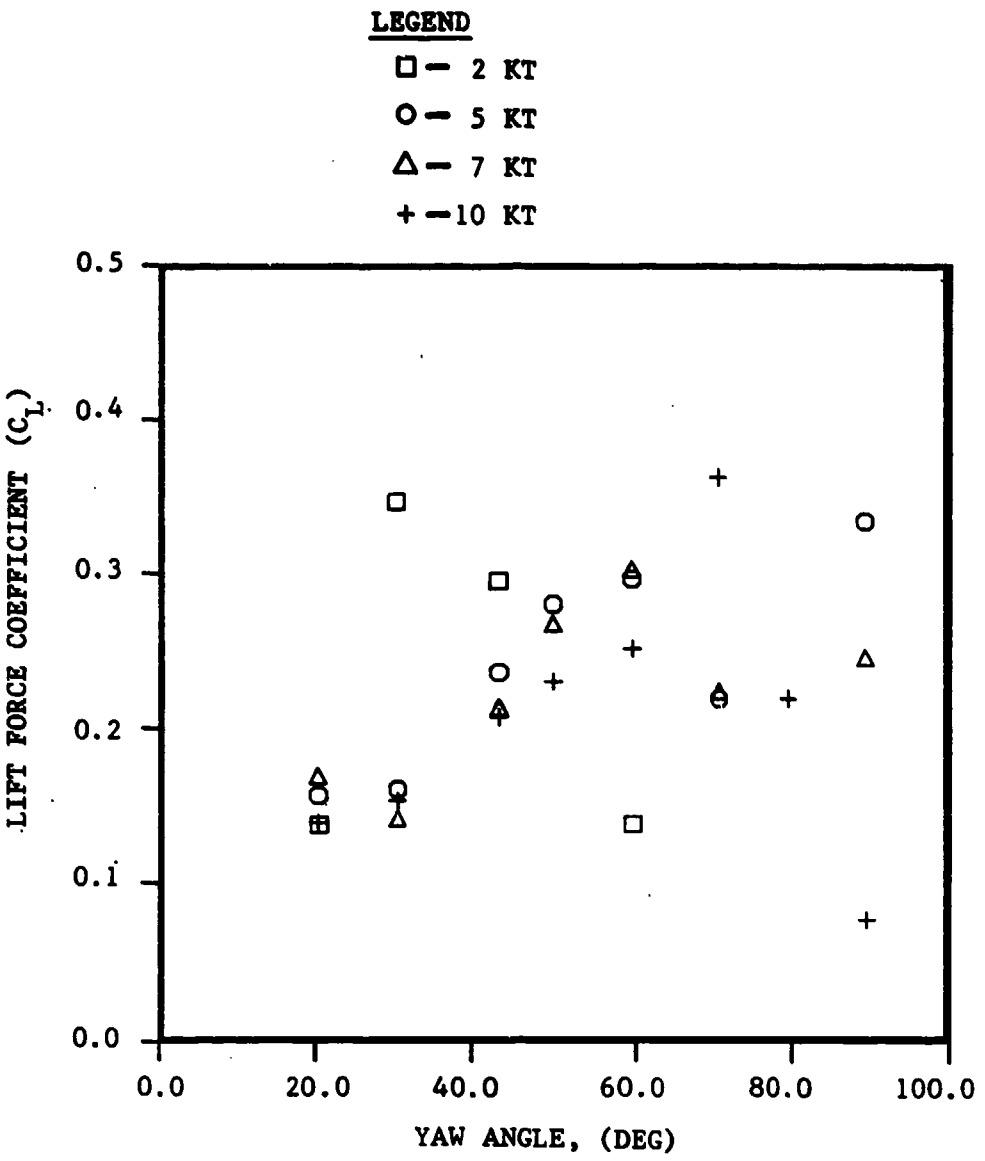

FIGURE 29(a). MEASURED LIFT FORCE COEFFICIENT VERSUS CABLE YAW ANGLE FOR THE 3 x 19 CABLE MODEL - LOW TENSION (Sheet 1 of 2)

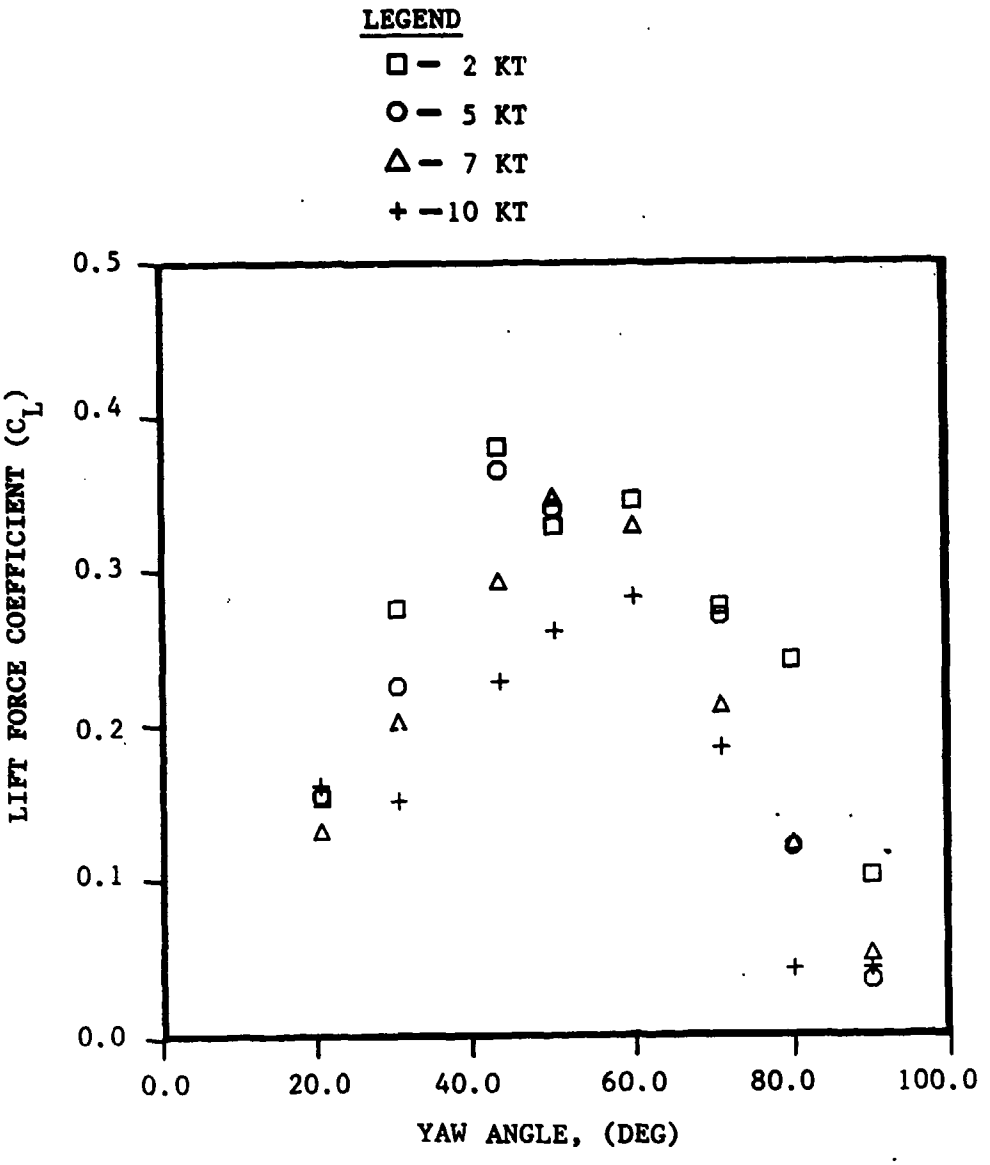

FIGURE 29(b). HIGH TENSION (Sheet 2 of 2)

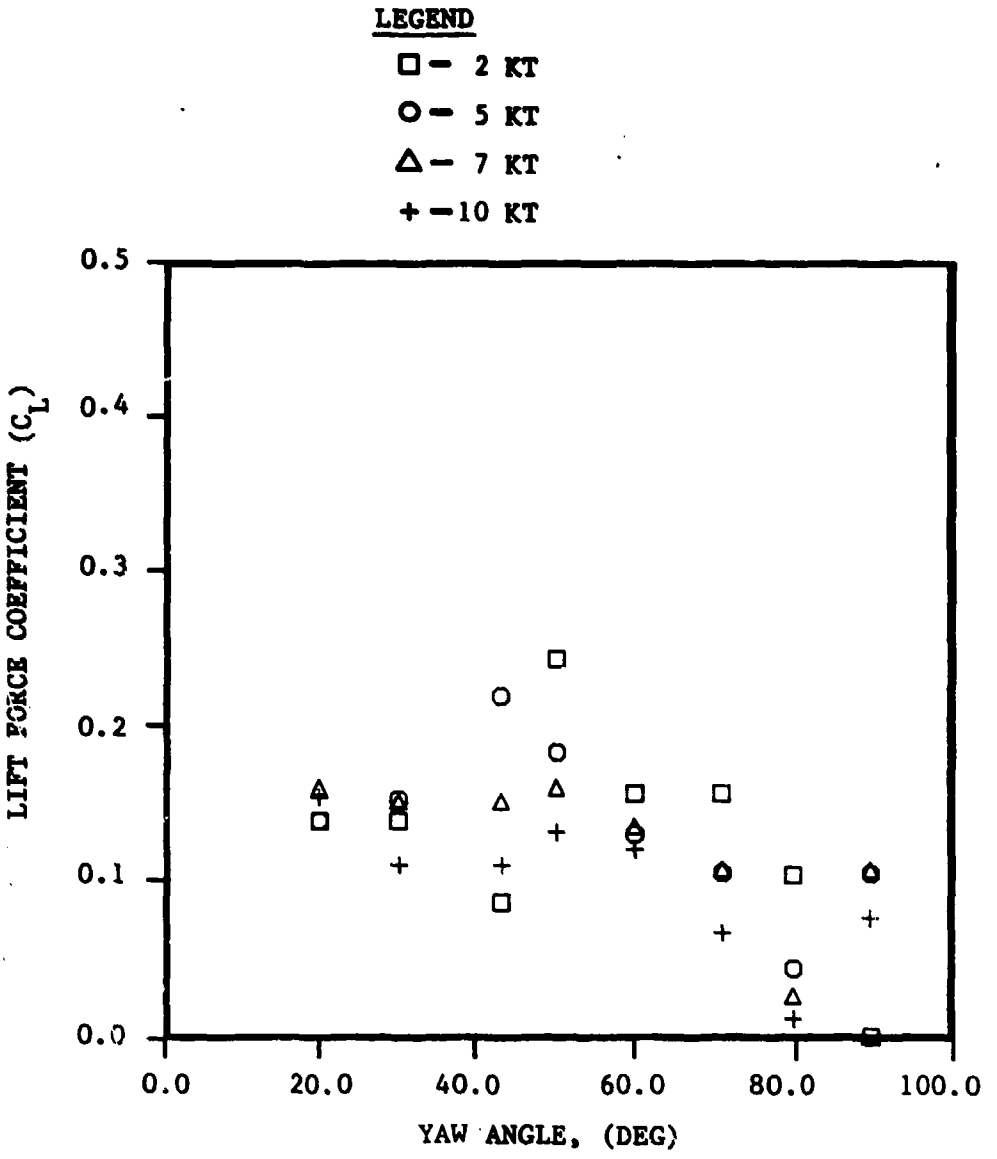

FIGURE 30(a). MEASURED LIFT FORCE COEFFICIENT VERSUS CABLE YAW ANGLE FOR THE 4 x 7 CABLE MODEL - LOW TENSION (Sheet 1 of 2)

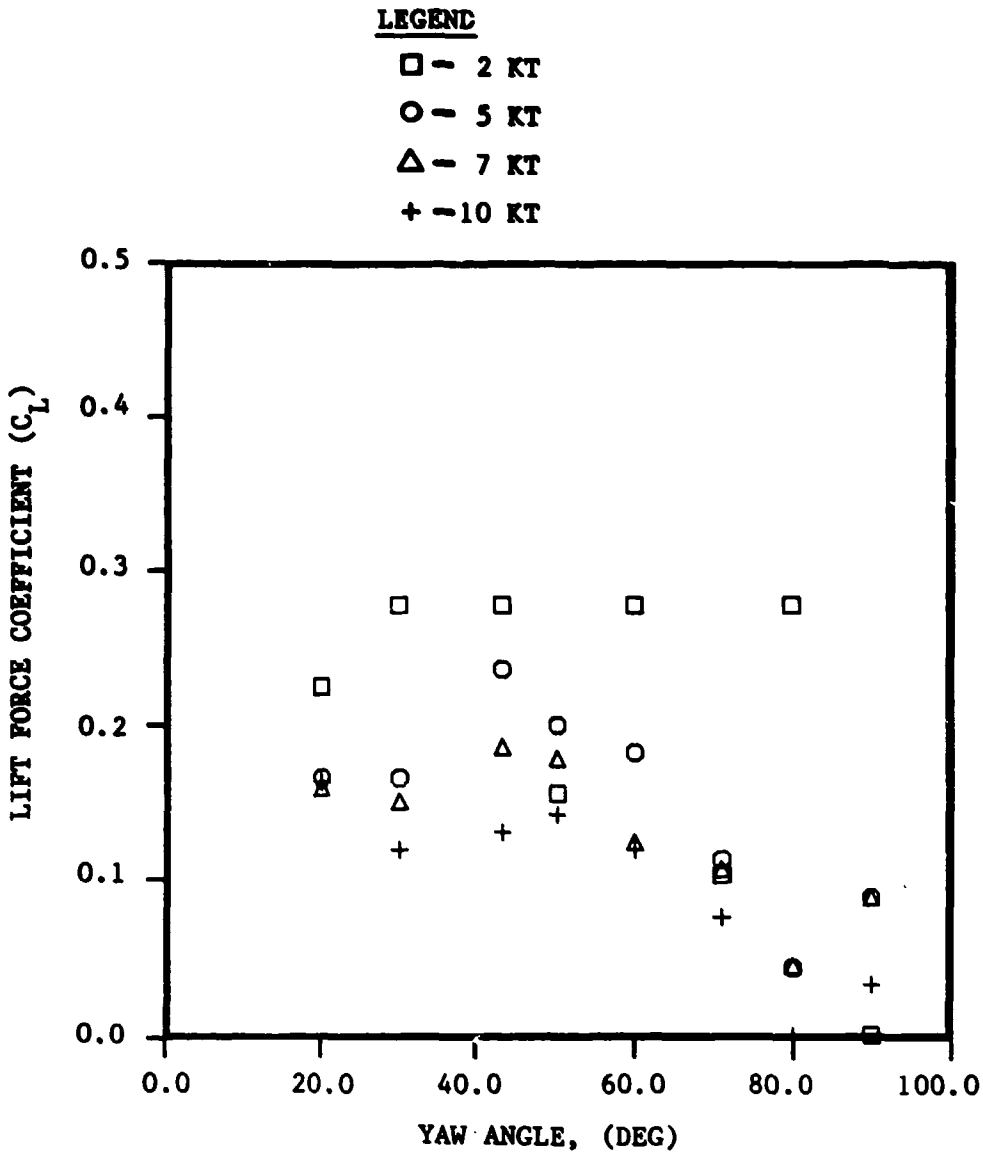

FIGURE 30(b). HIGH TENSION (Sheet 2 of 2)

TABLE 7

AVERAGE LIFT COEFFICIENTS FOR THE FOUR CABLE MODELS

Cable Model	C_ℓ Average	Standard Deviation
1 x 19	0.139	0.0812
7 x 7	0.116	0.0572
3 x 19	0.222	0.1000
4 x 7	0.139	0.0610

Values of $C_{\ell n}$ for β = 50 to 90 degrees are plotted versus the crossflow Reynolds number in Figure 31. Previous application of the Independence Principle in Figure 23 showed it to be an effective means of scaling the normal drag data. Figure 31 shows that the Independence Principle is less successful in scaling the lift force data. The values of $C_{\ell n}$ are widely scattered over the range of Reynolds numbers, with values for the 3 x 19 cable model showing an especially large scatter compared to the other cable models. The effect of yaw angle is not removed from the lift force data as was observed for the normal drag data.

In the method used for obtaining the lift force loading functions, significant data scatter forced a "double smoothing" technique to fit the data. For a given cable model the first step involves fitting a least squares curve to the measured lift force at each speed, resulting in four expressions of the form

$$f_\ell(\beta) = a_o + a_1 \beta + a_2 \beta^2 + a_3 \beta^3 + a_4 \beta^4 \qquad (13)$$

where $f_\ell(\beta)$ is normalized with the maximum lift force. The curves determined for each cable are presented in dimensional form in Figure 32 along with the lift force data. Values for the normalized lift force are obtained from the above expression for use in the second step of the smoothing process. The data are used to determine the coefficients of the loading function, Equation (12), based on a least squares solution. The resulting expression is the lift force loading function, $f_\ell(\beta)$. This method of "double-smoothing" the data enables a curve fit to be performed on the scattered lift force data. No boundary conditions were imposed on the lift force loading function; however, it was assumed that the lift force data were zero at β = 0 and 90 degrees.

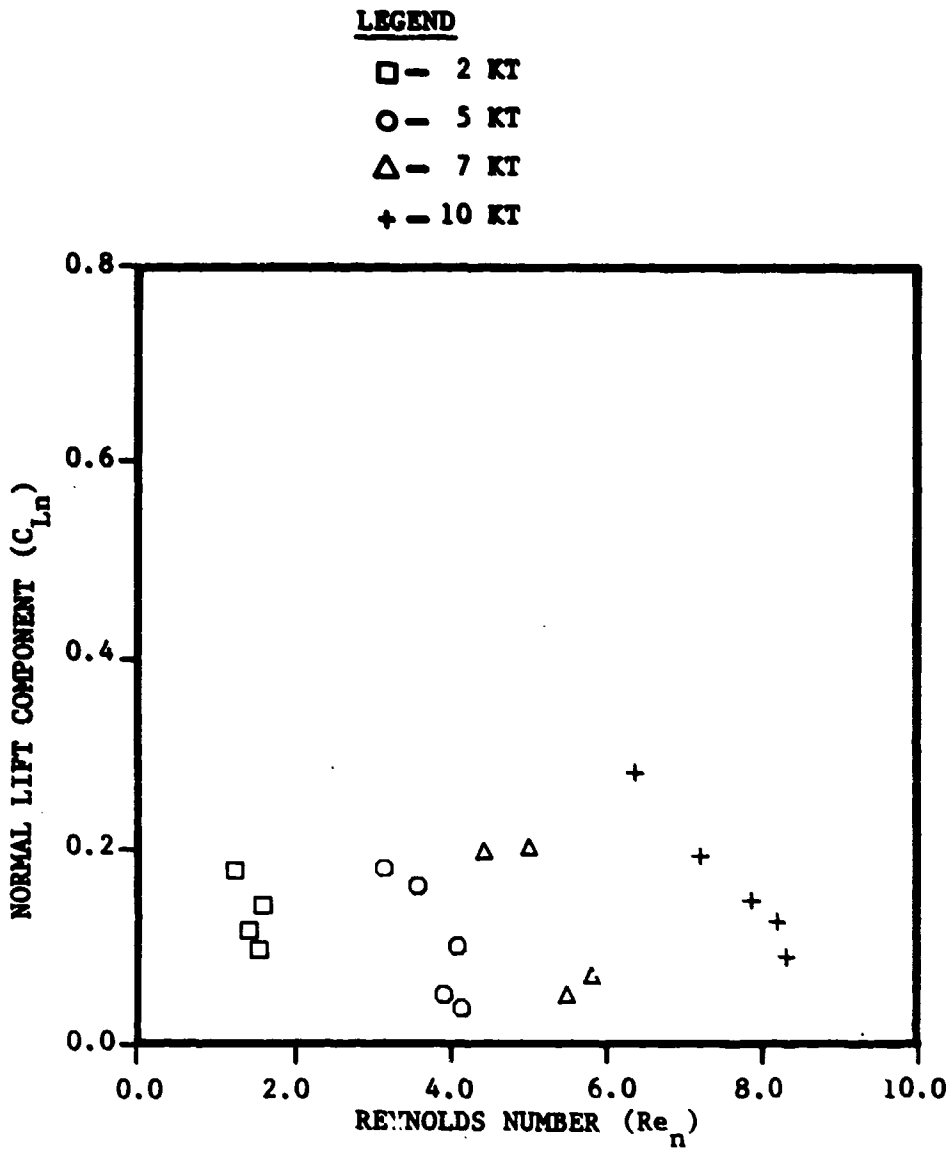

FIGURE 31(a). MEASURED LIFT COEFFICIENT BASED ON NORMAL VELOCITY COMPONENT VERSUS CROSSFLOW REYNOLDS NUMBER FOR HIGH TENSION 1 x 19 CABLE (Sheet 1 of 4)

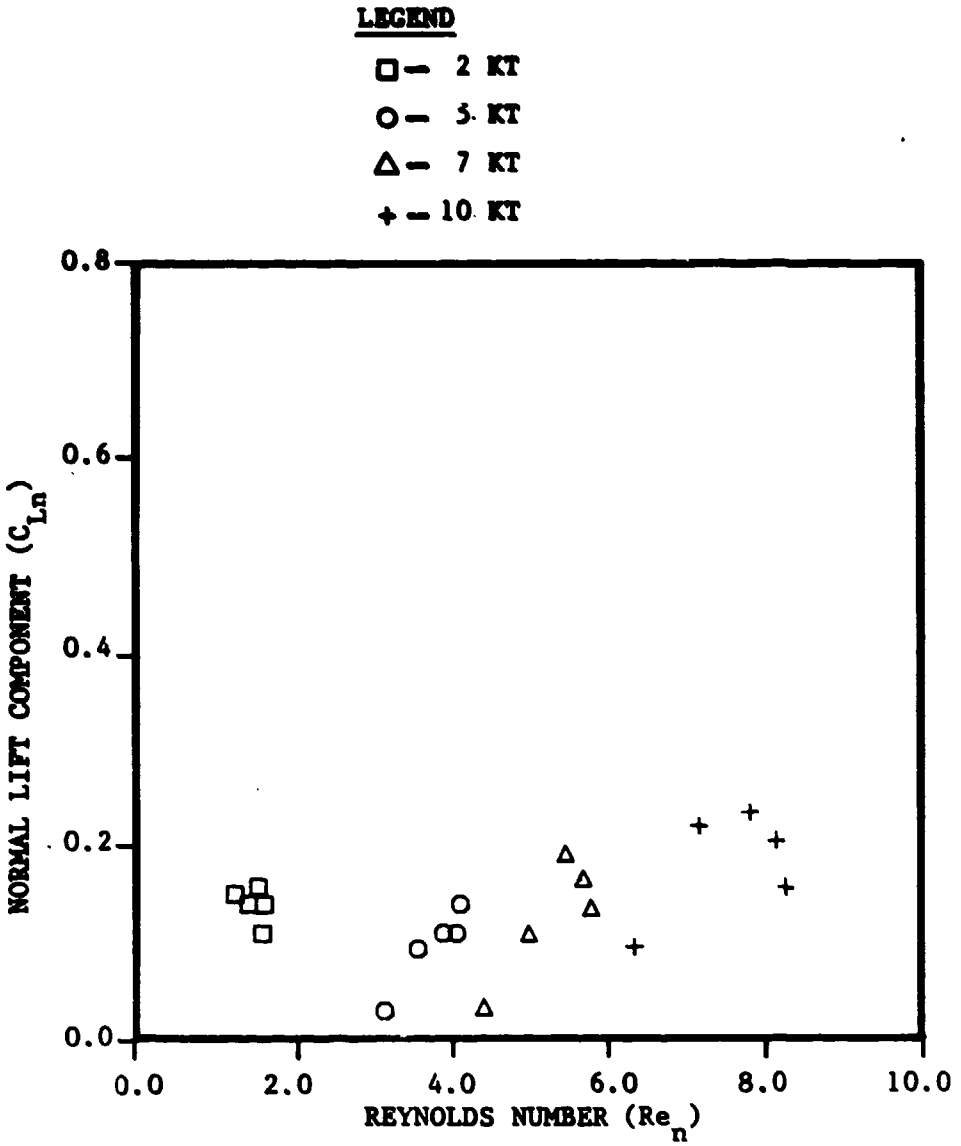

FIGURE 31(b). 7 x 7 CABLE (Sheet 2 of 4)

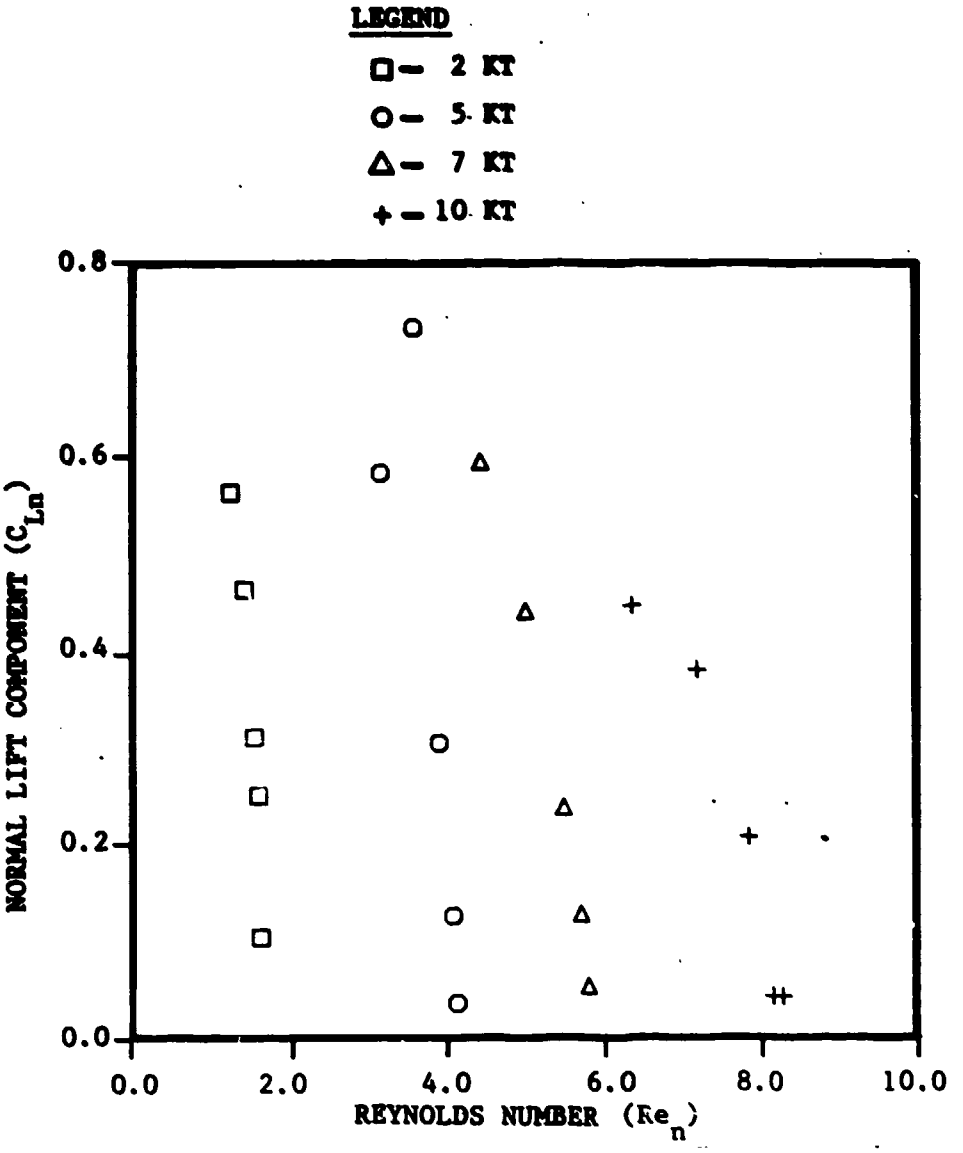

FIGURE 31(c). 3 x 19 CABLE (Sheet 3 of 4)

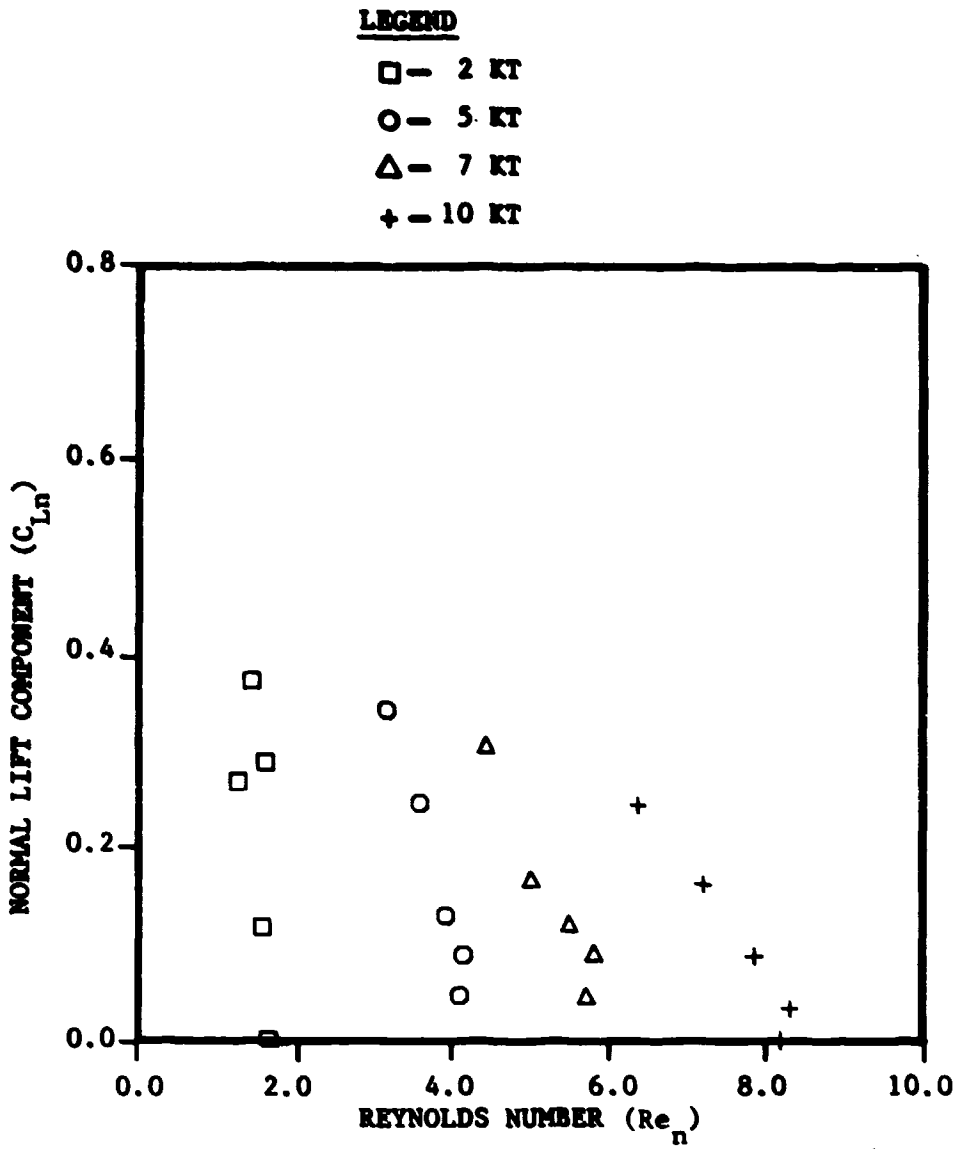

FIGURE 31(d). 4 x 7 CABLE (Sheet 4 of 4)

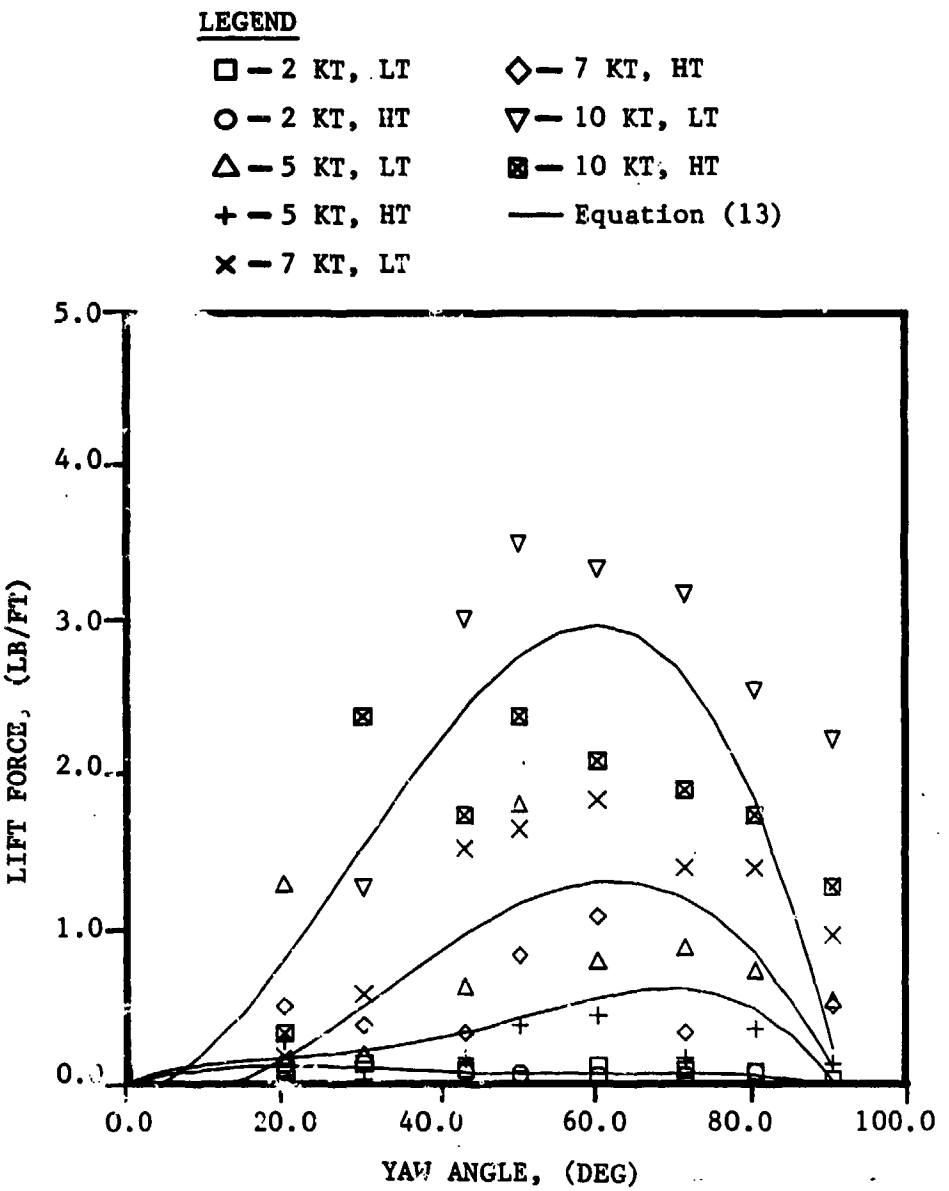

FIGURE 32(a). MEASURED LIFT FORCE VERSUS CABLE YAW ANGLE
1 x 19 CABLE (Sheet 1 of 4)

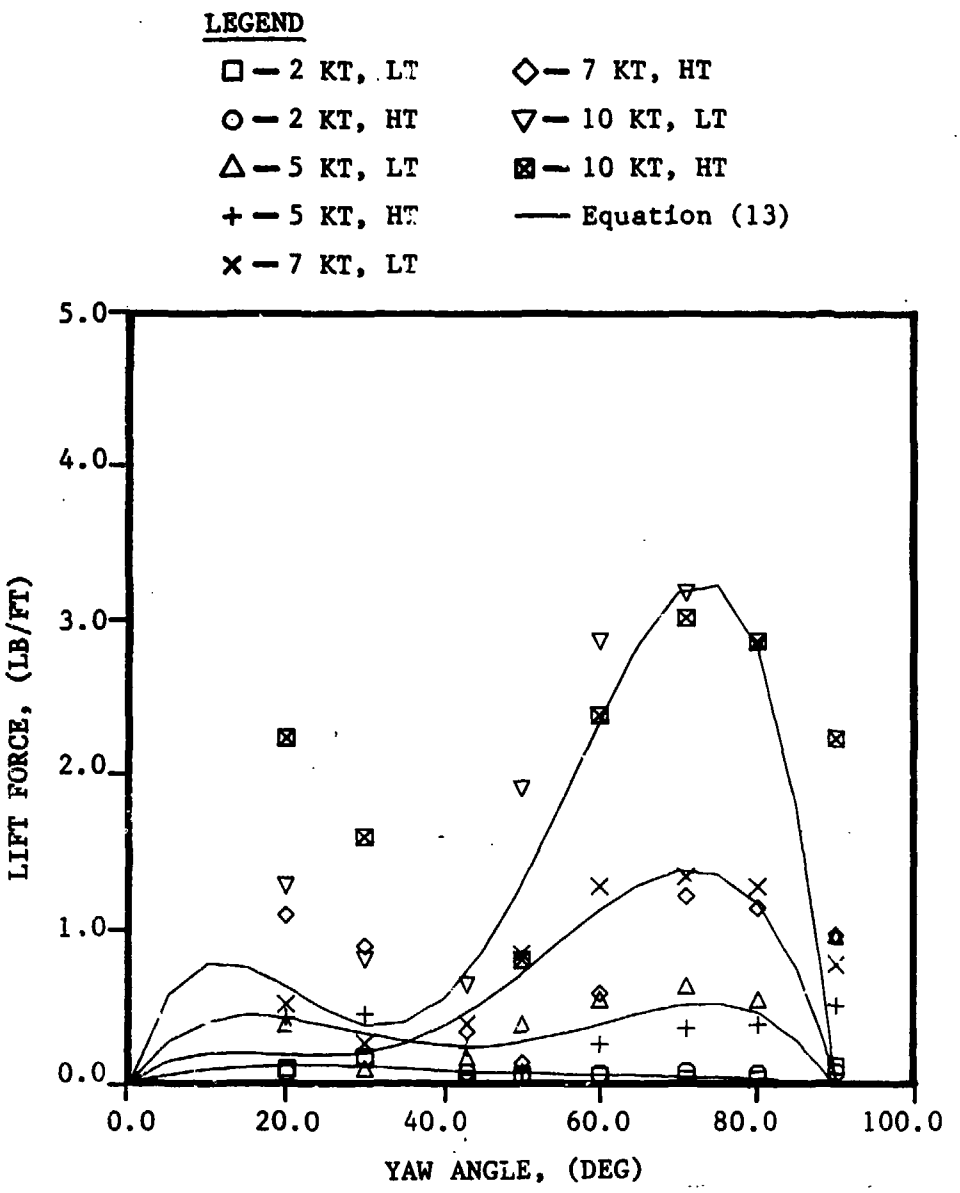

FIGURE 32(b). 7 x 7 CABLE (Sheet 2 f 4)

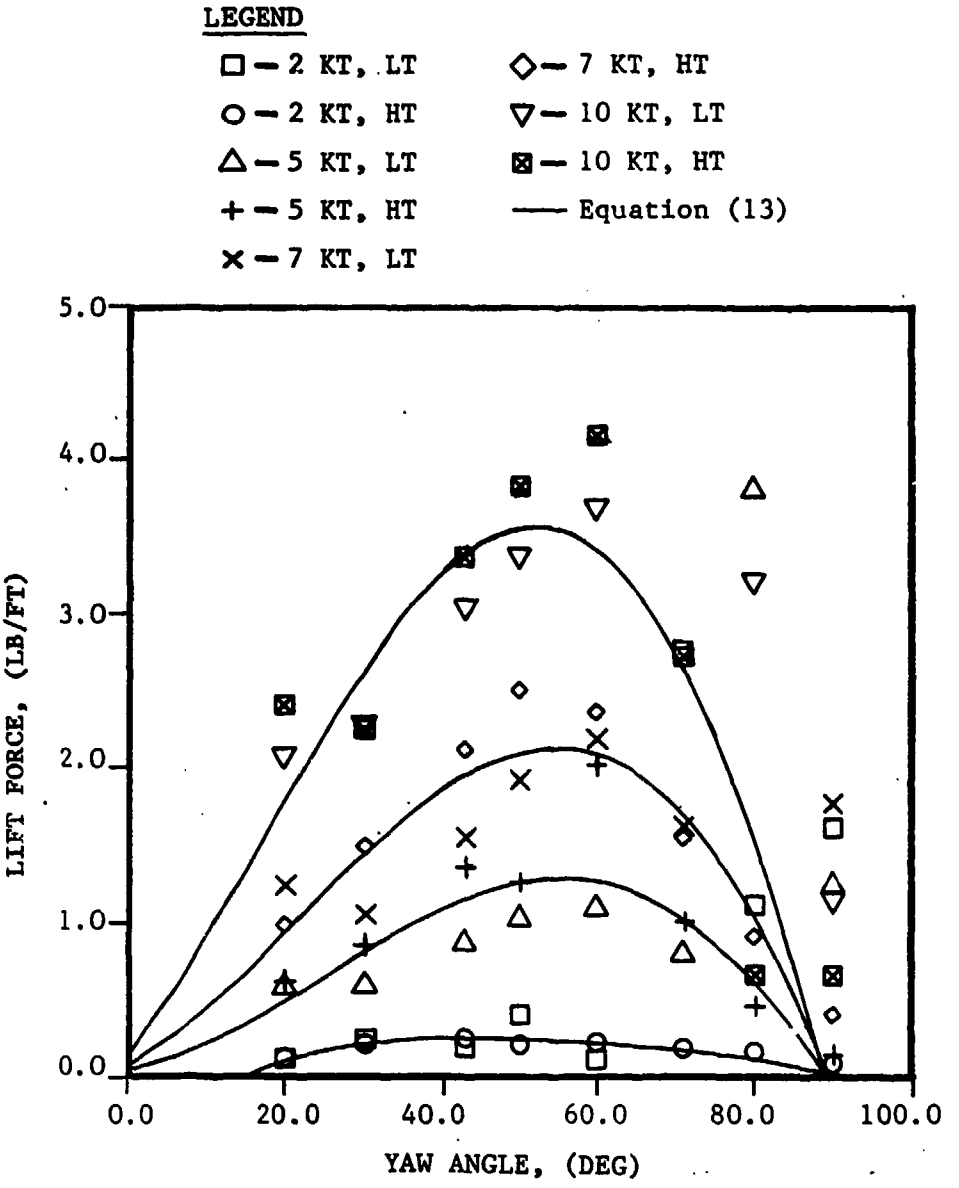

FIGURE 32(c). 3 x 19 CABLE (Sheet 3 of 4)

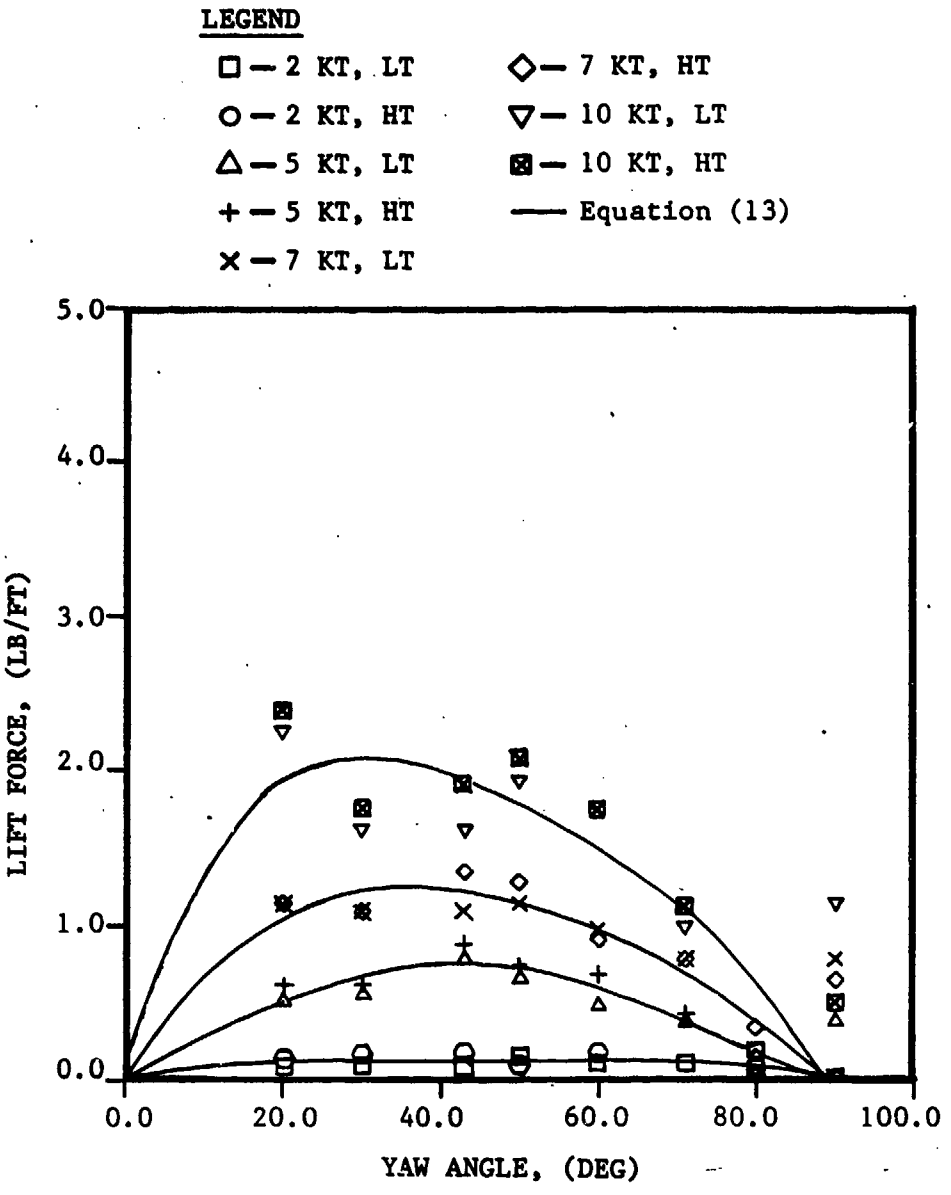

FIGURE 32(d). 4 x 7 CABLE (Sheet 4 of 4)

The lift force loading functions for each cable model are shown in Figure 33. As with the normal drag loading functions, the low and high tension data are combined to obtain one expression for each cable model. Although the loading functions stated provide a better estimate of the lift forces developed on various cables than in the past, the usefulness of the lift force loading functions for quantitative analysis is limited due to the significant scatter in the data used to derive these curves. However, the expressions for $f_\ell(\beta)$ are useful in showing the qualitative differences in the lift characteristics among the four cable models. In particular, the curves highlight the observation made in Figures 27 through 30 concerning the angle at which the maximum lift force is generated. As shown in Figure 33, the angle of maximum lift force for the cable models varies from 40 to 70 degrees. As noted in the lift force coefficient data, the 7 x 7 cable model shows a second peak at the lower angles. The shape of the loading functions differ significantly among the four cable models. It is not possible to generate a common lift force loading function as was done with the normal drag force. This serves to emphasize the important effect of geometry on the out-of-plane force generated by stranded cables. Table 8 presents the lift loading function coefficients for each cable model evaluated.

TABLE 8

HYDRODYNAMIC LIFT LOADING FUNCTION COEFFICIENTS
FOR THE FOUR CABLE MODELS

Cable Model	Coefficients $f_\ell(\beta) = A_o + A_1 \cos\beta + B_1 \sin\beta + A_2 \cos 2\beta + B_2 \sin 2\beta$				
	A_o	A_1	B_1	A_2	B_2
1 x 19	-7.0246	8.9808	5.0718	-1.9575	-2.2012
7 x 7	-29.7559	31.5478	27.9747	-1.7925	-11.9774
3 x 19	0.6240	0.3496	-1.5954	-0.9774	1.2234
4 x 7	-3.8616	3.0695	4.6514	0.7931	-0.6304

Although nonzero lift forces were measured at $\beta = 90$ degrees, the assumption that the loading function is zero at 90 degrees was maintained in order to derive the loading functions. It is well known that the direction of lift force changes as the relative angle to the flow exceeds 90 degrees. One explanation for nonzero lift force measurements is that at 90 degrees the experimental setup might have influenced the data; that is, perhaps the cable model was not at 90 degrees due to

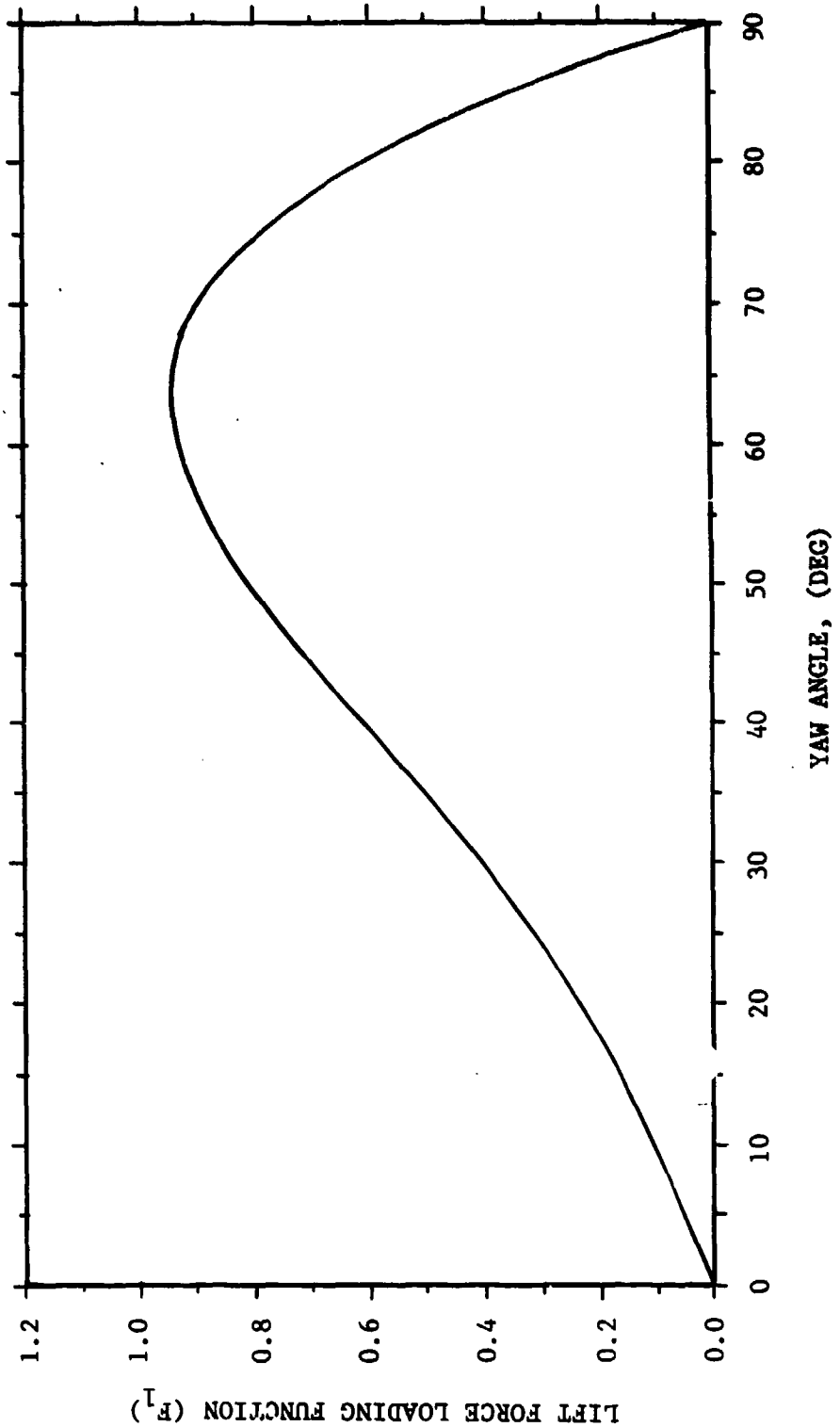

FIGURE 33(a). LIFT FORCE LOADING FUNCTION VERSUS CABLE YAW ANGLE
1 x 19 CABLE (SHEET 1 OF 4)

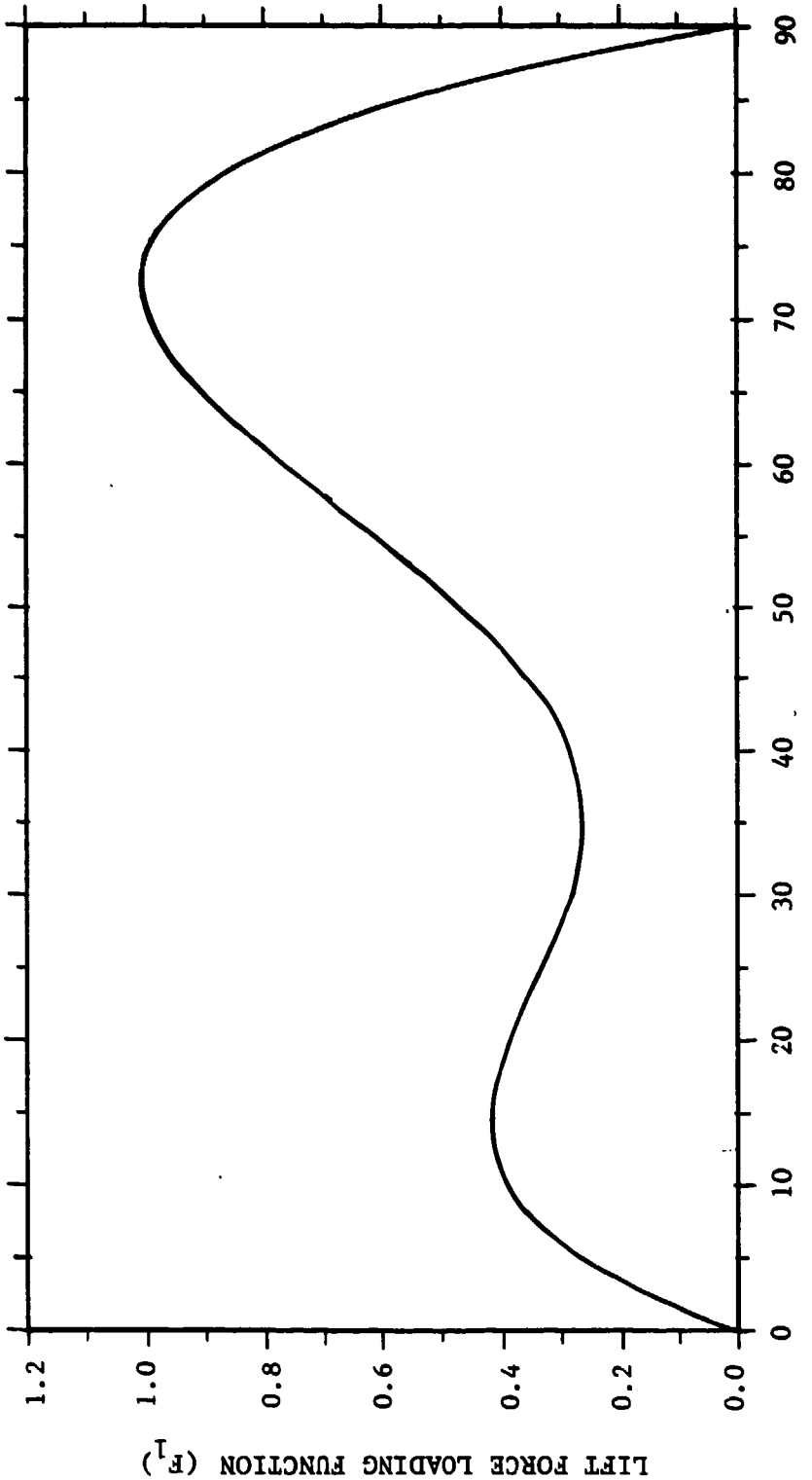

FIGURE 33(b). 7 x 7 CABLE (SHEET 2 OF 4)

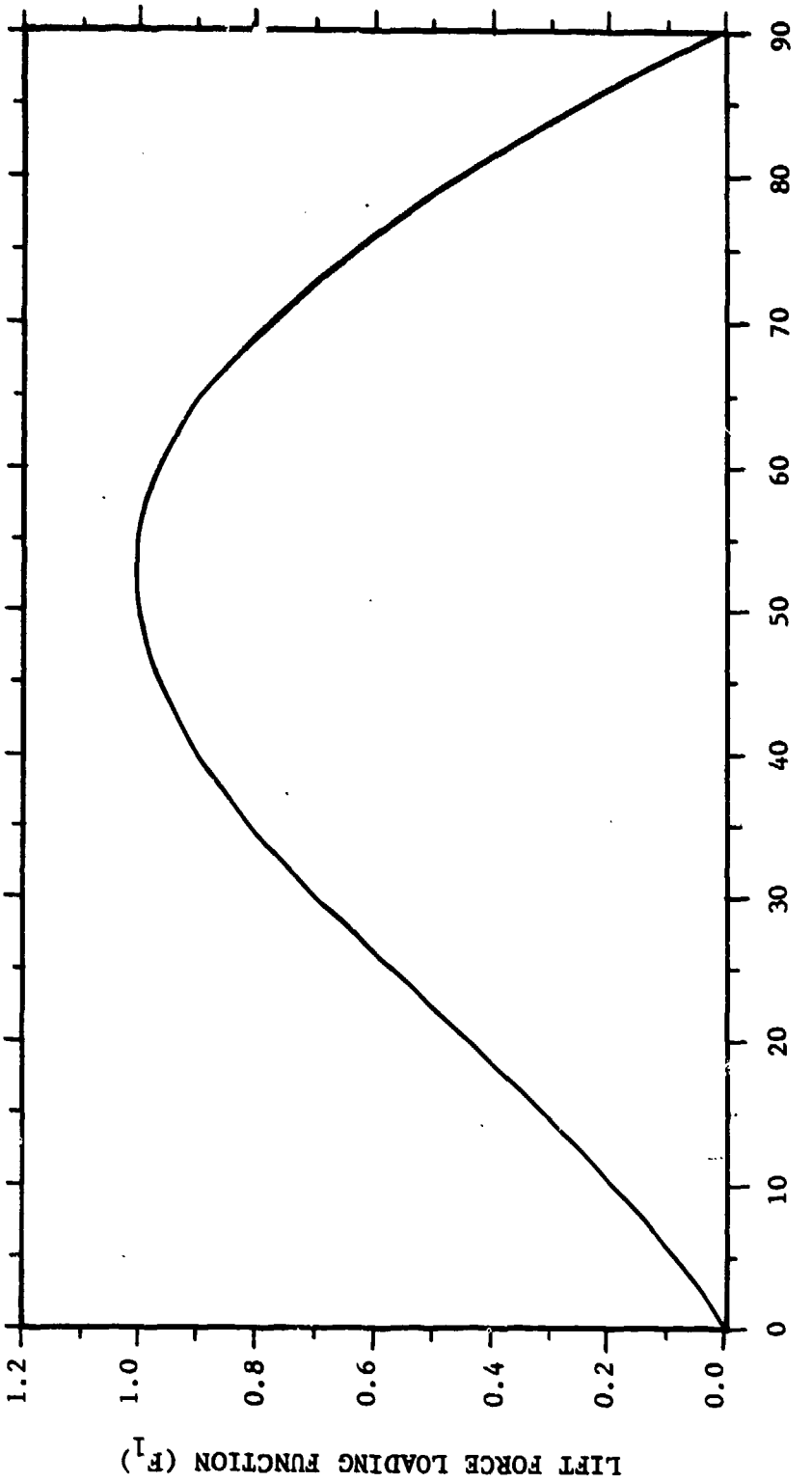

FIGURE 33(c). 3 x 19 CABLE (SHEET 3 OF 4)

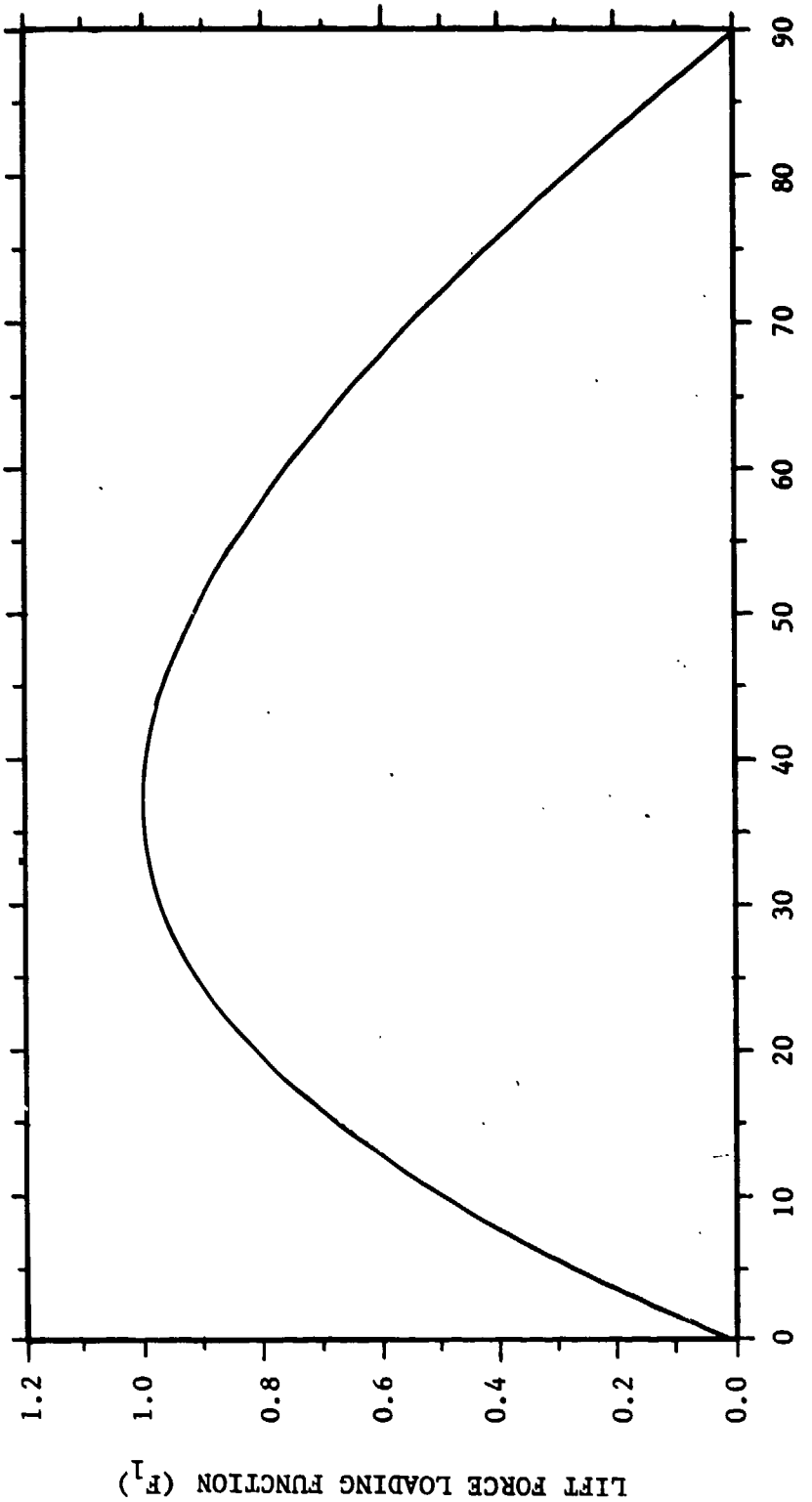

FIGURE 33(d). 4 x 7 CABLE (SHEET 4 OF 4)

strut flexure, misalignment, etc. Previous work using the same rig has indicated a lift force is produced at $\beta = 90$ degrees.[9] As previously discussed, the steady lift force data show scatter at all angles due to the large overlying fluctuating forces. That scatter might be reflected in the data measured at $\beta = 90$ degrees.

Tangential Drag

An initial analysis of the steady tensile (tangential drag) forces measured at the end of the cable model was performed. It was determined that the tensile data are not appropriate for use in determining tangential loading functions. The tangential drag measurements were influenced by the development of a shallow catenary in the cable model under tow caused by the normal drag force. As a consequence of the catenary the tensile force in the cable model increased as a function of the square of the velocity even for the 90-degree runs. In this configuration no tangential drag should be recorded if the entire length of the cable model is normal to the flow. The tensile forces have been reduced but no further analysis has been performed. Potential effects of the catenary shape on measured lift and normal drag have not been evaluated.

CABLE DYNAMIC PROPERTIES

Cable dynamic properties were measured with a single accelerometer pair located at the midspan of the cable. Another accelerometer pair, located at the quarterspan, is typically used to more accurately define the cable mode shape. Unfortunately, as mentioned before, only one accelerometer pair was available for this test.

This section presents a sample of the data collected by the midspan accelerometers. For each cable model, the cable frequency and acceleration were measured as a function of speed, yaw angle, and tension. The acceleration data were double integrated to estimate the amplitude at the midspan. Results presented below show the effect of speed, yaw angle, and tension on the dynamic properties of a cable. In addition, the effect of cable geometry is investigated by comparing accelerometer data of the four cable models. Two important dynamic quantities, the vortex shedding frequency and the cable natural frequency, are estimated to aid in the interpretation of the accelerometer data.

Vortex shedding frequency is typically measured using a hot-wire anenometer placed in the test sample wake. Since no measurements of the vortex shedding frequency were made in these tests, f_v is estimated using Equation (5). Figure 5 showed that for a circular cylinder the

[9] op. cit.

Strouhal number has a constant value of S ~ 0.2 over a wide range of Reynolds numbers, $10^3 < Re < 10^5$. Previous cable experiments have shown that the Strouhal number for cables does not vary significantly from the circular cylinder value.[13] Using the value of S = 0.20 the shedding frequency ranges from about 13 hertz at 2 knots to 64 hertz at 10 knots for a 5/8-inch cable normal to the flow. The shedding frequency is reduced as the yaw angle is decreased, varying as the sine of the angle.

Cable natural frequencies may be estimated with the taut string equation expressed in Equation (6), which has been shown to be accurate within 2 to 4 percent as applied to cables.[14] The calculated natural frequencies through the 12th mode are presented in Table 9 for the two tensions. High and low estimates of the frequency for each mode are given to account for variance of the cable model tension during the course of the experiments. As shown in the table, the fundamental frequencies vary from 5 to 7 hertz, while the 12th mode frequencies range from 55 to 84 hertz. The cable tension at the beginning and end of each test run can be found in Appendix A.

Predictions from Equations (5) and (6) are used to interpret the frequency data collected by the accelerometer. During lock-on Equation (6) is an accurate estimate of the cable frequency because the cable is vibrating at or near one of its natural frequencies. The vortices are forced to shed at the cable natural frequency; consequently, Equation (5) does not accurately predict a shedding frequency in this regime. Outside of the lock-on regime the cable is forced to vibrate at the vortex shedding frequency.

Effect of Geometry and Yaw Angle on Cable Dynamics

Both x- and y-amplitudes were estimated from the accelerometer data. Only the y-amplitude data is discussed in this section. The x-amplitude data is listed in Appendix B.

The y-amplitude of the cable model as a function of frequency is plotted in Figures 34 and 35. The cable amplitude is nondimensionalized by the diameter, and the frequency is expressed in nondimensional form as the reduced velocity, V/fD. Amplitudes for the low tension case are plotted in Figure 34(a). Two major features are shown by the data: as the yaw angle is increased the cable frequency also increases, and; the largest amplitudes, Y/D = 1.1, are associated with the two smallest yaw angles, β = 20 and 30 degrees. Amplitudes for β = 20 degrees correspond to the lowest frequencies, hence the highest reduced velocities (V/fD = 14). Increasing the yaw angle to β = 30 degrees groups the data about a lower reduced velocity of V/fD = 12. The grouping of the data

[13]Votaw, C. W. and O. M. Griffin, "Vortex Shedding from Smooth Cylinders and Stranded Cables," Journal of Basic Engineering, September 1971.

[14]Naval Research Laboratory Report 7821, "Some Transverse Resonant Vibration Properties of Wire Rope with Application to Flow-Induced Cable Vibrations," by S. E. Ramberg and O. M. Griffin, December 1974.

TABLE 9(a)

CALCULATED NATURAL FREQUENCIES FOR EACH CABLE MODEL
DURING LOW TENSION (T ~ 550 lb) RUNS
(Sheet 1 of 3)

Cable	Mode	Minimum Frequency (Hz)	Maximum Frequency (Hz)
1 x 19	1	5	5
1 x 19	2	9	10
1 x 19	3	14	15
1 x 19	4	18	20
1 x 19	5	23	25
1 x 19	6	28	30
1 x 19	7	32	35
1 x 19	8	37	40
1 x 19	9	42	45
1 x 19	10	46	50
1 x 19	11	51	55
1 x 19	12	55	60
7 x 7	1	5	5
7 x 7	2	11	11
7 x 7	3	16	16
7 x 7	4	21	22
7 x 7	5	26	27
7 x 7	6	32	33
7 x 7	7	37	38
7 x 7	8	42	44
7 x 7	9	47	49
7 x 7	10	53	55
7 x 7	11	58	60
7 x 7	12	63	65
3 x 19	1	5	6
3 x 19	2	11	12
3 x 19	3	16	17
3 x 19	4	21	23
3 x 19	5	27	29
3 x 19	6	32	35
3 x 19	7	37	41
3 x 19	8	42	46
3 x 19	9	48	52
3 x 19	10	53	58
3 x 19	11	58	64
3 x 19	12	64	69

TABLE 9(a)
(Sheet 2 of 3)

Cable	Mode	Minimum Frequency (Hz)	Maximum Frequency (Hz)
4 x 7	1	5	5
4 x 7	2	10	10
4 x 7	3	15	15
4 x 7	4	20	21
4 x 7	5	24	26
4 x 7	6	29	31
4 x 7	7	34	36
4 x 7	8	39	41
4 x 7	9	44	46
4 x 7	10	49	51
4 x 7	11	54	56
4 x 7	12	59	62

TABLE 9(b)

CALCULATED NATURAL FREQUENCIES FOR EACH CABLE MODEL
DURING HIGH TENSION (T ~ 850 lb) RUNS
(Sheet 2 of 3)

Cable	Mode	Minimum Frequency (Hz)	Maximum Frequency (Hz)
1 x 19	1	6	6
1 x 19	2	12	12
1 x 19	3	18	18
1 x 19	4	24	24
1 x 19	5	30	30
1 x 19	6	36	36
1 x 19	7	42	42
1 x 19	8	48	48
1 x 19	9	54	54
1 x 19	10	60	60
1 x 19	11	66	66
1 x 19	12	72	72

TABLE 9(b)
(Sheet 3 of 3)

Cable	Mode	Minimum Frequency (Hz)	Maximum Frequency (Hz)
7 x 7	1	6	7
7 x 7	2	13	13
7 x 7	3	19	20
7 x 7	4	26	27
7 x 7	5	32	33
7 x 7	6	38	40
7 x 7	7	45	47
7 x 7	8	51	54
7 x 7	9	58	60
7 x 7	10	64	67
7 x 7	11	71	74
7 x 7	12	77	80
3 x 19	1	7	7
3 x 19	2	13	14
3 x 19	3	20	21
3 x 19	4	27	28
3 x 19	5	33	35
3 x 19	6	40	42
3 x 19	7	47	49
3 x 19	8	54	56
3 x 19	9	60	63
3 x 19	10	67	70
3 x 19	11	74	77
3 x 19	12	80	83
4 x 7	1	6	6
4 x 7	2	12	12
4 x 7	3	18	19
4 x 7	4	24	25
4 x 7	5	30	31
4 x 7	6	36	37
4 x 7	7	43	44
4 x 7	8	49	50
4 x 7	9	55	56
4 x 7	10	61	62
4 x 7	11	67	68
4 x 7	12	73	75

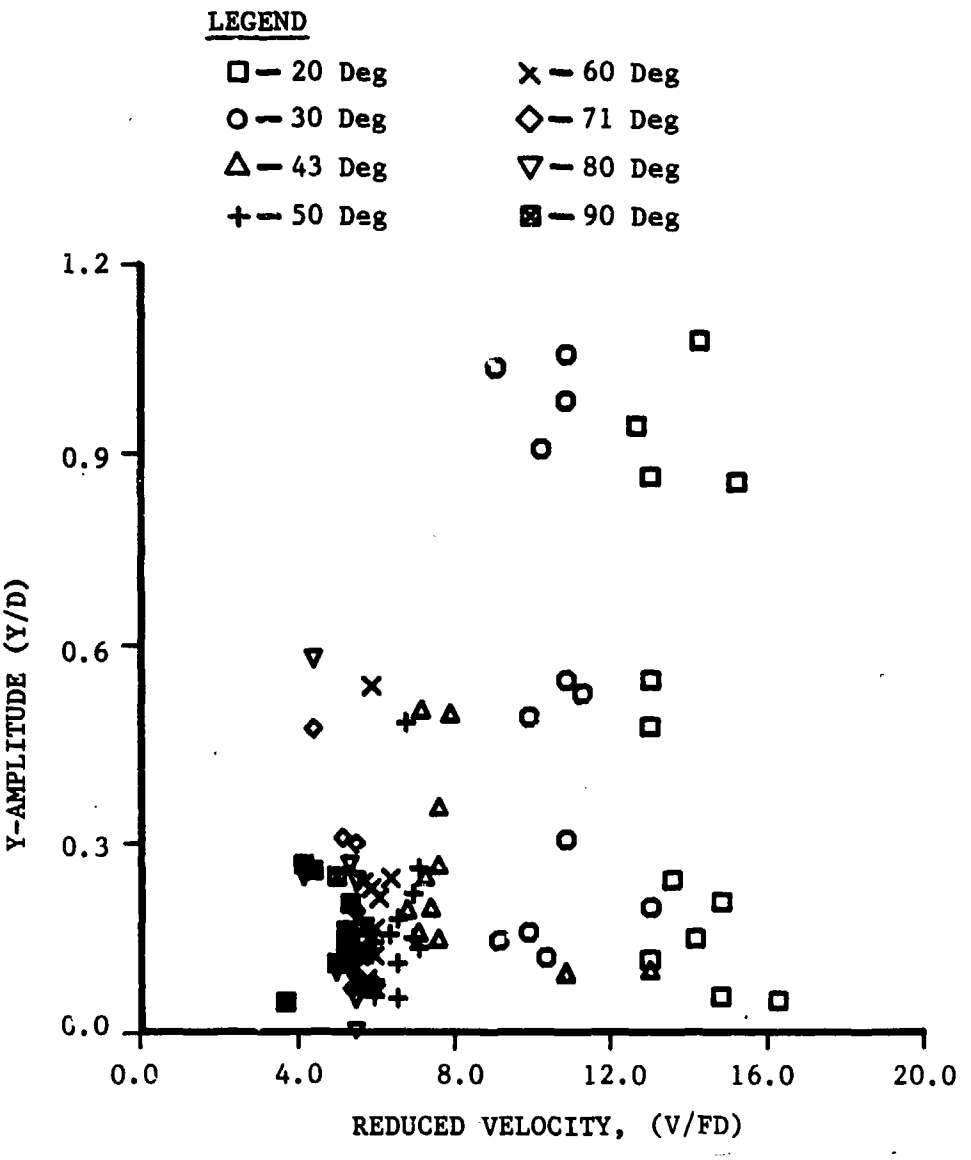

FIGURE 34(a). MEASURED Y-AMPLITUDE AT CABLE MIDSPAN VERSUS REDUCED VELOCITY - LOW TENSION (Sheet 1 of 2)

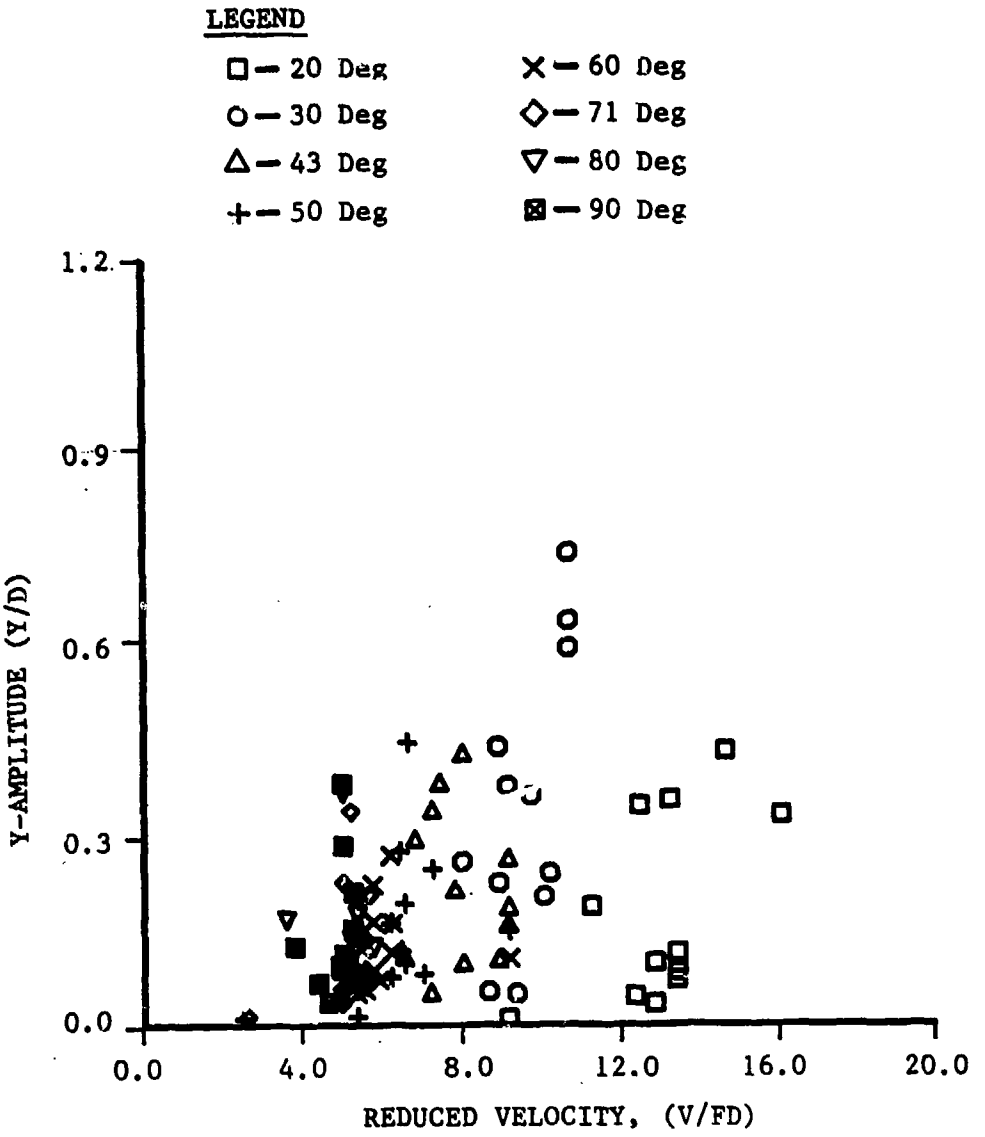

FIGURE 34(b). HIGH TENSION (Sheet 2 of 2)

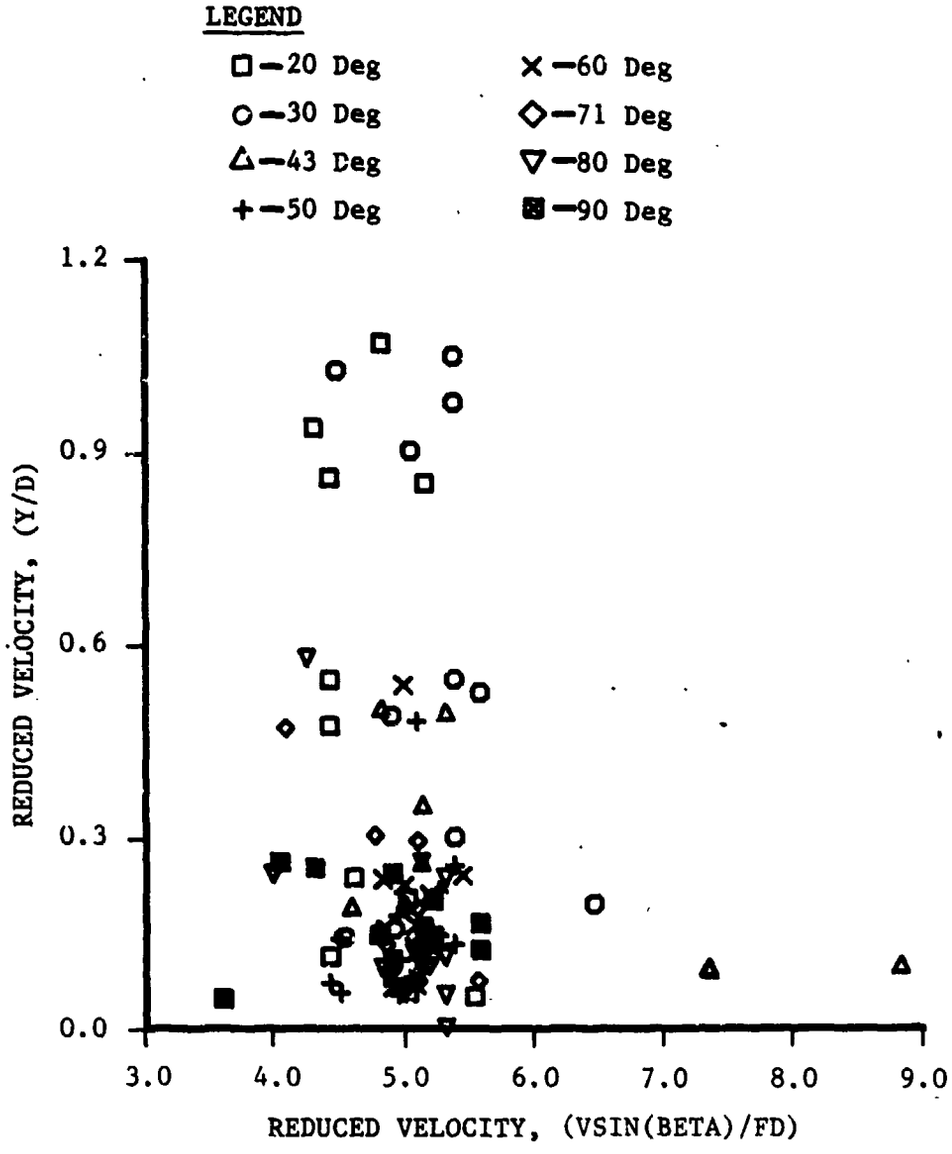

FIGURE 35(a). MEASURED Y-AMPLITUDE AT CABLE MIDSPAN VERSUS REDUCED VELOCITY BASED ON NORMAL VELOCITY COMPONENT LOW TENSION (Sheet 1 of 2)

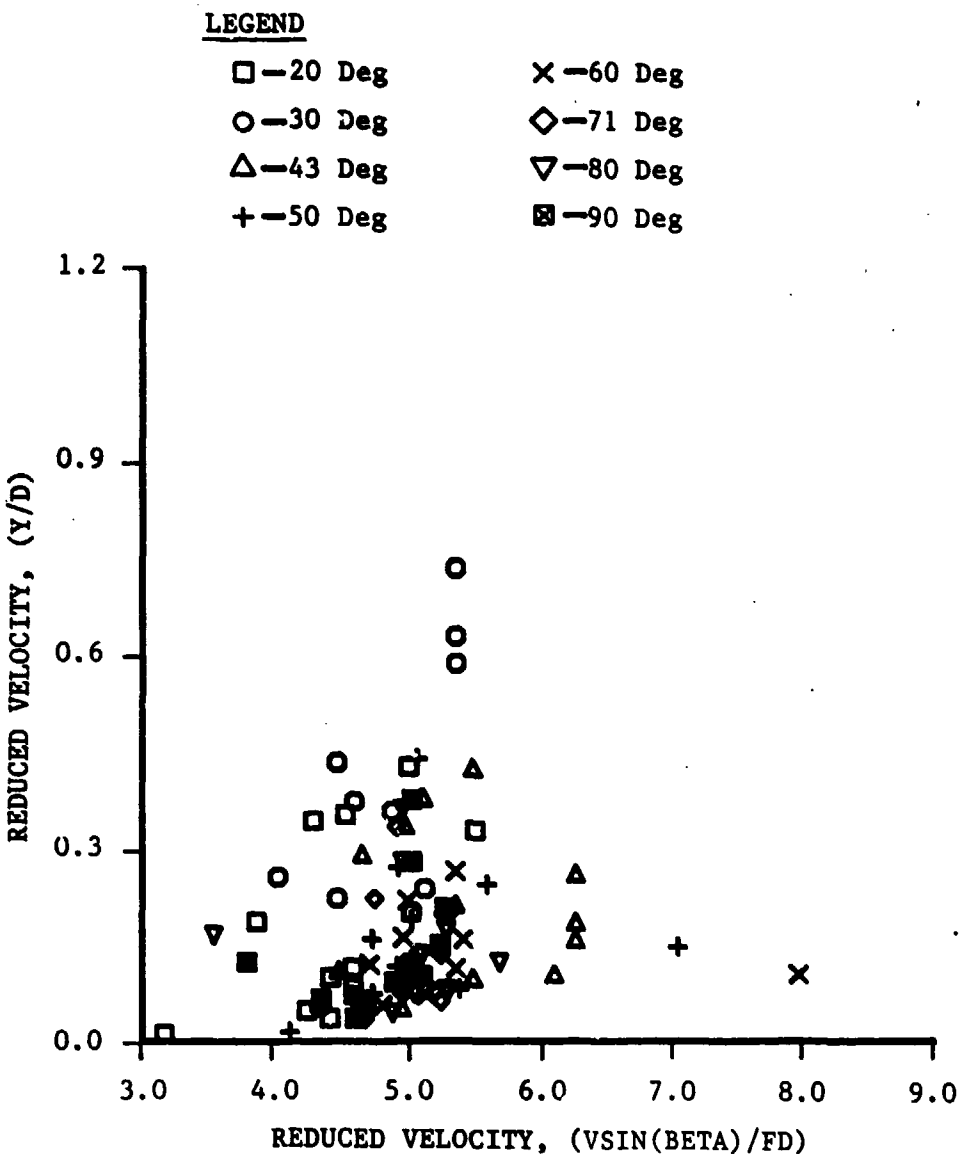

FIGURE 35(b). HIGH TENSION (Sheet 2 of 2)

about smaller reduced velocities for increasing yaw angle is still apparent for $43° < \beta < 90°$, although these data show less of an effect due to yaw angle. Amplitudes in this range of angles are centered about a reduced velocity of 5.0 to 6.0, and the maximum Y/D is 0.6.

In Figure 34(b) y-amplitude data are plotted versus reduced velocity for the high tension case. The systematic effect of yaw angle is similar to that observed for the low tension case of Figure 34(a). However, smaller and more uniform maximum amplitudes are observed for the higher tension. Except for the 30-degree data, the maximum amplitudes do not exceed Y/D = 0.45 and are insensitive to yaw angle variations.

The effect of yaw angle on the amplitude data can be explained by the Independence Principle. Recall that the Independence Principle predicts that the maximum vortex shedding frequency occurs at $\beta = 90$ degrees, and then decreases as the sine of the yaw angle (Equation (5)). Since f_v is the forcing function which causes the cable to vibrate, the relatively high shedding frequencies at large yaw angles excite high cable frequencies and the associated high mode shapes. Similarly, at small angles the reduced shedding frequencies excite the lower mode shapes. This explains the grouping of the data as a function of reduced velocity and the larger amplitudes at small yaw angles.

From the Independence Principle improved scaling of the y-amplitude data can be achieved by using the reduced velocity based on the normal velocity component. This is shown in Figure 35. For both tensions the y-amplitude data fall within a relatively narrow band of reduced velocities, $4.0 < \frac{V \sin \beta}{fD} < 5.5$. The effect of yaw angle has been removed, confirming the success of the Independence Principle in scaling the data.

Next considered is the effect of cable geometry on the amplitude and frequency characteristics. The shape of the cable in the cross-flow plane affects the vortex shedding from the cable and, therefore, influences the vibration of the cable. The cross-sectional geometries of the cable models were compared in Figure 13. Of the five cable models tested, the 1 x 19 is the smoothest (i.e., most nearly circular) and the 4 x 7 serrated is the roughest. Results for these two cables are presented in Figures 36 and 37 to show geometry effects on the cable dynamics.

Figure 36 compares y-amplitudes versus yaw angle for the 1 x 19 and 4 x 7 cables at low tension. As previously shown in Figure 34 the highest amplitudes are observed at small angles. The maximum amplitude for the 4 x 7 cable, Y/D = 1.6, is 60 percent higher than that for the smoother 1 x 19 cable. The amplitudes for both cables are sensitive to speed variation, although no systematic effect due to speed is apparent. High tension results are shown in Figure 37. The maximum Y/D for the 4 x 7 cable is reduced from 1.6 for low tension to approximately 1.0,

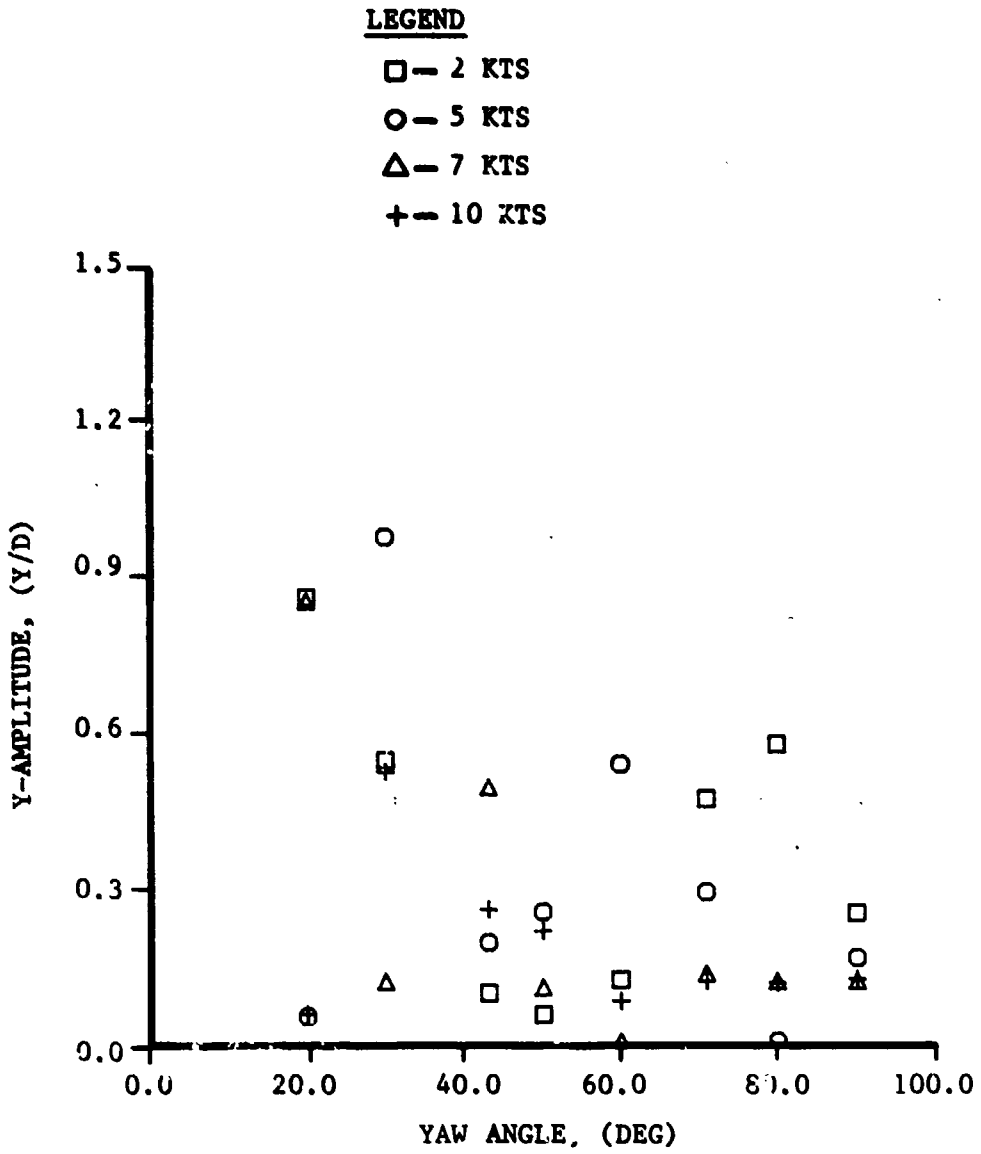

FIGURE 36(a). MEASURED Y-AMPLITUDE AT CABLE MIDSPAN VERSUS YAW ANGLE FOR THE 1 x 19 AND 4 x 7 CABLE MODELS AT LOW TENSION
1 x 19 CABLE (Sheet 1 of 2)

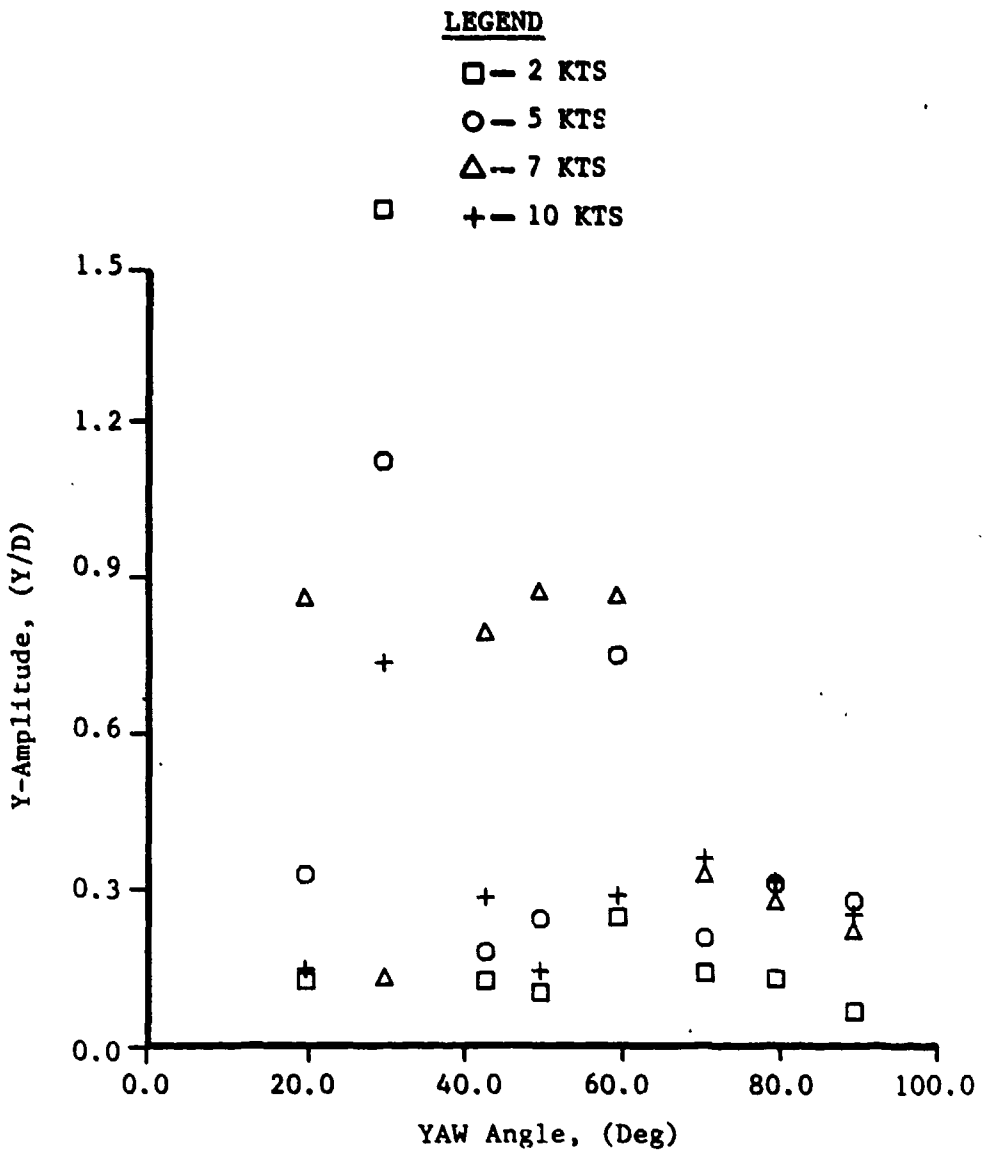

FIGURE 36(b). 4 x 7 CABLE (Sheet 2 of 2)

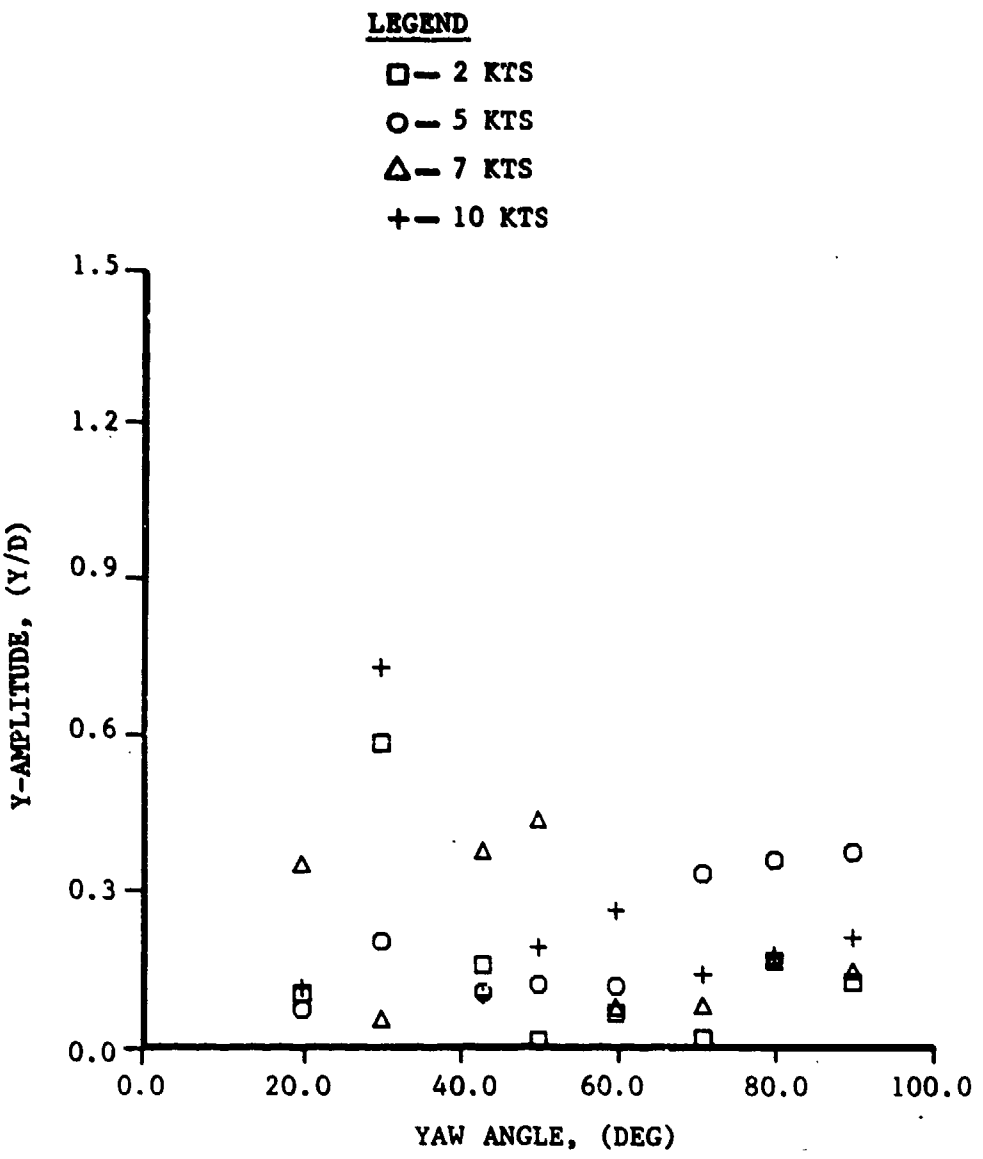

FIGURE 37(a). MEASURED Y-AMPLITUDE AT CABLE MIDSPAN VERSUS YAW ANGLE FOR THE 1 x 19 AND 4 x 7 CABLE MODELS AT HIGH TENSION
1 x 19 CABLE (Sheet 1 of 2)

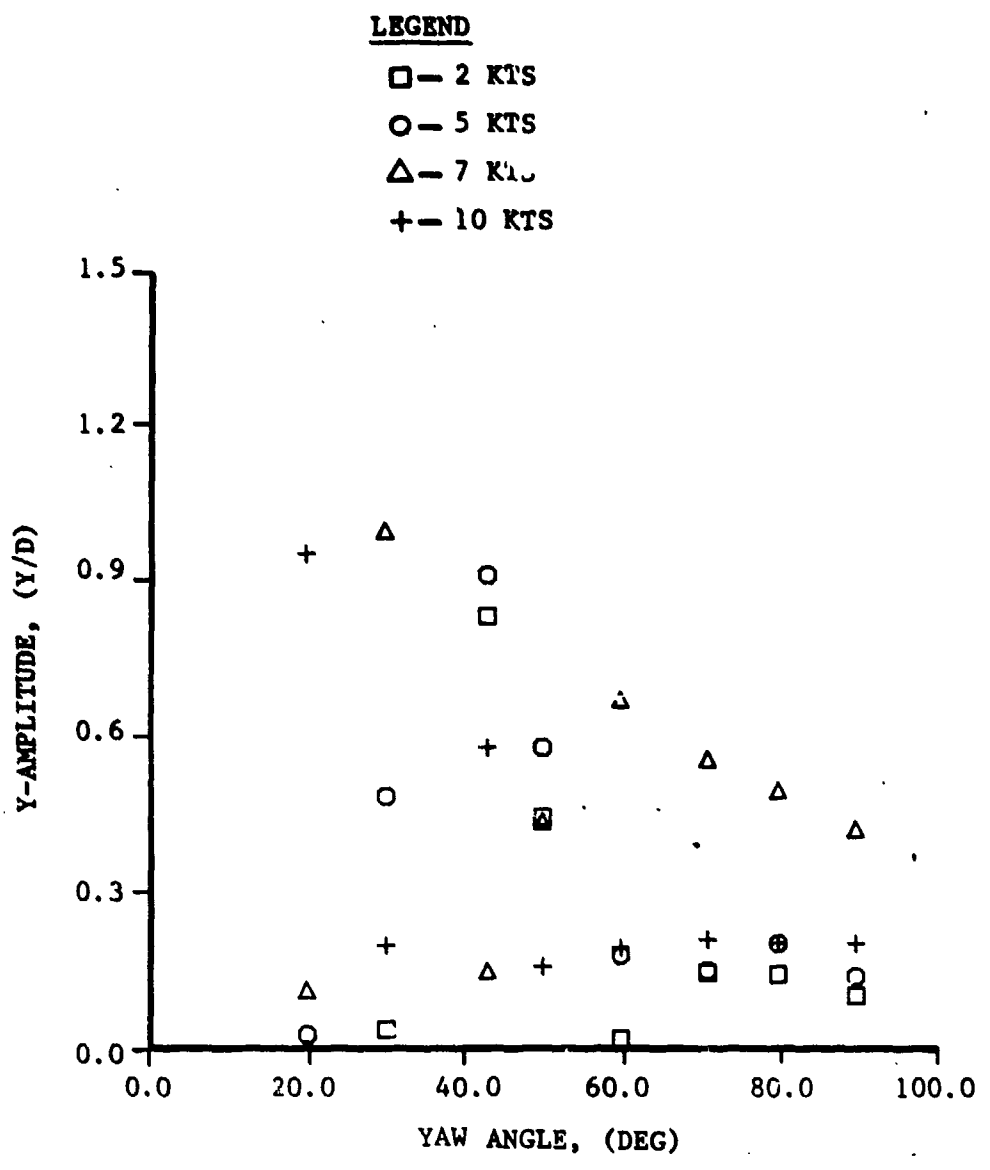

FIGURE 37(b). 4 x 7 CABLE (Sheet 2 of 2)

while the maximum amplitude for the 1 x 19 cable is less affected by the increased tension. The results of Figures 36 and 37 indicate that the smoother 1 x 19 cable develops a smaller maximum amplitude in comparison with the rougher 4 x 7 cable. In addition, the effect of speed (i.e., Reynolds number) is shown to be significant.

Lock-On Effects

All of the frequency data showed evidence of the lock-on phenomenon. Typical results are shown in Figure 38. Measured frequencies are plotted as a function of yaw angle for two cable models, 1 x 19 and 4 x 7, at low tension. At the lowest test speed of 2 knots, both cable models vibrate at their fundamental frequency for small yaw angles. The 1 x 19 cable shifts to the second mode for intermediate yaw angles, and to the third mode at the highest angles. For speeds greater than 2 knots lock-on is more difficult to detect, because higher mode shapes are excited at the increased tow speeds. The 10-degree spacing between measurements and the consistency of the cable tension are not sufficient to resolve the lock-on plateaus at these speeds.

The full set of cable frequency data is presented in Figures 39 and 40. The frequency data are nondimensionalized to create a cable Strouhal number, fD/V, where f corresponds to the cable frequency. In contrast the "true" Strouhal number is defined as the nondimensional vortex shedding frequency, $f_v D/V$. Since f_v was not measured in the cable strumming tests, the true Strouhal number is estimated using the vortex shedding frequency predicted by Equation (5). This equation is shown as the curve in Figures 39 and 40. It corresponds to the predicted Strouhal number for a nonvibrating yawed circular cylinder with S = 0.2.

Figure 39 shows nondimensional cable frequencies for the low tension case. Low tension frequencies for the 1 x 19 cable are shown in Figure 39(a). Except for the 2-knot case good scaling of the data is observed, with the cable Strouhal numbers in good agreement with the predicted values. The scatter in the 2-knot data is consistent with the lock-on effect discussed in Figure 38. At this speed the cable forces the vortex wake at the cable natural frequency over a relatively wide range of yaw angles. This produces a large deviation from the predicted vortex shedding frequency. At higher speeds the cable frequency more closely follows the shedding frequency because the lock-on plateaus are relatively smaller. Similar results are shown in Figures 39(b) and 39(c) which correspond to the 7 x 7 and the 3 x 19 cable models, respectively. The measured frequencies for the 4 x 7 cable, Figure 39(d), are consistently higher than the predicted values. The measured and predicted Strouhal numbers differ by roughly 10 percent. At present there is no evidence to suggest a bias error in the 4 x 7 frequency data that could explain this result. Therefore, the cross-section geometry of the 4 x 7 cable may alter the vortex wake such that higher cable frequencies are excited.

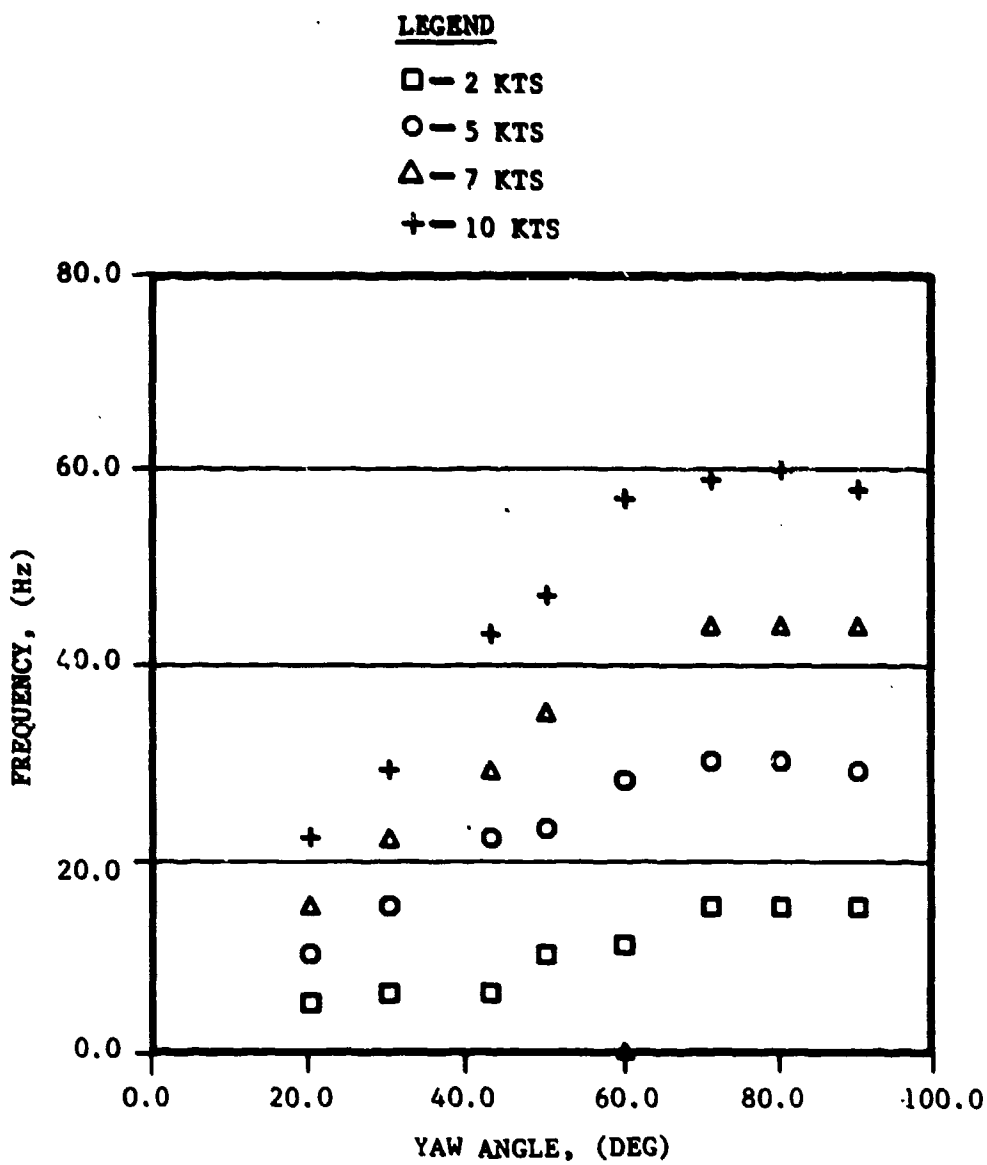

FIGURE 38(a). MEASURED CABLE FREQUENCY VERSUS YAW ANGLE FOR THE 1 x 19 AND 4 x 7 CABLE MODELS AT LOW TENSION
1 x 19 CABLE (Sheet 1 of 2)

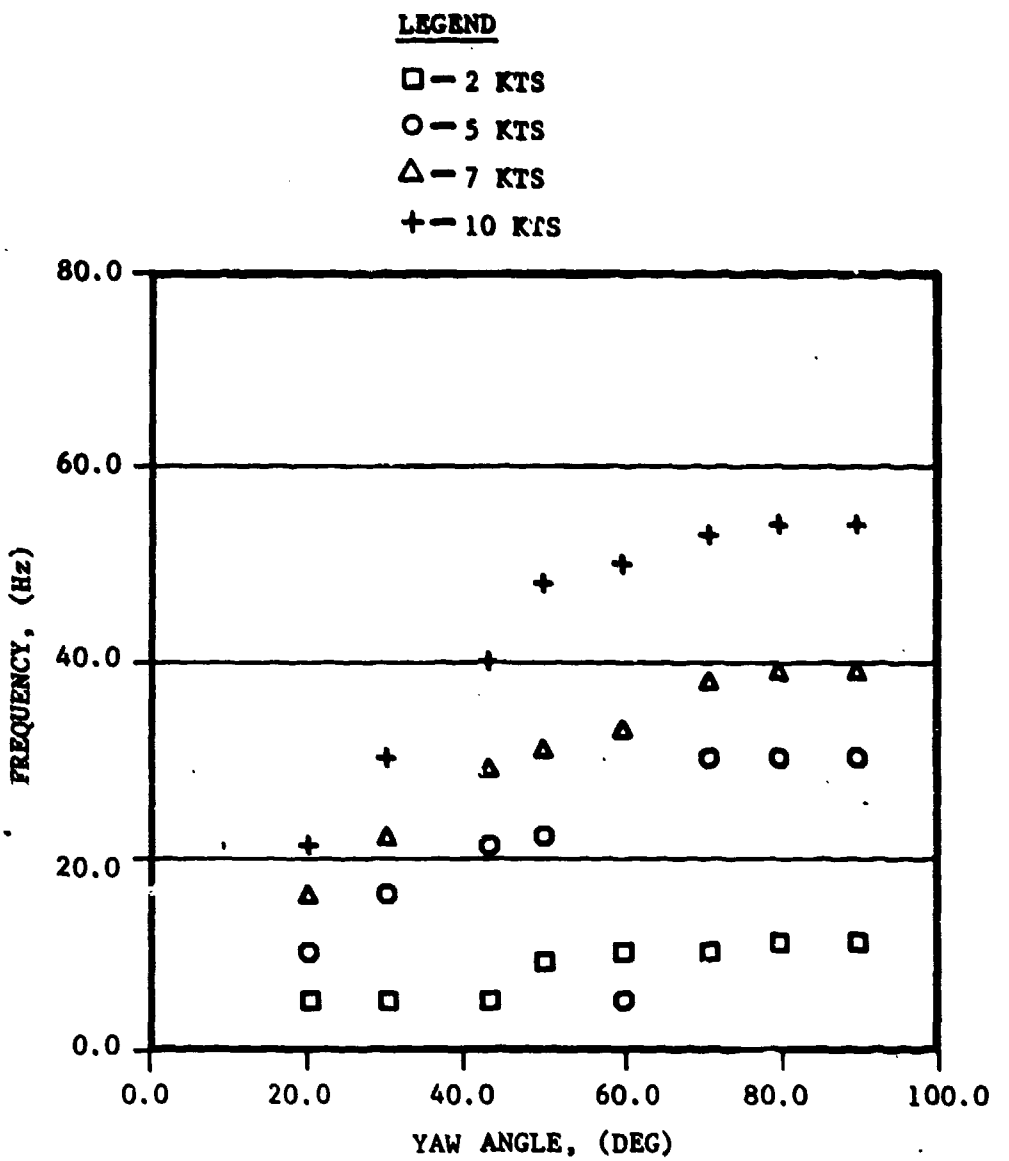

FIGURE 38(b). 4 x 7 CABLE (Sheet 2 of 2)

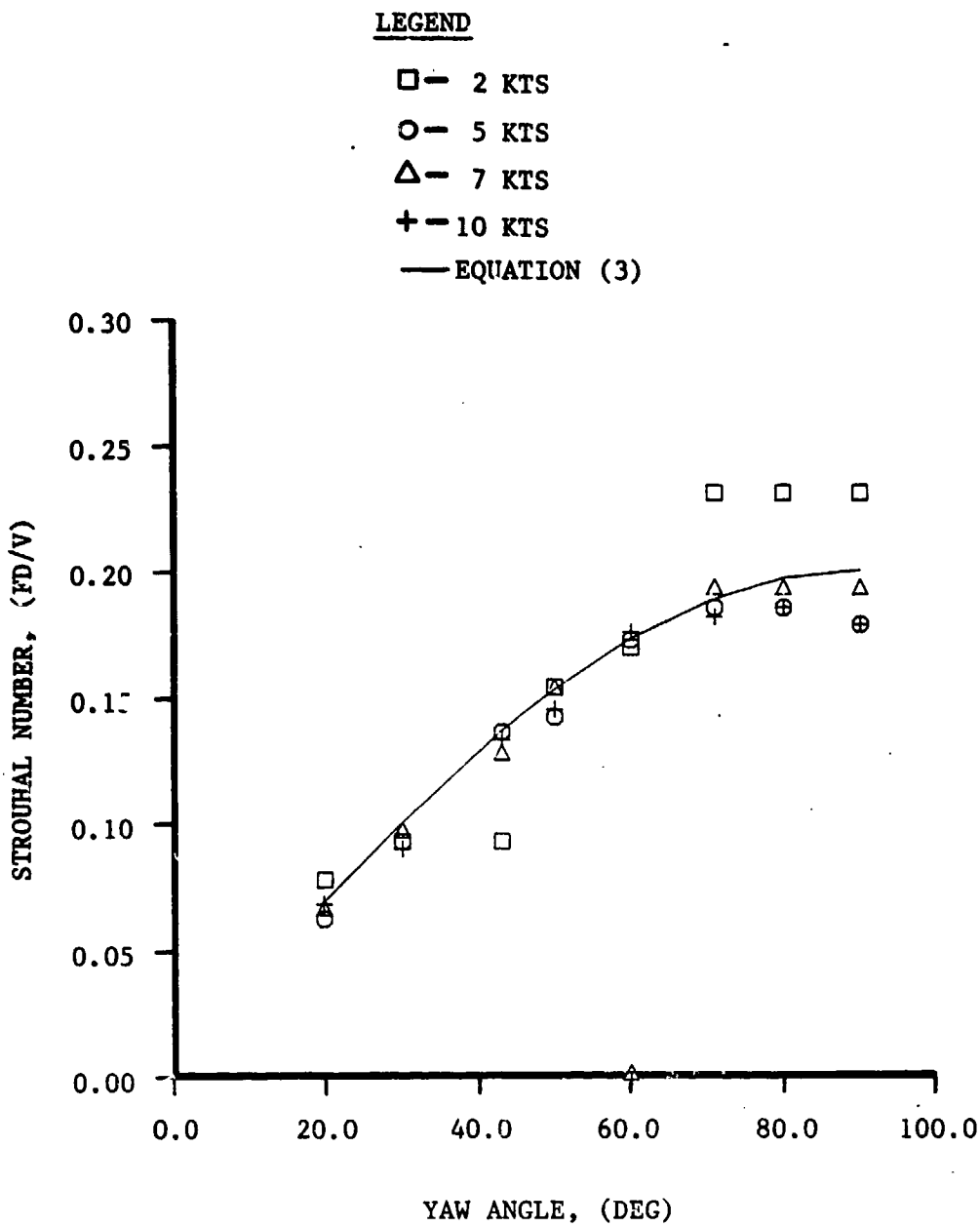

FIGURE 39(a). COMPARISON OF MEASURED CABLE STROUHAL NUMBERS AND PREDICTED STROUHAL NUMBERS VERSUS YAW ANGLE AT LOW TENSION 1 x 19 CABLE (Sheet 1 of 4)

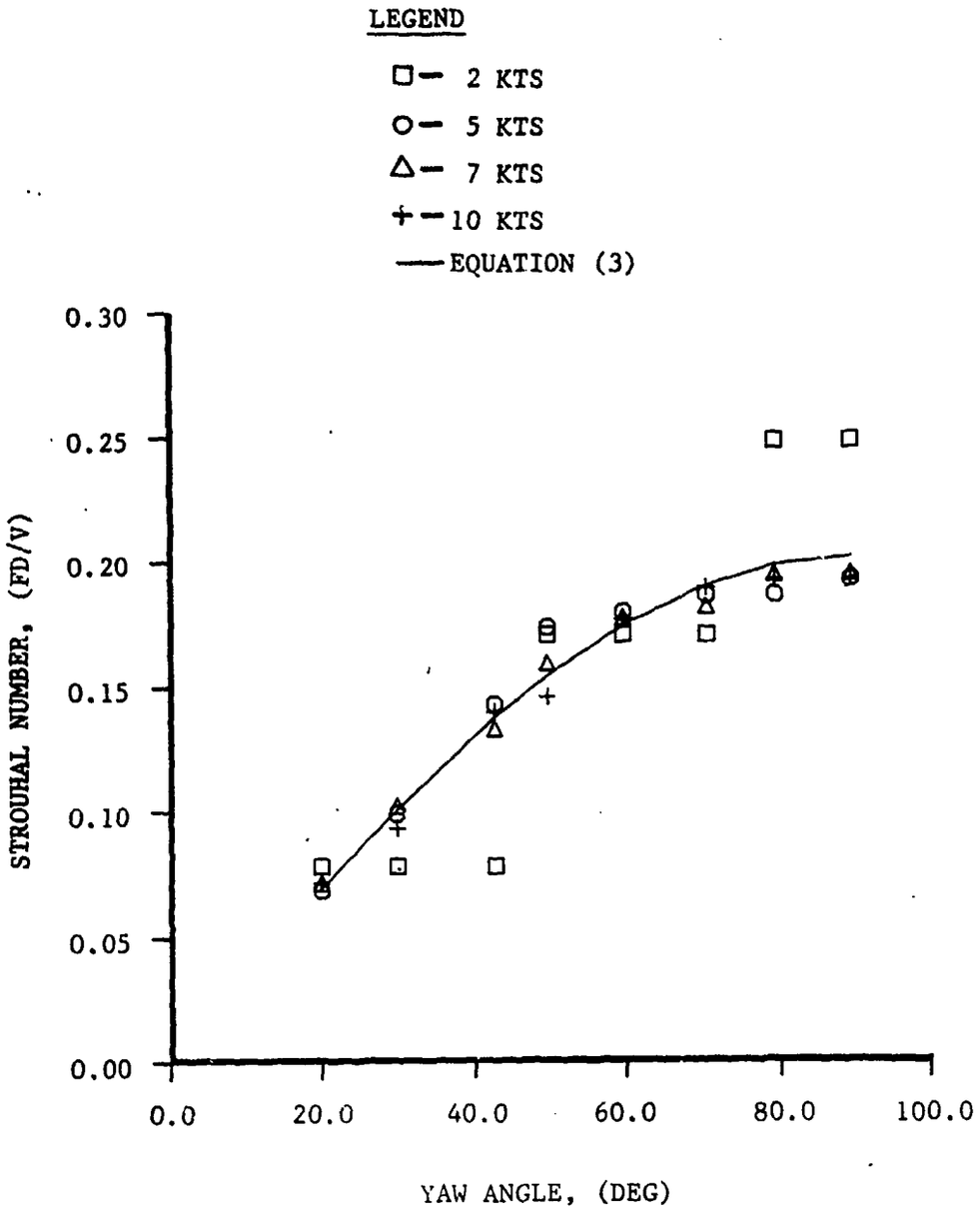

FIGURE 39(b). 7 x 7 CABLE (Sheet 2 of 4)

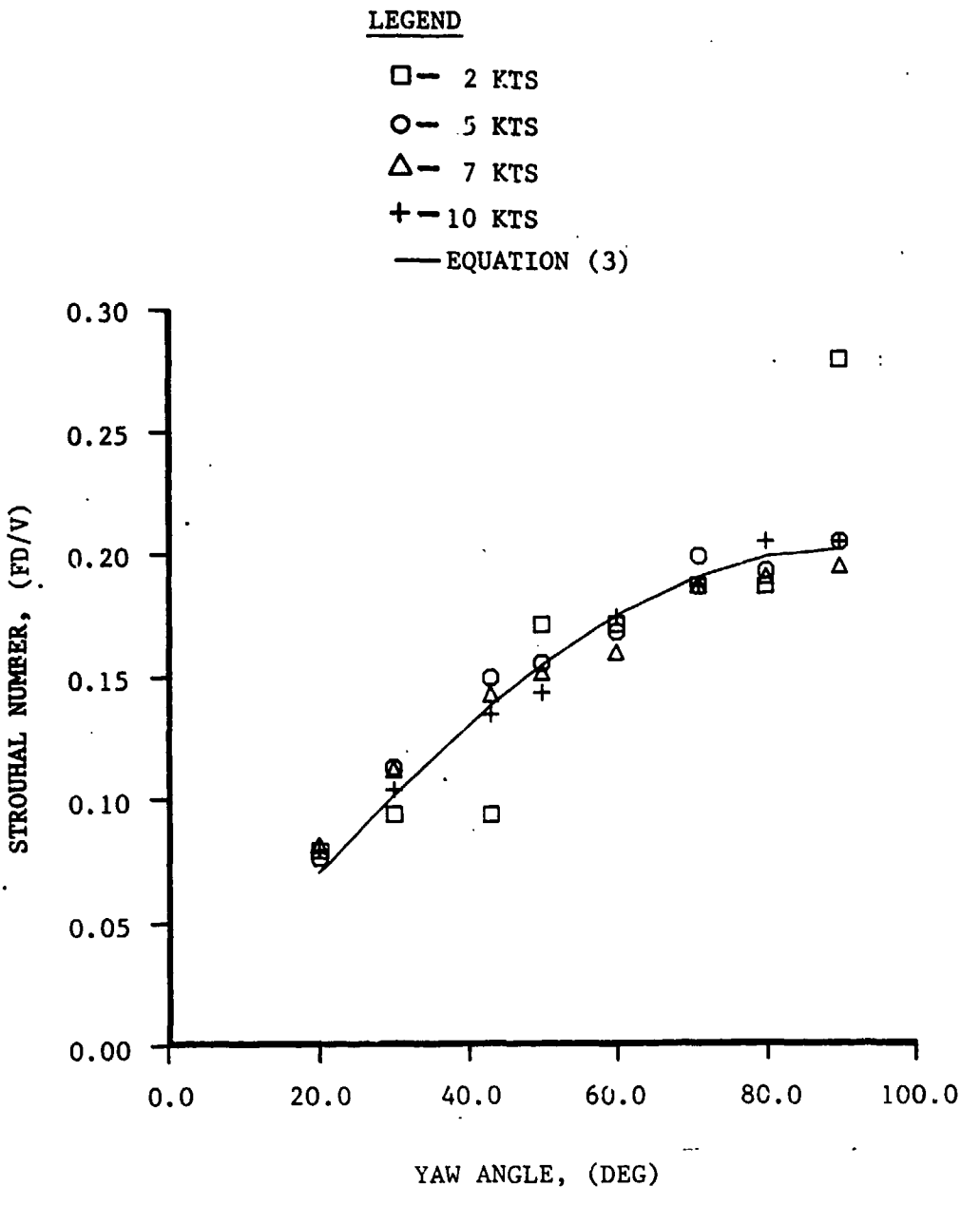

FIGURE 39(c). 3 x 19 CABLE (Sheet 3 of 4)

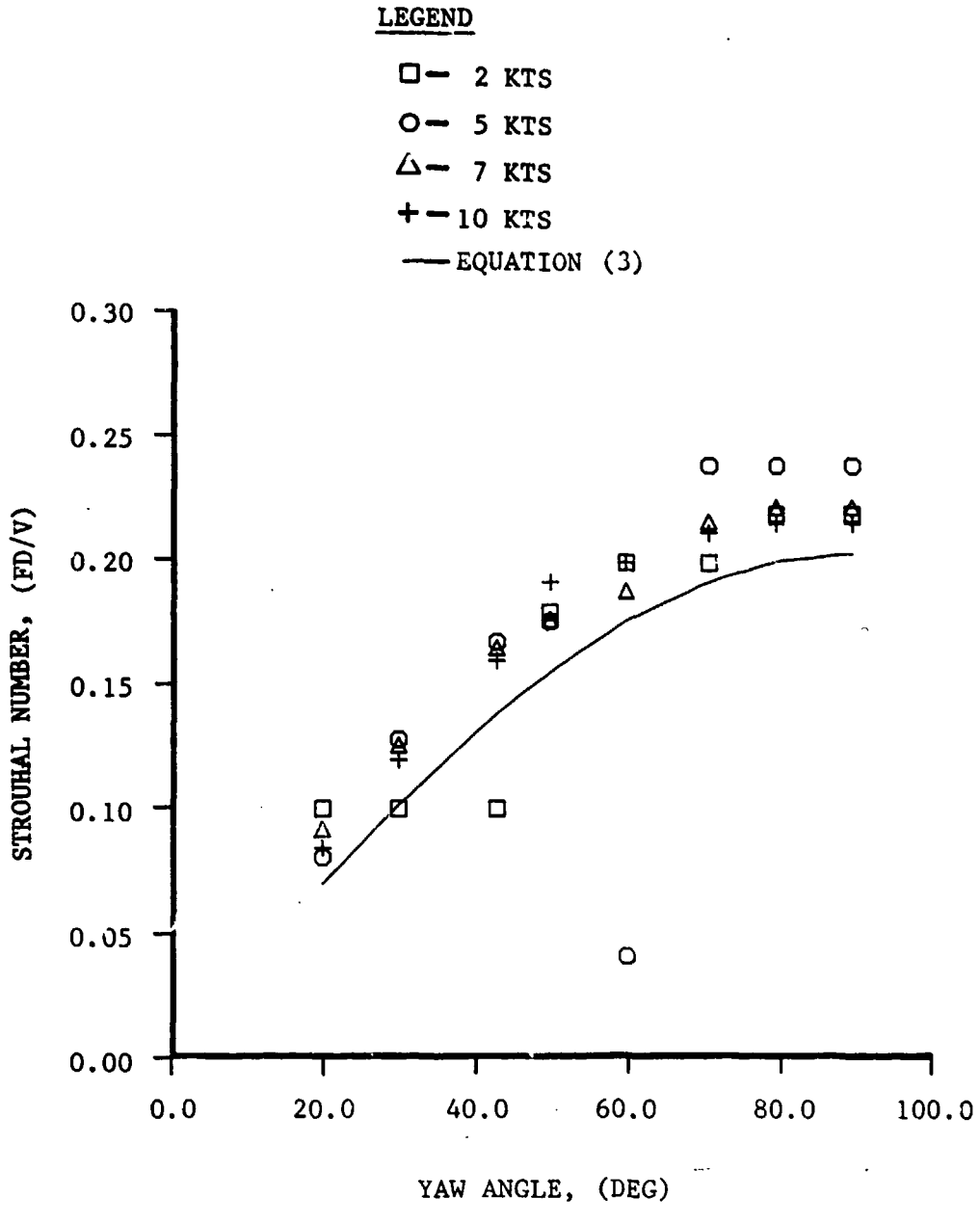

FIGURE 39(d). 4 x 7 CABLE (Sheet 4 of 4)

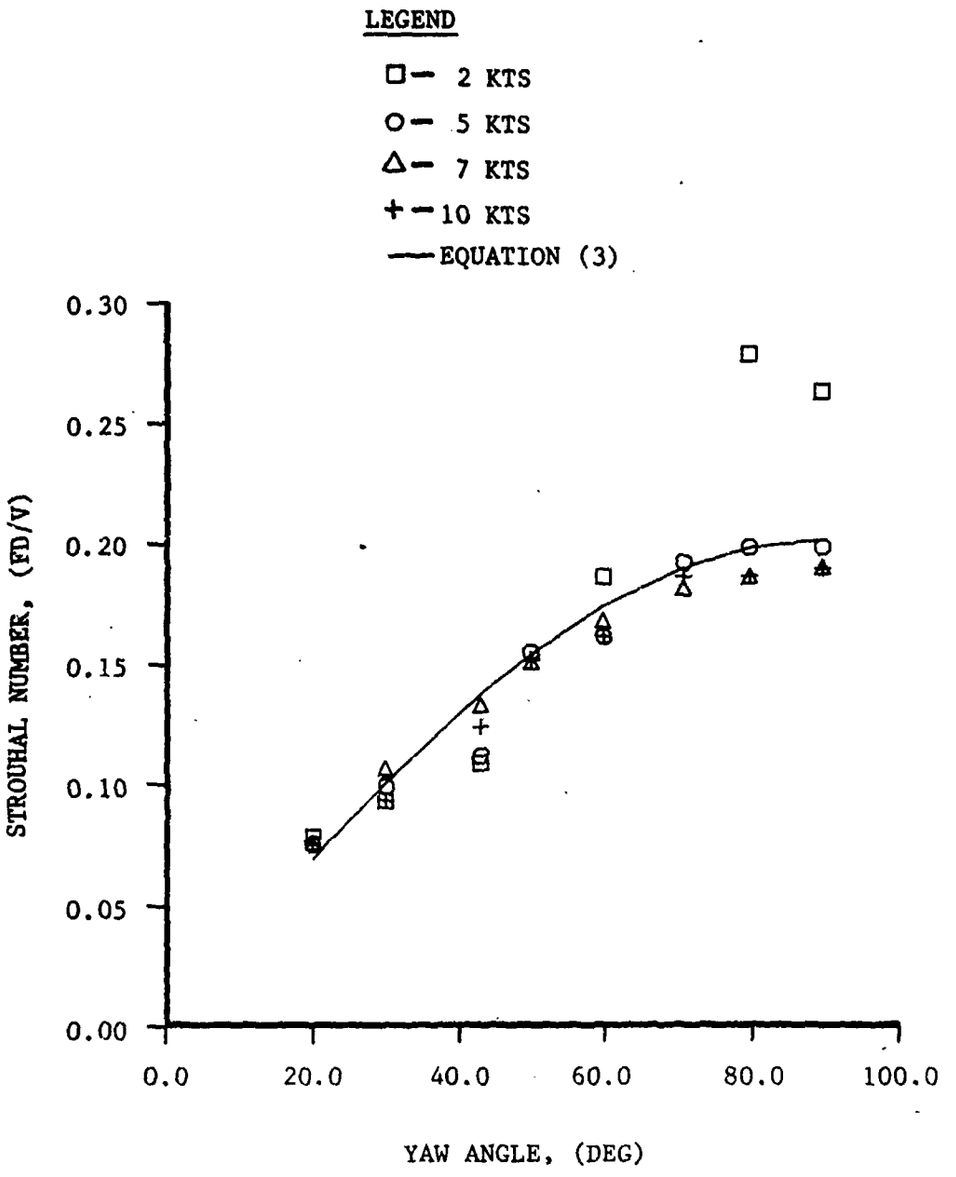

FIGURE 40(a). COMPARISON OF MEASURED CABLE STROUHAL NUMBERS AND PREDICTED STROUHAL NUMBERS VERSUS YAW ANGLE AT HIGH TENSION 1 x 19 CABLE (Sheet 1 of 4)

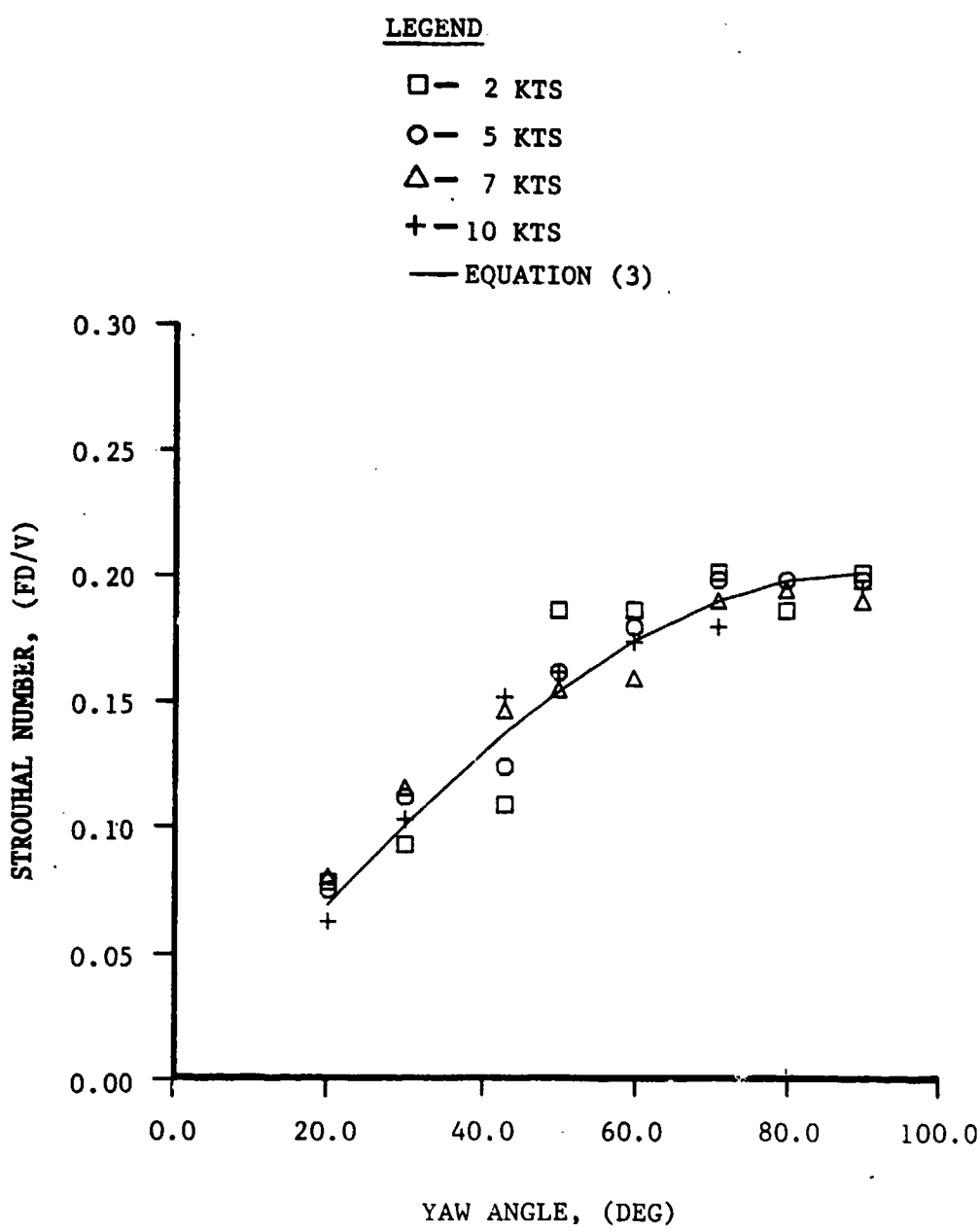

FIGURE 40(b). 7 x 7 CABLE (Sheet 2 of 4)

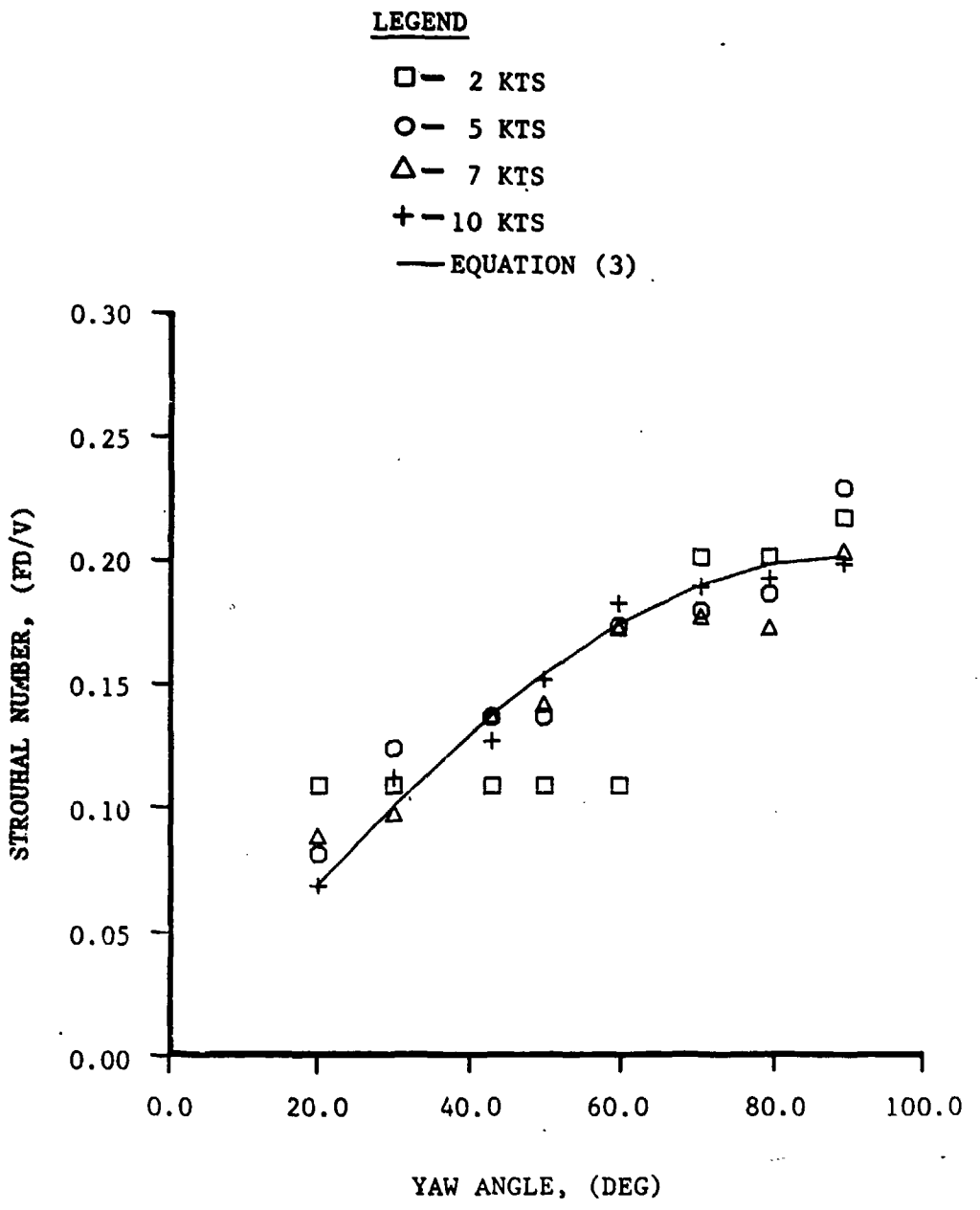

FIGURE 40(c). 3 x 19 CABLE (Sheet 3 of 4)

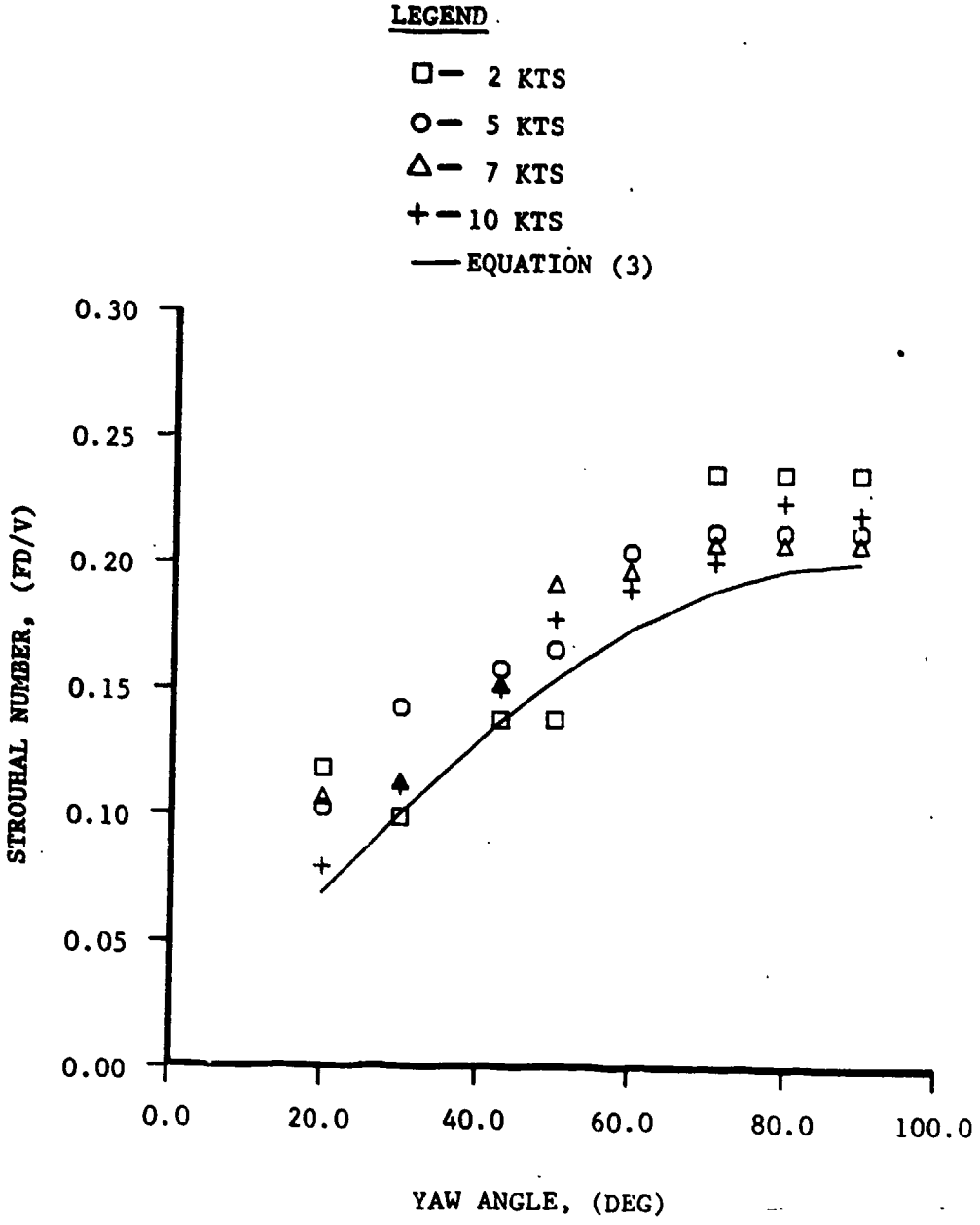

FIGURE 40(d). 4 x 7 CABLE (Sheet 4 of 4)

Figure 40 shows nondimensional cable frequencies for the high tension case. The cable natural frequencies for high tension are increased by about 20 percent over the low tension case. This difference is not sufficient to change the conclusions drawn in Figure 39. The distribution of nondimensional cable frequencies about the theory curve is generally similar to the results for the low tension case.

Effect of Geometry and Velocity on Cable Strouhal Number

Cable Strouhal numbers are plotted versus speed in Figure 41 for the cables normal to the flow, $\beta = 90$ degrees. The speed range of 2 to 10 knots corresponds to Reynolds numbers of $1.6 \times 10^4 < Re < 8.0 \times 10^4$. Again, the effect of lock-on is evident at the lowest speed. For both tensions the highest cable Strouhal numbers are observed at 2 knots. At this speed the average Strouhal number is $S = 0.24$. Values for the higher speeds are roughly centered about $S = 0.20$. Table 10 lists the cable Strouhal numbers at $\beta = 90$ degrees averaged for the speeds of 5, 7, and 10 knots. As noted previously the 1 x 19 cable has the smoothest, or most nearly circular cross section. The 4 x 7 has the roughest cross section, and the 7 x 7 and 3 x 19 cables have cross sections of intermediate roughness. This table shows that the cable Strouhal numbers vary from a low of $S = 0.18$ for the 1 x 19 cable to a high value of $S = 0.22$ for the 4 x 7 cable. The cable Strouhal numbers for $\beta = 90$ degrees show an apparent systematic effect due to cable geometry. Yet the effect does not seem too significant since the average Strouhal numbers of Table 10 are within 10 percent of $S = 0.2$, which is the circular cylinder value.

CONCLUSIONS

Five wire ropes were tested for their drag, lift, and strum properties using the DTNSRDC rotatable twin strut assembly. The wire ropes investigated were of five constructions: 1 x 19, 7 x 7, 3 x 19, 4 x 7 serrated, and 6 x 25 lang lay. The test rig was suitable for measuring the steady and unsteady normal drag and lift forces and strum accelerations on the cable models. Another test method is required in order to determine accurate tangential drag measurements. The 1 x 19, 7 x 7, 3 x 19, and 4 x 7 ropes were tested at four speeds, two tensions, and eight angles. The data from these four ropes were used to determine lift and drag coefficients, lift and drag loading functions, and strum properties. The 6 x 25 lang lay rope was tested at two speeds, two tensions, and three angles. The data from this rope was used to determine its drag coefficient only. The test Reynolds number range based on model diameter was approximately $10^4 < Re < 10^5$.

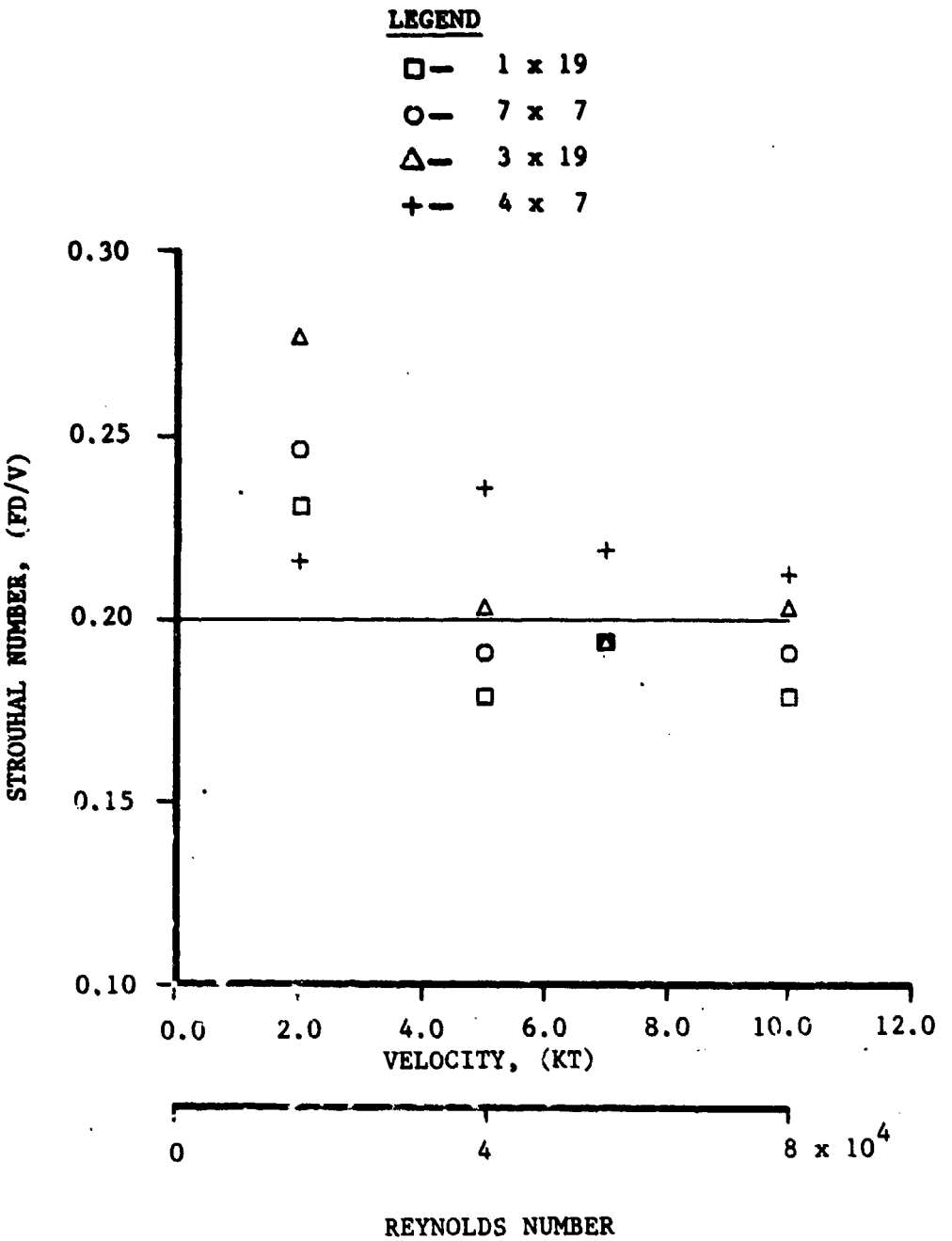

FIGURE 41(a). CABLE STROUHAL NUMBER VERSUS VELOCITY AT β = 90 DEGREES LOW TENSION (Sheet 1 of 2)

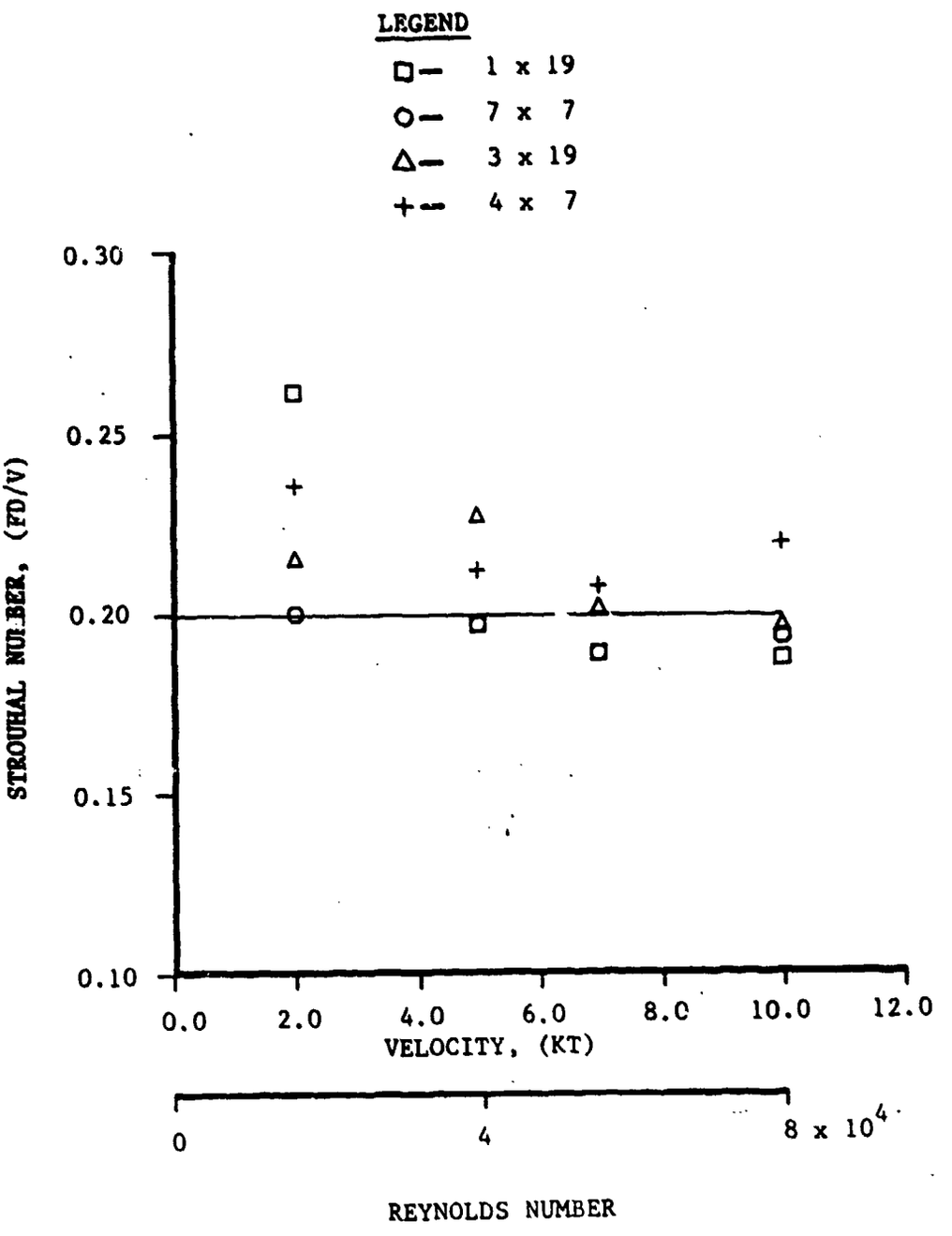

FIGURE 41(b). HIGH TENSION (Sheet 2 of 2)

TABLE 10

AVERAGE CABLE STROUHAL NUMBERS FOR V = 5, 7, 10 KNOTS
AT β = 90 DEGREES

Cable	Low Tension fD/V @ 90°	High Tension fD/V @ 90°
1 x 19	0.18	0.19
7 x 7	0.19	0.19
3 x 19	0.20	0.21
4 x 7	0.22	0.21

LOADING FUNCTIONS

Using this rig, the measured steady drag forces were much larger than the measured unsteady drag forces. The four wire ropes analyzed displayed similar normal drag characteristics and as a result a common drag coefficient and loading function can be used to predict normal drag on these four cables within the Reynolds number range. Normal drag loading functions were determined for each cable and a common loading function was developed:

1 x 19: $f_n(\beta) = -0.9300 + 1.2272 \cos \beta + 1.6328 \sin \beta - 0.2972 \cos 2\beta - 0.5643 \sin 2\beta$

7 x 7: $f_n(\beta) = -1.9580 + 2.3201 \cos \beta + 2.5960 \sin \beta - 0.3621 \cos 2\beta - 0.9870 \sin 2\beta$

3 x 19: $f_n(\beta) = -0.4018 - 0.1597 \cos \beta + 0.3561 \sin \beta - 0.2421 \cos 2\beta - 0.0126 \sin 2\beta$

4 x 7 Serrated: $f_n(\beta) = 0.1571 + 0.2518 \cos \beta + 0.4341 \sin \beta - 0.4089 \cos 2\beta - 0.0868 \sin 2\beta$

Common: $f_n(\beta) = -0.6686 + 0.9888 \cos \beta + 1.3483 \sin \beta - 0.3202 \cos 2\beta - 0.45 \sin 2\beta$

The common drag coefficient determined from these tests was 1.46. For the Reynolds number range, no evidence of transition can be seen based on the normal drag coefficients determined over a range of angles based on the Independence Principle.

The measured steady lift forces were much smaller than the unsteady lift forces. Scatter was introduced into the steady lift data as a result of the large unsteady to steady force ratio. However, from the data, cable geometry and Reynolds number clearly affect the lift characteristics of stranded wire ropes. The lift coefficients determined for the runs displayed scatter over the Reynolds number range. The Independence Principle does not successfully scale the lift coefficients determined for each cable. No function based on Reynolds number was determined to describe the lift coefficients. In addition, a separate lift loading function must be used for each cable. The average lift coefficients and loading functions determined for the cables are:

1 x 19: $C_\ell = 0.139$

$$f_\ell(\beta) = -7.0246 + 8.9808 \cos\beta + 5.0718 \sin\beta - 1.9575 \cos 2\beta - 2.2012 \sin 2\beta$$

7 x 7: $C_\ell = 0.116$

$$f_\ell(\beta) = -29.7559 + 31.5478 \cos\beta + 27.9747 \sin\beta - 1.7925 \cos 2\beta - 11.9774 \sin 2\beta$$

3 x 19: $C_\ell = 0.222$

$$f_\ell(\beta) = 0.6240 + 0.3496 \cos\beta - 1.5954 \sin\beta - 0.9774 \cos 2\beta + 1.2234 \sin 2\beta$$

4 x 7
Serrated: $C_\ell = 0.139$

$$f_{\ell(\beta)} = -3.8616 + 3.0695 \cos\beta + 4.6514 \sin\beta + 0.7931 \cos 2\beta - 0.6304 \sin 2\beta$$

CABLE DYNAMIC PROPERTIES

The measurements by the midspan accelerometer pair show the importance of yaw angle, speed, tension and geometry on the dynamic characteristics of a cable. Cable geometry influences both the amplitude and frequency of cable vibration. The highest amplitudes are

observed for the 4 x 7 cable, which is the roughest cable of the four tested. The highest vibration amplitudes are observed at the smallest tow angles. This means that a small tow angle does not insure that strumming will be negligible.

The Independence Principle successfully scales the amplitude data. The amplitudes are roughly centered about a reduced velocity of V sin (β)/fD = 5.0. Predicted Strouhal numbers from the Independence Principle are generally within 10 percent of the measured cable Strouhal numbers. At β = 90 degrees the cable Strouhal numbers for the rougher cables (3 x 19, 4 x 7) are approximately 10 percent greater than for the smoother cables (1 x 19, 7 x 7).

RECOMMENDATIONS

FUTURE ANALYSIS

A detailed error analysis of the data measurement system is recommended to provide a confidence limit on the data obtained and to provide information on possible future refinements of the measurement system. This includes an estimate of measurement errors affecting the estimation of vibration amplitude from acceleration data.

An analysis of the reduced steady tangential force data is recommended to determine if a tangential drag loading function can be estimated from the available data, and to make that estimation if possible. An investigation of other techniques to accurately measure tangential drag is also recommended.

It is recommended that the unsteady force data be reduced in order to estimate the magnitude of the oscillatory forces and associated frequencies. This information can be used to augment the analysis of the accelerometer data and to provide information for a fatigue analysis.

The lift coefficient data available from this test should be examined further to determine the nature of the steady lift dependence on Reynolds number. An analysis of steady lift production and steady-unsteady lift force coupling is also recommended to improve our understanding of lift force production.

FUTURE TESTS

For many tow applications the hydrodynamic properties of the towed cables are desired at low angles of incidence. Since these tests apply only to yaw angles greater than 20 degrees, it is recommended that similar tests be designed to quantify the characteristics of the tested

wires at yaw angles less than 20 degrees. In addition, the development of test techniques to determine the tangential drag on these wire ropes should be pursued.

The present series of cable tests represent the first stage of experiments required to develop accurate cable modeling techniques for cable systems. To further develop such techniques a second stage of experiments is recommended. Measurements of the vortex shedding and lift production characteristics of a cable would aid in interpreting the force and strum data collected in these tests. Flow field measurements would provide insight into the complex flow physics associated with strumming cables.

Very little data is available for the vortex shedding characteristics of stranded cables. This is because researchers in the aerospace and hydrodynamic communities have traditionally focused their attention on smooth cylinders. The hydrodynamics of cables differ from smooth cylinders; for example, a cable generates a steady lift component while a smooth circular cylinder does not. Therefore, the vortex shedding characteristics of cables are likewise expected to differ from smooth cylinders. A systematic series of flow field measurements could answer many questions about the poorly understood hydrodynamics of strumming cables. Some of these questions are listed below.

1. How does the helical stranding of a cable affect the location of boundary layer separation and formation of a vortex wake?

2. By what flow mechanism is steady lift developed?

3. What effect do changes in the tow speed, cable geometry, and angle of incidence have on the stability of the shed vortex wake and the shedding frequency?

4. Is there a flow field mechanism which couples the steady and unsteady loads acting on the cable?

To answer these questions two broad categories of flow field measurements are required: qualitative flow field visualization and quantitative measurements. Flow visualization is achieved by introducing tracer particles into the flow (smoke, dye, etc.) which follow the streamlines and can be photographed. Flow visualization methods give a picture of the flow about the cable which can be used to determine the overall structure and stability of the vortex wake. Quantitative methods involve the use of probes placed in the flow to measure mean flow velocities, vortex shedding frequency, and boundary layer characteristics. Suggested measurement techniques for both categories are discussed below.

Flow visualization about the cable may be achieved in a wind tunnel by injecting smoke upstream of the test section. The visualized flow field is recorded with still photography or high-speed motion picture

cameras. Strobe lights can be used to "freeze" the flow at a given instant. Typical results of smoke injection are shown in Figure 42.[15] Results similar to Figure 42 can be achieved in a water tunnel with dye injection. A recent innovation in flow visualization involves the use of a laser light source.[16] A laser-produced sheet of light is used for its ability to show a cross section of the flow. As shown in Figure 43 a particular advantage of this method is the ability to capture both the total smoke pattern and the cross-sectional sheet pattern in a single photograph.

The traditional instrument for quantitative measurements of an unsteady flow field is the hot-wire probe. Mean flow and fluctuating turbulent velocities are measured by the hot-wire probe at a particular point in the flow field. The measured velocities are used to determine the vortex shedding frequency, energy spectra of the vortex wake, and the location of boundary layer separation. Laser Doppler Velocimetry (LDV) is an alternative means of measuring the flow field. LDV is a technique by which the instantaneous velocity is measured at a point in the flow from the Doppler frequency shift of light scattered from particles moving with the fluid. Its advantage over hot-wire anemometry is that LDV is a nonintrusive measurement technique (i.e., no probes are placed in the flow).

Ideally, the flow field measurements described above are desired for the full set of cable models with the same speed and yaw angle range of the present tests. Additionally, tests on rigid and vibrating cable models, supplemented with force measurements, are needed to study the effect of cable motion. Due to the cost of flow field measurements, it is recommended that the experimental program be divided into two phases. The Phase I test program would consider rigid cable models, while Phase II tests cable models which are free to vibrate.

To further reduce the cost and complexity of the experimental program, it is recommended that the tests be restricted to two cable models, with a circular cylinder included to serve as a baseline case. For the rigid cable model tests of Phase I, the flow field measurements may be conducted in air to produce the same results as tests conducted in water. This is achieved by adjusting the Reynolds number in air to equal the Reynolds number of the cable operating in water. Testing in a wind tunnel simplifies the setup of the cable model and operation of electrical instrumentation required for the flow field measurements. The tests of Phase II require the use of a water tunnel to ensure dynamic scaling.

---

[15]Nelson, R. C. and T. N. Mouch, "Cylinder/Splitter-Plate Data Illustrating High α Support Interference," Journal of Spacecraft and Rockets, Vol. 16, No. 2, March-April 1979.

[16]Nelson, R. C., "The Use of Flow Visualization for Vortex Trajectory Mapping," presented at the Third International Flow Visualization Symposium, University of Michigan, Ann Arbor, Michigan, September 1983.

Flow visualization of the crossflow plane is required for at least three spanwise stations along the cable. This will check the stability and spanwise coherence of the vortex wake. Quantitative measurements, performed at the same spanwise stations, should include the frequency of vortex shedding and the location of boundary layer separation.

REFERENCES

1. David W. Taylor Model Basin Report R-312, "Wind-Tunnel Tests of Mine Sweeper Cables," Aero Report 705, December 1949.

2. David W. Taylor Model Basin Report 1645, "Wind-Tunnel Determination of the Aerodynamic Characteristics of Several Twisted Wire Ropes," by M. P. Schultz, Aero Report 1028, June 1962.

3. David W. Taylor Naval Ship Research and Development Center Report 2424, "Generalized Hydrodynamic Loading Functions for Bare and Faired Cables in Two-Dimensional Steady-State Cable Configurations," by G. B. Springston, Jr., June 1967.

4. Imperial College of Science and Technology Report 117, "Lift and Drag Measurements on Stranded Cables," by J. Counihan, United Kingdom, 1963.

5. Simpson, A., "Fluid Dynamic Stability Aspects of Cables," Proceedings of the Mechanics of Wave-Induced Forces on Cylinders, T. L. Shaw, ed., Pitman Advanced Publishing Program, London, 1979, pp. 90-132.

6. MAR, Inc. Technical Report 122, "A Survey of Vortex Shedding from Circular Cylinders with Application Toward Towed Arrays," by J. S. Diggs, July 1974.

7. Naval Civil Engineering Laboratory Technical Note 1608, "The Strumming Vibrations of Marine Cables: State of the Art," by O. M. Griffin, S. E. Ramberg, and R. A. Skop, May 1981.

8. Blevins, R. D., Flow-Induced Vibration, Van Nostrand Reinhold Company, New York, 1977, Ch. 3, pp. 11-54.

9. David W. Taylor Naval Ship Research and Development Center Report SPD 766-01, "Measurement Technique to Obtain Strumming Characteristics of Model Mooring Cables in Uniform Currents," by J. H. Pattison, April 1977.

10. National Aeronautics and Space Administration Report CR 134695, "Improved Solution for Potential Flow About Arbitrary Axisymmetric Bodies by the Use of a Higher-Order Surface Source Method, Part I, Theory," by D. M. Friedman, July 1974.

11. Hoerner Fluid Dynamics, Fluid Dynamic Drag, Brick Town, NJ, 1965.

12. Brogan, W. L., Modern Control Theory, Prentice-Hall, Inc./Quantum Publishers, Inc., NJ, 1982, pp. 90-92.

13. Votaw, C. W. and C. M. Griffin, "Vortex Shedding from Smooth Cylinders and Stranded Cables," Journal of Basic Engineering, September 1971.

14. Naval Research Laboratory Report 7821, "Some Transverse Resonant Vibration Properties of Wire Rope with Application to Flow-Induced Cable Vibrations," by S. E. Ramberg and O. M. Griffin, December 1974.

15. Nelson, R. C. and T. N. Mouch, "Cylinder/Splitter-Plate Data Illustrating High α Support Interference," Journal of Spacecraft and Rockets, Vol. 16, No. 2, March-April 1979.

16. Nelson, R. C., "The Use of Flow Visualization for Vortex Trajectory Mapping," presented at the Third International Flow Visualization Symposium, University of Michigan, Ann Arbor, Michigan, September 1983.

APPENDIX A

A BIBLIOGRAPHY FOR TOWED SYSTEM ANALYSIS AND DESIGN

APPENDIX A

CONTENTS

APPENDIX A

SECTION 1
CABLE STEADY LIFT AND DRAG REFERENCES

Alexander, C. M., "The Complex Vibrations and Implied Drag of a Long Oceanographic Wire," Ocean Engineering, Vol. 8, No. 4, pp. 379-406, 1981.

Collier, Lowell, Arthur Brisbane, and Leonard Davis, "Investigation of Hydrodynamic Loading Functions on Two Faired Towlines," Hydrospace Research Corporation Report 142, November 1966.

Counihan, J., "Lift and Drag Measurements on Stranded Cables," Imperial College of Science and Technology Report 117, UK, 1963.

Diggs, Jesse S., "Hydrodynamic Characterization of Various Towed Array Cables," MAR, Inc. Technical Report 128, August 1974.

Every, M. J., "A Brief Survey of the Steady-drag Data Available for Application to Unfaired Umbilical Cables," British Hydromechanics Research Association Report RR1715, 1981.

Folb, Reece and John Nelligan, "Investigation of the Hydrodynamic Loads on Ribbon Towcable," David Taylor Naval Shipyard Research and Development Center SPD 1030-01, 1982.

Folb, Reece and John J. Nelligan, "Hydrodynamic Loading on Armored Towcables," David Taylor Naval Shipyard Research and Development Center DTNSRDC-82/116, February 1983.

Gay, S. M., A. Brisbane, L. I. Davis et al, "Investigation of Hydrodynamic Loading on Faired Towline Hydrospace Research Corporation Report 119, June 1964.

Holler, R. A., "Drag Measurements of Long Cables in the Ocean," Naval Air Development Center NADC-84086-30, March 1984

Landweber, L. and M. H. Protter, "The Shape and Tension of a Light, Flexible Cable in a Uniform Current," David Taylor Model Basin Report 533, October 1944.

McGlothlin, J. C., "Drag Coefficients of Long Flexible Cylinders Subject to Vortex Induced Vibrations," Massachusetts Institute of Technology Ocean Engineering M.S. Thesis, January 1982.

Moses, H. L. and S. A. Brantley, Jr., "Feasibility Study of Methods for the Accurate Determination of Hydrodynamic Forces on Stranded Cables," Naval Research Laboratory, Office of Naval Research Contract Number N00014-69-C-0458 (Virginia Polytech), September 1970.

Ramsey, J. and D. Dillon, "Empirical Hydrodynamic Characteristics of Two Bare Double Armored Towlines," Hydrospace Research Corporation Report 293, 1970.

Relf, E. F. and C. H. Powell, "Tests on Smooth and Stranded Wires Inclined to the Wind Direction, and a Comparison of Results on Stranded Wires in Air and Water," National Advisory Committee for Aeronautics Reports and Memoranda (New Series) No. 307, 1917.

Schultz, Mark P., "Wind-Tunnel Determination of the Aerodynamic Characteristics of Several Twisted Wire Ropes," David Taylor Model Basin Report 1645 (Aero Report 1028), June 1962.

SECTION 2
CABLE STRUMMING THEORY REFERENCES

Anand, G. V., "Nonlinear Resonance in Stretched Strings with Viscous Damping," Journal of the Acoustical Society of America, Vol. 40, No. 6, pp. 1517-1528.

Blevins, R. and T. Burton, "Fluid Forces Induced by Vortex Shedding," American Society of Mechanical Engineers Publication 75-FE-10, 1975.

Chiu, W. S. and J. H. Lienhard, "On Real Fluid Flow over Yawed Circular Cylinders," Washington State University College of Engineering Bulletin 299, 1966.

Coder, David W., "Hydrodynamic Forces on Oscillating and Nonoscillating Smooth Circular Cylinders in Cross-flow," David Taylor Naval Ship Research and Development Center Report 3639, October 1972.

Dale, J., H. Mensel, and J. McCandless, "Dynamic Characteristics of Underwater Cables: Flow Induced Transverse Vibrations," Naval Air Development Center NADC-AE-6620, 1966.

Dale, J. R., " Fluid-excitation Criteria for a Cylinder Oscillating in a Steady Flow," Naval Air Development Center NADC-AE-6768, May 1968.

Dale, J. R. and J. M. McCandless, "Water Drag Effects of Flow Induced Cable Vibrations," American Society of Mechanical Engineers Paper 68-WA/FE-47, December 1968.

Gerrard, J. H., "The Three-Dimensional Structure of the Wake of a Circular Cylinder," Journal of Fluid Mechanics, Vol. 25, Part 1, pp. 143-164, 1966.

Griffin, O. M., "OTEC Cold Water Pipe Design for Problems Caused by Vortex Excited Oscillations," Ocean Engineering, Vol. 8, pp. 129-209, 1981.

Griffin, O. M., "Steady Hydrodynamic Loads Due to Vortex Shedding from the OTEC Cold Water Pipe," Naval Research Laboratory Memorandum Report 4698, January 1982.

Griffin, O. M. and S. E. Ramberg, "The Vortex-Street Wakes of Vibrating Cylinders," Journal of Fluid Mechanics, Vol. 66, Part 3, pp. 553-576, 1974.

Griffin, O. M. and S. E. Ramberg, "The Strumming Vibrations of Marine Cables: State of the Art," Civil Engineering Laboratory Technical Note 1608, May 1981.

Griffin, O. M. and S. E. Ramberg, "On Vortex Strength and Drag in Bluff Body Wakes," Journal of Fluid Mechanics, Vol. 69, No. 4, pp. 721-728, 1975.

Griffin, O. M., J. K. Vandiver, R. A. Skop et al, "The Strumming Vibrations of Marine Cables," Ocean Science and Engineering, Vol. 7, No. 4, pp. 461-498, 1982.

Griffin, O. M. and J. K. Vandiver, "Vortex-Induced Strumming Vibrations of Marine Cables with Attached Masses," American Society of Mechanical Engineers Transactions, Vol. 106, p. 458, December 1984.

Griffin, O. M. and J. K. Vandiver, " Flow-induced Vibrations of Taut Marine Cables with Attached Masses," Civil Engineering Laboratory Report CR 84.004, November 1983.

Griffin, Owen M., John Pattison, R. Skop et al, "Vortex-Excited Vibrations of Marine Cables," American Society of Chemical Engineers Proceedings, Journal of the Waterways, Port, Coastal, and Ocean Division, Vol. 106, pp. 183-204, 1980.

Hanson, A. R., "Vortex Shedding from Yawed Cylinders," American Institute of Aeronautics and Astronautics Journal, Vol. 4, No. 4, pp. 738-774, 1966.

Iwan, W. D. and N. P. Jones, "NATFREQ Users Manual - A FORTRAN IV Program for Computing Natural Frequencies, Mode Shapes, and Drag Coefficients for Taut Strumming Cables with Attached Masses," Naval Civil Engineering Laboratory Report CR 84.026, June 1984.

Jong, Jen-Yi and J. Kim Vandiver, "The Quadratic Correlation Between In-line and Cross-flow, Vortex-induced Vibrations of Long Flexible Cylinders, Massachusetts Institute of Technology Report 84-10, August 1984.

Kennedy, Robert M. and Eric S. Strahan, "A Linear Theory of Transverse Cable Dynamics at Low Frequencies," Naval Underwater Systems Center Technical Report 6463, June 1981.

King, R., "A Review of Vortex Shedding Research and Its Application," Ocean Engineering, Vol. 4, pp. 141-171, 1977.

King, R., "An Investigation of the Criteria Controlling Sustained Self-excited Oscillations of Cylinders in Flowing Water," Biennial Symposium on Turbulence in Liquids, 4th Proceedings, 1975.

Ramberg, S. and O. Griffin, "The Effects of Vortex Coherence, Spacing, and Circulation on Flow-induced Forces on Vibrating Cables and Bluff Structures," Naval Research Laboratory Report 7945, 1976.

Ramberg, S. E., "The Influence of Yaw Angle upon the Vortex Wakes of Stationary and Vibrating Cylinders," Naval Research Laboratory Memorandum Report 3822, August 1978.

Ramberg, S. E., O. M. Griffin, and R. A. Skop, "Some Resonant Vibration Properties of Marine Cables with Application to the Prediction of Vortex-Induced Structural Vibrations," Naval Research Laboratory, American Society of Mechanical Engineers reprint.

Sarpaya, T., "Vortex-induced Oscillations, A Selective Review," American Society of Mechanical Engineers Transactions, Journal of Applied Mechanics, Vol. 46, pp. 241-258, 1979.

Sergev, S. and W. D. Iwan, "Natural Frequencies and Mode Shapes of Cables with Attached Masses," Civil Engineering Laboratory Technical Note N-1583, August 1980.

Peltzer, R. D., "Vortex Shedding from a Vibrating Cable with Attached Spherical Masses in a Linear Shear Flow," Naval Research Laboratory Memorandum Report 4940, October 1982.

SECTION 3
CABLE STRUMMING EXPERIMENTAL REFERENCES

Bloor, M. S. and J. H. Gerrard, "Measurements on Turbulent Vortices in a Cylinder Wake," Royal Society Proceedings, Series A, Vol. 294, pp. 319-342, London, 1966.

Borden, A., D. B. Young, W. M. Ellsworth, Jr., "Hydrodynamic Induced Vibrations of Cylinders Towed in Various Combinations," David Taylor Model Basin Report C-452, September 1951.

Brown, D. F., L. M. Sieracki, and M. L. Collier, "Longitudinal Oscillations of a Cable-Experiment and Theory," Hydrospace Research Corporation Technical Report 204-3, May 1969.

Buranall, W. J. and L. W. Lofting, "Experimental Investigation of the Pressure Distribution About a Yawed Circular Cylinder in the Critical Reynolds Number Range," National Advisory Committee for Aeronautics Technical Note 2463, 1961.

Chey, Y., "Strum and Drag Measurement of Underwater Cables," General Electric Technical Memorandum 990-2014, June 1975.

Dalton, William L., "A Survey of Available Data on the Normal Drag Coefficients of Cables Subjected to Crossflow," Civil Engineering Laboratory Report CR 78.001, August 1977.

Davis, N. B. and S. D. Jessup, "Cable Strumming Experiments," Massachusetts Institute of Technology Report MIT-DOE-Rept-74-19, (DTIC AD/A-005 894), November 1974.

Fabula, A. G. and R. L. Bedore, "Cable Strum Suppression Experiments with Helical Ridges," US Navy Journal of Underwater Acoustics, Vol. 24, No. 4, UNCLASSIFIED pp. 563-582, October 1974, CONFIDENTIAL.

Hafen, B. E. and D. Meggitt, "Cable Strumming Suppression," Civil Engineering Laboratory Technical Note N-1499, September 1977.

Jong, Jen-Yi and J. Kim Vandiver, "Response Analysis of the Flow-induced Vibration of Flexible Cylinders Tested at Castine, Maine in July and August of 1981," Massachusetts Institue of Technology Ocean Engineering Department Report, 15 January 1983.

Kim, Yang-Hann, J. Kim Vandiver, and Roger Holler, "Vortex-induced Vibration and Drag Coefficients of Long Cables Subjected to Sheared Flows," American Society of Mechanical Engineers, 4th International Symposium on Offshore Mechanics and Arctic Engineering, Paper 264.

King, R., "Vortex Excited Oscillations of Yawed Circular Cylinders," American Society of Mechanical Engineers Transactions, Journal of Fluids Engineering, Vol. 99, No. 3, pp. 495-502, 1977.

Kline, J. E. and A. Brisbane, "Experimental Study of Strumming Suppression Devices - Test Plan," MAR, Inc. Test Plan 112, 1978.

Kline, J. E., J. J. Nelligan, and J. S. Diggs, "A Survey of Recent Investigations into the Nature of Cable Strumming, Its Mechanisms and Suppression," MAR, Inc. Technical Report 210, July 1978.

Kline, Jeffrey, Arthur Brisbane, and Edward Fitzgerald, "A Study of Cable Strumming Suppression, MAR, Inc. Technical Report 249, October 1980.

Koopmann, G. H., "Wind-induced Vibrations of Skewed Circular Cylinders," Catholic University of America, Civil and Mechanical Engineering Department Report 70-11, 1970.

Maxel, Charles H., "Vortex-excited Vibrations of Marine Cables," Massachusetts Institute of Technology N00014-75-C-0961, June 1976.

Pattison, John H., "Measurement Technique to Obtain Strumming Characteristics of Model Mooring Cables in Uniform Currents," David Taylor Naval Ship Research and Development Center Report SPD 776-01, April 1977.

Peltzer, R. D. and D. M. Rooney, "Near Wake Properties of a Strumming Marine Cable: An Experimental Study," Journal of Fluids Engineering, Vol. 107, pp. 86-91, March 1985.

Peltzer, R. D. and D. M. Rooney, "Vortex Shedding in a Linear Shear Flow from a Vibrating Marine Cable with Attached Bluff Bodies," Journal of Fluids Engineering, Vol. 107, pp. 61-65, March 1985.

Rispin, P., B. Webster, and J. Stasiewicz, "An Evaluation of Several Techniques for Reducing Cable Strum," David Taylor Ship Research and Development Center Report SPD 732-01, November 1977.

Sarpkaya, Turgut, "In-line and Transverse Forces on Smooth and Sand-roughened Cylinders in Oscillatory Flow at High Reynolds," Naval Postgraduate School 69SL76062, June 1976.

SECTION 4
CABLE SYSTEMS REFERENCES

Abkowitz, M. A., "Paper 4. Towed Bodies," Journal of Mechanical Engineering Science, Vol. 14, No. 7, pp. 20-28, 1972.

Carroll, D., "Parametric Design and Analysis of Target Towlines," Naval Air Development Center 74151-30, September 1974.

Carter, N. A., "Effect of Fairings on Drag Characteristics of a Straincable When Towing a Heavy Body," Admiralty Underwater Weapons Establishment Publication 65593, 1982.

Casarella, Mario J., "Dynamics of Cable Systems," Catholic University of America AD-A022 119, August 1975.

Casarella, Mario J. and Michael Parsons, "Cable Systems Under Hydrodynamic Loading," Marine Technical Society Journal, Vol. 4, No. 4, pp. 27-44, July-August 1970.

Choo, Y. and M. J. Casarella, "Hydrodynamic Resistance of Towed Cables," Journal of Hydronautics, Vol. 5, No. 4, October 1971.

Collier, M. Lowell and M. E. Schultz, "The Determination of the Natural Frequency of a Cable Catenary Fixed at Both Ends, Volume 1," Hydrospace Research Corporation Technical Report 204-1, May 1969.

DeLaurier, James D., "A First Order Theory for Predicting the Stability of Cable Towed and Tethered Bodies Where the Cable Has a General Curvature and Tension Variation," Von Karman Institute for Fluid Dynamics Technical Note 68, December 1970.

Durelli, A. J., J. A. Clark, and V. J. Parks, "Analysis of Stresses Generated by Surface Waves in a Buoy-Cable System Model," Catholic University of America Report 70-12, November 1970.

Every, M. J., "Fluid Dynamic Problems of Cables Used for Remotely Operated Vehicles," British Hydrodynamics Research Association Offshore Applications Conference, Aberdeen, January 1983.

Every, M. J. and M. E. Davies, "Predictions of the Drag and Performance of Umbilical Cables," Marine Technology Society, Remotely Operated Vehicles Conference, 1984.

Gay, Shelton M., Jr., "New Engineering Techniques for Application to Deep-Water Mooring," American Society of Mechanical Engineers Paper 66-PET-31, 1966.

Gibbons, Thomas and C. O. Walton, "Evaluation of Two Methods for Predicting Towline Tensions and Configurations of a Towed Body System Using Bare Cable," David Taylor Model Basin Report 2313, December 1966.

Griffin, O. M. and F. Rosenthal, "The Dynamics of Slack Marine Cables," Naval Research Laboratory Memorandum Report 5559, 13 May 1985.

Griffin, O. M., R. A. Skop, and S. E. Ramberg, "The Vortex-Excited Resonant Vibrations of Structures and Cable Systems," Offshore Technology Conference, Preprint OTC 2319, 1975.

Iwan, W. D., "The Vortex-induced Vibration of Nonuniform Structural Systems," Journal of Sound and Vibration, Vol. 79, pp. 291-302, November 1981.

Jeffrey, N. E., "Influence of Design Features on Underwater Towed System Stability," Journal of Hydronautics, Vol. 2, No. 4, pp. 205-213, October 1968.

Kretshmer, G. A., G. A. Edgerton, and N. D. Albertsen, "Seafloor Construction Experiment, Seacon II," Civil Engineering Laboratory Technical Report R-848, December 1976.

Lo, Alain and John W. Leonard, "Dynamic Analysis of Underwater Cables," American Society of Chemical Engineers Proceedings, Journal of Engineering Mechanics Division, Vol. 108, No. EM4, pp. 605-621, August 1982.

McLeod, A. R., "On the Action of Wind on Flexible Cables with Applications to Cables Towed Below Aeroplanes, and Balloon Cables," National Advisory Committee for Aeronautics Reports and Memos No. 554, October 1918.

Merritt, Paul H. and David K. Cunningham, "Some Aerodynamic Characteristics of Tow Targets and Towlines," Air Proving Ground Center TR-65-65, September 1965.

Nair, S. and G. Hegemier, G., "Stability of Faired Underwater Towing Cables," Journal of Hydronautics, Vol. 13, No. 1, 1979.

Pattison, J. H., P. P. Rispin, and N. T. Tsai, "Handbook on Hydrodynamic Characteristics of Moored Array Components," David Taylor Naval Ship Research and Development Center SPD-745-01, March 1977.

Pattison, John H., "Components of Force Generated by Harmonic Oscillations of Small-scale Mooring Lines in Water," David Taylor Naval Ship Research and Development Center SPD 589-01, January 1977.

Phillips, William H., "Theoretical Analysis of Oscillations of Towed Cables," Navy Mine Defense Laboratory Technical Note 1796, January 1949.

Ramberg, S. E. and O. M. Griffin, "Free Vibrations of Taut and Slack Marine Cables," American Society of Chemical Engineers Proceedings, Journal of the Structural Division, Vol. 103, No. ST11, pp. 2079-2092, November 1977.

Rispin, P. and J. S. Diggs, "At-Sea Evaluation of the Hydrodynamic Performance of a Simulated Depressor-towed Array," David Taylor Naval Ship Research and Development Center SPD 0953-01, March 1981.

Saxon, D. S. and A. E. Cahn, "Modes of Vibration of a Suspended Cable," Quarterly Journal of Mechanics and Applied Mathematics, Vol. 6, Par 3, pp. 273-285, 1953.

Shepard, G. Dudley, "Mooring Line Forces on an Oscillating Buoy in a Uniform Current," Charles Stark Draper Laboratory, Inc. Report AD-773 956, July 1973.

SECTION 5
GENERAL REFERENCES

Blevins, Robert D., "Flow Induced Vibration," Van Nostrand Reinhold Company, New York, 1977.

Every, M. J., R. King, and O. M. Griffin, "Hydrodynamic Loads on Flexible Marine Structures Due to Vortex Shedding," American Society of Mechanical Engineers Paper 81-WA/FE-24, 1981.

Hallam, M. G., N. J. Heat, and L. R. Wootton, "Dynamics of Marine Structures," Construction Industry Research and Information Association (CIRIA), London, 1978.

APPENDIX B

CABLE STRUM DATA

APPENDIX B

CONTENTS

APPENDIX B

INTRODUCTION

The reduced data from the cable drag, lift, and strum tests described in this report are presented in the following sections. The data include mean steady forces, acceleration spectra, tabulated information from the spectra, and quantities calculated from the spectra.

The forces and accelerations are defined for a right-hand coordinate system. The x- and z-axes lie in the cable-flow plane with the x-axis normal to the cable and the z-axis along the cable. The positive axes correspond to the normal and tangential drag directions. The y-axis lies transverse to the x- and z-axes according to the right-hand rule. β is defined to be the angle between the z-axis and the relative flow velocity.

For this test setup, all data reduction has been completed as if the coordinate system described were applied to a left lay cable. From previous tests[1,2] and tow experience it has been shown that the drag forces developed on right and left lay cables are equivalent at the same yaw angles. The lift force developed on a right lay cable over the angle range $0° < \beta < 90°$ is equivalent to that developed by a left lay cable except the direction of the lift vector is reversed. All lift force data tabulated in the appendix are listed as positive forces regardless of the lay of the corresponding cable tested. The reader who chooses to use the loading functions developed for system design must take care to insure the correct sign is attached to the lift loading function depending on whether the design cable is right or left lay.

MEAN FORCE DATA

Three-dimensional dynamic force data were available from the tri-axial force gage attached to one end of the cable. The dynamic data were reduced to provide the mean steady forces acting on the cable during each test run. For each run, the x, y, and z mean steady forces

---

[1]David W. Taylor Model Basin Report R-312, "Wind-Tunnel Tests of Mine Sweeper Cables," Aero Report 705, December 1940.

[2]David W. Taylor Model Basin Report 1645, "Wind-Tunnel Determination of the Aerodynamic Characteristics of Several Twisted Wire Ropes," by M. P. Schultz, Aero Report 1028, June 1962.

are reported in tabular form. Dimensional loads in pounds are given by fx, fy, fz corresponding to the x, y, and z directions. These forces are divided by the cable length (L = 14 ft) to give the loading per foot. The force coefficients are defined as

$$C_x = \frac{f_x}{\frac{1}{2} \rho V^2 D L}$$

$$C_y = \frac{f_y}{\frac{1}{2} \rho V^2 D L}$$

$$C_z = \frac{f_z}{\frac{1}{2} \rho V^2 D L}$$

where the water density iS ρ = 1.94 lbm/ft and D is the nominal cable diameter (D = 51/64 inch for the 4 x 7 model and D = 5/8 inch for the remaining models). Undefined values in the table are denoted by "******."

cable: 1x19
diameter (in): 5/8
length (in): 160.0
tension: low

speed (kt)	angle (deg)	cx	cy	cz	fx (lb)	fy (lb)	fz (lb)	fx/l (lb/ft)	fy/l (lb/ft)	fz/l (lb/ft)
2	20	0.31	0.14	0.14	2.58	1.18	1.18	0.18	0.08	0.08
2	30	0.52	0.23	0.14	4.20	1.88	1.12	0.30	0.13	0.08
2	45	0.68	0.16	0.19	5.46	1.26	1.54	0.39	0.09	0.11
2	50	1.13	0.03	1.85	9.10	0.28	10.08	0.65	0.02	0.72
2	60	1.34	0.19	1.41	10.78	1.54	11.34	0.77	0.11	0.81
2	71	1.54	0.16	1.41	12.46	1.26	11.34	0.89	0.09	0.81
2	80	1.49	0.14	0.84	12.04	1.12	1.96	0.86	0.08	0.14
2	90	1.60	0.05	1.20	12.88	0.42	9.66	0.92	0.03	0.69
5	20	0.12	0.36	0.12	6.50	18.06	6.16	0.46	1.29	0.44
5	30	0.47	0.05	0.74	25.26	2.36	37.10	1.69	0.19	2.65
5	45	0.76	0.17	1.41	58.80	8.82	71.26	2.75	0.65	5.09
5	50	0.19	0.50	0.51	9.52	25.20	15.82	0.68	1.80	1.15
5	60	1.06	0.22	2.05	55.34	11.06	105.18	3.81	0.79	7.37
5	71	1.24	0.24	2.52	62.44	12.32	117.04	4.46	0.88	8.36
5	80	1.35	0.20	2.45	65.52	10.08	122.36	4.68	0.72	8.74
5	90	0.70	0.15	0.77	35.14	7.56	38.64	2.51	0.54	2.76
7	20	******	0.05	0.34	******	2.52	33.88	******	0.18	2.42
7	30	0.48	0.08	0.95	47.18	7.98	93.66	3.37	0.57	6.69
7	45	0.71	0.21	1.42	69.86	21.14	140.56	4.99	1.51	10.04
7	50	0.83	0.23	1.81	82.32	22.96	178.92	5.88	1.64	12.78
7	60	1.04	0.26	2.24	103.04	25.68	221.48	7.36	1.85	15.82
7	71	1.21	0.20	2.52	119.56	19.46	255.64	8.54	1.39	18.26
7	80	1.34	0.20	2.80	132.02	19.46	276.92	9.43	1.39	19.78
7	90	1.38	0.13	3.13	136.08	13.30	308.98	9.72	0.95	22.07
10	20	0.26	0.00	0.42	53.34	0.00	85.12	3.81	0.00	6.08
10	30	0.41	0.09	0.84	82.32	17.64	170.38	5.88	1.26	12.17
10	45	0.61	0.21	1.38	125.62	41.86	286.28	8.85	2.99	19.08
10	50	0.78	0.24	1.80	156.80	48.58	362.18	11.20	3.47	25.87
10	60	0.98	0.23	2.22	198.10	46.34	447.58	14.15	3.31	31.97
10	71	1.17	0.22	2.64	235.34	44.10	532.84	16.81	3.15	38.06
10	80	1.23	0.17	2.64	247.80	35.28	532.84	17.70	2.52	38.06
10	90	1.29	0.15	2.96	260.12	30.94	596.82	18.58	2.21	42.63

cable: 1x19
diameter (in): 5/8
length (in): 160.0
tension: high

speed (kt)	angle (deg)	cx	cy	cz	fx (lb)	fy (lb)	fz (lb)	fx/l (lb/ft)	fy/l (lb/ft)	fz/l (lb/ft)
2	20	0.52	0.23	0.35	4.80	1.82	2.80	0.30	0.13	0.20
2	30	.....	.....	.....	.....	.....	.....	.....	.....	.....
2	43	0.57	0.14	0.21	4.68	1.12	1.68	0.33	0.08	0.12
2	50	0.85	0.10	0.24	6.86	0.84	1.96	0.49	0.06	0.14
2	60	1.16	0.09	1.37	9.38	0.70	11.06	0.67	0.05	0.78
2	71	1.46	0.09	1.35	11.76	0.70	10.92	0.84	0.05	0.78
2	80	1.61	0.14	1.51	13.02	1.12	12.12	0.93	0.08	0.87
2	90	.....	.....	.....	.....	.....	.....	.....	.....	.....
5	20	0.19	0.08	0.19	9.52	3.92	9.38	0.68	0.28	0.67
5	30	0.34	0.01	0.27	16.94	0.42	13.72	1.21	0.03	0.98
5	43	0.73	0.04	0.86	36.82	2.24	43.54	2.63	0.16	2.11
5	50	0.94	0.11	1.33	47.60	5.32	66.92	3.40	0.38	4.78
5	60	1.14	0.12	1.58	57.54	6.16	79.80	4.11	0.44	5.70
5	71	1.30	0.04	1.83	65.80	2.24	92.54	4.70	0.16	6.61
5	80	1.38	0.10	2.00	69.86	4.90	101.08	4.99	0.35	7.22
5	90	1.43	0.04	1.86	72.38	1.82	93.66	5.17	0.13	6.69
7	20	0.35	0.07	0.86	34.72	7.00	85.12	2.48	0.50	6.08
7	30	0.56	0.05	0.39	55.44	5.32	38.22	3.96	0.38	2.73
7	43	0.73	0.05	1.03	71.96	4.48	102.20	5.14	0.32	7.30
7	50	0.89	0.12	1.46	88.48	11.48	144.76	6.32	0.82	10.34
7	[illegible]	1.08	0.15	1.94	107.10	14.98	191.66	7.65	1.07	13.69
7	[illegible]	1.08	0.05	1.94	107.10	4.48	191.66	7.65	0.32	13.69
7	80	.....	.....	.....	.....	.....	.....	.....	.....	.....
7	90	1.38	0.07	2.37	136.08	7.00	234.36	9.72	0.50	16.74
10	20	0.16	0.04	0.21	32.76	4.48	42.42	2.34	0.32	3.03
10	30	0.41	0.16	1.11	82.32	33.04	223.72	5.88	2.36	15.98
10	43	0.70	0.12	1.21	140.28	24.22	245.00	10.02	1.73	17.50
10	50	0.82	0.16	1.53	165.06	33.04	308.98	11.79	2.36	22.07
10	60	0.98	0.14	1.95	198.10	29.12	394.24	14.15	2.08	28.16
10	71	1.21	0.15	0.79	243.60	26.46	159.74	17.40	1.89	11.41
10	80	1.31	0.12	2.53	264.32	24.22	511.42	18.88	1.73	36.53
10	90	1.29	0.09	2.53	260.12	17.64	511.42	18.58	1.26	36.53

cable: 7x7
diameter (in): 5/8
length (in): 160.0
tension: low

speed (kt)	angle (deg)	cx	cy	cz	fx (lb)	fy (lb)	fz (lb)	fx/l (lb/ft)	fy/l (lb/ft)	fz/l (lb/ft)
2	20	0.42	0.16	0.09	3.36	1.26	0.70	0.24	0.09	0.06
2	30	0.57	0.28	0.19	4.62	2.24	1.54	0.33	0.16	0.11
2	43	0.97	0.05	0.61	7.84	0.42	4.90	0.56	0.03	0.35
2	50	1.23	0.09	1.87	9.94	0.70	15.12	0.71	0.05	1.08
2	60	1.44	0.09	1.77	11.62	0.70	14.28	0.83	0.05	1.02
2	71	1.86	0.03	2.62	14.98	0.28	21.14	1.07	0.02	1.51
2	80	1.80	0.05	0.21	14.56	0.42	1.68	1.04	0.03	0.12
2	90	1.80	0.19	0.45	14.56	1.54	3.64	1.04	0.11	0.26
5	20	0.40	0.11	0.42	20.30	5.32	21.14	1.45	0.38	1.51
5	30	0.61	0.02	1.01	30.66	1.26	50.96	2.19	0.09	3.64
5	43	0.94	0.04	2.36	47.18	2.24	119.14	3.37	0.16	8.51
5	50	1.14	0.11	2.04	57.54	5.32	155.50	4.11	0.38	10.96
5	60	1.30	0.15	3.89	65.80	7.56	196.00	4.70	0.54	14.00
5	71	1.55	0.17	4.98	78.26	8.82	251.44	5.59	0.63	17.96
5	80	1.72	0.15	5.41	86.52	7.56	272.72	6.18	0.54	19.48
5	90	1.26	0.26	3.80	63.70	13.30	191.66	4.55	0.95	13.69
7	20	0.31	0.07	0.60	50.66	7.00	59.50	3.19	0.50	4.25
7	30	0.50	0.04	1.29	48.28	3.50	127.68	3.52	0.25	9.12
7	43	0.79	0.05	2.67	78.26	5.32	264.18	5.59	0.38	18.87
7	50	0.96	0.12	3.68	94.78	11.48	357.98	6.77	0.82	25.57
7	60	1.21	0.18	4.66	119.56	17.64	460.32	8.54	1.26	32.88
7	71	1.48	0.19	5.69	146.44	18.48	562.66	10.46	1.32	40.19
7	80	1.56	0.18	5.76	154.70	17.64	571.20	11.05	1.26	40.80
7	90	0.88	0.11	6.21	86.52	10.64	615.76	6.18	0.76	43.84
10	20	0.29	0.09	0.74	57.54	17.64	149.10	4.11	1.26	10.65
10	30	0.45	0.05	1.48	90.58	11.06	298.34	6.47	0.79	21.31
10	43	0.72	0.04	2.75	144.34	8.82	554.12	10.31	0.63	39.58
10	50	0.92	0.13	3.80	185.64	26.46	767.54	13.26	1.89	54.81
10	60	1.13	0.20	4.75	227.08	39.76	959.14	16.22	2.84	68.51
10	71	1.35	0.22	5.70	272.58	44.10	******	19.47	3.15	82.82
10	80	1.47	0.20	5.92	297.36	39.76	******	21.24	2.84	85.27
10	90	1.29	0.46	14.05	260.12	92.68	******	18.58	6.62	808.53

cable: 7x7
diameter (in): 5/8
length (in): 160.0
tension: high

speed (kt)	angle (deg)	cx	cy	cz	fx (lb)	fy (lb)	fz (lb)	fx/l (lb/ft)	fy/l (lb/ft)	fz/l (lb/ft)
2	20	0.29	0.10	0.05	2.38	0.84	0.42	0.17	0.06	0.03
2	30	0.47	0.28	0.09	3.78	2.24	0.70	0.27	0.16	0.05
2	43	0.47	0.10	0.14	3.78	0.84	1.12	0.27	0.06	0.08
2	50	0.73	0.09	0.14	5.88	0.70	1.12	0.42	0.05	0.08
2	60	1.11	0.10	0.47	8.96	0.84	3.78	0.64	0.06	0.27
2	71	1.54	0.14	0.75	12.46	1.12	6.02	0.89	0.08	0.43
2	80	1.46	0.10	0.54	11.76	0.84	4.34	0.84	0.06	0.31
2	90	1.49	0.14	0.35	12.04	1.12	2.80	0.86	0.08	0.20
5	20	0.21	0.11	0.21	10.36	5.74	10.50	0.74	0.41	0.75
5	30	0.44	0.12	0.19	21.98	6.16	9.38	1.57	0.44	0.67
5	43	0.80	0.06	0.57	40.18	3.08	28.56	2.87	0.22	2.04
5	50	0.94	0.02	0.56	47.60	0.84	43.54	3.40	0.06	3.11
5	60	1.17	0.07	1.16	59.22	3.50	58.38	4.23	0.25	4.17
5	71	1.29	0.10	1.39	64.96	4.90	70.14	4.64	0.35	5.01
5	80	1.42	0.11	1.55	71.54	5.32	77.98	5.11	0.38	5.57
5	90	1.35	0.14	1.62	68.32	7.00	81.90	4.88	0.50	5.86
7	20	0.29	0.15	0.26	28.56	14.98	28.34	2.04	1.07	1.81
7	30	0.46	0.12	0.30	45.08	12.32	29.68	3.22	0.88	2.12
7	43	0.82	0.05	0.60	81.60	4.48	59.50	4.40	0.32	4.25
7	50	0.88	0.02	1.08	86.52	1.82	106.40	6.18	0.13	7.60
7	60	1.10	0.02	1.51	109.20	7.98	149.10	7.80	0.57	10.65
7	71	1.29	0.17	2.07	127.68	16.80	204.54	9.13	1.20	14.61
7	80	0.16	0.16	0.47	16.10	15.82	46.76	1.15	1.13	3.34
7	90	1.48	0.15	2.20	146.44	13.30	217.28	10.46	0.95	15.52
10	20	0.29	0.15	0.21	57.54	30.94	42.48	4.11	2.21	3.06
10	30	0.45	0.11	0.42	90.58	22.12	85.12	6.47	1.58	6.08
10	43	0.72	0.00	1.06	144.54	0.00	212.94	10.31	0.00	15.21
10	50	0.84	0.05	1.43	169.12	11.06	287.56	12.08	0.79	20.54
10	60	1.06	0.18	1.80	214.62	35.04	368.18	15.33	2.50	26.27
10	71	1.27	0.21	2.38	256.06	41.86	479.80	18.29	2.99	34.25
10	80	1.35	0.20	2.52	272.58	39.76	511.42	19.47	2.84	36.53
10	90	1.43	0.15	2.27	289.10	30.94	486.22	20.65	2.21	32.73

cable: 3x19
diameter (in): 5/8
length (in): 160.0
tension: low

speed (kt)	angle (deg)	cx	cy	cs	fx (lb)	fy (lb)	fs (lb)	fx/l (lb/ft)	fy/l (lb/ft)	fs/l (lb/ft)
2	30	0.26	0.14	0.03	8.10	1.12	0.88	0.15	0.08	0.08
2	30	0.49	0.35	0.09	3.92	2.80	0.70	0.28	0.20	0.05
2	45	0.68	0.29	0.14	5.46	2.28	1.12	0.39	0.17	0.08
2	50	0.83	0.66	0.48	6.72	5.32	3.33	0.48	0.38	0.24
2	60	1.28	0.14	0.29	10.36	1.12	2.35	0.74	0.08	0.17
2	71	1.60	4.70	1.02	12.88	37.94	8.26	0.92	2.71	0.59
2	80	1.70	1.86	0.97	13.72	14.98	7.84	0.98	1.07	0.56
2	90	1.88	2.74	1.02	14.98	22.12	8.26	1.07	1.58	0.59
5	20	0.25	0.16	0.21	12.46	7.98	10.50	0.89	0.57	0.75
5	30	0.88	0.18	1.16	44.24	8.12	58.38	3.16	0.58	4.17
5	45	0.75	0.24	0.99	37.66	11.90	49.84	2.69	0.88	3.56
5	50	0.93	0.28	1.41	46.76	14.14	71.26	3.34	1.01	5.09
5	60	1.26	0.30	1.94	63.70	14.98	97.86	4.55	1.07	6.98
5	71	1.43	0.22	2.45	71.96	11.06	122.15	5.14	0.79	8.58
5	80	1.55	1.06	2.62	78.26	52.92	132.02	5.59	3.78	9.45
5	90	1.67	0.33	2.91	84.42	16.80	146.86	6.03	1.20	10.49
7	20	0.28	0.17	0.34	31.36	16.80	25.34	1.84	1.20	1.66
7	30	0.48	0.14	0.60	47.18	14.14	59.50	3.37	1.01	4.26
7	45	0.73	0.21	1.29	71.96	21.14	127.68	5.14	1.51	9.12
7	50	0.92	0.27	1.71	90.58	26.46	169.98	6.47	1.89	12.07
7	60	1.08	0.30	4.27	107.10	29.96	421.96	7.65	2.14	30.14
7	71	1.23	0.28	2.67	121.66	28.18	264.18	8.69	1.58	18.87
7	80	1.40	1.12	5.56	138.18	110.32	549.92	9.87	7.88	39.28
7	90	1.50	0.24	2.89	148.54	24.22	285.46	10.61	1.73	20.39
10	20	0.19	0.14	0.31	37.66	28.28	61.60	2.69	2.02	4.40
10	30	0.43	0.15	0.74	58.52	30.94	148.10	6.18	2.21	10.58
10	45	0.70	0.21	1.53	140.28	41.86	308.98	10.02	2.99	22.07
10	50	0.86	0.23	1.90	173.32	46.34	385.60	12.38	3.31	27.40
10	60	1.00	0.25	2.22	202.30	50.68	447.58	14.45	3.62	31.97
10	71	0.88	0.36	2.69	177.38	72.80	543.48	12.67	5.20	38.82
10	80	1.35	0.22	2.90	272.58	44.10	586.04	19.47	3.15	41.86
10	90	1.43	0.08	2.84	289.10	15.40	558.84	20.65	1.10	38.06

cable: 3x19
diameter (in): 5.8
length (in): 160.0
tension: high

speed (kt)	angle (deg)	cx	cy	cz	fx (lb)	fy (lb)	fz (lb)	fx/l (lb/ft)	fy/l (lb/ft)	fz/l (lb/ft)
2	20	0.19	0.18	0.09	1.54	1.26	0.70	0.11	0.09	0.05
2	30	0.47	0.28	0.18	2.75	2.24	1.26	0.27	0.16	0.09
2	43	0.69	0.38	0.24	5.60	3.08	1.96	0.40	0.22	0.14
2	50	0.73	0.33	0.24	3.88	2.66	1.96	0.42	0.19	0.14
2	60	1.06	0.35	0.26	3.54	2.80	2.80	0.61	0.20	0.20
2	71	1.39	0.28	0.61	11.20	2.24	4.90	0.80	0.16	0.35
2	80	1.41	0.24	0.98	11.34	1.96	7.42	0.81	0.14	0.53
2	90	1.08	0.10	0.35	3.68	0.84	2.80	0.68	0.06	0.20
5	20	0.26	0.18	0.21	12.53	7.98	10.50	0.92	0.57	0.75
5	30	0.42	0.25	0.27	21.14	11.48	13.72	1.51	0.82	0.98
5	43	0.80	0.37	0.65	40.18	18.48	38.90	2.87	1.32	2.35
5	50	0.91	0.34	0.95	45.92	17.22	47.74	3.28	1.23	3.41
5	60	1.83	0.55	2.35	92.26	27.72	143.64	6.59	1.98	10.26
5	71	1.34	0.27	1.73	67.48	13.72	87.22	4.82	0.98	6.23
5	80	1.13	0.12	1.69	57.12	6.16	85.12	4.08	0.44	6.08
5	90	1.40	0.04	1.82	70.70	1.82	81.90	5.05	0.13	5.85
7	20	0.27	0.15	0.21	26.46	15.30	21.14	1.89	0.96	1.51
7	30	0.46	0.21	0.39	45.08	20.30	38.22	3.22	1.43	2.73
7	43	0.79	0.29	0.95	78.26	29.12	95.66	5.59	2.08	6.69
7	50	0.94	0.35	1.29	98.68	34.44	187.88	6.66	2.46	9.13
7	60	1.10	0.35	1.64	109.20	33.62	161.84	7.80	2.33	11.56
7	71	1.27	0.21	2.07	125.72	21.14	204.54	8.98	1.51	14.61
7	80	1.34	0.12	2.11	132.02	12.32	208.74	9.43	0.88	14.91
7	90	1.34	0.05	2.11	132.02	5.32	208.74	9.43	0.38	14.91
10	20	0.38	0.18	0.38	53.34	25.04	53.06	3.81	2.33	3.79
10	30	0.41	0.15	0.47	58.52	30.94	95.76	5.88	2.21	6.84
10	43	0.78	0.25	1.21	144.54	46.34	245.00	10.31	3.31	17.50
10	50	0.82	0.26	1.53	165.06	52.92	308.98	11.79	3.78	22.07
10	60	1.00	0.28	1.85	202.30	57.40	378.98	14.45	4.10	26.84
10	71	1.19	0.19	2.38	239.40	37.52	478.50	17.10	2.68	34.26
10	80	1.27	0.04	2.38	256.06	8.82	478.50	18.29	0.63	34.26
10	90	1.31	0.04	2.22	264.38	8.82	447.38	18.86	0.63	31.97

cable: 4x7
diameter (in): 51/64
length (in): 160.0
tension: low

speed (kt)	angle (deg)	cx	cy	cz	fx (lb)	fy (lb)	fz (lb)	fx/l (lb/ft)	fy/l (lb/ft)	fz/l (lb/ft)
2	20	0.20	0.11	0.04	2.10	1.18	0.48	0.16	0.08	0.03
2	30	0.38	0.11	0.08	3.98	1.18	0.84	0.28	0.08	0.06
2	43	0.23	0.07	0.03	2.38	0.70	0.28	0.17	0.05	0.02
2	50	0.71	0.19	0.19	7.28	1.96	1.96	0.52	0.14	0.14
2	60	1.33	0.12	0.71	13.72	1.26	7.28	0.98	0.09	0.52
2	71	4.95	0.12	0.83	50.96	1.26	8.54	3.64	0.09	0.61
2	80	1.51	0.08	0.75	15.44	0.84	7.70	0.96	0.06	0.55
2	90	0.68	0.00	0.75	7.00	0.00	7.70	0.50	0.00	0.55
5	20	0.18	0.11	0.14	11.76	7.00	8.84	0.84	0.50	0.66
5	30	0.37	0.12	0.37	24.08	7.70	85.66	1.72	0.55	1.69
5	43	0.65	0.17	0.82	41.86	11.06	53.06	2.99	0.79	3.79
5	50	0.83	0.14	1.27	53.34	9.24	81.90	3.81	0.66	5.85
5	60	1.12	0.10	1.79	71.96	6.58	114.94	5.14	0.47	8.21
5	71	1.18	0.08	2.12	75.74	5.32	136.22	5.41	0.38	9.73
5	80	1.22	0.05	2.25	78.26	2.24	144.76	5.59	0.16	10.34
5	90	1.23	0.08	2.35	78.96	5.32	151.20	5.64	0.38	10.80
7	20	0.23	0.13	0.20	28.56	16.52	25.54	2.04	1.18	1.81
7	30	0.39	0.12	0.52	49.28	14.98	65.94	3.52	1.07	4.71
7	43	0.67	0.12	1.18	84.42	14.98	149.10	6.03	1.07	10.65
7	50	0.83	0.15	1.69	105.14	15.38	212.94	7.51	1.15	15.21
7	60	1.03	0.11	2.23	129.92	13.30	281.26	9.28	0.95	20.09
7	71	1.13	0.08	2.40	142.24	10.64	302.54	10.16	0.76	21.61
7	80	1.21	0.02	2.60	152.60	2.66	328.16	10.90	0.19	23.44
7	90	1.23	0.08	5.24	154.70	10.64	660.66	11.05	0.76	47.19
10	20	0.21	0.12	0.25	53.34	30.94	63.70	3.81	2.21	4.55
10	30	0.37	0.09	0.70	94.78	22.12	181.02	6.77	1.58	12.93
10	43	0.63	0.09	1.41	160.86	22.12	362.18	11.49	1.58	25.87
10	50	0.77	0.10	1.74	198.10	26.46	447.58	14.15	1.89	31.97
10	60	0.91	0.09	2.11	235.34	24.22	543.48	16.81	1.73	38.82
10	71	1.09	0.05	2.53	280.84	13.30	650.02	20.06	0.95	46.43
10	80	1.17	0.01	2.57	301.56	2.24	660.66	21.54	0.16	47.19
10	90	1.16	0.06	2.40	297.36	15.40	618.10	21.24	1.10	44.15

cable: 4x7
diameter (in): 51/64
length (in): 160.0
tension: high

speed (kt)	angle (deg)	cx	cy	cz	fx (lb)	fy (lb)	fz (lb)	fx/l (lb/ft)	fy/l (lb/ft)	fz/l (lb/ft)
2	20	0.24	0.18	0.04	2.52	1.92	0.42	0.18	0.13	0.03
2	30	0.42	0.22	0.19	4.34	2.24	1.96	0.31	0.16	0.14
2	43	0.65	0.22	0.04	6.72	2.24	0.42	0.48	0.16	0.03
2	50	0.71	0.12	0.19	7.28	1.26	1.96	0.52	0.09	0.14
2	60	0.80	0.22	0.27	8.26	2.24	2.80	0.59	0.16	0.20
2	71	1.14	0.08	0.42	11.76	0.84	4.34	0.84	0.06	0.31
2	80	1.37	0.22	0.48	14.14	2.24	4.90	1.01	0.16	0.35
2	90	1.31	0.00	0.68	13.44	0.00	10.08	0.96	0.00	0.72
5	20	0.80	0.13	0.08	18.88	8.40	8.18	0.98	0.60	0.37
5	30	0.59	0.13	0.23	25.20	8.40	14.70	1.80	0.60	1.05
5	43	0.71	0.19	0.51	45.98	11.90	38.90	3.28	0.85	8.35
5	50	0.82	0.16	0.71	52.50	10.08	45.64	3.75	0.72	3.26
5	60	1.00	0.14	1.12	64.12	9.24	72.24	4.58	0.66	5.16
5	71	1.20	0.09	1.42	77.42	5.74	91.42	5.53	0.41	6.53
5	80	1.28	0.03	1.55	82.32	2.24	99.96	5.88	0.16	7.14
5	90	1.44	0.07	1.52	92.68	4.48	97.86	6.62	0.32	6.99
7	20	0.24	0.13	0.17	30.66	15.82	21.14	2.19	1.13	1.51
7	30	0.41	0.12	0.37	51.38	14.98	46.76	3.67	1.07	3.34
7	43	0.74	0.15	0.84	92.68	18.48	106.40	6.62	1.32	7.60
7	50	0.83	0.14	1.12	105.14	17.64	140.56	7.51	1.26	10.04
7	60	1.03	0.10	1.62	129.92	12.32	204.54	9.28	0.88	14.61
7	71	1.23	0.08	2.03	154.70	10.64	255.64	11.05	0.76	18.26
7	80	1.26	0.04	2.03	158.90	4.48	255.64	11.35	0.32	18.26
7	90	1.29	0.07	1.99	162.96	8.82	251.44	11.64	0.63	17.96
10	20	0.22	0.13	0.16	57.54	33.04	42.42	4.11	2.36	3.03
10	30	0.40	0.09	0.50	103.04	24.22	127.68	7.36	1.73	9.12
10	43	0.67	0.10	1.08	173.32	26.46	276.92	12.38	1.89	19.78
10	50	0.79	0.11	1.37	202.30	28.70	351.54	14.45	2.05	25.11
10	60	0.96	0.09	1.82	247.80	24.22	468.86	17.70	1.73	33.49
10	71	1.11	0.06	2.07	284.90	15.40	532.84	20.35	1.10	38.06
10	80	1.17	0.00	2.11	301.56	0.00	543.48	21.54	0.00	38.82
10	90	1.03	0.03	1.99	264.32	6.58	511.42	18.88	0.47	36.53

cable: 6x25
diameter (in): 5/8
length (in): 160.0
tension: low

speed (kt)	angle (deg)	cx	cy	cz	fx (lb)	fy (lb)	fz (lb)	fx/l (lb/ft)	fy/l (lb/ft)	fz/l (lb/ft)
2	30	0.42	0.42	0.14	3.36	3.36	1.12	0.24	0.24	0.08
2	60	1.27	0.38	1.06	10.22	3.08	8.54	0.73	0.22	0.61
2	90	1.18	0.05	0.90	9.52	0.42	7.28	0.68	0.03	0.52
5	30	0.44	0.40	0.44	21.98	20.30	22.12	1.57	1.45	1.58
5	60	1.11	0.52	1.98	55.86	26.46	99.96	3.99	1.89	7.14
5	90	0.07	0.07	0.26	3.78	3.50	12.60	0.27	0.26	0.90
7	30	0.43	0.38	0.60	42.98	37.94	59.50	3.07	2.71	4.26
7	60	1.00	0.49	2.20	98.84	48.58	217.28	7.06	3.47	15.52
7	90	0.52	0.26	1.21	51.38	25.62	119.14	3.67	1.83	8.51
10	30	0.41	0.32	0.69	82.32	63.98	138.32	5.88	4.57	9.88
10	60	0.94	0.42	2.22	189.84	83.86	447.58	13.56	5.99	31.97
10	90	1.51	0.02	2.80	264.32	4.48	564.76	18.88	0.32	40.34

cable: 6x25
diameter (in): 5/8
length (in): 160.0
tension: high

speed (kt)	angle (deg)	cx	cy	cz	fx (lb)	fy (lb)	fz (lb)	fx/l (lb/ft)	fy/l (lb/ft)	fz/l (lb/ft)
2	30	0.47	0.42	0.16	3.78	3.36	1.26	0.27	0.24	0.09
2	60	0.31	0.09	0.92	2.52	0.70	7.42	0.18	0.05	0.53
2	90	1.39	0.14	0.75	11.20	1.12	6.02	0.80	0.08	0.43
5	30	0.45	0.31	0.44	22.82	15.40	22.12	1.63	1.10	1.58
5	60	1.04	0.46	1.31	52.50	23.38	65.94	3.75	1.67	4.71
5	90	1.40	0.04	1.60	70.70	1.82	80.64	5.05	0.13	5.76
7	30	0.43	0.30	0.47	42.98	29.96	46.76	3.07	2.14	3.34
7	60	1.02	0.53	1.68	100.94	52.08	166.04	7.21	3.72	11.86
7	90	1.51	0.05	1.90	129.92	4.48	187.46	9.28	0.32	13.39
10	30	0.45	0.33	0.58	90.58	66.22	117.04	6.47	4.73	8.36
10	60	0.98	0.42	1.90	198.10	83.86	383.60	14.15	5.99	27.40
10	90	1.21	0.09	1.98	243.60	17.64	394.24	17.40	1.26	28.16

REDUCED ACCELEROMETER DATA

A variety of values have been noted from the accelerometer spectra and are presented in tabular form. For each set of runs including the eight angles for each cable, speed, and tension range, the following values are tabulated:

RUN	Test run number corresponding to the number of the associated spectral plot.
ANGLE	Yaw angle, β.
FREQ(HZ)	First harmonic vibration frequency chosen from the y-spectrum as the frequency corresponding to the highest acceleration amplitude.
X-AMP(DB)	Decibel level from the x-spectrum at the associated frequency.
Y-AMP(DB)	Decibel level from the y-spectrum at the associated frequency.
GAIN	Accelerometer amplifier gain.
T1(LB)	Applied tension at the beginning of the run in pounds.
T2(LB)	Applied tension at the end of the run in pounds.

REDUCED ACCELEROMETER DATA

2 knots 1x19 Low tension

RUN	ANGLE	FREQ(HZ)	X-AMP(DB)	Y-AMP(DB)	GAIN	T1(LB)	T2(LB)
13	90.	15.	-18.2	-22.1	10.	504.5	--
16	80.	15.	-16.5	-14.8	10.	601.0	--
21	71.	15.	-16.3	-16.6	10.	560.5	--
25	60.	11.	-27.5	-33.9	10.	--	--
30	50.	10.	-32.4	-42.6	10.	--	--
34	43.	6.	-45.6	-46.4	10.	--	--
38	30.	6.	-32.2	-31.2	10.	--	--
42	20.	5.	-30.2	-30.4	10.	--	--

2 knots 7x7 Low tension

RUN	ANGLE	FREQ(HZ)	X-AMP(DB)	Y-AMP(DB)	GAIN	T1(LB)	T2(LB)
47	90.	16.	-38.0	-20.6	10.	--	--
52	80.	16.	-37.0	-21.3	10.	595.7	593.9
56	71.	11.	-52.0	-38.1	10.	567.6	566.2
60	60.	11.	-52.0	-38.9	10.	567.8	566.5
64	50.	11.	-50.4	-40.7	10.	560.8	560.6
68	43.	5.	-50.0	-49.3	10.	562.3	562.0
72	30.	5.	-46.0	-43.4	10.	556.6	556.6
76	20.	5.	-39.0	-35.6	10.	557.6	557.7

2 knots 3x19 Low tension

RUN	ANGLE	FREQ(HZ)	X-AMP(DB)	Y-AMP(DB)	GAIN	T1(LB)	T2(LB)
83	90.	18.	-35.9	-33.5	10.	592.7	592.1
87	80.	12.	-34.0	-39.6	10.	523.2	522.8
91	71.	12.	-33.2	-36.6	10.	604.6	603.6
95	60.	11.	-54.2	-31.4	10.	621.0	619.1
99	50.	11.	-54.5	-32.6	10.	597.2	596.7
103	43.	6.	-57.0	-46.7	10.	591.8	591.5
107	30.	6.	-42.1	-25.5	10.	591.6	591.3
111	20.	5.	-51.1	-34.4	10.	577.1	577.6

2 knots 4x7 serrated Low tension

RUN	ANGLE	FREQ(HZ)	X-AMP(DB)	Y-AMP(DB)	GAIN	T1(LB)	T2(LB)
117	90.	11.	-47.0	-37.0	10.	610.9	610.7
121	80.	11.	-43.0	-31.2	10.	603.0	601.7
125	71.	10.	-40.0	-32.0	10.	573.4	573.2
129	60.	10.	-38.0	-27.0	10.	564.7	564.1
133	50.	9.	-41.0	-36.7	10.	569.0	568.6
137	43.	5.	-52.0	-45.0	10.	556.2	556.1
141	30.	5.	-63.0	-42.8	1.	564.3	564.5
145	20.	5.	-58.0	-45.0	10.	564.6	564.6

2 knots 1x19 High tension

RUN	ANGLE	FREQ(HZ)	X-AMP(DB)	Y-AMP(DB)	GAIN	T1(LB)	T2(LB)
259	90.	17.	-30.8	-26.2	10.	864.8	864.0
263	80.	18.	-26.4	-22.6	10.	853.4	853.3
267	71.	25.	-35.7	-39.2	10.	858.4	857.4
271	60.	12.	-42.0	-38.0	10.	850.8	850.7
275	50.	26.	-42.0	-42.0	10.	849.0	848.8
279	43.	7.	-48.4	-39.4	10.	852.4	852.4
283	30.	6.	-42.0	-30.6	10.	845.9	845.2
287	20.	5.	-53.0	-49.3	10.	845.0	845.1

2 knots 7x7 High tension

RUN	ANGLE	FREQ(HZ)	X-AMP(DB)	Y-AMP(DB)	GAIN	T1(LB)	T2(LB)
222	90.	13.	-46.6	-34.0	10.	889.1	887.7
226	80.	12.	-52.5	-36.0	10.	827.8	828.0
230	71.	13.	-55.0	-38.0	10.	824.0	824.0
234	60.	12.	-55.8	-40.0	10.	898.2	897.4
238	50.	12.	-57.6	-52.4	10.	883.8	883.1
242	43.	7.	-60.1	-38.0	10.	880.9	881.5
246	30.	6.	-43.0	-30.0	10.	883.3	883.7
250	20.	5.	-64.1	-58.6	10.	880.5	883.1

2 knots 3x19 High tension

RUN	ANGLE	FREQ(HZ)	X-AMP(DB)	Y-AMP(DB)	GAIN	T1(LB)	T2(LB)
187	90.	14.	-50.8	-41.0	10.	892.0	890.0
192	80.	13.	-50.3	-40.0	10.	836.8	836.9
196	71.	13.	-52.5	-42.0	10.	835.1	834.9
200	60.	7.	-50.2	-43.0	10.	897.7	897.3
204	50.	7.	-41.6	-40.0	10.	876.7	876.5
208	43.	7.	-43.1	-35.0	10.	879.9	879.9
212	30.	7.	-36.2	-31.9	10.	879.1	879.2
216	20.	7.	-59.0	-64.5	10.	859.5	859.5

2 knots 4x7 serrated High tension

RUN	ANGLE	FREQ(HZ)	X-AMP(DB)	Y-AMP(DB)	GAIN	T1(LB)	T2(LB)
149	90.	12.	-39.2	-31.9	10.	890.0	890.7
153	80.	12.	-42.0	-28.8	10.	870.9	--
157	71.	12.	-42.0	-28.7	10.	861.5	861.4
161	60.	18.	-60.0	-40.0	10.	860.5	860.2
165	50.	7.	-41.0	-28.2	10.	861.0	860.7
171	43.	7.	-35.0	-22.7	10.	861.2	861.2
175	30.	5.	-57.0	-56.2	10.	865.9	865.9
179	20.	6.	-35.0	-18.9	10.	897.3	896.4

5 knots 1x19 Low tension

RUN	ANGLE	FREQ(HZ)	X-AMP(DB)	Y-AMP(DB)	GAIN	T1(LB)	T2(LB)
14	90.	29.	-15.4	-14.4	10.	496.2	--
18	80.	30.	-14.9	-8.8	10.	564.6	--
23	71.	30.	-36.3	-34.7	1.	547.4	--
27	60.	28.	-10.0	-10.6	10.	--	--
32	50.	23.	-14.1	-20.6	10.	--	--
36	43.	22.	-24.7	-17.7	10.	--	--
40	30.	15.	-18.9	-10.2	10.	--	--
44	20.	10.	-40.6	-43.2	10.	--	--

5 knots 7x7 Low tension

RUN	ANGLE	FREQ(HZ)	X-AMP(DB)	Y-AMP(DB)	GAIN	T1(LB)	T2(LB)
50	90.	31.	-30.0	-11.5	10.	--	--
54	80.	30.	-38.0	-10.6	10.	569.8	571.7
58	71.	30.	-35.0	-8.7	10.	563.8	557.2
62	60.	29.	-40.0	-11.3	10.	566.4	566.6
66	50.	28.	-43.2	-22.2	10.	560.6	561.3
70	43.	23.	-27.0	-18.9	10.	565.5	565.4
74	30.	16.	-14.0	-9.8	10.	563.5	563.5
78	20.	11.	-33.0	-29.3	10.	556.9	556.9

5 knots 3x19 Low tension

RUN	ANGLE	FREQ(HZ)	X-AMP(DB)	Y-AMP(DB)	GAIN	T1(LB)	T2(LB)
85	90.	33.	-10.6	-8.7	10.	540.1	--
89	80.	31.	-12.7	-9.1	10.	526.8	528.3
93	71.	32.	-18.5	-7.3	10.	550.0	--
97	60.	27.	-25.7	-13.5	10.	594.2	594.3
101	50.	25.	-30.0	-16.3	10.	595.2	594.7
105	43.	24.	-29.3	-16.3	10.	592.7	592.3
109	30.	18.	-19.7	-6.6	10.	586.0	585.7
113	20.	12.	-47.1	-26.5	10.	581.2	580.7

5 knots 4x7 serrated Low tension

RUN	ANGLE	FREQ(HZ)	X-AMP(DB)	Y-AMP(DB)	GAIN	T1(LB)	T2(LB)
119	90.	30.	-25.0	-7.0	10.	529.3	529.4
123	80.	30.	-42.0	-26.0	1.	568.1	568.8
127	71.	30.	-22.0	-9.6	10.	565.7	566.2
131	60.	5.	-46.0	-29.4	10.	562.2	562.7
135	50.	22.	-14.0	-13.5	10.	563.6	563.6
139	43.	21.	-16.0	-17.0	10.	563.7	563.7
143	30.	16.	-22.0	-5.7	10.	564.7	564.6
147	20.	10.	-36.0	-24.5	10.	564.4	564.4

5 knots 1x19 High tension

RUN	ANGLE	FREQ(HZ)	X-AMP(DB)	Y-AMP(DB)	GAIN	T1(LB)	T2(LB)
261	90.	32.	-36.6	-5.4	10.	856.4	856.4
265	80.	32.	-28.8	-5.8	10.	859.0	859.6
269	71.	31.	-23.9	-7.0	10.	854.8	855.3
273	60.	26.	-21.8	-19.4	10.	853.4	853.8
277	50.	25.	-23.0	-19.9	10.	852.0	852.8
281	43.	18.	-27.0	-26.7	10.	845.0	845.2
285	30.	16.	-27.0	-22.9	10.	845.2	845.3
289	20.	12.	-34.7	-37.2	10.	845.1	844.9

5 knots 7x7 High tension

RUN	ANGLE	FREQ(HZ)	X-AMP(DB)	Y-AMP(DB)	GAIN	T1(LB)	T2(LB)
224	90.	32.	-36.8	-8.0	10.	8[illegible].9	831.6
228	80.	32.	-34.4	-8.0	10.	826.0	826.1
232	71.	32.	-32.9	-10.0	10.	840.0	824.8
236	60.	29.	-33.0	-24.0	10.	884.1	884.0
240	50.	26.	-33.1	-23.4	10.	881.6	881.6
244	43.	20.	-31.3	-12.5	10.	880.5	880.8
248	30.	18.	-30.3	-14.2	10.	879.6	880.0
252	20.	12.	-55.7	-35.8	10.	879.0	880.1

5 knots 3x19 High tension

RUN	ANGLE	FREQ(HZ)	X-AMP(DB)	Y-AMP(DB)	GAIN	T1(LB)	T2(LB)
189	90.	37.	-31.1	-18.4	10.	843.3	842.9
194	80.	30.	-36.6	-20.7	10.	834.0	834.0
198	71.	29.	-35.4	-23.1	10.	831.2	831.6
202	60.	28.	-29.1	-20.5	10.	877.7	877.4
206	50.	22.	-23.0	-15.7	10.	880.5	880.1
210	43.	22.	-20.9	-12.9	10.	879.1	879.1
214	30.	20.	-26.4	-17.0	10.	879.1	879.1
218	20.	13.	-53.8	-39.4	10.	859.5	859.4

5 knots 4x7 serrated High tension

RUN	ANGLE	FREQ(HZ)	X-AMP(DB)	Y-AMP(DB)	GAIN	T1(LB)	T2(LB)
151	90.	27.	-24.9	-15.0	10.	894.7	890.0
155	80.	27.	-23.9	-11.7	10.	861.2	860.8
159	71.	27.	-24.1	-14.3	10.	859.5	860.2
163	60.	26.	-20.1	-13.4	10.	860.9	860.9
167	50.	21.	-23.9	-6.8	10.	862.4	862.6
173	43.	20.	-21.6	-3.7	10.	866.3	866.0
177	30.	18.	-25.7	-11.0	10.	864.0	863.8
181	20.	13.	-54.0	-43.0	10.	856.0	856.0

7 knots 1x19 Low tension

RUN	ANGLE	FREQ(HZ)	X-AMP(DB)	Y-AMP(DB)	GAIN	T1(LB)	T2(LB)
15	90.	44.	-34.8	-30.1	1.	505.0	--
18	80.	44.	-34.0	-30.0	1.	564.6	--
24	71.	44.	-34.5	-29.0	1.	556.0	--
28	60.	--	--	--	1.	--	--
33	50.	35.	-48.0	-34.8	1.	--	--
37	43.	29.	-39.8	-24.7	1.	--	--
41	30.	22.	-51.8	-42.1	1.	--	--
45	20.	15.	-39.0	-31.4	1.	--	--

7 knots 7x7 Low tension

RUN	ANGLE	FREQ(HZ)	X-AMP(DB)	Y-AMP(DB)	GAIN	T1(LB)	T2(LB)
51	90.	44.	-33.1	-7.5	10.	--	--
55	80.	44.	-47.4	-29.3	1.	571.7	575.5
59	71.	41.	-43.3	-29.4	1.	567.2	572.3
63	60.	40.	-54.0	-36.9	1.	566.6	570.0
67	50.	36.	-53.1	-31.3	1.	561.3	568.2
71	43.	30.	-32.9	-27.1	1.	564.3	566.4
75	30.	23.	-43.8	-38.8	1.	563.5	561.9
79	20.	16.	-31.6	-28.3	1.	556.9	556.2

7 knots 3x19 Low tension

RUN	ANGLE	FREQ(HZ)	X-AMP(DB)	Y-AMP(DB)	GAIN	T1(LB)	T2(LB)
86	90.	44.	-28.8	-29.0	1.	523.7	533.9
90	80.	43.	-33.2	-32.0	1.	528.5	524.2
94	71.	42.	-36.0	-26.7	1.	537.2	544.6
98	60.	36.	-35.9	-27.3	1.	594.1	602.9
102	50.	34.	-30.9	-22.2	1.	594.9	597.0
106	43.	32.	-31.5	-22.9	1.	592.6	592.7
110	30.	25.	-50.4	-38.1	1.	585.7	584.9
114	20.	18.	-39.7	-27.4	1.	580.8	580.3

7 knots 4x7 serrated Low tension

RUN	ANGLE	FREQ(HZ)	X-AMP(DB)	Y-AMP(DB)	GAIN	T1(LB)	T2(LB)
120	90.	39.	-36.1	-24.4	1.	529.4	534.2
124	80.	39.	-33.1	-22.4	1.	568.8	575.0
128	71.	38.	-32.8	-21.4	1.	566.4	572.7
132	60.	33.	-27.5	-15.4	1.	562.6	568.2
136	50.	31.	-28.4	-16.4	1.	563.7	567.3
140	43.	29.	-31.0	-18.4	1.	563.8	563.5
144	30.	22.	-35.1	-38.9	1.	564.6	564.6
148	20.	16.	-43.2	-28.0	1.	564.5	564.2

7 knots 1x19 High tension

RUN	ANGLE	FREQ(HZ)	X-AMP(DB)	Y-AMP(DB)	GAIN	T1(LB)	T2(LB)
262	90.	43.	-47.9	-28.5	1.	856.5	856.5
266	80.	42.	-39.9	-27.6	1.	859.5	858.8
270	71.	41.	-40.7	-34.9	1.	855.2	854.2
274	60.	38.	-41.0	-36.9	1.	853.8	953.7
278	50.	34.	-35.0	-23.0	1.	852.8	853.0
282	43.	30.	-40.8	-26.5	1.	845.0	855.5
286	30.	24.	-53.2	-48.2	1.	845.1	845.1
290	20.	17.	-43.0	-37.0	1.	845.1	844.8

7 knots 7x7 High tension

RUN	ANGLE	FREQ(HZ)	X-AMP(DB)	Y-AMP(DB)	GAIN	T1(LB)	T2(LB)
225	90.	43.	-45.2	-28.4	1.	831.6	837.5
229	80.	44.	-47.3	-34.2	1.	826.1	833.6
233	71.	43.	-45.6	-34.4	1.	824.8	828.4
237	60.	36.	-39.4	-30.9	1.	883.7	883.5
241	50.	35.	-37.6	-26.7	1.	881.6	881.2
245	43.	33.	-40.6	-27.1	1.	880.8	881.0
249	30.	26.	-63.0	-46.2	1.	880.0	880.0
253	20.	18.	-50.2	-36.2	1.	880.4	880.4

7 knots 3x19 High tension

RUN	ANGLE	FREQ(HZ)	X-AMP(DB)	Y-AMP(DB)	GAIN	T1(LB)	T2(LB)
190	90.	46.	-24.5	-11.3	10.	842.9	847.2
195	80.	39.	-47.0	-31.8	1.	833.9	836.0
199	71.	40.	-38.8	-26.9	1.	831.6	833.4
203	60.	39.	-37.9	-26.7	1.	877.3	877.2
207	50.	32.	-42.9	-39.0	1.	880.0	879.9
211	43.	31.	-45.9	-43.0	1.	879.1	879.1
215	30.	22.	-45.9	-36.0	1.	879.2	879.1
219	20.	20.	-54.2	-39.7	1.	859.4	858.1

7 knots 4x7 serrated High tension

RUN	ANGLE	FREQ(HZ)	X-AMP(DB)	Y-AMP(DB)	GAIN	T1(LB)	T2(LB)
152	90.	37.	-27.6	-19.7	1.	889.8	885.4
156	80.	37.	-26.6	-18.3	1.	860.9	863.0
160	71.	37.	-25.8	-17.3	1.	860.2	861.1
164	60.	35.	-25.9	-16.6	1.	860.9	860.6
168	50.	34.	-32.9	-20.9	1.	862.6	862.0
174	43.	27.	-43.3	-34.3	1.	866.0	864.3
178	30.	20.	-39.0	-22.9	1.	863.8	863.4
182	20.	19.	-58.0	-43.0	1.	856.0	856.6

10 knots 1x19 Low tension

RUN	ANGLE	FREQ(HZ)	X-AMP(DB)	Y-AMP(DB)	GAIN	T1(LB)	T2(LB)
12	90.	58.	-30.9	-24.8	1.	506.0	--
17	80.	60.	-38.0	-25.0	1.	597.3	--
22	71.	59.	-41.1	-30.8	1.	560.5	--
26	60.	57.	-40.3	-34.9	1.	--	--
31	50.	47.	-38.0	-23.6	1.	--	--
35	43.	43.	-35.7	-23.5	1.	--	--
39	30.	29.	-39.0	-24.2	1.	--	--
43	20.	22.	-50.3	-48.6	1.	--	--

10 knots 7x7 Low tension

RUN	ANGLE	FREQ(HZ)	X-AMP(DB)	Y-AMP(DB)	GAIN	T1(LB)	T2(LB)
48	90.	62.	-27.1	-22.3	1.	--	--
53	80.	62.	-29.9	-25.7	1.	593.9	577.1
57	71.	61.	-33.6	-29.1	1.	566.2	563.9
61	60.	57.	-34.9	-28.5	1.	566.5	566.4
65	50.	47.	-36.9	-27.0	1.	560.6	560.6
69	43.	45.	-33.3	-23.3	1.	562.0	570.0
73	30.	30.	-34.5	-28.5	1.	556.6	567.8
77	20.	23.	-43.4	-39.3	1.	557.7	556.6

10 knots 3x19 Low tension

RUN	ANGLE	FREQ(HZ)	X-AMP(DB)	Y-AMP(DB)	GAIN	T1(LB)	T2(LB)
84	90.	66.	-1.3	-3.9	10.	590.7	541.7
88	80.	66.	-29.4	-30.8	1.	522.6	526.8
92	71.	60.	-36.0	-33.0	1.	588.5	549.5
96	60.	56.	-30.5	-26.2	1.	618.9	604.6
100	50.	46.	-40.3	-34.3	1.	596.6	603.5
104	43.	43.	-42.0	-34.6	1.	591.5	599.2
108	30.	33.	-36.9	-28.6	1.	591.2	591.0
112	20.	25.	-57.7	-46.2	1.	577.7	578.4

10 knots 4x7 serrated Low tension

RUN	ANGLE	FREQ(HZ)	X-AMP(DB)	Y-AMP(DB)	GAIN	T1(LB)	T2(LB)
118	90.	54.	-33.8	-23.6	1.	610.7	537.4
122	80.	54.	-24.7	-15.7	1.	601.6	576.3
126	71.	53.	-30.2	-20.8	1.	573.2	573.0
130	60.	50.	-34.4	-23.8	1.	564.0	568.9
134	50.	48.	-41.4	-30.5	1.	568.6	569.2
138	43.	40.	-37.1	-27.8	1.	556.1	568.2
142	30.	30.	-35.6	-24.5	1.	564.5	564.7
146	20.	21.	-42.3	-44.7	1.	564.6	563.7

10 knots 1x19 High tension

RUN	ANGLE	FREQ(HZ)	X-AMP(DB)	Y-AMP(DB)	GAIN	T1(LB)	T2(LB)
260	90.	61.	-52.3	-25.4	1.	864.1	869.1
264	80.	60.	-48.1	-27.2	1.	853.3	862.5
268	71.	60.	-41.9	-23.3	1.	857.5	863.0
272	60.	52.	-38.5	-20.1	1.	850.7	853.2
276	50.	49.	-42.4	-30.0	1.	848.8	862.1
280	43.	40.	-48.2	-39.4	1.	852.4	852.3
284	30.	30.	-38.0	-20.7	1.	845.2	845.3
288	20.	24.	-46.0	-41.0	1.	845.2	844.9

10 knots 7x7 High tension

RUN	ANGLE	FREQ(HZ)	X-AMP(DB)	Y-AMP(DB)	GAIN	T1(LB)	T2(LB)
223	90.	63.	-24.5	-25.0	1.	887.7	843.3
227	80.	--	--	--	1.	828.1	836.3
231	71.	58.	-23.2	-24.0	1.	823.9	834.6
235	60.	56.	-29.1	-29.1	1.	896.9	893.3
239	50.	52.	-33.5	-30.5	1.	883.1	893.2
243	43.	49.	-43.2	-34.8	1.	881.5	885.1
247	30.	33.	-44.3	-31.3	1.	883.7	880.2
251	20.	20.	-52.2	-40.8	1.	883.1	879.4

10 knots 3x19 High tension

RUN	ANGLE	FREQ(HZ)	X-AMP(DB)	Y-AMP(DB)	GAIN	T1(LB)	T2(LB)
188	90.	64.	-38.4	-24.0	1.	890.8	851.6
193	80.	62.	-38.6	-23.0	1.	836.9	844.1
197	71.	61.	-35.0	-24.0	1.	834.9	841.3
201	60.	59.	-41.1	-30.9	1.	897.2	882.4
205	50.	49.	-37.7	-30.0	1.	876.6	888.9
209	43.	41.	-41.5	-32.1	1.	879.9	879.9
213	30.	36.	-42.3	-28.0	1.	879.2	879.3
217	20.	22.	-47.1	-36.8	1.	859.5	858.2

10 knots 4x7 serrated High tension

RUN	ANGLE	FREQ(HZ)	X-AMP(DB)	Y-AMP(DB)	GAIN	T1(LB)	T2(LB)
150	90.	56.	-31.3	-25.1	1.	890.5	815.3
154	80.	57.	-32.0	-24.7	1.	870.2	873.0
158	71.	51.	-30.0	-20.4	1.	861.4	871.1
162	60.	48.	-31.0	-22.1	1.	860.1	870.8
166	50.	45.	-35.0	-25.0	1.	860.7	873.0
170	43.	38.	-26.0	-16.5	1.	862.4	861.7
176	30.	28.	-45.0	-31.2	1.	865.9	863.9
180	20.	20.	-40.0	-23.3	1.	896.4	855.5

QUANTITIES CALCULATED FROM ACCELEROMETER DATA

For each set of runs including all eight angles for each speed, tension range, and cable, the following quantitites are calculated and tabulated:

FUNDAMENTAL X ACCELERATIONS, G-S: The acceleration of the cable in the x-direction has been converted from decibels to g's (32.17 ft/sec. sec).

FUNDAMENTAL X AMPLITUDE, INCHES: A simple double integration based on acceleration and frequency has been used to estimate the vibrational amplitude of the cable in the x-direction in inches.

FUNDAMENTAL Y ACCELERATIONS, G-S: The acceleration of the cable in the y-direction has been converted from decibels to g's (32.17 ft/sec. sec).

FUNDAMENTAL Y AMPLITUDE, INCHES: A simple double integration based on acceleration and frequency has been used to estimate the vibrational amplitude of the cable in the y-direction in inches.

VECTOR ADDITION OF SUPERPOSED AMPLITUDES, INCHES: The x- and y-amplitudes have been added vectorially to estimate a maximum vibrational amplitude.

AMPLITUDE TO DIAMETER RATIO: The maximum amplitude estimate has been divided by the maximum measured cable diameter to provide the amplitude to diameter ratio.

NOMINAL STROUHAL NUMBERS: The ratio St = (f D)/V with

St = nominal Strouhal number for the cable
f = fundamental vibrational frequency in Hz
D = cable diameter
V = flow velocity

has been calculated.

The acceleration in g's was calculated from the spectra by the following procedure:

1. Actual decibel level was calculated from the displayed decibel level based on the full scale voltage of the spectral plot:

$$dB_a = dB_p + 20 \log (\text{scale})$$

dB_a = actual decibel level

dB_p = plotted decibel level

scale = full scale voltage of the plot.

The full scale voltage is noted on each plot in the top right corner as:

A 1V B 1V

where A and B designate Spectra A and B, and 1V designates a 1V full scale voltage. The full scale voltages used were 0.5V, 1V, and 2V.

2. Actual voltage was determined by converting the actual dB level to voltage by

$$v = 10 \exp(dB_a/20)$$

3. G's were calculated from the actual voltages based on the amplifier gain:

$$g = 0.0022 \, K \, v$$

where g = acceleration in g's
K = accelerometer amplifier gain.

2 knots, low tension

FUNDAMENTAL X ACCELERATION, G-S

DEGREES	1X19	7X7	3X19	4X7
90.00000	5.59213	0.57224	0.72875	0.20304
80.00000	6.80107	0.64206	0.90694	0.32179
71.00000	6.95949	0.11418	0.99444	0.45455
60.00000	1.91680	0.11418	0.08863	0.57224
50.00000	1.09038	0.13727	0.08562	0.40511
43.00000	0.23855	0.14374	0.06421	0.11418
30.00000	1.11578	0.22781	0.35693	0.32179
20.00000	1.40468	0.51001	0.12664	0.05722

FUNDAMENTAL X AMPLITUDE, INCHES

DEGREES	1X19	7X7	3X19	4X7
90.00000	0.24303	0.02186	0.02199	0.01641
80.00000	0.29558	0.02453	0.06159	0.02601
71.00000	0.30246	0.00923	0.06753	0.04445
60.00000	0.15490	0.00923	0.00716	0.05596
50.00000	0.10662	0.01109	0.00692	0.04891
43.00000	0.06480	0.05622	0.01744	0.04466
30.00000	0.30307	0.08911	0.09695	0.12587
20.00000	0.54943	0.19949	0.04953	0.02238

FUNDAMENTAL Y ACCELERATION, G-S

DEGREES	1X19	7X7	3X19	4X7
90.00000	3.56925	4.24207	0.96068	0.64206
80.00000	8.27137	3.91361	0.47597	1.25192
71.00000	6.72322	0.56569	0.67232	1.14247
60.00000	0.91744	0.51591	1.22343	2.03038
50.00000	0.33696	0.41935	1.06556	0.66463
43.00000	0.21756	0.15580	0.21017	0.25561
30.00000	1.25192	0.30731	2.41311	3.29289
20.00000	1.37271	0.75436	0.86612	0.25561

FUNDAMENTAL Y AMPLITUDE, INCHES

DEGREES	1X19	7X7	3X19	4X7
90.00000	0.15512	0.16204	0.02899	0.05189
80.00000	0.35947	0.14949	0.03232	0.10117
71.00000	0.29219	0.04572	0.04565	0.11165
60.00000	0.07414	0.04169	0.09887	0.19854
50.00000	0.03295	0.03389	0.08611	0.08024
43.00000	0.05909	0.00094	0.05709	0.09998
30.00000	0.34005	0.12020	0.65546	1.28798
20.00000	0.53692	0.29506	0.33877	0.09998

VECTOR ADDITION OF SUPERPOSED AMPLITUDES, INCHES

DEGREES	1X19	7X7	3X19	4X7
90.00000	0.28832	0.16350	0.03639	0.05442
80.00000	0.46539	0.15149	0.06955	0.10446
71.00000	0.42055	0.04664	0.08151	0.12017
60.00000	0.17173	0.04270	0.09913	0.20628
50.00000	0.11160	0.03566	0.08639	0.09397
43.00000	0.08770	0.08291	0.05969	0.10950
30.00000	0.45551	0.14963	0.66259	1.29412
20.00000	0.76822	0.35617	0.34238	0.10245

AMPLITUDE TO DIAMETER RATIO

DEGREES	1X19	7X7	3X19	4X7
90.00000	0.45620	0.25547	0.05917	0.07774
80.00000	0.73637	0.23670	0.11309	0.14923
71.00000	0.66542	0.07287	0.13254	0.17167
60.00000	0.27173	0.06672	0.16119	0.29468
50.00000	0.17658	0.05572	0.14047	0.13424
43.00000	0.13876	0.12955	0.09706	0.15643
30.00000	0.72075	0.23379	1.07739	1.84874
20.00000	1.21553	0.55651	0.55671	0.14636

NOMINAL STROUHAL NUMBERS

DEGREES	1X19	7X7	3X19	4X7
90.00000	0.23400	0.25280	0.27324	0.19008
80.00000	0.23761	0.25670	0.18497	0.19301
71.00000	0.24749	0.18382	0.19266	0.18276
60.00000	0.19815	0.20069	0.19281	0.19953
50.00000	0.20365	0.22688	0.21798	0.20302
43.00000	0.13725	0.11584	0.13355	0.12669
30.00000	0.18720	0.15800	0.18216	0.17280
20.00000	0.22806	0.23098	0.22192	0.25262

2 knots, high tension

FUNDAMENTAL X ACCELERATION, G-S

DEGREES	1X19	7X7	3X19	4X7
90.00000	1.31092	0.21261	0.13109	0.49840
80.00000	2.17559	0.10779	0.13886	0.36106
71.00000	0.74572	0.08083	0.10779	0.36106
60.00000	0.36106	0.07372	0.14047	0.04545
50.00000	0.36106	0.05992	0.37807	0.40511
43.00000	0.17281	0.04493	0.31811	0.80831
30.00000	0.36106	0.32179	0.70401	0.06421
20.00000	0.10176	0.02835	0.05100	0.80831

FUNDAMENTAL X AMPLITUDE, INCHES

DEGREES	1X19	7X7	3X19	4X7
90.00000	0.04436	0.01230	0.00654	0.03384
80.00000	0.06566	0.00732	0.00803	0.02452
71.00000	0.01167	0.00468	0.00624	0.02452
60.00000	0.02452	0.00501	0.02803	0.00137
50.00000	0.00522	0.00407	0.07545	0.08085
43.00000	0.03449	0.00897	0.06348	0.16131
30.00000	0.09807	0.08741	0.14049	0.02511
20.00000	0.03980	0.01109	0.01018	0.21956

FUNDAMENTAL Y ACCELERATION, G-S

DEGREES	1X19	7X7	3X19	4X7
90.00000	2.22627	0.90694	0.40511	1.15499
80.00000	3.36959	0.72041	0.45455	1.65036
71.00000	0.49840	0.57224	0.36106	1.66946
60.00000	0.57224	0.45455	0.32179	0.45455
50.00000	0.36106	0.10904	0.45455	1.76839
43.00000	0.48705	0.57224	0.80831	3.33102
30.00000	1.34146	1.43740	1.15499	0.07040
20.00000	0.15580	0.05340	0.02708	5.15914

FUNDAMENTAL Y AMPLITUDE, INCHES

DEGREES	1X19	7X7	3X19	4X7
90.00000	0.07533	0.05248	0.02021	0.07843
80.00000	0.10170	0.04892	0.02630	0.11207
71.00000	0.00780	0.03311	0.02089	0.11337
60.00000	0.03886	0.03087	0.06422	0.01372
50.00000	0.00522	0.00740	0.09071	0.35290
43.00000	0.09720	0.11420	0.16131	0.66474
30.00000	0.36437	0.39043	0.23049	0.02754
20.00000	0.06094	0.02089	0.00540	1.40135

VECTOR ADDITION OF SUPERPOSED AMPLITUDES, INCHES

DEGREES	1X19	7X7	3X19	4X7
90.00000	0.08742	0.05390	0.02124	0.08542
80.00000	0.12105	0.04946	0.02750	0.11472
71.00000	0.01403	0.03344	0.02180	0.11599
60.00000	0.04595	0.03127	0.07007	0.01379
50.00000	0.00739	0.00845	0.11799	0.36204
43.00000	0.10313	0.11455	0.17335	0.68404
30.00000	0.37734	0.40010	0.26993	0.03727
20.00000	0.07279	0.02365	0.01152	1.41845

AMPLITUDE TO DIAMETER RATIO

DEGREES	1X19	7X7	3X19	4X7
90.00000	0.13832	0.08422	0.03454	0.12203
80.00000	0.19154	0.07729	0.04472	0.16389
71.00000	0.02220	0.05225	0.03545	0.16570
60.00000	0.07270	0.04886	0.11393	0.01970
50.00000	0.01169	0.01320	0.19185	0.51721
43.00000	0.16319	0.17898	0.28187	0.97719
30.00000	0.59706	0.62515	0.43892	0.05324
20.00000	0.11517	0.03695	0.01874	2.02636

NOMINAL STROUHAL NUMBERS

DEGREES	1X19	7X7	3X19	4X7
90.00000	0.26520	0.20540	0.21252	0.20736
80.00000	0.28513	0.19253	0.20039	0.21056
71.00000	0.41247	0.21724	0.20871	0.21931
60.00000	0.21616	0.21893	0.12270	0.35916
50.00000	0.52948	0.24751	0.13871	0.15790
43.00000	0.16012	0.16217	0.15581	0.17736
30.00000	0.18720	0.18960	0.21252	0.17280
20.00000	0.22806	0.23098	0.31069	0.30314

5 knots, low tension

FUNDAMENTAL X ACCELERATION, G-S

DEGREES	1X19	7X7	3X19	4X7
90.00000	7.71929	1.43740	13.41459	2.55610
80.00000	8.17669	0.57224	10.53361	3.61058
71.00000	13.91898	0.80831	5.40228	3.61058
60.00000	7.18699	0.45455	2.35818	0.22781
50.00000	4.48278	0.31447	1.43740	9.06937
43.00000	2.64592	2.03038	1.55804	7.20406
30.00000	5.15914	9.06937	4.70519	3.61058
20.00000	0.42421	1.01760	0.20071	0.72041

FUNDAMENTAL X AMPLITUDE, INCHES

DEGREES	1X19	7X7	3X19	4X7
90.00000	0.08975	0.01463	0.12045	0.02777
80.00000	0.08884	0.00622	0.10718	0.03923
71.00000	0.15123	0.00878	0.05159	0.03923
60.00000	0.08964	0.00529	0.03163	0.08911
50.00000	0.08286	0.00392	0.02249	0.18323
43.00000	0.05346	0.03753	0.02645	0.15974
30.00000	0.22422	0.34643	0.14201	0.13791
20.00000	0.04148	0.08224	0.01363	0.07045

FUNDAMENTAL Y ACCELERATION, G-S

DEGREES	1X19	7X7	3X19	4X7
90.00000	8.66119	12.09420	16.69465	20.30380
80.00000	16.50355	13.41459	15.94327	22.78124
71.00000	16.73429	16.69465	19.61450	15.05141
60.00000	26.82918	12.37592	9.60677	1.54020
50.00000	8.48413	3.52840	6.95949	9.60677
43.00000	5.92348	5.15914	6.95949	6.42062
30.00000	14.04680	14.70880	21.26069	23.58182
20.00000	0.31447	1.55804	2.15069	2.70756

FUNDAMENTAL Y AMPLITUDE, INCHES

DEGREES	1X19	7X7	3X19	4X7
90.00000	0.10071	0.12306	0.14991	0.22060
80.00000	0.00000	0.14575	0.16223	0.24752
71.00000	0.18182	0.18139	0.18731	0.16353
60.00000	0.33463	0.14390	0.12886	0.60244
50.00000	0.15683	0.04401	0.10889	0.19409
43.00000	0.11968	0.09537	0.11815	0.14237
30.00000	0.61048	0.56184	0.64166	0.90076
20.00000	0.03075	0.12591	0.14605	0.26476

VECTOR ADDITION OF SUPERPOSED AMPLITUDES, INCHES

DEGREES	1X19	7X7	3X19	4X7
90.00000	0.13490	0.12393	0.19231	0.22234
80.00000	0.08884	0.14588	0.19444	0.25061
71.00000	0.23649	0.18160	0.19428	0.16817
60.00000	0.34643	0.14399	0.13269	0.60899
50.00000	0.17737	0.04418	0.11118	0.26692
43.00000	0.13107	0.10249	0.12107	0.21397
30.00000	0.65035	0.66005	0.65719	0.91126
20.00000	0.05164	0.15039	0.14668	0.27397

AMPLITUDE TO DIAMETER RATIO

DEGREES	1X19	7X7	3X19	4X7
90.00000	0.21345	0.19364	0.31269	0.31763
80.00000	0.14057	0.22794	0.31616	0.35801
71.00000	0.37420	0.28375	0.31590	0.24025
60.00000	0.54815	0.22499	0.21575	0.86999
50.00000	0.28066	0.06904	0.18079	0.38131
43.00000	0.20739	0.16013	0.19687	0.30568
30.00000	1.02903	1.03134	1.06860	1.30180
20.00000	0.08170	0.23498	0.23850	0.39139

NOMINAL STROUHAL NUMBERS

DEGREES	1X19	7X7	3X19	4X7
90.00000	0.18096	0.19592	0.20038	0.20736
80.00000	0.19009	0.19253	0.19114	0.21056
71.00000	0.19799	0.20053	0.20550	0.21931
60.00000	0.20175	0.21164	0.18931	0.03991
50.00000	0.18735	0.23101	0.19816	0.19851
43.00000	0.20129	0.21314	0.21368	0.21284
30.00000	0.18720	0.20224	0.21860	0.22119
20.00000	0.18245	0.20327	0.21304	0.20210

5 knots, high tension

FUNDAMENTAL X ACCELERATION, G-S

DEGREES	1X19	7X7	3X19	4X7
90.00000	0.67232	0.65702	1.26642	2.58570
80.00000	1.65036	0.86612	0.67232	2.90120
71.00000	2.90120	1.02938	0.77193	2.83516
60.00000	3.69468	1.01760	1.59433	4.49342
50.00000	3.21794	1.00595	3.21794	2.90120
43.00000	2.03038	1.23759	4.09805	3.78074
30.00000	2.03038	1.38860	2.17559	2.35818
20.00000	0.83671	0.07457	0.09281	0.09069

FUNDAMENTAL X AMPLITUDE, INCHES

DEGREES	1X19	7X7	3X19	4X7
90.00000	0.00642	0.00627	0.00905	0.03468
80.00000	0.01576	0.00827	0.00730	0.03892
71.00000	0.02952	0.00983	0.00898	0.03803
60.00000	0.05344	0.01183	0.01989	0.06500
50.00000	0.05035	0.01455	0.06501	0.06433
43.00000	0.06128	0.03025	0.08280	0.09243
30.00000	0.07756	0.04191	0.05319	0.07117
20.00000	0.05682	0.00506	0.00537	0.00525

FUNDAMENTAL Y ACCELERATION, G-S

DEGREES	1X19	7X7	3X19	4X7
90.00000	24.41054	18.09578	5.46484	8.08309
80.00000	23.31188	18.09578	4.19351	11.81891
71.00000	20.30380	14.37399	3.18110	8.76148
60.00000	4.87054	2.86799	4.29119	9.71801
50.00000	4.59809	3.07310	7.45723	20.77674
43.00000	2.10173	10.77897	10.29384	29.68775
30.00000	3.25520	8.86293	6.42062	12.81083
20.00000	0.62745	0.73719	0.48705	0.32179

FUNDAMENTAL Y AMPLITUDE, INCHES

DEGREES	1X19	7X7	3X19	4X7
90.00000	0.23310	0.17280	0.03903	0.10842
80.00000	0.22261	0.17280	0.04556	0.15853
71.00000	0.20660	0.13726	0.03699	0.11752
60.00000	0.07045	0.03335	0.05352	0.14057
50.00000	0.07194	0.04445	0.15066	0.46069
43.00000	0.06343	0.26351	0.20797	0.72576
30.00000	0.12434	0.26749	0.15696	0.38664
20.00000	0.04261	0.05006	0.02818	0.01862

VECTOR ADDITION OF SUPERPOSED AMPLITUDES, INCHES

DEGREES	1X19	7X7	3X19	4X7
90.00000	0.23319	0.17292	0.04007	0.11384
80.00000	0.22317	0.17300	0.04614	0.16324
71.00000	0.20870	0.13761	0.03806	0.12352
60.00000	0.08843	0.03538	0.05710	0.15487
50.00000	0.08781	0.04677	0.16409	0.46516
43.00000	0.08820	0.26524	0.22385	0.73162
30.00000	0.14654	0.27075	0.16573	0.39313
20.00000	0.07102	0.05032	0.02869	0.01934

AMPLITUDE TO DIAMETER RATIO

DEGREES	1X19	7X7	3X19	4X7
90.00000	0.36898	0.27018	0.06515	0.16262
80.00000	0.35312	0.27031	0.07503	0.23320
71.00000	0.33022	0.21502	0.06189	0.17646
60.00000	0.13992	0.05529	0.09284	0.22125
50.00000	0.13894	0.07308	0.26682	0.66452
43.00000	0.13955	0.41443	0.36398	1.04517
30.00000	0.23187	0.42305	0.26947	0.56162
20.00000	0.11237	0.07862	0.04665	0.02764

NOMINAL STROUHAL NUMBERS

DEGREES	1X19	7X7	3X19	4X7
90.00000	0.19968	0.20224	0.22466	0.18662
80.00000	0.20276	0.20536	0.18497	0.18950
71.00000	0.20459	0.21389	0.18624	0.19738
60.00000	0.18734	0.21164	0.19632	0.20752
50.00000	0.20365	0.21451	0.17438	0.18948
43.00000	0.16469	0.18534	0.19587	0.20270
30.00000	0.19968	0.22752	0.24288	0.24884
20.00000	0.21894	0.22174	0.23080	0.26273

7 knots, low tension

FUNDAMENTAL X ACCELERATION, G-S

DEGREES	1X19	7X7	3X19	4X7
90.00000	8.27137	1.00595	16.50355	7.12160
80.00000	9.06937	1.93900	9.94437	10.05952
71.00000	8.56204	3.10869	7.20406	10.41303
60.00000	0.00000	0.90694	7.28748	19.16802
50.00000	1.80958	1.00595	12.95918	17.28134
43.00000	4.65133	10.29384	12.09420	12.81083
30.00000	1.16836	2.93479	1.37271	7.99056
20.00000	5.10008	11.95576	4.70519	3.14469

FUNDAMENTAL X AMPLITUDE, INCHES

DEGREES	1X19	7X7	3X19	4X7
90.00000	0.04178	0.00508	0.08336	0.04578
80.00000	0.04581	0.00979	0.05259	0.06467
71.00000	0.04325	0.01808	0.03993	0.07052
60.00000	0.00000	0.00554	0.05499	0.17212
50.00000	0.01444	0.00759	0.10962	0.17584
43.00000	0.05408	0.11184	0.11549	0.14895
30.00000	0.02361	0.05425	0.02148	0.16144
20.00000	0.22165	0.45668	0.14201	0.12012

FUNDAMENTAL Y ACCELERATION, G-S

DEGREES	1X19	7X7	3X19	4X7
90.00000	14.20945	19.16802	16.12788	27.38907
80.00000	14.37399	15.58036	11.41767	34.48080
71.00000	16.12788	15.40201	21.01732	38.68810
60.00000	0.00000	6.49497	19.61450	77.19290
50.00000	8.27137	12.37592	35.28396	68.79824
43.00000	26.45924	20.07138	32.55198	54.64839
30.00000	3.56925	5.21888	5.65689	5.15914
20.00000	12.23425	17.48145	19.38998	18.09578

FUNDAMENTAL Y AMPLITUDE, INCHES

DEGREES	1X19	7X7	3X19	4X7
90.00000	0.07177	0.09682	0.08146	0.17608
80.00000	0.07260	0.07869	0.06038	0.22168
71.00000	0.08146	0.08959	0.11651	0.26199
60.00000	0.00000	0.03969	0.14799	0.69314
50.00000	0.06603	0.09338	0.29846	0.70005
43.00000	0.30765	0.21808	0.31085	0.63541
30.00000	0.07211	0.09647	0.08851	0.10423
20.00000	0.53170	0.66774	0.58520	0.69121

VECTOR ADDITION OF SUPERPOSED AMPLITUDES, INCHES

DEGREES	1X19	7X7	3X19	4X7
90.00000	0.08304	0.09695	0.11655	0.18194
80.00000	0.08585	0.07930	0.08007	0.23092
71.00000	0.09223	0.09140	0.12316	0.27131
60.00000	0.00000	0.04008	0.15788	0.71419
50.00000	0.06759	0.09369	0.31796	0.72179
43.00000	0.31237	0.24508	0.33161	0.65264
30.00000	0.07588	0.11068	0.09107	0.19216
20.00000	0.57605	0.80897	0.60218	0.70157

AMPLITUDE TO DIAMETER RATIO

DEGREES	1X19	7X7	3X19	4X7
90.00000	0.13140	0.15148	0.18951	0.25991
80.00000	0.13583	0.12391	0.13020	0.32988
71.00000	0.14593	0.14281	0.20026	0.38759
60.00000	0.00000	0.06262	0.25671	1.02028
50.00000	0.10694	0.14638	0.51701	1.03113
43.00000	0.49425	0.38294	0.53921	0.93234
30.00000	0.12006	0.17293	0.14809	0.27452
20.00000	0.91147	1.26402	0.97916	1.00224

NOMINAL STROUHAL NUMBERS

DEGREES	1X19	7X7	3X19	4X7
90.00000	0.19611	0.19863	0.19083	0.19255
80.00000	0.19914	0.20169	0.18937	0.19552
71.00000	0.20742	0.19575	0.19266	0.19842
60.00000	0.18734	0.20851	0.18029	0.18813
50.00000	0.20365	0.21215	0.19250	0.19980
43.00000	0.18953	0.19858	0.20351	0.20994
30.00000	0.19612	0.20766	0.21686	0.21724
20.00000	0.19548	0.21119	0.22826	0.23097

7 knots, high tension

FUNDAMENTAL X ACCELERATION, G-S

DEGREES	1X19	7X7	3X19	4X7
90.00000	1.83053	2.49791	2.70756	18.94861
80.00000	4.59809	1.96145	2.03038	21.26068
71.00000	4.19351	2.38549	5.21888	23.31188
60.00000	4.05114	4.87054	5.78865	23.04504
50.00000	8.08309	5.99208	3.25520	10.29384
43.00000	4.14550	4.24206	2.30450	3.10869
30.00000	0.99444	0.32179	2.30450	5.10008
20.00000	3.21793	1.40468	0.88629	0.57224

FUNDAMENTAL X AMPLITUDE, INCHES

DEGREES	1X19	7X7	3X19	4X7
90.00000	0.00968	0.01321	0.01251	0.13535
80.00000	0.02549	0.00991	0.01305	0.15186
71.00000	0.02439	0.01262	0.03190	0.16651
60.00000	0.02743	0.03675	0.03722	0.18396
50.00000	0.06837	0.04783	0.03108	0.08707
43.00000	0.04504	0.03809	0.02345	0.04170
30.00000	0.01688	0.00465	0.04656	0.12468
20.00000	0.10888	0.04239	0.02167	0.01550

FUNDAMENTAL Y ACCELERATION, G-S

DEGREES	1X19	7X7	3X19	4X7
90.00000	17.08352	17.28134	12.37592	47.05192
80.00000	18.94861	8.86293	11.68362	55.28119
71.00000	8.17668	8.66119	20.53891	62.02651
60.00000	6.49497	12.95918	21.01732	67.23219
50.00000	32.17936	21.01732	5.10008	40.98051
43.00000	21.50687	20.07138	3.21793	8.76148
30.00000	1.76839	2.22627	7.20406	32.55198
20.00000	6.42063	7.04007	4.70519	3.21793

FUNDAMENTAL Y AMPLITUDE, INCHES

DEGREES	1X19	7X7	3X19	4X7
90.00000	0.09035	0.09139	0.05719	0.33608
80.00000	0.10504	0.04477	0.07511	0.39486
71.00000	0.04756	0.04581	0.12553	0.44304
60.00000	0.04398	0.09778	0.13512	0.53668
50.00000	0.27220	0.16777	0.04870	0.34665
43.00000	0.23367	0.18023	0.03274	0.11752
30.00000	0.03002	0.03220	0.14555	0.79578
20.00000	0.21725	0.21247	0.11502	0.08717

VECTOR ADDITION OF SUPERPOSED AMPLITUDES, INCHES

DEGREES	1X19	7X7	3X19	4X7
90.00000	0.09086	0.09234	0.05854	0.36231
80.00000	0.10809	0.04585	0.07624	0.42306
71.00000	0.05346	0.04751	0.12951	0.47330
60.00000	0.05184	0.10446	0.14015	0.56733
50.00000	0.28066	0.17446	0.05778	0.35742
43.00000	0.23797	0.18421	0.04027	0.12470
30.00000	0.03444	0.03254	0.15281	0.80548
20.00000	0.24300	0.21666	0.11705	0.08853

AMPLITUDE TO DIAMETER RATIO

DEGREES	1X19	7X7	3X19	4X7
90.00000	0.14377	0.14429	0.09519	0.51759
80.00000	0.17102	0.07164	0.12397	0.60437
71.00000	0.08458	0.07424	0.21059	0.67615
60.00000	0.08202	0.16321	0.22789	0.81047
50.00000	0.44408	0.27259	0.09395	0.51060
43.00000	0.37654	0.28783	0.06549	0.17814
30.00000	0.05450	0.05084	0.24848	1.15069
20.00000	0.38450	0.33853	0.19032	0.12648

NOMINAL STROUHAL NUMBERS

DEGREES	1X19	7X7	3X19	4X7
90.00000	0.19166	0.19411	0.19951	0.18267
80.00000	0.19009	0.20169	0.17176	0.18549
71.00000	0.19327	0.20530	0.18348	0.19320
60.00000	0.19558	0.18766	0.19532	0.19953
50.00000	0.19783	0.20626	0.18118	0.21913
43.00000	0.19607	0.21844	0.19715	0.19546
30.00000	0.21395	0.23475	0.19084	0.19749
20.00000	0.22154	0.23758	0.25362	0.27427

VELOCITY=10 KNOTS AND LOW TENSION

FUNDAMENTAL X ACCELERATION, G-S

DEGREES	1X19	7X7	3X19	4X7
90.00000	12.95918	20.07138	39.13608	18.56125
80.00000	5.72239	14.54043	30.80402	26.45924
71.00000	8.00954	9.49680	14.40812	28.09359
60.00000	8.78228	8.17668	27.13984	17.32237
50.00000	5.72239	6.49497	8.78228	7.73762
43.00000	7.45723	9.83054	7.22117	12.69426
30.00000	5.10008	8.56204	12.98994	15.08716
20.00000	1.38860	3.07310	1.18470	6.97601

FUNDAMENTAL X AMPLITUDE, INCHES

DEGREES	1X19	7X7	3X19	4X7
90.00000	0.03767	0.05106	0.08785	0.06224
80.00000	0.01554	0.03699	0.06915	0.08873
71.00000	0.02250	0.02496	0.03914	0.09780
60.00000	0.02643	0.02461	0.08463	0.06775
50.00000	0.02533	0.02875	0.04058	0.03284
43.00000	0.03944	0.04747	0.03819	0.07758
30.00000	0.05930	0.09303	0.11664	0.16392
20.00000	0.02805	0.05681	0.01854	0.15468

FUNDAMENTAL Y ACCELERATION, G-S

DEGREES	1X19	7X7	3X19	4X7
90.00000	26.15636	34.88007	29.01198	60.06304
80.00000	25.56097	23.58182	26.21847	74.57227
71.00000	26.21847	15.94327	20.35201	82.91010
60.00000	16.35337	17.08352	44.52535	58.69584
50.00000	30.03152	20.30380	17.52295	27.13984
43.00000	30.37927	31.08690	16.92807	37.03458
30.00000	28.02704	17.08352	33.77593	54.15110
20.00000	1.68880	4.92694	4.45253	5.29185

FUNDAMENTAL Y AMPLITUDE, INCHES

DEGREES	1X19	7X7	3X19	4X7
90.00000	0.07603	0.08873	0.06513	0.20142
80.00000	0.06943	0.05999	0.05886	0.25007
71.00000	0.07365	0.04190	0.05528	0.28862
60.00000	0.04922	0.05142	0.13884	0.22958
50.00000	0.13294	0.08988	0.08098	0.11519
43.00000	0.16066	0.15012	0.08952	0.22634
30.00000	0.32588	0.18561	0.30329	0.58835
20.00000	0.03412	0.09107	0.06966	0.11734

VECTOR ADDITION OF SUPERPOSED AMPLITUDES, INCHES

DEGREES	1X19	7X7	3X19	4X7
90.00000	0.08485	0.10237	0.10936	0.21081
80.00000	0.07115	0.07048	0.09081	0.26535
71.00000	0.07701	0.04877	0.06773	0.30474
60.00000	0.05587	0.05700	0.16260	0.23937
50.00000	0.13533	0.09436	0.09058	0.11978
43.00000	0.16543	0.15744	0.09733	0.23927
30.00000	0.33123	0.20762	0.32494	0.61076
20.00000	0.04417	0.10734	0.07209	0.19415

AMPLITUDE TO DIAMETER RATIO

DEGREES	1X19	7X7	3X19	4X7
90.00000	0.13426	0.15995	0.17782	0.30116
80.00000	0.11258	0.11012	0.14765	0.37906
71.00000	0.12185	0.07620	0.11013	0.43534
60.00000	0.08840	0.08907	0.26438	0.34196
50.00000	0.21413	0.14745	0.14728	0.17111
43.00000	0.26176	0.24600	0.15826	0.34181
30.00000	0.52410	0.32441	0.52836	0.87252
20.00000	0.06989	0.16772	0.11721	0.27736

NOMINAL STROUHAL NUMBERS

DEGREES	1X19	7X7	3X19	4X7
90.00000	0.18096	0.19592	0.20038	0.18662
80.00000	0.19009	0.19894	0.20347	0.18950
71.00000	0.19469	0.20387	0.19266	0.19372
60.00000	0.20535	0.20799	0.19632	0.19953
50.00000	0.19143	0.19388	0.18231	0.21655
43.00000	0.19672	0.20851	0.19142	0.20270
30.00000	0.18096	0.18960	0.20038	0.20736
20.00000	0.20069	0.21251	0.22192	0.21220

10 knots and high tension

FUNDAMENTAL X ACCELERATION, G-S

DEGREES	1X19	7X7	3X19	4X7
90.00000	2.20601	27.07555	5.46484	24.75183
80.00000	3.57773	0.00000	5.34044	22.83533
71.00000	3.65239	31.44686	8.08309	14.37399
60.00000	5.40228	31.88653	8.00954	12.81083
50.00000	.616	19.21354	5.92349	8.08309
43.00000	3.53677	6.28937	7.64905	22.78124
30.00000	5.72239	5.54124	3.48801	2.55610
20.00000	2.27812	2.23155	4.01428	4.54545

FUNDAMENTAL X AMPLITUDE, INCHES

DEGREES	1X19	7X7	3X19	4X7
90.00000	0.00580	0.06671	0.01305	0.07718
80.00000	0.00972	0.00000	0.01359	0.06873
71.00000	0.00992	0.09141	0.02124	0.05404
60.00000	0.01454	0.09943	0.02250	0.05437
50.00000	0.02809	0.06948	0.02412	0.03903
43.00000	0.02162	0.02561	0.04450	0.15427
30.00000	0.06217	0.04976	0.02632	0.03188
20.00000	0.03867	0.05455	0.08110	0.11112

FUNDAMENTAL Y ACCELERATION, G-S

DEGREES	1X19	7X7	3X19	4X7
90.00000	48.82108	25.56097	28.67988	50.53674
80.00000	39.68325	0.00000	32.17936	52.91846
71.00000	31.08690	28.67988	28.67988	43.40876
60.00000	44.93423	31.88653	25.91835	35.69253
50.00000	28.74797	27.13984	14.37399	25.56097
43.00000	9.74108	16.54274	22.57394	68.01071
30.00000	41.93506	24.75183	18.09578	12.51922
20.00000	4.05114	8.29101	13.14036	31.08690

FUNDAMENTAL Y AMPLITUDE, INCHES

DEGREES	1X19	7X7	3X19	4X7
90.00000	0.12830	0.06298	0.06847	0.15758
80.00000	0.10470	0.00000	0.08186	0.15927
71.00000	0.08444	0.08337	0.07537	0.16320
60.00000	0.16250	0.09943	0.07281	0.15148
50.00000	0.11708	0.09815	0.05854	0.12343
43.00000	0.05953	0.06737	0.13131	0.46056
30.00000	0.45563	0.22226	0.13654	0.15615
20.00000	0.06877	0.20268	0.26548	0.75996

VECTOR ADDITION OF SUPERPOSED AMPLITUDES, INCHES

DEGREES	1X19	7X7	3X19	4X7
90.00000	0.12843	0.09174	0.06970	0.17547
80.00000	0.10823	0.00000	0.08298	0.17346
71.00000	0.08502	0.12372	0.07830	0.17191
60.00000	0.16367	0.14061	0.07620	0.16095
50.00000	0.12040	0.12025	0.06332	0.12946
43.00000	0.06334	0.07208	0.13865	0.48571
30.00000	0.45985	0.22776	0.13905	0.15937
20.00000	0.07890	0.20990	0.27759	0.76804

AMPLITUDE TO DIAMETER RATIO

DEGREES	1X19	7X7	3X19	4X7
90.00000	0.20321	0.14334	0.11333	0.25067
80.00000	0.17125	0.00000	0.13492	0.24781
71.00000	0.13453	0.19331	0.12732	0.24559
60.00000	0.25897	0.21970	0.12391	0.22992
50.00000	0.19051	0.18789	0.10295	0.18494
43.00000	0.10022	0.11262	0.22544	0.69387
30.00000	0.72761	0.35587	0.22610	0.22767
20.00000	0.12485	0.32797	0.45137	1.09720

NOMINAL STROUHAL NUMBERS

DEGREES	1X19	7X7	3X19	4X7
90.00000	0.19032	0.19908	0.19430	0.19354
80.00000	0.19009	0.19894	0.19114	0.20003
71.00000	0.19799	0.19384	0.19587	0.18641
60.00000	0.18734	0.20434	0.20684	0.19155
50.00000	0.19957	0.21451	0.19420	0.20302
43.00000	0.18299	0.22704	0.18252	0.19257
30.00000	0.18720	0.20856	0.21860	0.19354
20.00000	0.21894	0.18479	0.19529	0.20210

DISTRIBUTION LIST

		Copy No.
162	Commander, Naval Air Systems Command	
	(APC-210, B. Emshwiller)	1
	(APC-210, K. Haas)	2
---	Commander, Naval Civil Engineering Laboratory, Port Hueneme, CA 93043	
	(Code L43, D. Meggit)	3
	(Code L03C, J. Dummer)	4
	(Code L44, Dr. W. Nordell)	5
223	Commander, Naval Research Laboratory	
	(Code 5841, Dr. R. Peltzer)	6
	(Code 5841, Dr. O. M. Griffin)	7
427	Commander, Naval Sea Systems Command	
	(PMS 407D, D. Potter)	8
236	Commander, David W. Taylor Naval Ship Research and Development Center	
	(Code 1541, D. Charvoz)	9
	(Code 1541, R. Crispin)	10
266	Commander, Naval Underwater Systems Center, Newport	
	(Code 8333, S. Hassan)	11
---	Chief of Naval Research (Office of Naval Technology) 800 North Quincy Street, Arlington, VA 22217-5000	
	(Code 23, Dr. A. J. Faulstich)	12
	(Code 235, W. Ching)	13
146	Commander, Mine Warfare Command	
	(Code N4A, G. Pollitt)	14
075	Director, Defense Technical Information Center	15-16